



## UvA-DARE (Digital Academic Repository)

### Ophthalmic molecular imaging and the role of the proteasome in retinal diseases

Ramos de Carvalho, J.E.

**Publication date**

2018

**Document Version**

Final published version

**License**

Other

[Link to publication](#)

**Citation for published version (APA):**

Ramos de Carvalho, J. E. (2018). *Ophthalmic molecular imaging and the role of the proteasome in retinal diseases*. [Thesis, fully internal, Universiteit van Amsterdam].

**General rights**

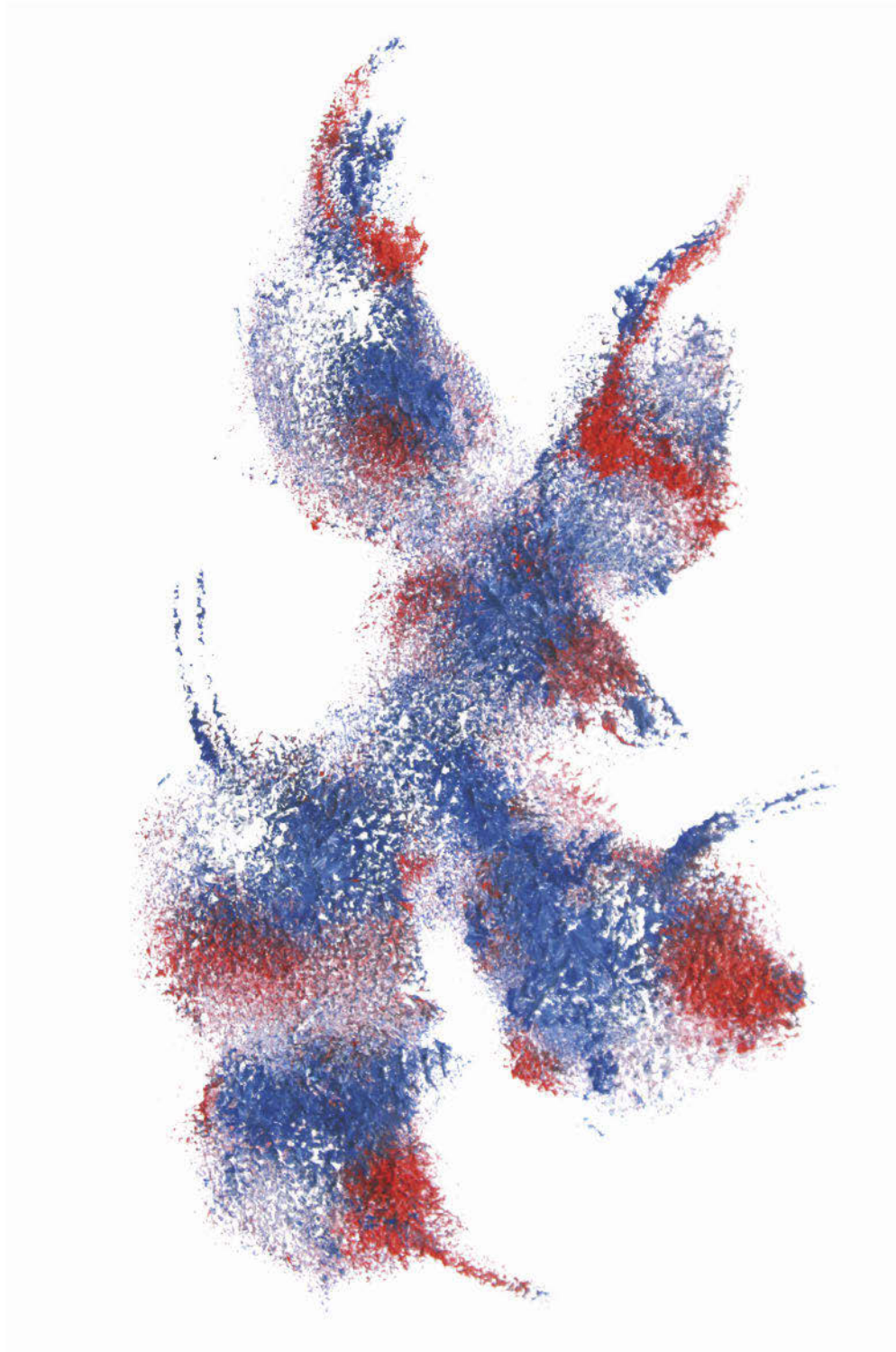
It is not permitted to download or to forward/distribute the text or part of it without the consent of the author(s) and/or copyright holder(s), other than for strictly personal, individual use, unless the work is under an open content license (like Creative Commons).

**Disclaimer/Complaints regulations**

If you believe that digital publication of certain material infringes any of your rights or (privacy) interests, please let the Library know, stating your reasons. In case of a legitimate complaint, the Library will make the material inaccessible and/or remove it from the website. Please Ask the Library: <https://uba.uva.nl/en/contact>, or a letter to: Library of the University of Amsterdam, Secretariat, P.O. Box 19185, 1000 GD Amsterdam, The Netherlands. You will be contacted as soon as possible.

Ophthalmic Molecular Imaging  
and the Role of the Proteasome  
in Retinal Diseases

Emanuel  
Ramos de Carvalho





# Ophthalmic Molecular Imaging and the Role of the Proteasome in Retinal Diseases

Emanuel  
Ramos de Carvalho

Ophthalmic molecular imaging and the role of the proteasome in retinal diseases  
Academic Thesis, University of Amsterdam, Amsterdam, The Netherlands

ISBN: 978-94-6182-916-0

Author: J. Emanuel Ramos de Carvalho

Layout: J. Emanuel Ramos de Carvalho and Andrea Dell'Anna

Cover artwork: Ana da Silva Ramos de Carvalho

Printing: Off Page

Copyright © by J. E. Ramos de Carvalho, Amsterdam, The Netherlands. All rights reserved. No part of this thesis may be reproduced, stored in a retrieval system or transmitted in any form or by any means, without prior authorisation of the author.

Financial support was kindly provided by Criel, Facol, Bayer, Novartis, Academic Medical Centre, Landelijke Stichting voor Blinden en Slechtzienden and Oculenti.

# Ophthalmic Molecular Imaging and the Role of the Proteasome in Retinal Diseases

## ACADEMISCH PROEFSCHRIFT

ter verkrijging van de graad van doctor  
aan de Universiteit van Amsterdam  
op gezag van de Rector Magnificus  
prof. dr. ir. K. I. J. Maex  
ten overstaan van een door het College voor Promoties ingestelde  
commissie,  
in het openbaar te verdedigen in de Aula der Universiteit  
op woensdag dag 28 november 2018, te 11:00 uur

door

João Emanuel Ramos de Carvalho  
geboren te Barcelos, Braga, Portugal



## **Promotiecommissie**

<b>Promotores:</b>	Prof. dr. R. O. Schlingemann	AMC-UvA
	Prof. dr. C. J. F. van Noorden	AMC-UvA
<b>Copromotor:</b>	Prof. dr. M. C. G. Aalders	AMC-UvA
	Dr. I. Klaassen	AMC-UvA
<b>Overige leden:</b>	Prof. dr. E. Aronica	AMC-UvA
	Prof. dr. A. G. J. M van Leeuwen	AMC-UvA
	Prof. dr. C. W. G. M. Löwik	Erasmus Universiteit Rotterdam
	Prof. dr. H. Tan	AMC-UvA
	Prof. dr. P. van der Valk	Vrije Universiteit Amsterdam
	Prof. dr. J. R. Vingerling	Erasmus Universiteit Rotterdam

## **Faculteit der Geneeskunde**



To my parents



## Table of contents

1	General introduction	11
2	Aims of the thesis	25
3	Complement factor C3a alters proteasome function in human RPE cells and in an animal model of age-related RPE degeneration	29
4	Involvement of the ubiquitin-proteasome system in the expression of extracellular matrix genes in retinal pigment epithelial cells	55
5	Modulation of the proteasome pathway by nano-curcumin and curcumin in retinal pigment epithelial cells	81
6	Reversal of threatening blindness after initiation of eculizumab in Purtscher-like retinopathy secondary to atypical hemolytic uremic syndrome	101
7	Spectral imaging of the ocular fundus using a 7-band retinal multispectral imaging system	117
8	Recent advances in ophthalmic molecular imaging	137
9	Summary and conclusions	175
10	Nederlandse samenvatting	181
11	Addendum	187

1

# General introduction

## Age-related macular degeneration

Age-related macular degeneration (AMD) is the leading cause of irreversible blindness in the Western world,<sup>97</sup> with a prevalence that is expected to rise to 97% by the year 2050 alongside increased life expectancy.<sup>116</sup> The disease has a broad phenotypical presentation, but is usually divided into exudative versus non-exudative. The non-exudative or dry form is characterized by the development of geographic atrophy with degeneration of the retinal pigment epithelium (RPE), outer layers of the neurosensory retina and the choriocapillaris. The exudative or wet or neovascular form is defined by the development of choroidal neovascularization, in which neovascular complexes infiltrate the subretinal space or the anatomical space located between the RPE and Bruch's membrane.<sup>97</sup> Both subtypes, although linked to distinct pathogenic pathways, ultimately lead to atrophy of the neurosensory retina and ensuing irreversible visual loss. Other relatively common causes of visual loss include development of subretinal fibrosis and hemorrhage.<sup>14; 26</sup> Subretinal fibrosis in AMD occurs within a context of a dysregulated wound response often secondary to choroidal neovascularization.<sup>14; 26; 127</sup> The multifactorial cascade of events leading to AMD is complex and involves numerous pathogenic pathways. One of the first features of "early" AMD is the accumulation of focal deposits of extracellular material located under the RPE (classical soft and cuticular drusen) or above the RPE (subretinal drusenoid deposits).<sup>134</sup> Drusen contain carbohydrates, zinc and nearly 150 proteins, including vitronectin, apolipoproteins E and B, clusterin, connective tissue growth factor (CTGF) and complement system components.<sup>24; 107</sup> The RPE cell monolayer is regarded as the primary mediator of disease initiation and progression in AMD. RPE cells participate in the visual cycle and are responsible for phagocytosis of photoreceptor outer segments, maintenance of the outer blood-retina barrier, secretion of neurotrophic, inflammatory and vasculotropic growth factors, fluid movement from the subretinal space and ionic transport regulation between the choroid and the retina.<sup>73; 135</sup> In addition, thickening of Bruch's

membrane, combined with accumulation of diffuse lipid aggregates has been reported to contribute to AMD pathogenesis by affecting RPE cell adhesion and migration and impeding choroidal and retinal cell migration.<sup>157</sup> Impaired outer retinal perfusion due to choriocapillaris changes has also been proposed as a pathogenic causative factor.<sup>157</sup> In the past two decades, several contributing environmental and genetic risk factors associated with the development of AMD have been identified. Smoking is the most consistently established environmental risk factor.<sup>131; 139</sup> Additionally, obesity, sunlight exposure and nutritional factors, such as antioxidant and fat intake have been identified as important risk factors.<sup>10; 22; 49; 85; 88; 101; 110; 130; 133</sup> The discovery of genetic risk variants in genes involved in inflammation and immune pathways was a major breakthrough in the understanding of AMD, attributing a role for chronic local inflammation and immune-mediated effects in its pathogenesis.<sup>7; 8; 30; 31; 37; 38; 41; 55; 67; 68; 79; 89</sup> Variants in genes involved in regulation of the complement pathway, namely Complement Factor H (*CFH*), Complement Factor B (*CFB*), Complement Component C2, Complement Component C3 and Complement Factor I (*CFI*) as well as others unrelated to the complement pathway such Age-Related Maculopathy Susceptibility 2 (*ARMS2*) and High Temperature Requirement A Serine Peptidase 1 (*HTRA1*) account for a large proportion of the genetic risk.<sup>8</sup>

Presently, the sole recommended treatment for patients with intermediate to advanced AMD in one eye is supplementation with a specific formulation of antioxidants and minerals which has been demonstrated to modestly reduce the risk of developing advanced AMD, including neovascular AMD.<sup>1</sup> For neovascular AMD, the advent of treatment options directed at vascular endothelial growth factor (VEGF) has greatly impacted the natural history of the disorder.<sup>21</sup> Notwithstanding, in spite of the immense progress achieved over the past two decades, AMD remains a complex multifactorial disease, often refractory to current treatment modalities. Assessment and characterization of novel molecular pathways are of paramount importance to drive the development of new therapeutic targets aimed at preventing or treating events associated with irreversible visual loss in advanced AMD, such as fibrosis, macular atrophy and choroidal neovascularization refractory to anti-VEGF treatment.

### **The ubiquitin-proteasome system**

The ubiquitin-proteasome system (UPS) is a multisubunit protein complex that is responsible for non-lysosomal proteolysis in all types of eukaryotic cells.<sup>23; 29</sup> In 2014, the Nobel Prize in Chemistry was awarded to Aaron Ciechanover, Avram Herschko and Irwin Rose for their discovery of ubiquitin-mediated proteolysis and in recognition of the importance of this pathway in maintenance of a regular protein homeostasis (proteostasis).<sup>113; 48</sup>

Protein quality control encompasses mechanisms of protein synthesis, folding, unfolding and clearance or turnover.<sup>124</sup> The first quality control mechanism is mediated

by molecular chaperones, a group of multidomain proteins, that recognize misfolded proteins. Proteins are then arrested or unfolded and targeted for protein refolding which is accomplished by heat shock proteins (HSPs).<sup>123</sup> If this fails, proteins are targeted to be cleared. Protein turnover in eukaryotic cells relies on two main pathways: the UPS and the lysosomal/autophagosomal degradation system. The latter targets long-lived proteins and large structures such as protein aggregates. Improper clearance by autophagy, alongside reduced lysosomal activity, results in the accumulation of toxic pro-inflammatory aggregates.<sup>48</sup> The UPS is responsible for the turnover of short-lived and misfolded proteins which comprise the majority (80-90%) of cellular proteins in eukaryotic cells.<sup>58; 59; 60</sup> The importance of efficient proteostasis mechanisms for the health of cells and longevity of organisms is attested by the fact that 1% of the total cellular protein content represents UPS-related proteins.<sup>23</sup> In recent years, UPS dysfunction has been implied in the pathogenesis of many diseases including various ophthalmic conditions such as AMD.<sup>15; 34; 36; 42; 43; 44; 45; 47; 48; 52; 61; 65; 75; 76; 77; 82; 83; 84; 95; 98; 104; 119;</sup>

<sup>125; 128; 143; 152; 156; 159; 160</sup> Taking this into account, targeting of the UPS has been proposed as a powerful therapeutic strategy in cancer therapy and in other diseases in which abnormal proteostasis is considered to play a primary role.<sup>20; 25; 32; 36; 40; 54; 92; 147</sup>

Proteins are targeted for proteasomal degradation by a process that involves tagging by a poly-ubiquitin chain in an ATP-dependent reaction after activation by an E1 ubiquitin-activating enzyme, followed by binding to an E2 conjugating enzyme and consecutive binding of the ubiquitin moiety to a lysine residue present in the protein to be degraded via an E3 ligase. Successive ubiquitination ultimately forms a poly-ubiquitin chain which enables recognition of the protein and consequent unfolding and degradation by the 26S proteasome.<sup>57</sup> The 26S proteasome is composed of the 20S core proteasome and the 19S regulatory particle. The 19S regulatory particle is involved in recognition and de-ubiquitination of the poly-ubiquitinated substrate facilitating its entry into the 20S core. The 20S proteolytic core consists of four stacked rings, each composed of seven catalytic subunits.<sup>64; 140</sup> The two outer rings, composed of the  $\alpha$ -subunits, control the opening and closure of the cylindrical core. The inner two rings contain seven  $\beta$ -subunits of which three have proteolytic activity for a specific set of amino acids;  $\beta 1$  with caspase-like activity (proteolysis of acidic residues),  $\beta 2$  with trypsin-like activity (proteolysis of basic residues) and  $\beta 5$  with chymotrypsin-like activity (proteolysis of hydrophobic residues). The amino acid chains are cleaved by the N-terminal threonine residue of the catalytic subunits.<sup>9; 64; 132; 140</sup> After release, these smaller peptides can be processed by peptidases for antigen presentation or recycled into amino acids. The proteasome activator (PA)28 $\gamma$  or the PA28A $\beta$  activating cap can replace the 19S cap. Opening of the  $\alpha$ -gate is achieved either by recognition of substrates by the 19S cap or by docking of the proteasome activators.<sup>50; 99</sup> The PA28 caps, unlike the 19S cap, are ATP independent and unable to recognize ubiquitinated and folded proteins. However, depending on the substrate, the peptidase activity of the proteasome can, in this manner, be stimulated up to 200-fold.<sup>99; 141</sup> PA28 $\alpha\beta$  expression can be induced by interferon- $\gamma$  (IFN $\gamma$ ) which was used to demonstrate maximal proteasomal activation throughout

our experiments. When PA28 $\alpha\beta$  is bound to the proteasome, proteolytic activities of all three catalytic subunits are elevated<sup>114</sup> due to a structural change of the 20S core and increased accessibility of the catalytic subunits.<sup>33; 63</sup> Furthermore, by opening the  $\alpha$ -gate, peptide release is increased, enabling more peptides to be recognized for antigen processing through binding to major histocompatibility complex (MHC) class I molecules.<sup>153</sup> The second proteasome activator, PA28 $\gamma$ , participates in a wider range of cellular processes including cell cycle regulation and apoptosis.<sup>115</sup> Proteasome activation by PA28 $\gamma$  mainly increases trypsin-like ( $\beta$ 2) activity.<sup>53; 93</sup> The constitutive catalytic subunits  $\beta$ 1,  $\beta$ 2 and  $\beta$ 5 can be replaced by the inducible immunosubunits  $\beta$ 1i (LMP2),  $\beta$ 2i (MECL1) and  $\beta$ 5i (LMP7), forming the so-called immunoproteasome. Interferon- $\gamma$  is one of the inducers of the immunoproteasome. This change in conformation induces significant changes in the level of proteasome-mediated proteolytic activity, namely downregulation of the caspase-like activity and upregulation of the trypsin-like and chymotrypsin-like activity.<sup>4; 39; 51</sup> The immunoproteasome is involved in several cellular processes such as generation of immunogenic peptides for MHC class I recognition,<sup>46; 60; 121</sup> degradation of oxidized proteins,<sup>35</sup> cell signaling<sup>71; 76</sup> and neuroprotection.<sup>46</sup> Therefore, the ratio between the constitutive and inducible subunits is considered to be a marker of cellular stress.

### **The ubiquitin-proteasome system and the role of the complement pathway in the retinal pigment epithelium**

Similar to other cells, the RPE depends on functional protein degradation systems to dispose of unwanted proteins and preserve cellular functions under normal and pathogenic conditions. Impairment of protein degradation has been associated with the development of several age-related degenerative disorders, especially in post-mitotic cells, such as neurons and RPE cells.<sup>19</sup> The RPE and the retina are constantly exposed to high oxidative stress conditions triggered by light exposure, and the high rate of metabolism and heterophagy which results in protein damage and subsequent protein unfolding. The toxic effects incurred by accumulation of protein aggregates and lipofuscin may tip the balance from a para-inflammatory state to the chronic inflammatory state that is observed in AMD.<sup>48</sup>

The proteasome is involved in several aspects of retinal physiology. The immunoproteasome, which is constitutively expressed in immune cells, has also been shown to be present, albeit in low concentrations, in the uninjured retina and RPE. As previously mentioned, the immunoproteasome has a role in modulation of pathways involved in cellular stress responses.<sup>100; 128</sup> Its expression is significantly upregulated during retinal injury by cytotoxic T-lymphocytes or optic nerve crush,<sup>47; 128</sup> oxidative stress,<sup>75</sup> inflammation<sup>62</sup> and aging.<sup>76</sup> Moreover, RPE cells deficient in LMP7 and MECL1 immuno-subunits have been shown to be less resistant to oxidative stress.<sup>75</sup> On the other hand, knock-out of the LMP2 immuno-subunit confers neuroprotective effects

in traumatic optic neuropathy.<sup>128</sup> The pool of proteasomes present in cells appears to be dynamic and changes over time. In fact, increased levels of immunoproteasomes have been demonstrated in the retina of human donors with AMD,<sup>42</sup> and the total content of proteasomes was increased (3-fold) when compared to age-matched controls.<sup>28</sup> Likewise, ubiquitin conjugates have been demonstrated in drusen under the macula of donors with AMD suggesting that these may occur secondary to impaired proteolysis by the UPS.<sup>106; 122; 145; 146</sup> In addition, proteasome activity in the neural retina has been shown to increase alongside AMD progression,<sup>42</sup> although this cannot be assumed to reflect the activity of the proteasome in RPE cells, since the effects of cellular stress on proteasome function are likely cell-specific.<sup>48</sup>

The accumulation of lipofuscin granules within the RPE is a recognized hallmark of aging and has been suggested to play a role in the development of AMD. Lipofuscin is a polymeric substance, located in lysosomal storage bodies or melanosomes of RPE cells<sup>80</sup> and primarily composed of cross-linked protein residues that are the result of iron-catalyzed oxidative processes.<sup>18</sup> With lipofuscin accumulation, both phagocytic (heterophagic) and autophagic processes become impaired which in turn results in increased transcytosis and exocytosis of proteins and ensuing drusen formation.<sup>81; 87; 137; 145</sup> Human retinal lipofuscin contains the 13-cis isomer iso-A2E and the bis-retinoid pyridinium compound, A2E. A2E inhibits lysosomal-driven proteolysis by mechanisms involving inhibition of the ATP-driven protein pump<sup>13</sup> and increase in lysosomal pH.<sup>91</sup> Melanosomes accumulate lipofuscin, due to higher oxygen consumption and reactive oxygen species production, which may then lead to retinal degeneration and local complement activation.<sup>154</sup> Activation of the complement system is an established pathogenic event linked to AMD and other retinal disorders. The complement system, as part of the innate immune response, can be activated via various pathways, namely the classical, alternative and lectin pathways.<sup>37; 38</sup> Briefly, complement system activation involves the following steps: initiation, formation of a C3 convertase, cleavage of C3, formation of a C5 convertase, cleavage of C5 and, ultimately, formation of the membrane attack complex (C5b-9) that directly lyses targeted (opsonized) pathogens or damaged cells. During this cascade of events, complement effector molecules, including complement anaphylatoxins C3a and C5a, are released.<sup>16</sup> These are potent pro-inflammatory molecules that attract and activate leukocytes through interaction with their cognate G-protein-coupled receptors.<sup>109</sup> Several other non-immune functions have been attributed to the complement system such as promotion of tissue regeneration, angiogenesis, recruitment of stem cells, neural development and control of embryo implantation.<sup>118</sup> The effector function of the complement system is non-specific which may result in unwanted effects in bystander cells. This response can be amplified and become pathogenic whenever activation of the complement persists, for instance, due to abnormalities in complement regulation. Several complement regulators act at different steps of the complement cascade. These can be identified in the fluid phase as well as on the surface of tissues and circulating cells.<sup>69</sup> AMD is one of the human disorders that has been linked to complement dysregulation.<sup>8</sup> As such,

modulation of the complement in AMD and other disorders has been proposed as a potential therapeutic strategy.<sup>117; 149</sup> Thus far, trials investigating the use of molecules blocking the complement pathway at various stages of its activation failed in halting progression of AMD.<sup>12; 155</sup>

## Curcumin

Curcumin [1,7-bis-(4-hydroxy-3-methoxyphenyl)-1,6-heptadiene-3,5-dione] is the pigment extract of turmeric, a widely-used food condiment in the Indian subcontinent that is known for its beneficial effects in the prevention and treatment of various pro-inflammatory chronic diseases including neurodegenerative, cardiovascular, pulmonary, metabolic, autoimmune and malignant diseases. The number of research studies assessing the cellular and molecular effects of curcumin has been increasing steadily.<sup>3; 11; 17; 56; 66; 108; 120; 126; 142</sup> The pleiotropic effects of curcumin include inhibition of pro-inflammatory transcription factor nuclear factor-kappaB (NF- $\kappa$ B), inhibition of signal transducer and activator of transcription-3, activation of peroxisome proliferator-activated receptor- $\gamma$  (PPAR $\gamma$ ), nuclear factor (erythroid-derived) factor-2 (Nrf2) cell-signaling pathways, upregulation of adiponectin, modulation of several inflammatory proteins and cell survival proteins such as histone acetylase, histone deacetylase, protein kinases, protein reductases, glyoxalase I, human immunodeficiency virus type 1 (HIV1) integrase and HIV1 protease.<sup>2; 27; 66</sup> Furthermore, one of the effects attributed to curcumin is its ability to modulate proteolytic activity by the proteasome.<sup>70</sup> In spite of the numerous pre-clinical studies, curcumin has not yet been approved as a specific treatment because its use is hampered by its poor bioavailability when administered orally.<sup>6</sup> Different strategies have been proposed to increase the absorption of curcumin such as concomitant administration of piperin, or incorporation of curcumin in nanoparticles, liposomes, micelles, or phospholipid complexes.<sup>111; 148</sup>

Similarly to the effects described in other tissues and organs, curcumin has been demonstrated to have favorable in vitro effects on corneal epithelial cells,<sup>21</sup> RPE cells<sup>74; 86; 96</sup> and neurosensory retina,<sup>94; 129; 144; 150; 151; 158</sup> suggesting a potential role for curcumin in ophthalmic disorders. Contradictorily, other studies have warned of potential toxic effects of curcumin in RPE cells<sup>5; 72; 136</sup> and retinal endothelial cells<sup>112</sup> suggesting that retinal function ought to be monitored during concomitant intake of curcumin.<sup>72</sup> One should take into account that the effects of curcumin are highly dependent on levels achieved at the target site<sup>102; 103</sup> and the formulation of curcumin used.<sup>105</sup> Indeed, curcumin is known to be a hormetic compound, i.e. toxic at high doses but able to exert adaptive stress responses at lower doses.<sup>102; 103</sup> Therefore, extrapolation of pre-clinical findings and effects of curcumin in the retina and RPE cells may not be as straightforward as initially presumed.

## Ophthalmic molecular imaging

In recent years, molecular imaging has been hailed as the next frontier in medicine and one of the crucial steps in driving medicine towards an era of personalized care. The purpose of molecular imaging is to “directly or indirectly monitor and record the spatiotemporal distribution of molecular or cellular processes for biochemical, biological, diagnostic, or therapeutic applications”.<sup>138</sup> In other words, the goal of molecular imaging techniques is to target and visualize molecular processes in vivo.<sup>90</sup> It is presumed that implementation of molecular imaging will facilitate disease detection at a preliminary stage, prior to the development of structural changes and organ dysfunction. This allows early diagnosis and targeted intervention with more favorable outcomes.

Broadly speaking, the introduction of molecular imaging techniques in the clinical setting has been delayed by two major obstacles: approval of contrast agents and development of feasible imaging modalities. Molecular imaging relies on the use of extrinsic contrast agents that are specific for the molecular processes of interest. Development of these contrast agents and approval for use in human subjects has been slower than expected. At present, most studies have been confined to small animals. Furthermore, applicability of these techniques depends on the development of feasible, non-invasive and reproducible imaging techniques that allow the visualization of such contrast agents. In spite of these inherent difficulties, several molecular imaging clinical applications have already been described.<sup>78</sup>

The myriad of ophthalmic imaging modalities attests to the accessibility of the human eye. Indeed, ophthalmology may be one of the first medical fields to streak ahead in the race to introduce molecular imaging in clinical care.

## References

1. Age-Related Eye Disease Study Research G: A randomized, placebo-controlled, clinical trial of high-dose supplementation with vitamins C and E, beta carotene, and zinc for age-related macular degeneration and vision loss: AREDS report no. 8. *Arch Ophthalmol* 119:1417-1436, 2001
2. Aggarwal BB: Targeting inflammation-induced obesity and metabolic diseases by curcumin and other nutraceuticals. *Annu Rev Nutr* 30:173-199, 2010
3. Aggarwal BB, Harikumar KB: Potential therapeutic effects of curcumin, the anti-inflammatory agent, against neurodegeneration, cardiovascular, pulmonary, metabolic, autoimmune and neoplastic diseases. *Int J Biochem Cell Biol* 41:40-59, 2009
4. Aki M, Shimbara N, Takashina M, et al.: Interferon-gamma induces different subunit organizations and functional diversity of proteasomes. *J Biochem-Tokyo* 115:257-269, 1994
5. Alex AF, Spitznas M, Tittel AP, et al.: Inhibitory effect of epigallocatechin gallate (EGCG), resveratrol, and curcumin on proliferation of human retinal pigment epithelial cells in vitro. *Curr Eye Res* 35:1021-1033, 2010
6. Anand P, Kunnumakkara AB, Newman RA, Aggarwal BB: Bioavailability of curcumin: problems and promises. *Mol Pharmacol* 4:807-818, 2007
7. Anderson DH, Mullins RF, Hageman GS, Johnson LV: Perspective - A role for local inflammation in the formation of drusen in the aging eye. *Am J Ophthalmol* 134:411-431, 2002
8. Anderson DH, Radeke MJ, Gallo NB, et al.: The pivotal role of the complement system in aging and age-related macular degeneration: Hypothesis re-visited. *Prog Ret Eye Res* 29:95-112, 2010
9. Arendt CS, Hochstrasser M: Identification of the yeast 20S proteasome catalytic centers and subunit interactions required for active-site formation. *Proc Natl Acad Sci U S A* 94:7156-7161, 1997
10. Arnault E, Barrau C, Nanteau C, et al.: Phototoxic action spectrum on a retinal pigment epithelium model of age-related macular degeneration exposed to sunlight normalized conditions. *PLoS One* 8:e71398, 2013
11. Bar-Sela G, Epelbaum R, Schaffer M: Curcumin as an anti-cancer agent: Review of the gap between basic and clinical applications. *Curr Med Chem* 17:190-197, 2010
12. Behar-Cohen F: AMD and complement pathway in 2017. *Rev Med Suisse* 14:64-69, 2018
13. Bergmann M, Schutt F, Holz FG, Kopitz J: Inhibition of the ATP-driven proton pump in RPE lysosomes by the major lipofuscin fluorophore A2-E may contribute to the pathogenesis of age-related macular degeneration. *FASEB J* 18:562-+, 2004
14. Bloch SB, Lund-Andersen H, Sander B, Larsen M: Subfoveal fibrosis in eyes with neovascular age-related macular degeneration treated with intravitreal ranibizumab. *Am J Ophthalmol* 156:116-124, 2013
15. Bousman C: The ubiquitin proteasome system is dysregulated in the blood and brain of individuals with schizophrenia. *Neuropsychopharmacol* 43:S92-S92, 2017
16. Bradley DT, Zipfel PF, Hughes AE: Complement in age-related macular degeneration: a focus on function. *Eye* 25:683-693, 2011
17. Bruck R, Ashkenazi M, Weiss S, et al.: Prevention of liver cirrhosis in rats by curcumin. *Liver Int* 27:373-383, 2007
18. Brunk UT, Terman A: Lipofuscin: Mechanisms of age-related accumulation and influence on cell function. *Free Radic Biol Med* 33:611-619, 2002
19. Carvalhal Marques F, Volovik Y, Cohen E: The roles of cellular and organismal aging in the development of late-onset maladies. *Annu Rev Pathol* 10:1-23, 2015
20. Chao A, Wang TH: Molecular mechanisms for synergistic effect of proteasome inhibitors with platinum-based therapy in solid tumors. *Taiwan J Obstet Gynecol* 55:3-8, 2016
21. Chew EY, Clemons TE, Agron E, et al.: Long-term effects of vitamins C and E, beta-carotene, and zinc on age-related macular degeneration AREDS Report No. 35. *Ophthalmology* 120:1604-1611, 2013
22. Cho E, Seddon JM, Rosner B, et al.: Prospective study of intake of fruits, vegetables, vitamins, and carotenoids and risk of age-related maculopathy. *Arch Ophthalmol* 122:883-892, 2004
23. Coux O, Tanaka K, Goldberg AL: Structure and functions of the 20S and 26S proteasomes. *Annu Rev Biochem* 65:801-847, 1996
24. Crabb JW, Miyagi M, Gu XR, et al.: Drusen proteome analysis: An approach to the etiology of age-related macular degeneration. *Proc Natl Acad Sci U S A* 99:14682-14687, 2002
25. Crawford LJ, Walker B, Irvine AE: Proteasome inhibitors in cancer therapy. *J Cell Commun Signal* 5:101-110, 2011
26. Daniel E, Toth CA, Grunwald JE, et al.: Risk of scar in the comparison of age-related macular degeneration treatments trials. *Ophthalmology* 121:656-666, 2014
27. de Porras VR, Gines A, Vallejo S, et al.: Curcumin-mediated oxaliplatin resistance reversal in CRC cell lines through modulation of NF- $\kappa$ B, STAT3 and CDK5 signaling pathways. *Eur J Cancer* 49:S172-S172, 2013
28. Decanini A, Nordgaard CL, Feng X, et al.: Changes in select redox proteins of the retinal pigment epithelium in age-related macular degeneration. *Am J Ophthalmol* 143:607-615, 2007
29. DeMartino GN, Slaughter CA: The proteasome, a novel protease regulated by multiple mechanisms. *J Biol Chem* 274:22123-22126, 1999
30. Despret DDG, Klaver CCW, Witteman JCM, et al.: Complement factor H polymorphism, complement activators, and risk of age-related macular degeneration. *JAMA* 296:301-309, 2006
31. Despret DDG, van Duijn CM, Oostra BA, et al.: Complement component C3 and risk of age-related macular degeneration. *Ophthalmology* 116:474-480, 2009
32. Dick LR, Fleming PE: Building on bortezomib: second-generation proteasome inhibitors as anti-cancer therapy. *Drug Discov Today* 15:243-249, 2010
33. Dick TP, Ruppert T, Groettrup M, et al.: Coordinated dual cleavages induced by the proteasome regulator PA28 lead to dominant MHC ligands. *Cell* 86:253-262, 1996
34. Ding QX, Keller JN: Proteasome inhibition in oxidative stress neurotoxicity: implications for heat shock proteins. *J Neurochem* 77:1010-1017, 2001
35. Ding QX, Martin S, Dimayuga E, et al.: LMP2 knock-out mice have reduced proteasome activities and increased levels of oxidatively damaged proteins. *Antiox Redox Signal* 8:130-135, 2006
36. Doepfner TR, Kaltwasser B, Kuckelkorn U, et al.: Systemic proteasome inhibition induces sustained post-stroke neurological recovery and neuroprotection via mechanisms involving reversal of peripheral immunosuppression and preservation of blood-brain-barrier integrity. *Mol Neurobiol* 53:6332-6341, 2016

37. Donoso LA, Kim D, Frost A, et al.: The role of inflammation in the pathogenesis of age-related macular degeneration. *Surv Ophthalmol* 51:137-152, 2006
38. Donoso LA, Vrabec T, Kuivaniemi H: The role of complement factor H in age-related macular degeneration: a review. *Surv Ophthalmol* 55:227-246, 2010
39. Driscoll J, Brown MG, Finley D, Monaco JJ: MHC-linked LMP gene-products specifically alter peptidase activities of the proteasome. *Nature* 365:262-264, 1993
40. Dudek EJ, Shang F, Liu Q, et al.: Selectivity of the ubiquitin pathway for oxidatively modified proteins: relevance to protein precipitation diseases. *FASEB J* 19:1707-+, 2005
41. Edwards AO, Ritter R, Abel KJ, et al.: Complement factor H polymorphism and age-related macular degeneration. *Science* 308:421-424, 2005
42. Ethen CM, Hussong SA, Reilly C, et al.: Transformation of the proteasome with age-related macular degeneration. *FEBS Lett* 581:885-890, 2007
43. Fernandes AF, Guo WM, Zhang XY, et al.: Proteasome-dependent regulation of signal transduction in retinal pigment epithelial cells. *Exp Eye Res* 83:1472-1481, 2006
44. Fernandes AF, Zhou JL, Zhang XY, et al.: Oxidative inactivation of the proteasome in retinal pigment epithelial cells - A potential link between oxidative stress and up-regulation of interleukin-8. *J Biol Chem* 283:20745-20753, 2008
45. Fernandes R, Giraó H, Pereira P: High glucose downregulates intercellular communication in retinal endothelial cells by enhancing degradation of connexin 43 by a proteasome-dependent mechanism. *J Biol Chem* 279:27219-27224, 2004
46. Ferrington DA, Gregerson DS: Immunoproteasomes: structure, function, and antigen presentation. *Prog Mol Biol Transl Sci* 109:75-112, 2012
47. Ferrington DA, Hussong SA, Roehrich H, et al.: Immunoproteasome responds to injury in the retina and brain. *J Neurochem* 106:158-169, 2008
48. Ferrington DA, Sinha D, Kaarniranta K: Defects in retinal pigment epithelial cell proteolysis and the pathology associated with age-related macular degeneration. *Prog Retin Eye Res* 51:69-89, 2016
49. Fletcher AE, Bentham GC, Agnew M, et al.: Sunlight exposure, antioxidants, and age-related macular degeneration. *Arch Ophthalmol* 126:1396-1403, 2008
50. Forster A, Masters EI, Whitby FG, et al.: The 1.9 Å structure of a proteasome-11S activator complex and implications for proteasome-PAN/PA700 interactions. *Mol Cell* 18:589-599, 2005
51. Gaczynska M, Rock KL, Goldberg AL: Gamma-interferon and expression of MHC genes regulate peptide hydrolysis by proteasomes. *Nature* 374:290-290, 1995
52. Gandolfi S, Laubach JP, Hideshima T, et al.: The proteasome and proteasome inhibitors in multiple myeloma. *Cancer Metast Rev* 36:561-584, 2017
53. Gao XL, Li J, Pratt G, et al.: Purification procedures determine the proteasome activation properties of REG gamma (PA28 gamma). *Arch Biochem Biophys* 425:158-164, 2004
54. Gatti L, Zuco V, Zaffaroni N, Perego P: Drug combinations with proteasome inhibitors in antitumor therapy. *Curr Pharm Des* 19:4094-4114, 2013
55. Gehrs KM, Jackson JR, Brown EN, et al.: Complement, age-related macular degeneration and a vision of the future. *Arch Ophthalmol* 128:349-358, 2010
56. Ghosh S, Banerjee S, Sil PC: The beneficial role of curcumin on inflammation; diabetes and neurodegenerative disease: a recent update. *Food Chem Toxicol* 83:111-124, 2015
57. Glickman MH, Ciechanover A: The ubiquitin-proteasome proteolytic pathway: Destruction for the sake of construction. *Physiol Rev* 82:373-428, 2002
58. Goldberg AL: Protein degradation and protection against misfolded or damaged proteins. *Nature* 426:895-899, 2003
59. Goldberg AL, Akopian TN, Kisselev AF, et al.: New insights into the mechanisms and importance of the proteasome in intracellular protein degradation. *Biol Chem* 378:131-140, 1997
60. Goldberg AL, Cascio P, Saric T, Rock KL: The importance of the proteasome and subsequent proteolytic steps in the generation of antigenic peptides. *Mol Immunol* 39:147-164, 2002
61. Graham SH, Liu H: Life and death in the trash heap: the ubiquitin proteasome pathway and UCHL1 in brain aging, neurodegenerative disease and cerebral ischemia. *Ageing Res Rev* 34:30-38, 2017
62. Gregerson DS, Lew KL, McPherson SW, et al.: RPE cells resist bystander killing by CTLs, but are highly susceptible to antigen-dependent CTL killing. *Invest Ophthalmol Vis Sci* 47:5385-5394, 2006
63. Groettrup M, Soza A, Eggers M, et al.: A role for the proteasome regulator PA28alpha in antigen presentation. *Nature* 381:166-168, 1996
64. Groll M, Ditzel L, Lowe J, et al.: Structure of 20S proteasome from yeast at 2.4 angstrom resolution. *Nature* 386:463-471, 1997
65. Guo W, Gallagher M, Taylor A, Shang F: Impairment of ubiquitin-proteasome pathway in retinal pigment epithelial cells enhances expression and secretion of vascular endothelial growth factor. *Invest Ophthalmol Vis Sci* 46, 2005
66. Gupta SC, Prasad S, Kim JH, et al.: Multitargeting by curcumin as revealed by molecular interaction studies. *Nat Prod Rep* 28:1937-1955, 2011
67. Hageman GS, Anderson DH, Johnson LV, et al.: A common haplotype in the complement regulatory gene factor H (HF1/CFH) predisposes individuals to age-related macular degeneration. *Proc Natl Acad Sci U S A* 102:7227-7232, 2005
68. Haines JL, Hauser MA, Schmidt S, et al.: Complement factor H variant increases the risk of age-related macular degeneration. *Science* 308:419-421, 2005
69. Harder MJ, Anliker M, Hochsmann B, et al.: Comparative analysis of novel complement-targeted inhibitors, MiniFH, and the natural regulators factor H and factor H-like protein 1 reveal functional determinants of complement regulation. *J Immunol* 196:866-876, 2016
70. Hasima N, Aggarwal BB: Targeting proteasomal pathways by dietary curcumin for cancer prevention and treatment. *Curr Med Chem* 21:1583-1594, 2014
71. Hayashi T, Faustman D: NOD mice are defective in proteasome production and activation of NF-kappa B. *Mol Cell Biol* 19:8646-8659, 1999
72. Hollborn M, Chen R, Wiedemann P, et al.: Cytotoxic effects of curcumin in human retinal pigment epithelial cells. *PLoS One* 8, 2013
73. Holz FG, Schmitz-Valckenberg S, Fleckenstein M: Recent developments in the treatment of age-related macular degeneration. *J Clin Invest* 124:1430-1438, 2014
74. Howell JC, Chun E, Farrell AN, et al.: Global microRNA expression profiling: Curcumin (diferuloylmethane) alters oxidative stress-responsive microRNAs in human ARPE-19

- cells. *Mol Vis* 19:544-560, 2013
75. Hussong SA, Kapphahn RJ, Phillips SL, et al.: Immunoproteasome deficiency alters retinal proteasome's response to stress. *J Neurochem* 113:1481-1490, 2010
  76. Hussong SA, Rochrich H, Kapphahn RJ, et al.: A novel role for the immunoproteasome in retinal function. *Invest Ophthalmol Vis Sci* 52:714-723, 2011
  77. Iuvone PM, Brown AD, Haque R, et al.: Retinal melatonin production: role of proteasomal proteolysis in circadian and photic control of arylalkylamine N-acetyltransferase. *Invest Ophthalmol Vis Sci* 43:564-572, 2002
  78. Jaffer FA, Weissleder R: Molecular imaging in the clinical arena. *JAMA* 293:855-862, 2005
  79. Johnson LV, Leitner WP, Staples MK, Anderson DH: Complement activation and inflammatory processes in drusen formation and age related macular degeneration. *Exp Eye Res* 73:887-896, 2001
  80. Kaarniranta K: Techniques for studying mechanisms of autophagy in RPE cells. *Acta Ophthalmol* 91, 2013
  81. Kaarniranta K, Sinha D, Blasiak J, et al.: Autophagy and heterophagy dysregulation leads to retinal pigment epithelium dysfunction and development of age-related macular degeneration. *Autophagy* 9:973-984, 2013
  82. Kapphahn RJ, Bigelow EJ, Ferrington DA: Age-dependent inhibition of proteasome chymotrypsin-like activity in the retina. *Exp Eye Res* 84:646-654, 2007
  83. Kapphahn RJ, Giwa BM, Berg KM, et al.: Retinal proteins modified by 4-hydroxynonenal: Identification of molecular targets. *Exp Eye Res* 83:165-175, 2006
  84. Keck S, Nitsch R, Grune T, Ullrich O: Proteasome inhibition by paired helical filament-tau in brains of patients with Alzheimer's disease. *J Neurochem* 85:115-122, 2003
  85. Khan JC, Shahid H, Thurlby DA, et al.: Age related macular degeneration and sun exposure, iris colour, and skin sensitivity to sunlight. *Br J Ophthalmol* 90:29-32, 2006
  86. Khanobdee K, Wongprasert K, Kitiyanant Y: In vitro protection against hydrogen peroxide-induced oxidative stress and cell death in ARPE-19 cells by curcumin. *Planta Med* 76:1242-1242, 2010
  87. Kim JY, Zhao H, Martinez J, et al.: Noncanonical autophagy promotes the visual cycle. *Cell* 155:725-726, 2013
  88. Klein BE, Howard KP, Iyengar SK, et al.: Sunlight exposure, pigmentation, and incident age-related macular degeneration. *Invest Ophthalmol Vis Sci* 55:5855-5861, 2014
  89. Klein RJ, Zeiss C, Chew EY, et al.: Complement factor H polymorphism in age-related macular degeneration. *Science* 308:385-389, 2005
  90. Krestin GP, Bernsen MR: Molecular imaging in radiology: the latest fad or the new frontier? *Eur Radiol* 16:2383-2385, 2006
  91. Lamb LE, Simon JD: A2E: A component of ocular lipofuscin. *Photochem Photobiol* 79:127-136, 2004
  92. Landis-Piwowar KR: Proteasome inhibitors in cancer therapy: a novel approach to a ubiquitous problem. *Clin Lab Sci* 25:38-44, 2012
  93. Li J, Gao XL, Ortega JQ, et al.: Lysine 188 substitutions convert the pattern of proteasome activation by REG gamma to that of REGs alpha and beta. *EMBO J* 20:3359-3369, 2001
  94. Li J, Wang PP, Zhu YX, et al.: Curcumin inhibits neuronal loss in the retina and elevates Ca<sup>2+</sup>/calmodulin-dependent protein kinase II activity in diabetic rats. *J Ocul Pharmacol Th* 31:555-562, 2015
  95. Li Y, Wang YS, Shen XF, et al.: Alterations of activity and intracellular distribution of the 20S proteasome in ageing retinal pigment epithelial cells. *Exp Gerontol* 43:1114-1122, 2008
  96. Li Y, Zou X, Cao K, et al.: Curcumin analog 1, 5-bis (2-trifluoromethylphenyl)-1, 4-pentadien-3-one exhibits enhanced ability on Nrf2 activation and protection against acrolein-induced ARPE-19 cell toxicity. *Toxicol Appl Pharm* 272:726-735, 2013
  97. Lim LS, Mitchell P, Seddon JM, et al.: Age-related macular degeneration. *Lancet* 379:1728-1738, 2012
  98. Louie JL, Kapphahn RJ, Ferrington DA: Proteasome function and protein oxidation in the aged retina. *Exp Eye Res* 75:271-284, 2002
  99. Ma CP, Slaughter CA, DeMartino GN: Identification, purification, and characterization of a protein activator (PA28) of the 20 S proteasome (macropain). *J Biol Chem* 267:10515-10523, 1992
  100. Maldonado M, Kapphahn RJ, Terluk MR, et al.: Immunoproteasome deficiency modifies the alternative pathway of NF kappa B signaling. *PLoS One* 8, 2013
  101. Mares-Perlman JA, Brady WE, Klein R, et al.: Serum antioxidants and age-related macular degeneration in a population-based case-control study. *Arch Ophthalmol* 113:1518-1523, 1995
  102. Mattson MP: Dietary factors, hormesis and health. *Ageing Res Rev* 7:43-48, 2008
  103. Mattson MP, Cheng AW: Neurohormetic phytochemicals: low-dose toxins that induce adaptive neuronal stress responses. *Trends Neurosci* 29:632-639, 2006
  104. Moritz K, Burnett B: Alterations of proteasome dynamics following traumatic brain injury. *J Neurotraum* 32:A92-A92, 2015
  105. Mujtaba T, Kanwar J, Wan SB, et al.: Sensitizing human multiple myeloma cells to the proteasome inhibitor bortezomib by novel curcumin analogs. *Int J Mol Med* 29:102-106, 2012
  106. Mullins RF, Russell SR, Anderson DH, Hageman GS: Drusen associated with aging and age-related macular degeneration contain proteins common to extracellular deposits associated with atherosclerosis, elastosis, amyloidosis, and dense deposit disease. *FASEB J* 14:835-846, 2000
  107. Nagai N, Klimava A, Lee WH, et al.: CTGF is increased in basal deposits and regulates matrix production through the ERK (p42/p44(mapk)) MAPK and the p38 MAPK signaling pathways. *Invest Ophthalmol Vis Sci* 50:1903-1910, 2009
  108. Naksuriya O, Okonogi S, Schifflers RM, Hennink WE: Curcumin nanoformulations: A review of pharmaceutical properties and preclinical studies and clinical data related to cancer treatment. *Biomaterials* 35:3365-3383, 2014
  109. Noris M, Remuzzi G: Overview of complement activation and regulation. *Semin Nephrol* 33:479-492, 2013
  110. Parekh N, Voland RP, Moeller SM, et al.: Association between dietary fat intake and age-related macular degeneration in the carotenoids in Age-Related Eye Disease Study (CAREDS): an ancillary study of the Women's Health Initiative. *Arch Ophthalmol* 127:1483-1493, 2009
  111. Prasad S, Tyagi AK, Aggarwal BB: Recent developments in delivery, bioavailability, absorption and metabolism of curcumin: the golden pigment from golden spice. *Cancer Res Treat* 46:2-18, 2014
  112. Premanand C, Rema M, Sameer MZ, et al.: Effect of curcumin on proliferation of human retinal endothelial cells under in vitro

- conditions. *Invest Ophthalmol Vis Sci* 47:2179-2184, 2006
113. A prize for protein degradation. *Nat Cell Biol* 6:1011, 2004
  114. Realini C, Jensen CC, Zhang ZG, et al.: Characterization of recombinant REG alpha, REG beta, and REG gamma proteasome activators. *J Biol Chem* 272:25483-25492, 1997
  115. Rechsteiner M, Hill CP: Mobilizing the proteolytic machine: cell biological roles of proteasome activators and inhibitors. *Trends Cell Biol* 15:27-33, 2005
  116. Rein DB, Wittenborn JS, Zhang X, et al.: Forecasting age-related macular degeneration through the year 2050: the potential impact of new treatments. *Arch Ophthalmol* 127:533-540, 2009
  117. Ren XY, Li J, Xu XX, et al.: IBI302, a promising candidate for AMD treatment, targeting both the VEGF and complement system with high binding affinity in vitro and effective targeting of the ocular tissue in healthy rhesus monkeys. *Exp Eye Res* 145:352-358, 2016
  118. Ricklin D, Hajishengallis G, Yang K, Lambris JD: Complement: a key system for immune surveillance and homeostasis. *Nat Immunol* 11:785-797, 2010
  119. Ritz MF, Grond-Ginsbach C, Fluri F, et al.: Cerebral small vessel disease is associated with dysregulation in the ubiquitin proteasome system and other major cellular pathways in specific brain regions. *Neurodegener Dis* 17:261-275, 2017
  120. Rivera-Espinoza Y, Muriel P: Pharmacological actions of curcumin in liver diseases or damage. *Liver Int* 29:1457-1466, 2009
  121. Rock KL, Gramm C, Rothstein L, et al.: Inhibitors of the proteasome block the degradation of most cell-proteins and the generation of peptides presented on MHC class-I molecules. *Cell* 78:761-771, 1994
  122. Ryhanen T, Hyttinen JMT, Kopitz J, et al.: Crosstalk between Hsp70 molecular chaperone, lysosomes and proteasomes in autophagy-mediated proteolysis in human retinal pigment epithelial cells. *J Cell Mol Med* 13:3616-3631, 2009
  123. Saibil H: Chaperone machines for protein folding, unfolding and disaggregation. *Nat Rev Mol Cell Bio* 14:630-642, 2013
  124. Saibil H: Chaperone machines for protein folding, unfolding and disaggregation. *Nat Rev Mol Cell Bio* 14:630-642, 2013
  125. Salazar I, Caldeira M, Duarte C: Interplay between the ubiquitin-proteasome system and calpains in brain ischemia. *J Neurochem* 142:181-181, 2017
  126. Salem M, Rohani S, Gillies ER: Curcumin, a promising anti-cancer therapeutic: a review of its chemical properties, bioactivity and approaches to cancer cell delivery. *Rsc Adv* 4:10815-10829, 2014
  127. Schlingemann RO: Role of growth factors and the wound healing response in age-related macular degeneration. *Graef Arch Clin Exp* 242:91-101, 2004
  128. Schuld NJ, Hussong SA, Kapphahn RJ, et al.: Immunoproteasome deficiency protects in the retina after optic nerve crush. *PLoS One* 10:e0126768, 2015
  129. Scott PA, Kaplan HJ, McCall MA: Prenatal exposure to curcumin protects rod photoreceptors in a transgenic Pro23His swine model of retinitis pigmentosa. *Transl Vis Sci Techn* 4, 2015
  130. Seddon JM, Cote J, Rosner B: Progression of age-related macular degeneration: association with dietary fat, transunsaturated fat, nuts, and fish intake. *Arch Ophthalmol* 121:1728-1737, 2003
  131. Seddon JM, Willett WC, Speizer FE, Hankinson SE: A prospective study of cigarette smoking and age-related macular degeneration in women. *JAMA* 276:1141-1146, 1996
  132. Seemuller E, Lupas A, Zuhl F, et al.: The proteasome from *Thermoplasma acidophilum* is neither a cysteine nor a serine protease. *FEBS Lett* 359:173-178, 1995
  133. Smith W, Mitchell P, Leeder SR: Dietary fat and fish intake and age-related maculopathy. *Arch Ophthalmol* 118:401-404, 2000
  134. Spaide RF, Curcio CA: Drusen characterization with multimodal imaging. *Retina* 30:1441-1454, 2010
  135. Strauss O: The retinal pigment epithelium in visual function. *Physiol Rev* 85:845-881, 2005
  136. Sun Y, You ZP: Curcumin inhibits human retinal pigment epithelial cell proliferation. *Int J Mol Med* 34:1013-1019, 2014
  137. Sundelin S, Wihlmark U, Nilsson SEG, Brunk UT: Lipofuscin accumulation in cultured retinal pigment epithelial cells reduces their phagocytic capacity. *Curr Eye Res* 17:851-857, 1998
  138. Thakur M, Lentle BC: Report of a summit on molecular imaging. *Radiology* 236:753-755, 2005
  139. Tomany SC, Wang JJ, Van Leeuwen R, et al.: Risk factors for incident age-related macular degeneration: pooled findings from 3 continents. *Ophthalmology* 111:1280-1287, 2004
  140. Unno M, Mizushima T, Morimoto Y, et al.: The structure of the mammalian 20S proteasome at 2.75 angstrom resolution. *Structure* 10:609-618, 2002
  141. Ustrell V, Pratt G, Rechsteiner M: Effects of interferon-gamma and major histocompatibility complex-encoded subunits on peptidase activities of human multicatalytic proteases. *Proc Natl Acad Sci U S A* 92:7605-7605, 1995
  142. Vallianou NG, Evangelopoulos A, Schizas N, Kazazis C: Potential anticancer properties and mechanisms of action of curcumin. *Anticancer Res* 35:645-651, 2015
  143. van Hees HWH, Li YP, Ottenheijm CAC, et al.: Proteasome inhibition improves diaphragm function in congestive heart failure rats. *Am J Physiol-Lung C* 294:L1260-L1268, 2008
  144. Vasireddy V, Chavali VRM, Joseph VT, et al.: Rescue of photoreceptor degeneration by curcumin in transgenic rats with P23H rhodopsin mutation. *PLoS One* 6, 2011
  145. Viiri J, Amadio M, Marchesi N, et al.: Autophagy activation clears ELAVL1/HuR-mediated accumulation of SQSTM1/p62 during proteasomal inhibition in human retinal pigment epithelial Cells. *PLoS One* 8, 2013
  146. Viiri J, Hyttinen JMT, Ryhanen T, et al.: p62/sequestosome 1 as a regulator of proteasome inhibitor-induced autophagy in human retinal pigment epithelial cells. *Molecular Vision* 16:1399-1414, 2010
  147. Voorhees PM, Orlowski RZ: The proteasome and proteasome inhibitors in cancer therapy. *Annu Rev Pharmacol Toxicol* 46:189-213, 2006
  148. Vyas A, Dandawate P, Padhye S, et al.: Perspectives on new synthetic curcumin analogs and their potential anticancer properties. *Curr Pharm Design* 19:2047-2069, 2013
  149. Wagner E, Frank MM: Therapeutic potential of complement modulation. *Nat Rev Drug Discov* 9:43-56, 2010
  150. Wang LL, Li CZ, Guo H, et al.: Curcumin inhibits neuronal and vascular degeneration in retina after ischemia and reperfusion injury. *PLoS One* 6, 2011
  151. Wang YH, Yin ZY, Gao LX, et al.: Curcumin delays retinal degeneration by regulating microglia activation in the retina of rd1 mice. *Cell Physiol Biochem* 44:479-493, 2017
  152. Wayne D, Lawler K, Bedford L, et al.: Does the activity of the proteasome decline during human ageing and in the brains of Parkinsons disease patients? *Acta Physiol* 221:60-60, 2017
  153. Whitby FG, Masters EI, Kramer L, et al.: Structural basis for the activation of 20S proteasomes by 11S regulators. *Nature*

408:115-120, 2000

154. Wolkow N, Song Y, Wu TD, et al.: Aceruloplasminemia retinal histopathologic manifestations and iron-mediated melanosome degradation. *Arch Ophthalmol* 129:1466-1474, 2011
155. Yehoshua Z, Garcia CAA, Nunes RP, et al.: Systemic complement inhibition with eculizumab for geographic atrophy in age-related macular degeneration. *Ophthalmology* 121:693-701, 2014
156. Zaky W, Manton C, Miller CP, et al.: The ubiquitin-proteasome pathway in adult and pediatric brain tumors: biological insights and therapeutic opportunities. *Cancer Metast Rev* 36:617-633, 2017
157. Zarbin MA: Current concepts in the pathogenesis of age-related macular degeneration. *Arch Ophthalmol* 122:598-614, 2004
158. Zhang HJ, Xing YQ, Jin W, et al.: Effects of curcumin on interleukin-23 and interleukin-17 expression in rat retina after retinal ischemia-reperfusion injury. *Int J Clin Exp Pathol* 8:9223-9231, 2015
159. Zhang XY, Zhou JL, Fernandes AF, et al.: The proteasome: a target of oxidative damage in cultured human retina pigment epithelial cells. *Invest Ophthalmol Vis Sci* 49:3622-3630, 2008
160. Zheng QY, Huang T, Zhang LS, et al.: Dysregulation of ubiquitin-proteasome system in neurodegenerative diseases. *Front Aging Neurosci* 8, 2016

2

# Aims of the thesis

The primary aims of this thesis are the assessment of molecular mechanisms of complement-mediated proteasome regulation, the role of the proteasome in retinal pigment epithelium (RPE) fibrosis and proteasomal pharmacological modulation. Secondly, we assess the effects of a complement-modulating drug in the retina and describe the development of a multispectral imaging device that potentially allows the visualization of molecular processes in vivo.

In **Chapter 3**, we investigate whether the complement pathway is involved in modulation of proteasome activity and expression in RPE cells. Proteasome and immunoproteasome expression is first characterized in a mouse model of age-related RPE degeneration (monocyte chemoattractant protein-1-deficient CCL2<sup>-/-</sup> mouse). Subsequently, we assess the effects of complement activation by means of the complement anaphylatoxins C3a and C5a in human donor RPE cells.

In **Chapter 4**, we investigate the role of the proteasome in the expression of extracellular matrix genes and whether pharmacological inhibition of the proteasome downregulates transcription of extracellular matrix genes. Human RPE cells (ARPE-19) are stimulated with two of the main fibrogenic factors in the retina, transforming growth factor- $\beta$  (TGF $\beta$ ) and connective tissue growth factor (CTGF) and epoxomicin, an irreversible inhibitor of the proteasome. We then proceed to assess their effects on the expression of known retinal fibrogenic factors such as fibronectin (FN), fibronectin EDA domain (FN EDA), metalloproteinase-2 (MMP-2), tissue inhibitor of metalloproteinases-1 (TIMP-1) and peroxisome proliferator-associated receptor- $\gamma$  (PPAR $\gamma$ ).

In **Chapter 5**, we explore the potential proteasome-modulating effects of standard curcumin and nano-curcumin, which is a highly bioavailable form of curcumin dispersed with colloidal nanoparticles. Preliminary cytotoxicity studies are conducted in order to evaluate the safety of in vitro treatment of RPE cells (ARPE-19) with these drugs. We then characterize and compare the effects of both curcuminoid formulations with regards to proteasome gene transcription, protein transcription and proteolytic activity.

In **Chapter 6**, we describe the use of eculizumab, a monoclonal antibody directed against the complement protein C5 in one patient with Purtscher-like retinopathy. Eculizumab arrests the cleavage of C5 and halts the process of complement-mediated cell lysis. This antibody has already been approved in the treatment of life-threatening diseases that are characterized by dysregulated complement activation, namely atypical hemolytic uremic syndrome and paroxysmal nocturnal hemoglobinuria. Purtscher-like

retinopathy is used as a model of a retinal disorder primarily mediated by complement activation. Based on our findings, we review the molecular mechanisms of Purtscher-like retinopathy, highlighting the differences with the role of the complement pathway in age-related macular degeneration.

In previous experiments, we assessed the expression of the proteasome and its inducible counterpart, the immunoproteasome, in *CCL2<sup>-/-</sup>* mice.

In **Chapter 7**, we describe the development of a retinal spectral imaging device that is constructed to serve as an imaging tool for ophthalmic molecular imaging. The unavailability of approved proteasome-labeling agents and the poor spectral properties of nano-curcumin hindered our initial aim of visualizing living proteasomes and nano-curcumin in the retina. Instead, as a proof of concept, we used an intrinsic chromophore, hemoglobin, to exemplify the clinical applicability of the retinal spectral imaging device.

In **Chapter 8**, we review the most recent advances in the field of ophthalmic molecular imaging.

3

# Complement factor C3a alters proteasome function in human RPE cells and in an animal model of age-related RPE degeneration

J. Emanuel Ramos de Carvalho<sup>a</sup>, Ingeborg Klaassen<sup>a</sup>,  
Ilse M.C. Vogels<sup>a</sup>, Sabine Schipper-Krom<sup>b</sup>, Cornelis J.F.  
Van Noorden<sup>a,b</sup>, Eric A. Reits<sup>b</sup>, Theo G. Gorgels<sup>c</sup>, Arthur  
A. Bergen<sup>c</sup>, Reinier O. Schlingemann<sup>a</sup>

<sup>a</sup> Ocular Angiogenesis Group, Departments of  
Ophthalmology and Medical Biology, Academic  
Medical Center, University of Amsterdam, Amsterdam,  
The Netherlands <sup>b</sup> Department of Medical Biology,  
Academic Medical Center, University of Amsterdam,  
Amsterdam, The Netherlands <sup>c</sup> Netherlands Institute  
for Neuroscience (NIN), Royal Academy of Sciences  
(KNAW), Amsterdam, The Netherlands

Investigative Ophthalmology and Visual Science 54(10):6489-6501, 2013  
doi: 10.1167/iovs.13-12374

## Abstract

Complement activation plays an unequivocal role in the pathogenesis of age-related macular degeneration (AMD). More recent evidence suggests an additional role in AMD for the ubiquitin proteasome system (UPS), a protein-degradation nanomachinery present in all types of eukaryotic cells. The purpose of this study was to elaborate on these findings and investigate whether the complement system directly contributes to derangements in the UPS through the activated complement components C3a and C5a. In the retinal pigment epithelial cells (RPE) of monocyte chemoattractant protein-1-deficient  $CCL2^{-/-}$  mice, a mouse model that may serve as a model for age-related atrophic degeneration of the RPE, proteasome function was investigated by immunohistochemistry of household ( $\beta 5$ ) and immuno ( $\beta 5i$ ) subunit expression. Subsequently, proteasome overall activity was determined using the BodipyFl-Ahx<sub>3</sub>L<sub>3</sub>VS probe in primary-cultured human retinal pigment epithelial cells (HRPE) cells that were exposed to different stimuli including C3a and C5a, using confocal laser scanning microscopy and flow cytometry. Gene expression and protein levels of proteasome subunits  $\alpha 7$ , PA28 $\alpha$ ,  $\beta 5$ , and  $\beta 5i$  were also studied in RPE cells after exposure to interferon- $\gamma$  (IFN $\gamma$ ), C3a, and C5a by real-time PCR and Western blotting.

Retinal pigment epithelial cells of  $CCL2^{-/-}$  mice showed immunoproteasome upregulation. C3a, but not C5a supplementation, induced decreased proteasome overall activity in HRPE cells, whereas mRNA and protein levels of household proteasome and immunoproteasome subunits were unaffected.

In HRPE cells, C3a induces decreased proteasome-mediated proteolytic activity, whereas in a mouse model of age-related RPE atrophy, the immunoproteasome was upregulated, indicating a possible role for complement-driven posttranslational alterations in proteasome activity in the cascade of pathologic events that result in AMD.

## Introduction

Age-related macular degeneration (AMD) is the leading cause of irreversible blindness among the elderly worldwide.<sup>3; 36</sup> Abnormal complement pathway regulation and retinal pigment epithelium (RPE) cell dysfunction have both been implicated in the early pathogenesis of the disease,<sup>5; 16; 45</sup> and specifically in the formation of drusen.<sup>2; 25</sup> Approximately 70% of AMD patients are homo- or heterozygous for a specific polymorphism of the gene encoding for the endogenous complement pathway regulator Factor H (CFH), with additional contributions of polymorphisms in the genes encoding for Factors B, C2, and C3.<sup>35; 51; 62; 63</sup> The single nucleotide change (1277 T→C, rs1061170) in the CFH gene results in the substitution of histidine for tyrosine at codon 402 of the CFH protein, which subsequently leads to a more than 2-fold increase in risk of AMD in CT heterozygotes (carriers of one single copy of the C allele) and a 3- to 6-fold increase in individuals homozygous for the CC genotype compared with the TT genotype.<sup>18; 24; 27; 47; 71</sup> This results in a prolonged state of complement activation, which results in the assembly of the C5b-C9 membrane attack complex and cell lysis, concurrently with liberation of C3a and C5a, two small pro-inflammatory peptide fragments. Most of the complement pathway proteins are present in Bruch's membrane, drusen, and RPE of AMD patients.<sup>11; 26; 37; 38; 54; 56</sup> Although the involvement of the complement pathway in the pathogenesis of AMD has unambiguously been established, it is not exactly known how a chronically overactive complement system triggers the development of AMD.<sup>31</sup> Nonlysosomal proteolysis is essential for cell survival. In eukaryotic cells, the ubiquitin-proteasome system (UPS) is the major nonlysosomal proteolytic pathway.<sup>55</sup> Most cytoplasmic and nuclear proteins become ubiquitinated in order to target these proteins for degradation. Once ubiquitinated, these proteins are recognized by the 19S regulatory particle that together with the 20S catalytic core forms the 26S proteasome. Upon de-ubiquitination and unfolding, the protein enters the cylinder-shaped 20S core particle, which is formed by stacked catalytic subunits that possess hydrolytic activity for the cleavage of the carboxyl end of proteins. There are three catalytic subunits in the standard proteasome:  $\beta 1$  for acidic amino acids,  $\beta 2$  for basic amino acids, and  $\beta 5$  for hydrophobic amino acids. The immunoproteasome is formed upon replacement of the constitutive subunits in the standard proteasome by the inducible subunits, the so-called  $\beta 1i$ ,  $\beta 2i$ , and  $\beta 5i$ .<sup>12; 46</sup> The immunoproteasome is involved in specific, biological processes including generation of immunogenic peptides for antigen presentation,<sup>22; 59</sup> degradation of oxidized proteins,<sup>15</sup> cell signaling,<sup>2; 28; 29</sup> neuronal maintenance, and synaptic vesicle formation.<sup>20</sup> Therefore, the ratio between proteasomes containing the standard catalytical subunits ( $\beta 1$ ,  $\beta 2$ , and  $\beta 5$ ) or the corresponding inducible subunits ( $\beta 1i$ ,  $\beta 2i$ , and  $\beta 5i$ ) can change during inflammation and other stressful situations. Retinal pigment epithelial (RPE) cells have an active UPS, but relatively limited levels of endogenous ubiquitin, which render these cells more vulnerable to cellular stressors.<sup>72</sup> Abnormalities in the UPS have been implied in the pathogenesis of many ageing diseases, such as Alzheimer's disease,<sup>32</sup> Parkinson's disease,<sup>13</sup> and cataract.<sup>17; 34; 61</sup> The aim of the

present study was to investigate the involvement of the proteasome in AMD in relation to complement overactivation. The chymotrypsin-like activity ( $\beta 5$ ) of the proteasome appears to be the rate-limiting activity of the proteasome,<sup>10; 49</sup> and it has been shown that ageing affects its functioning in the retina.<sup>39</sup> For this reason,  $\beta 5$  proteasome subunit and its immunoproteasome counterpart  $\beta 5i$  were characterized both in cell cultures of complement-activated human retinal pigment epithelial cells (HRPE) and in a mouse model for age-related atrophic degeneration of the RPE.

## **Materials and methods**

### **Immunohistochemistry**

To characterize  $\beta 5$  and  $\beta 5i$  proteasome subunit expression in the RPE of AMD tissue, whole retinal sections (2- $\mu$ m thick) of 500 day-old monocyte chemoattractant protein-1-deficient *CCL2*<sup>-/-</sup> mice ( $n = 3$ ) and wild-type mice ( $n = 3$ ) were stained with mouse antibodies against the  $\beta 5$  and  $\beta 5i$  subunits of the 20S proteasome and the  $\beta 5i$  subunit of the 20S proteasome (Abcam, Cambridge, UK) and visualized by immunofluorescence. *CCL2*<sup>-/-</sup> mice were obtained from The Jackson Laboratory (B6.129S4-*Ccl2*<sup>tm1Roi</sup>/J, stock no. 004434; Bar Harbor, ME), and these do not contain the rd8 mutation.<sup>52</sup> All the animals were treated according to the ARVO Statement for the Use of Animals in Ophthalmic and Vision Research. Briefly, sections were fixed in 2% paraformaldehyde (Electron Microscopy Sciences, Hatfield, PA, USA), equilibrated, and rinsed in 1% PBS four times for 5 minutes, blocked in 10% normal goat serum (Invitrogen, Breda, The Netherlands) for 30 minutes, again rinsed in 1% PBS three times for 5 minutes. Then, sections were incubated in the presence of the primary antibodies for 1 hour at room temperature in a dilution of 1:500 followed by rinsing in PBS and incubation with appropriate secondary goat anti-mouse antibodies, conjugated with Cy3 in a dilution of 1:500 (Jackson, Suffolk, UK), and rinsed in PBS. Sudan Black B staining was performed by incubating sections in a freshly prepared solution of 1% Sudan Black B (Fisher Biotech, Pittsburgh, PA, USA) diluted in 70% ethanol for 10 minutes, followed by brief rinsing in 70% ethanol, and rinsing in distilled water. As controls, whole retinal sections with no antibody treatment nor Sudan Black B staining, as well as whole retinal sections with only Sudan Black B staining were used. Sections were counterstained with 4'-6-diamidino-2-phenylindole (DAPI; Vector, Burlingame, CA, USA).

### **Culture, maintenance and treatment of HRPE cells**

Donor eyes were obtained from the Euro Cornea Bank (Beverwijk, The Netherlands) after removal of corneal buttons for transplantation. Donor eyes were acquired with

consent of the donor or donor family to be used for medical research in accordance with the principles outlined in the Declaration of Helsinki. Characterization of the donors is summarized in Table 1.

Donor	Age	Sex	Postmortem time (h)	Primary Cause of Death
1	13	M	13	Trauma
2	23	M	15	Trauma
3	34	M	13	Trauma
4	37	M	16	Cardiac—endocarditis aorta
5	42	M	14	Respiratory—pulmonary embolism
6	47	F	10	Heart failure
7	49	M	18	Cardiac—heart failure
8	55	M	14	Cardiac—heart failure
9	57	F	10	Malignancy—unknown
10	61	M	7	Respiratory—pulmonary embolism
11	62	M	16	Cardiac—heart failure
12	64	F	9	Malignancy—glioblastoma multiforme
13	65	M	12	Respiratory—respiratory insufficiency
14	68	M	15	Multiorgan failure
15	70	F	5	Respiratory—respiratory insufficiency
16	72	M	6	Malignancy—hepatocarcinoma
17	76	M	8	Heart failure

**Table 1.** Characterization of the HRPE donors.

For isolation of the HRPE, donor eyes with a post mortem time of less than 15 hours (average postmortem time, 12 hours) were obtained from 17 donors between 13 and 76 years of age. The RPE was isolated from the sclera together with the choroid after dissection of the anterior and posterior segment of the eye. The tissue was subsequently incubated for 1 hour at 37°C in a 6-well plate with 2 mL digestion medium (TrypLE Express; Invitrogen). The RPE and choroid were separated after adding 2.5 mL of F99 medium to the digestion mixture and transferring the tissue to an empty well containing 2.5 mL of F99 medium. Medium containing the RPE cells was then transferred to a cell strainer with 70- $\mu$ m meshes and centrifuged for 10 minutes (400g, 1000 rpm). Supernatant was collected and diluted in 12 mL F99 medium. A suspension of cells in 1 mL F99 medium was transferred to a gelatin-coated 6-well plate.

Growth of cells was monitored and medium was changed every 2 days. After 8 days, the confluent cells were washed with PBS and 0.5 mL TrypLE Express, and 1 mL F99 medium was added. The contents of three wells were then transferred to a fibronectin-coated 75-cm<sup>2</sup> flask, which renders four flasks for passage 1 for each pair of eyes. The medium was replaced by human endothelial serum-free medium upon confluence. In passages 2 through 4, cells were used for experiments upon attaining 100% confluence. The cultured RPE cells exhibited an epithelial cell shape and contained

pigment granules in the perinuclear region. The expression of RPE-specific marker genes CRALBP, RPE65, and FGFR2as determined by RT-PCR analysis indicated the identity and high differentiation state of the cells as well. When cells were cultured on transwell inserts, a transepithelial resistance was obtained between 36 and 64  $\Omega$ -cm<sup>2</sup>. Proper polarization of HRPE cells was verified by a positive staining of ZO-1 and occludin protein (Fig. 1).

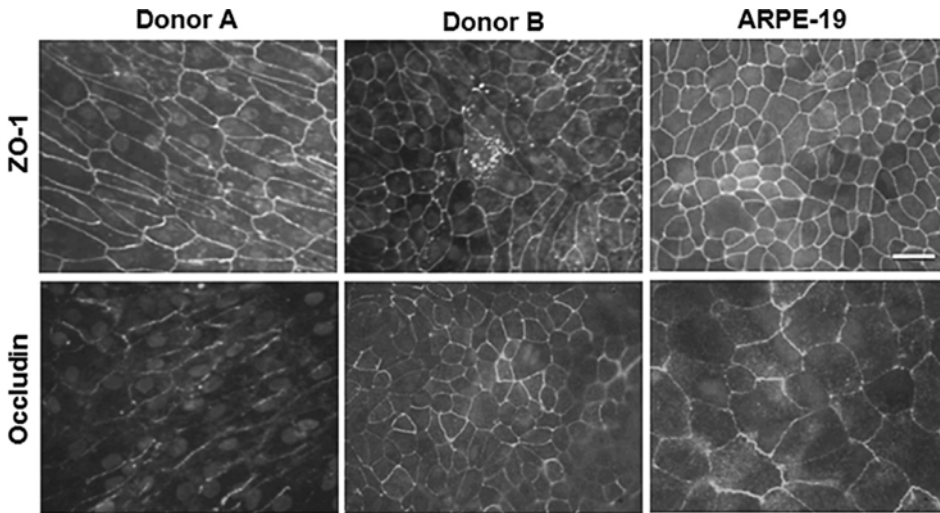


**Fig. 1.** Characterization of HRPE cells by immunofluorescence microscopy with antibodies against tight junction protein ZO-1 and occludin. Human donor RPE cells give positive immunostaining for ZO-1 and occludin, which is comparable to staining in the immortalized RPE cell line ARPE-19. Donors A and B are two representative examples. Scale bar: 50  $\mu$ m.

To investigate the effect of complement factors, inflammation, and oxidative stress, RPE cells were stimulated with C3a (50 ng/mL or 100 ng/mL; R&D Systems, Minneapolis, MN), C5a (50 ng/mL; R&D Systems), IFN $\gamma$  (50 U/mL; PBL Biomedical, Piscataway, NJ; and U-CyTech Biosciences, Utrecht, The Netherlands) in serum-free medium for 72 hours.

### Genotyping

Ten donors were genotyped for the CFH Y402H polymorphism (1277 T $\rightarrow$ C, rs1061170) in 2 ng genomic DNA extracted from RPE cells using a standard Taqman assay (Table 2).<sup>14</sup>

Genotype assessment for CFH Y402H polymorphism in the 10 donors used for protein

analysis showed six C allele carriers, of which three had the CC genotype, three the CT genotype, and four the TT genotype (Table 2).

Donor	Genotype
2	CT
4	TT
3	CT
6	TT
7	TT
8	CC
13	TT
14	CC
16	CC
17	CT

**Table 2.** Screening for polymorphisms in complement factor-H (CFH Y402H) in donors used for protein analysis.

### **Preparation of photoreceptor rod outer segments**

Photoreceptor outer segments (POS) were added to cultured HRPE cells to mimic the situation in vivo where RPE continually phagocytoses POS. Photoreceptor outer segments were isolated from bovine eyes obtained freshly from the slaughterhouse.<sup>53:</sup> <sup>57</sup> Photoreceptor outer segments were stored suspended in a solution of 10 mM sodium phosphate (pH 7.2), 0.1 M sodium chloride, and 2.5% sucrose at  $-80^{\circ}\text{C}$ . Before use, POS were thawed and labeled by addition of 20% volume of 1 mg/mL FITC (Molecular Probes, Invitrogen, Carlsbad, CA, USA) in 0.1 M sodium bicarbonate (pH 9.0), for 1 hour at room temperature in the dark. Photoreceptor outer segments were then washed and resuspended in cell culture media.

### **Proteasome activity measurements by flow cytometry of HRPE cells**

Proteasome activity was determined using the probe BodipyFl-Ahx<sub>3</sub>L<sub>3</sub>VS (provided by Hermen Overkleeft),<sup>66</sup> which has a similar affinity for all catalytically active subunits of proteasomes in living cells. This probe has a green emission spectrum ( $\lambda_{\text{ex}} = 480 \text{ nm}$ ,  $\lambda_{\text{em}} = 530 \text{ nm}$ ) and can be used for both flow cytometry (FACS) experiments and confocal laser scanning microscopy (CLSM).<sup>4; 66</sup>

The following cell culture samples were tested for proteasome activity by means of FACS: unstimulated HRPE, POS-fed RPE, C3a-stimulated HRPE, C3a-stimulated POS-fed

HRPE, IFN $\gamma$ -stimulated HRPE, and HRPE with and without C3a stimulation treated for 1 hour with 500 nM of the proteasome inhibitor epoxomicin (Ep; Sigma-Aldrich, St. Louis, MO). In total, seven human donors were used and divided in a “young age” group (n = 3; 13, 23, and 37 years old) and an “old age” group (n = 4; 47, 55, 57, and 65 years old).

Flow cytometry experiments were performed on a FACS LSRII (Becton Dickinson, Breda, The Netherlands). For uptake experiments, untreated cells, and C3a-treated cells were incubated with 500 nM BodipyFl-Ahx<sub>3</sub>L<sub>3</sub>VS for 2 hours. The treated cells were stimulated with 50 ng/mL recombinant human C3a. Cells were washed, trypsinized, and resuspended in medium, and intracellular fluorescence was measured. As a negative control, cells were incubated with 500 nM Ep overnight. Unstained HRPE cells were used to normalize the signal. Two or three parallel wells were used for each experimental condition. Approximately 10,000 of unfixed RPE cells were used for the experiments and a live gate was used to exclude cell fragments, POS particles, and other unwanted debris. The background fluorescence of the system, as assayed without any cells, was subtracted. A logarithmic scale of relative fluorescent intensity was used and signal intensity was calculated by subtracting the geometric mean autofluorescence of control cells from the geometric mean fluorescence of cells incubated with BodipyFl-Ahx<sub>3</sub>L<sub>3</sub>VS.

### **Confocal laser scanning microscopy**

To visualize active proteasomes in HRPE cells using a TCS SP2 CLSM (Leica, Rijswijk, The Netherlands), the following cell culture samples were incubated with BodipyFl-Ahx<sub>3</sub>L<sub>3</sub>VS: unstimulated HRPE, C3a-stimulated HRPE, IFN $\gamma$ -stimulated HRPE, and HRPE with and without C3a stimulation treated for 1 hour with Ep. Two samples of HRPE cells of two donors were studied. Untreated and C3a-treated cells were incubated for 2 hours with the probe and washed with medium before being imaged. Treated HRPE cells were stimulated with 50 ng/mL C3a. As a negative control, cells were incubated with 500 nM Ep overnight before incubation with the activity probe.

### **Protein extraction and Western blot analysis**

For Western blot analysis, protein lysates of 10 donors (three samples per experimental condition) were collected in 100  $\mu$ L lysis buffer (1% Triton X-100, 50 mM HEPES, 150 mM NaCl, 10% glycerol, 1.5 mM MgCl<sub>2</sub>, 1 mM EGTA, 1 mM phenylmethanesulfonyl fluoride, 1X phosphatase inhibitors, and 1X complete protease inhibitors; Roche Biochemicals, Almere, The Netherlands).

Western blot analyses were performed as described previously.<sup>60</sup> Twenty micrograms of protein were separated on a 12.5% SDS-PAGE, transferred to polyvinylidene difluoride membranes and semiquantitatively analyzed. Membranes were incubated for 16 hours

at 4°C with a monoclonal antibody against the  $\alpha 7$  and  $\alpha 2$  subunit of the 20S proteasome and one of the following polyclonal antibodies: anti- $\beta 5$  subunit of the 20S proteasome, anti- $\beta 5i$  subunit of the 20S proteasome, and anti-11S regulator subunit PA28 $\alpha$  (Enzo Life Sciences, Zandhoven, Belgium). All primary antibodies were diluted 1:500 in 3% nonfat dry milk (Bio-Rad, Hercules, CA) in TBS/0.05% Tween-20. Infrared dye-conjugated goat anti-rabbit (for  $\beta 5$ ,  $\beta 5i$ , and PA28 $\alpha$ ) and goat anti-mouse (for  $\alpha 7$  and  $\alpha 2$ ) secondary antibodies (LI-COR Biosciences, Lincoln, NE) were diluted 1:10,000. Immune reactions were quantified by densitometric analysis using Odyssey (LI-COR Biosciences). Anti- $\beta$ -actin antibody was used to stain a reference sample to normalize sample reactions and allowed for comparison between blots. All Western blot experiments were performed at least twice.

### **Proteasome activity measurements in cell extracts**

Retinal pigment epithelial cells from a young and old donor were harvested in TSDG buffer (10 mM Tris, pH 7.5, 25 mM KCl, 10 mM NaCl, 1.1 mM MgCl<sub>2</sub>, 0.1 mM EDTA, and 8% glycerol) and lysed by three freeze/thaw cycles in liquid nitrogen. After centrifugation (15 minutes, 21,000g), the protein concentration in the supernatant was determined by a Bradford protein assay (Serva, Heidelberg, Germany). Proteasomes were labeled in the lysate with 0.5  $\mu$ M Bodipy-Ep probe for 1 hour at 37°C.<sup>21</sup> Six times sample buffer (350 mM Tris/HCl, pH 6.8, 10% SDS, 30% glycerol, and 6%  $\beta$ -mercaptoethanol) was added to 30  $\mu$ g lysate. The samples were boiled for 3 minutes and loaded on a 12.5% SDS-PAGE gel. Afterwards, fluorescent imaging was performed on a Trio Thyphoon (GE Healthcare, Madison, WI) using the 580 bandpass (BP) 30 filter to detect the Bodipy-Ep probe directly in the gel. Subsequently, the gels were used for Western blot analysis to determine the proteasome levels using  $\alpha 2$  subunit levels as a loading control, using the MCP236 antibody (Enzo Life Sciences). Antibody detection was performed using the Odyssey detection system (LI-COR Biosciences).

### **RNA isolation and mRNA quantification**

For real-time quantitative PCR (qPCR) experiments, total RNA (6 samples per experimental condition) was isolated according to the manufacturer's instructions (TRIzol; Invitrogen) from the RPE of eight donors that were stimulated as indicated above. The amount of total RNA was approximately 3  $\mu$ g/sample. A 1- $\mu$ g aliquot of total RNA was treated with DNase-I (amplification grade; Invitrogen) and reverse transcribed into first strand cDNA (Superscript III and oligo[dT]),<sup>12-18</sup> Invitrogen). The specificity of the primers was confirmed by a nucleotide-nucleotide BLAST (available in the public domain at <http://www.ncbi.nlm.nih.gov/blast.cgi>; National Center for Biotechnology Information, Bethesda, MD) search. Primer details are given in Table 3. The presence of

a single PCR product was verified by both the presence of a single melting temperature peak and detection of a single band of the expected size on a 3% agarose gel. Quantitative PCR was performed (CFX96 system; Bio-Rad). For each primer set, a mastermix was prepared, consisting of 1X SYBR Green mix (iQ SYBR Green Supermix; Bio-Rad) and 2 pM primers with RNase-free water. One microliter of cDNA (diluted 1:20) in 19  $\mu$ L mastermix was amplified using the following PCR protocol: an activation step at 95°C for 15 minutes, followed by 40 cycles at 95°C for 10 seconds and at 60°C for 45 seconds, followed by 95°C for 1 minute and a melting program (60–95°C). Relative gene expression ( $R$ ) was calculated by using the equation:  $R = E^{-Ct}$ , where  $E$  is the mean efficiency of all samples for the gene being evaluated and  $Ct$  is the cycle threshold for the gene as determined during real-time PCR. The qPCR data were normalized with the expression of the *TWHAZ* gene, as determined by geNorm.<sup>65</sup>

Gene	GenBank	Forward Primer	Reverse Primer	Size, bp	Temp, °C
<i>RPE65</i>	NM_000329	GATGCCTTGGAAGAAGATGATGGTG	TCCTTGGCATTGAGAATCAGGAGAT	98	79
<i>RLBP1</i>	NM_000326	GAGAAGCTGCTGGAGAATGAGGAAA	TGGGAAGGAATCCTGGAGCATG	144	80
<i>FGFR2</i>	NM_022971	TGATGATGAGGGACTGTTGGCATG	TCGAGAGGTTGGCTGAGGTCCA	108	78
<i>PSME1</i>	NM_006263	CAGCCCCATGTGGGTGATTATC	GCTTCTCGAAGTTCTTCAGGATGAT	139	82
<i>PSMA7</i>	NM_002792	CCTGGAAGGCCAATGCCATAG	TTTGCCACCTGACTGAACCACTTC	149	82
<i>PSMB5</i>	NM_002797	CCATGATCTGTGGCTGGGATAAG	GGTCATAGGAATAGCCCGATC	144	83
<i>PSMB8</i>	NM_004159	CTGGAGGCGTTGTCAATATGTACC	GCAGCAGGTCCTGACATCTGTAC	81	76
<i>C5AR1</i>	NM_001736	CCCAGGAGACCAGAACATGAACTC	TGACCAAGGCCAGGATGTCTG	143	81
<i>C5L2</i>	NM_018485	GCCAGGACGAAAGTGTGGACAG	CCAGCTATGCCTGAAGCCAGTC	136	81
<i>C3AR</i>	NM_004054	ACCAGACAGGACTCGTGGAGACAT	GCAGAGAAAGACGCCATTGCTAAAC	90	77

**Table 3.** Primer details (gene nomenclature, GenBank accession code, primer sequences, and predicted size and  $T_m$  of the amplified product).

### Statistical analysis

Gene expression data showed a normal distribution. Differences in gene expression levels between groups were calculated by using single ANOVA with  $P < 0.05$  indicating significant differences (two-tailed).

For proteasome activity in FACS assays, the total fluorescence intensities from two independent preparations in each group were calculated. Data are presented as mean  $\pm$  SEM with statistical differences between groups analyzed by standard two-tailed  $t$ -test using GraphPad Prism (version 5.00 for Windows, www.graphpad.com; GraphPad

Software, San Diego, CA, USA) and a  $P < 0.05$  indicating statistically significant differences.

## **Results**

### **Increased $\beta 5i:\beta 5$ ratio in RPE of CCL2<sup>-/-</sup> mice**

Immunofluorescence of proteasome subunits  $\beta 5$  and  $\beta 5i$  in retinas of CCL2<sup>-/-</sup> mice ( $n = 3$ ) and wild-type mice ( $n = 3$ ) showed the subunits to be localized in nuclei and perinuclear regions of RPE cells. Retinal pigment epithelium of age-matched wild-type and CCL2<sup>-/-</sup> mice showed similar levels of  $\beta 5$  staining (Fig. 2A). However, the RPE of CCL2<sup>-/-</sup> mice also showed high levels of the  $\beta 5i$  subunit, while no  $\beta 5i$  subunit staining was observed in RPE of wild-type mice (Fig. 2B). This translated in a higher  $\beta 5i:\beta 5$  ratio in the RPE of CCL2<sup>-/-</sup> mice. These results suggest that proteasome activity may be altered in age-related maculopathy.

### **Overall activity of the RPE proteasome is decreased upon C3a stimulation in HRPE cells**

Overall proteasome activity was visualized in RPE cells at 72 hours by CLSM imaging and subsequently quantified by FACS assays using the activity probe BodipyFl-Ahx<sub>3</sub>L<sub>3</sub>VS. Confocal scanning laser microscope images showed active proteasomes in nuclei and cytoplasm of HRPE cells. In comparison to untreated cells, HRPE cells treated for 72 hours with C3a showed decreased proteasome activity. Cells treated with the proteasome inhibitor, Ep, showed 80% inhibition of proteasome activity ( $n = 7$ ;  $P < 0.01$ ; Fig. 3). C3a-treated HRPE cells of younger donors (13–37 years old,  $n = 3$ ) showed no differences in proteasome activity when compared with untreated HRPE ( $P > 0.05$ , Fig. 4A), whereas C3a-treated HRPE cells of older donors (47–65 years old,  $n = 4$ ) showed a 37% decrease in proteasome activity when compared to age-matched untreated HRPE cells ( $P < 0.05$ , Fig. 4B). Treatment of HRPE cells with IFN $\gamma$  caused a 76% increase in proteasome activity ( $n = 7$ ,  $P < 0.01$ ). Photoreceptor outer segments-fed cells did not show altered proteasome activity (data not shown). Moreover, the CFH Y402H polymorphism did not affect proteasome activity in untreated and C3a-treated HRPE cells. Overall, these results suggest that complement factor C3a causes decreased proteasome activity in HRPE cells of older individuals.

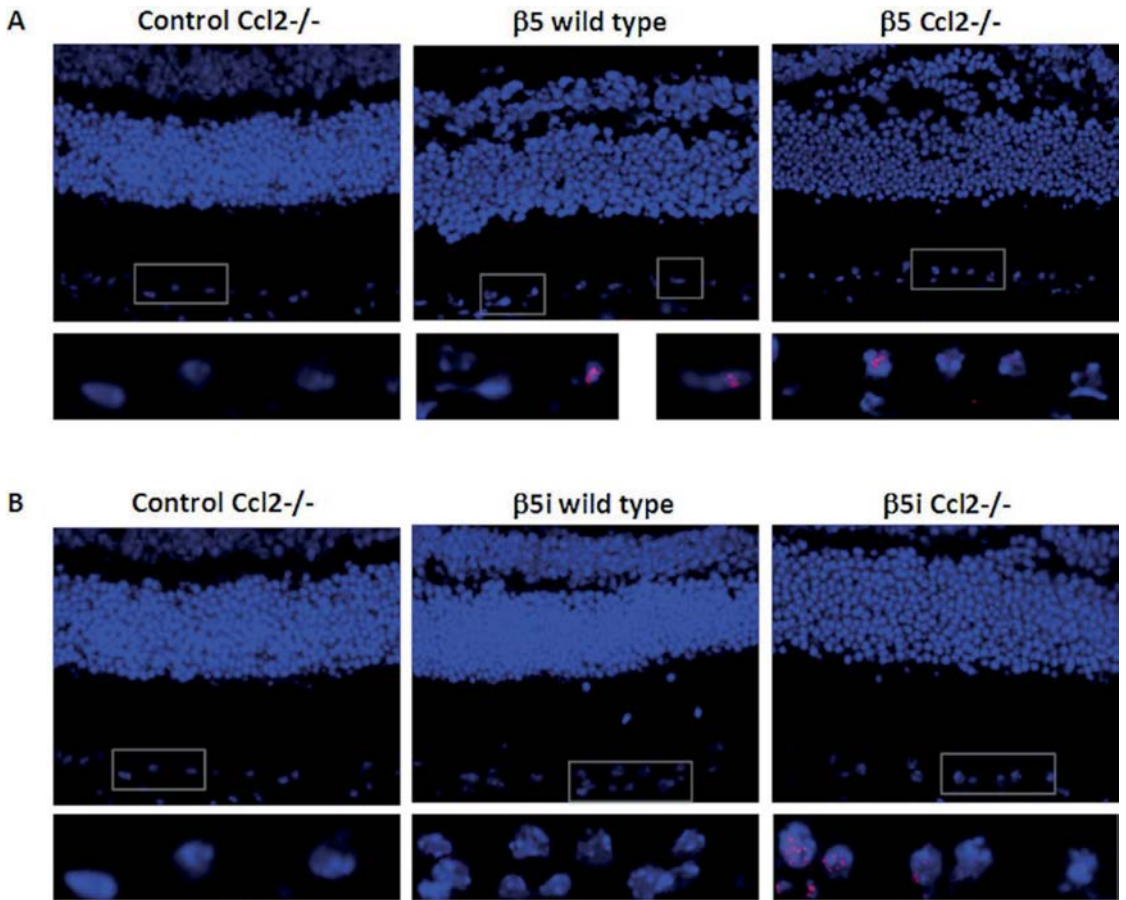


**Fig. 2.** (A) Proteasome  $\beta 5$  subunit content is constant in  $CCL2^{-/-}$  mice. Whole retina sections from wild-type and  $CCL2^{-/-}$  mice were stained with anti-proteasome  $\beta 5$  antibody and visualized by immunofluorescence microscopy (in pink). Proteasome  $\beta 5$  subunit was present in the nuclei and perinuclear region of the RPE of both wild-type and  $CCL2^{-/-}$  mice. (B) Proteasome  $\beta 5i$  subunit protein expression is upregulated in  $CCL2^{-/-}$  mice. Whole retina sections from wild-type and  $CCL2^{-/-}$  mice were stained with anti-proteasome  $\beta 5i$  antibody and visualized by immunofluorescence microscopy. Proteasome  $\beta 5i$  subunit was not present in the RPE of wild-type mice. Immunoproteasome  $\beta 5i$  subunit was upregulated in the nuclei and perinuclear regions of the RPE of  $CCL2^{-/-}$  mice.

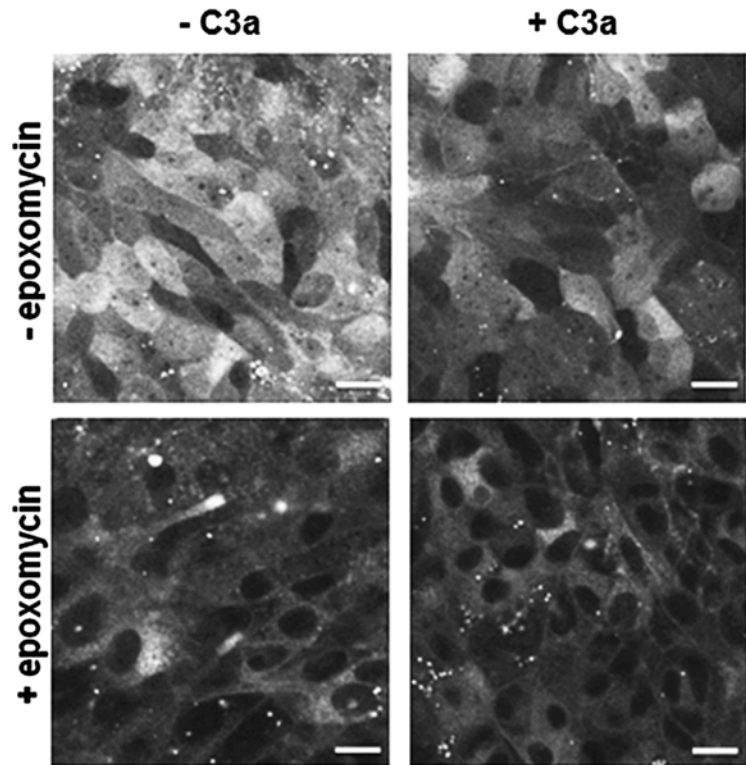


**Fig. 3.** Proteasome overall activity is decreased upon C3a stimulation of HRPE cells from old donors. Proteasome overall activity was assessed in the following conditions: unstimulated HRPE, 72-hour C3a stimulation in HRPE, and the same conditions after epoxomicin (Ep) treatment for 1 hour. Proteasome overall activity was visualized by confocal scanning laser microscopy after treatment with the probe BodipyFl-Ahx3L3VS for 2 hours. Epoxomicin, a proteasome inhibitor, is used as a negative control and represents minimal proteasomal activity.

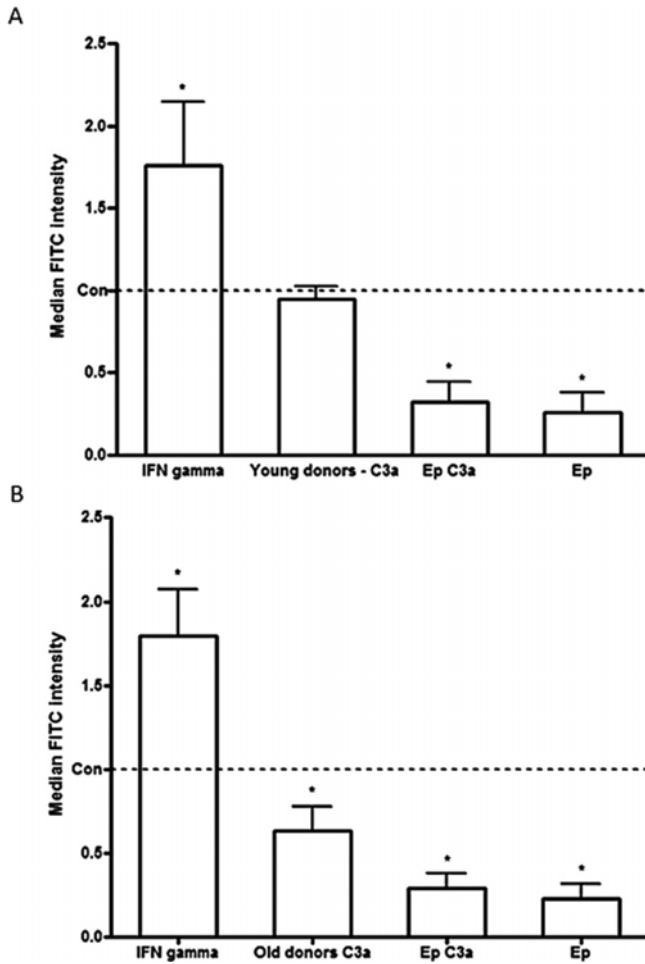


**Fig. 4.** Proteasome overall activity is decreased upon C3a stimulation of HRPE cells from old donors. Proteasome overall activity was assessed in the following conditions: unstimulated HRPE, 72-hour C3a stimulation in HRPE of young donors (13–37 years old, n = 3) (A), 72-hour C3a stimulation in HRPE of old donors (47–65 years old, n = 4) (B), 72-hour treatment of HRPE with IFN $\gamma$  and HRPE with and without C3a stimulation treated for 1 hour with Ep. Proteasome overall activity was measured by FACS assay after treatment with the probe BodipyFl-Ahx3L3VS for 2 hours. Data of HRPE treated with POS are not shown. Interferon- $\gamma$  is used as a positive control and represents the maximum proteasomal activity; Ep, a proteasome inhibitor, is used as a negative control and represents minimal proteasomal activity. Data are expressed as the median  $\pm$  SEM. \*, Significant change (P < 0.05).

### **Specific proteasome subunit activities are not affected by C3a in HRPE cells**

To further characterize whether decreased overall proteasome activity was due to changes in the activities of specific proteasome subunits, we used a Bodipy-Ep probe to label the individual catalytic proteasome subunit activities upon separation by SDS-PAGE (Fig. 5). Retinal pigment epithelial cells from young and old donors were used (ages 23 and 65 years old, respectively). As expected, IFN $\gamma$  caused increased activity of immunoproteasomes as indicated by the increase in  $\beta$ 2i (14.7-fold higher on average in all donors), and  $\beta$ 5:5i:1i levels in the young donor (2.7-fold higher when compared with control). However, treatment with either a high or low concentration of C3a did not induce any changes in  $\beta$ 2,  $\beta$ 2i,  $\beta$ 1, and  $\beta$ 5:5i:1i activity levels when compared with control HRPE cells. These results indicate that overall decreased proteasome activity upon C3a stimulation is not due to changes in the activity of specific proteasome subunit complexes.

### **Expression of proteasome is not affected by C3a stimulation in HRPE cells**

To assess whether the observed decrease in proteasome activity upon C3a treatment was due to an alteration in expression of proteasome subunits, we measured total proteasome content (Fig. 6). Levels of the different proteasome subunits were evaluated using the  $\alpha$ 7 and  $\alpha$ 2 subunits of the 20S core. Densitometric analysis revealed no statistically significant differences in the content of  $\alpha$ 7 (n = 6) and  $\alpha$ 2 (n = 8) proteasome subunits after treatment with C3a, C5a, or IFN $\gamma$ .

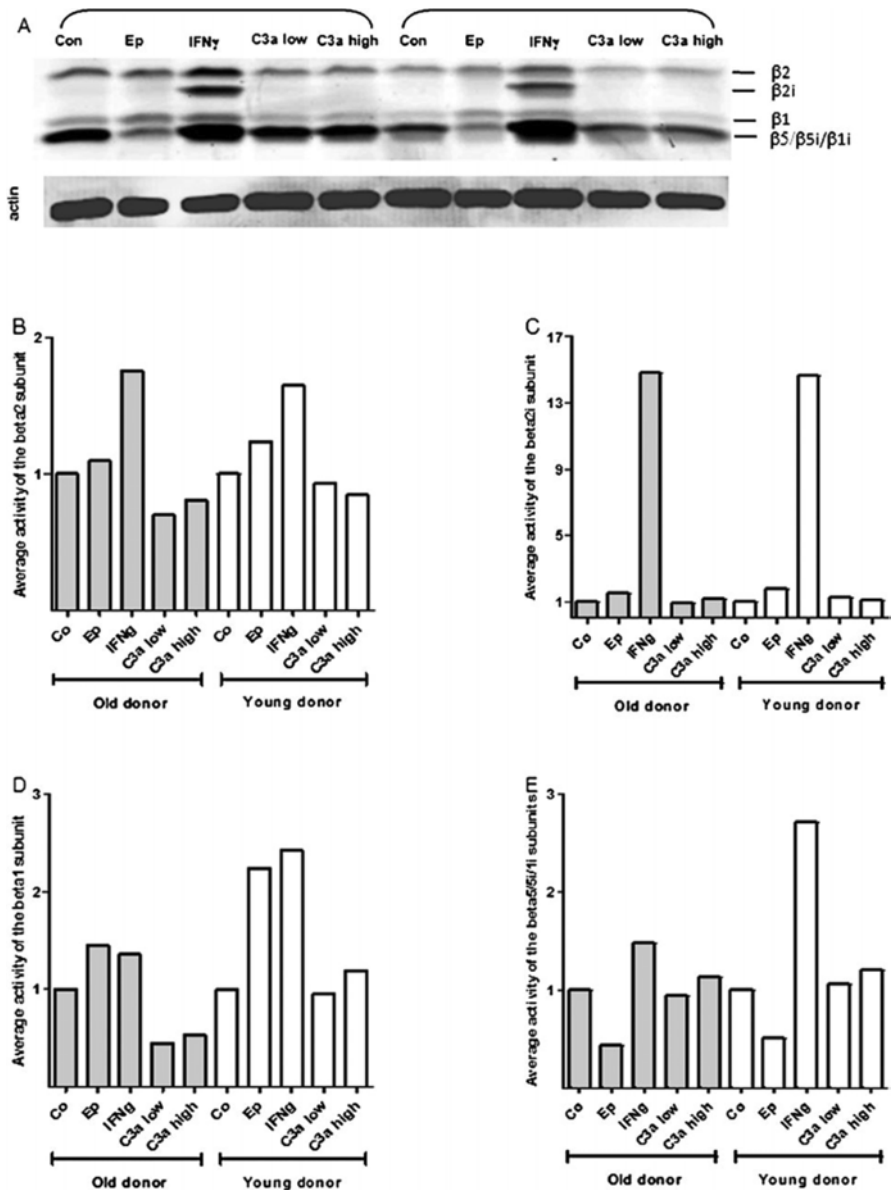


**Fig. 5.** Interferon- $\gamma$ , but not C3a, increases the average activity of proteasome subunits  $\beta 2$ ,  $\beta 2i$ ,  $\beta 1$ , and  $\beta 5:\beta 5i:\beta 1i$  complex both in an old donor (65 years old) and young donor (23 years old). (A) After treatment with Ep, IFN $\gamma$ , and high and low concentrations of C3a, HRPE cells were harvested, and proteasomes were labeled with a Bodipy-Ep probe. Detection of different proteasome subunit activities was performed by Western blotting. Quantitative data of the proteasome activity are presented per donor for proteasome subunit  $\beta 2$  (B),  $\beta 2i$  (C),  $\beta 1$  (D), and  $\beta 5:\beta 5i:\beta 1i$  complex (E).

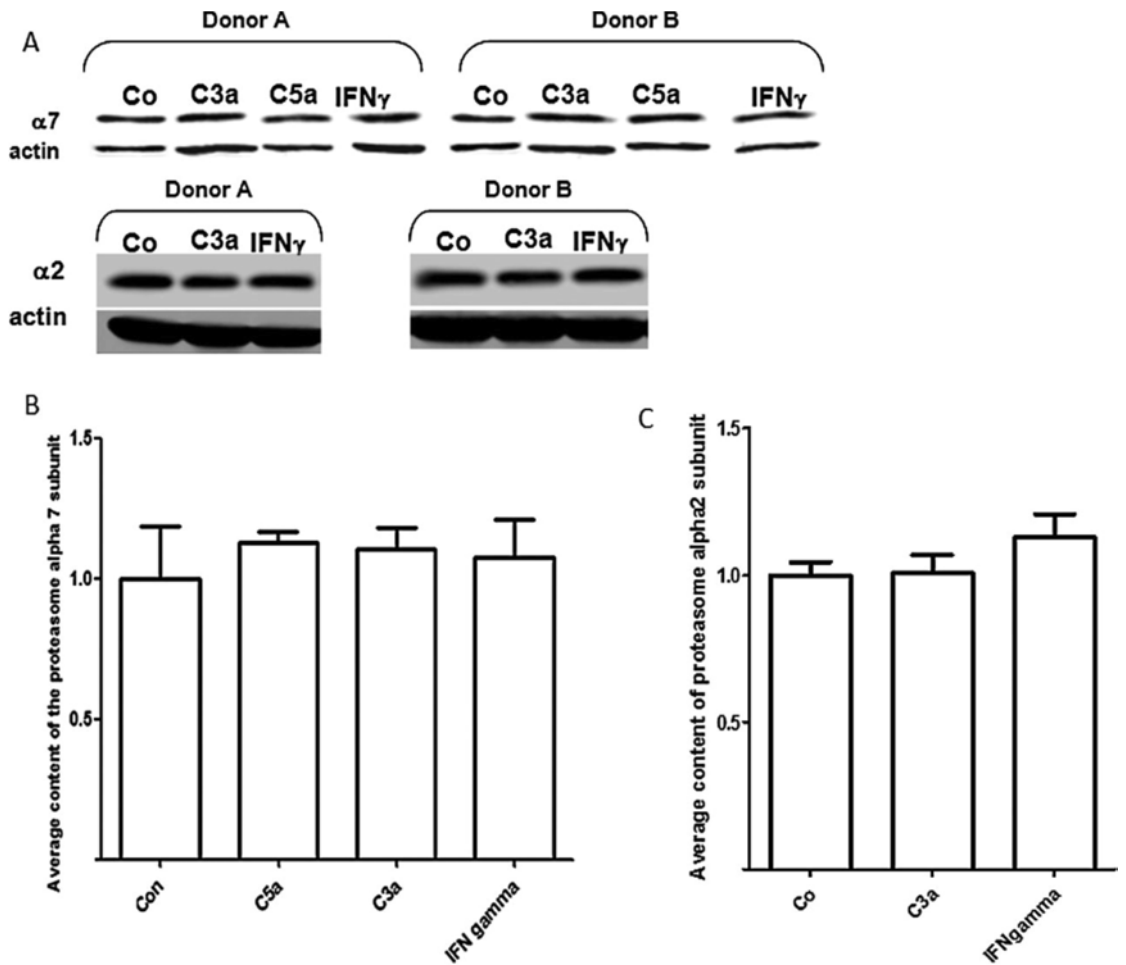


**Fig. 6.** The total content of the proteasome  $\alpha 7$  and  $\alpha 2$  subunit is not increased upon stimulation of HRPE cells with C3a. Human retinal pigment epithelial cells were incubated for 72 hours with or without C3a, C5a (only for  $\alpha 7$ ), or IFN $\gamma$ . (A)  $\alpha 7$  and  $\alpha 2$  levels were assessed by Western blot with actin expression as a loading control. (B) Quantitative data of the average content of  $\alpha 7$  in the different experimental conditions, corrected for actin, and relative to control samples in HRPE cells without C3a stimulation. (C) Quantitative data of the average content of  $\alpha 2$  in the different experimental conditions, corrected for actin expression, and relative to control samples in HRPE cells without C3a stimulation. Data are expressed as the mean  $\pm$  SEM. \*Significant change ( $P < 0.05$ ).

### Immunoproteasome expression is not affected by complement overactivation in HRPE cells

Untreated HRPE cells showed protein levels of both the constitutive subunit  $\beta 5$  and the inducible subunit  $\beta 5i$  of the proteasome that were similar in C3a-stimulated HRPE

cells ( $n = 8$ ,  $P > 0.05$ , Fig. 7). In IFN $\gamma$ -treated HRPE cells, the protein levels for the immuno-subunit  $\beta 5i$  were on average 1.8-fold higher than in control HRPE ( $n = 8$ ,  $P < 0.05$ ), whereas those of the constitutive  $\beta 5$  subunit were on average 0.8-fold lower than in untreated HRPE ( $n = 8$ ,  $P > 0.05$ ). This translated in a statistically significant increased average  $\beta 5i:\beta 5$  ratio of 2.3 for IFN $\gamma$ -treated HRPE cells ( $n = 8$ ,  $P < 0.01$ ). These results show that inflammatory mediators, but not complement activation, may explain the change in the conformation of the proteasome in RPE cells in mice, as the decreased proteasome overall activity found in the HRPE cells treated with C3a cannot be explained by changes in the content of  $\beta 5$  or  $\beta 5i$ . No significant association was found between age, CFH Y402H polymorphism and change in proteasome protein content.

### **No alterations in PA28 levels upon C3a stimulation in HRPE cells**

As changes in proteasome activity can also be induced by the proteasome activator PA28, which can replace the 19S cap as an alternative proteasome activator binding to the 20S proteasome core, we determined the total content of the proteasome regulatory complexes by antibody reactions against the  $\alpha$ -subunit of PA28, another proteasome regulatory complex.

We did not find any significant change in content of PA28 $\alpha$  protein levels due to C3a treatment. A significant 4.6-fold increase was found in IFN $\gamma$ -stimulated HRPE cells ( $n = 5$ ,  $P < 0.01$ , Fig. 8). These data suggest that decreased proteasome overall activity upon C3a stimulation is not due to altered PA28 levels, a mechanism by which IFN $\gamma$  and other inflammatory mediators are known to upregulate the level of the immunoproteasome.

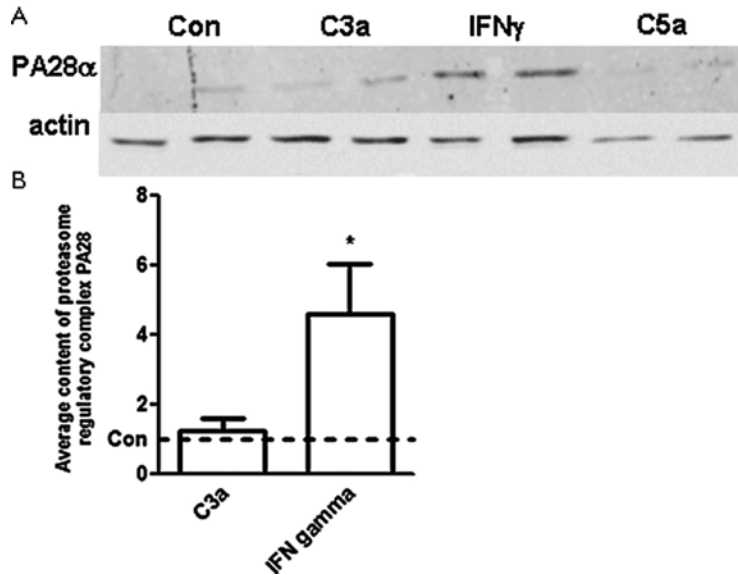


**Fig. 8.** The total content of the proteasome regulatory complex PA28 $\alpha$  is increased upon stimulation of HRPE cells with IFN $\gamma$ , but remains unchanged upon C3a stimulation. Human retinal pigment epithelial cells were incubated with or without C3a, C5a, or IFN $\gamma$ . (A) PA28 $\alpha$  levels were assessed by Western blot with actin used as a loading control. (B) Quantitative data of the content of the average content of PA28 $\alpha$ , corrected for actin, and relative to control samples in HRPE cells without C3a stimulation. Data are expressed as the mean  $\pm$  SEM. \*, Significant change ( $P < 0.05$ ).

### C3a stimulation in HRPE cells does not change mRNA expression of proteasome-related genes

We assessed mRNA levels of proteasome-related genes, *PSME1* (PA28), *PSMB5* ( $\beta$ 5 subunit), *PSMA7* ( $\alpha$ 7 subunit), and *PSMB8* ( $\beta$ 5i subunit) in untreated HRPE cells and HRPE cells treated with C3a, IFN $\gamma$ , and H<sub>2</sub>O<sub>2</sub>. Expression of the C5a receptors, human C5aR (hC5aR) and human C5L2 (hC5L2), as well as the C3a receptor, human C3aR (hC3aR), was also determined in order to confirm whether complement receptors were expressed in the RPE cells.

mRNA levels of proteasome-related genes did not significantly change after C3a, C5a, and H<sub>2</sub>O<sub>2</sub> treatment for 72 hours. However, IFN $\gamma$  treatment significantly increased mRNA levels of all genes, 4.9-fold for *PSMB5* ( $\beta$ 5 subunit), 11.9-fold for *PSMB8* ( $\beta$ 5i subunit), 3.2-fold for *PSMA7* ( $\alpha$ 7 subunit), and 3.0-fold for *PSME1* (PA28 subunit) ( $n = 8$ ,  $P < 0.05$ , Fig. 9). Expression of both hC5aR and hC3aR was detected in the HRPE, whereas hC5L2 expression was not detected (data not shown).

These results suggest that the complement factor C3a-induced changes in overall proteasome activity are not caused by alterations in gene expression.

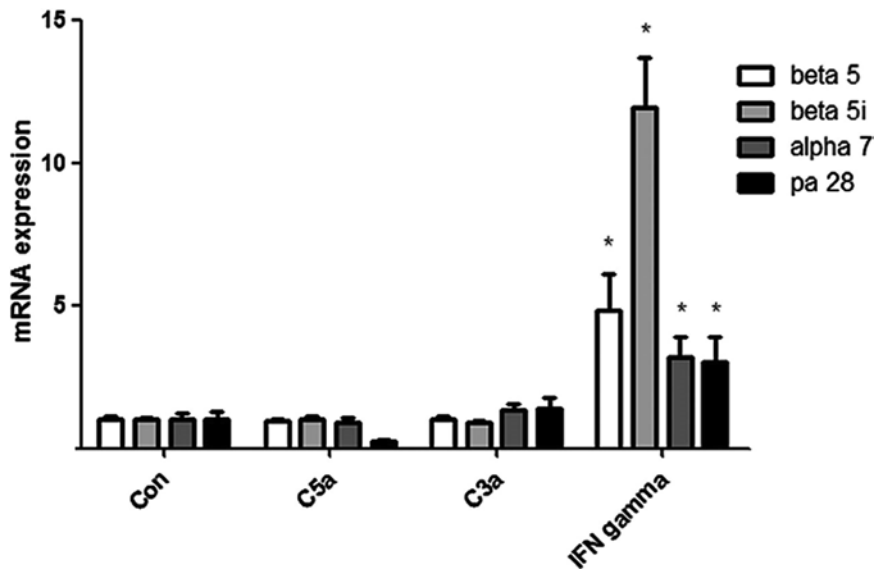


**Fig. 9.** Increased mRNA expression of  $\beta 5$  and  $\alpha 7$  subunits by C3a treatment in RPE cells. mRNA levels of PA28 $\alpha$ ,  $\beta 5$ ,  $\beta 5i$ , and  $\alpha 7$  subunits of the proteasome in HRPE cells, which were stimulated with IFN $\gamma$ , C3a, and C5a for 72 hours. Values represent mRNA expression levels (mean  $\pm$  SEM) relative to untreated control cells. \*, Significant change ( $P < 0.05$ ).

## Discussion

This study shows that in primary cultures of HRPE, C3a leads to decreased proteasome-mediated proteolytic activity, independent of changes in proteasome components at the protein or transcriptional level, while in a mouse model of age-related atrophic degeneration of the RPE, immunoproteasome upregulation was shown by an increased  $\beta 5i:\beta 5$  ratio. Our results support involvement of alterations in proteasome activity in the cascade of pathologic events that result in this disease process.

Interferon- $\gamma$  had no effect on the total level of proteasomes, but it did cause an increase in proteasome overall and specific activities, increased relative expression of proteasome regulatory complex PA28 $\alpha$ , and increased protein and mRNA expression of immunoproteasome subunits. Interferon- $\gamma$  caused a switch in the predominance of the inducible chymotrypsin-like subunit  $\beta 5i$  over its normal counterpart  $\beta 5$ . The resulting  $\beta 5i:\beta 5$  ratio increased by 2.27-fold when compared with unstimulated HRPE. This resulted in a high  $\beta 5i:\beta 5$  ratio, which is indicative of more immunoproteasomes. These results, which are in accordance with previous studies<sup>6; 58; 64</sup> show that the observed decreased proteasome activity upon stimulation with C3a cannot be explained by similar mechanisms.

48 Previous studies have shown that  $\beta 5$ -driven proteolytic activity is the rate-limiting

activity and the primary effector of protein degradation by the proteasome.<sup>10; 49</sup> Specific inhibition of its activity has the most significant consequences for key processes involved in cell survival under stressful conditions. Neuronal cells that over-expressed a mutant  $\beta 5$  subunit where the active site threonine had been mutated to an alanine were significantly hypersensitive to oxidative stress.<sup>48</sup> The aged retina is exposed to high oxygen tension, high metabolic activity, presence of photosensitive pigments, all culminating in generation of reactive oxygen species<sup>7</sup> that periodically lead to an imbalance in the cellular redox homeostasis. Additionally, and in agreement with our results, proteasome function in the retina is known to be affected by aging, with the  $\beta 5$  chymotrypsin-like activity of the proteasome being most affected.<sup>39</sup> Our results suggest that in addition to aging mechanisms, inflammatory mediators such as  $\text{IFN}\gamma$  and potentially complement overactivation may cause alterations in proteasome activity, which may render the RPE less tolerant to oxidative stress due to impairment in the clearance of oxidatively damaged proteins.

Decreased overall proteasome activity in the RPE may indirectly contribute to the development of age-related maculopathy. A recent study showed that experimental drug-induced proteasome inhibition in the ARPE-19 cell line, a human RPE cell line with differentiated properties, leads to accumulation of hypoxia-inducible factor 1-alpha and diminished activation of the nuclear factor kappa-light-chain-enhancer of activated B cells pathway (NF- $\kappa$ B). This led in turn to enhanced expression and secretion of pro-angiogenic factors such as VEGF and angiopoietin-2 together with an attenuated expression of monocyte chemoattractant protein-1.<sup>56; 19</sup> Pathologic angiogenesis due to upregulation of VEGF is one of the most important causes of visual deterioration in AMD.<sup>70</sup>

Furthermore, C3a-driven reduced proteasome activity in the RPE could lead to an abnormal regulation of key signaling pathways. For instance, the UPS plays a crucial role in the regulation of pathways that respond to light damage<sup>23; 69</sup> and to melatonin production.<sup>33</sup> Hence, complement-driven proteasome inhibition could impact the circadian cycles of melatonin production and the subsistence of the retina to light-induced damage.

Proteasome inhibition has been shown to increase lipofuscin accumulation and in turn, lipofuscin inhibits the proteasome system due to proteasomal binding to the lipofuscin surface motifs.<sup>30</sup> Lipofuscin, a highly oxidized aggregate, consists of covalently cross-linked proteins, lipids, and sugar residues and is one of the major lifespan-limiting factors in post mitotic ageing cells.<sup>30</sup> Lipofuscin accumulation in the RPE has been reported in aging and has been implicated in many ocular disorders such as AMD, Stargardt disease and Best vitelliform macular dystrophy. Potential noxious effects of lipofuscin include photochemical blue light damage, inhibition of lysosomal digestion and proteins, detergent-like disruption of membranes, RPE apoptosis, and DNA damage. Lipofuscinogenesis translates in increased autofluorescence of the retinal fundus. However, it is still unclear whether proteasome inhibition would have the same effects in the RPE because unlike in many cell types in which lipofuscin originates internally (autophagy), lipofuscin derives

primarily from phagocytosed photoreceptor outer segments in the RPE.<sup>7; 8; 40; 41; 42; 43; 44; 68</sup> Besides our studies in *in vitro* HRPE models, we also studied proteasome function in a mouse model for age-related atrophic degeneration of the RPE. Ambati et al. observed developing features of age-related maculopathy and AMD such as accumulation of lipofuscin, drusen beneath the RPE, photoreceptor atrophy, and choroidal neovascularization.<sup>1</sup> Deposition of complement C3 and C5 intermediates within the RPE and the choroid apparently precedes the accumulation of lipofuscin and deposits in Bruch's membrane. This chain of events is supposedly similar to the processes occurring in human eyes affected by AMD. Complement activation was not present in age-matched wild-type mice.<sup>1</sup> The use of CCL2<sup>-/-</sup> mice as a mouse model for AMD has been disputed in recent years. Studies have shown that dysfunction of the chemokine ligand-receptor pair CCL2-CCR2 may lead to dysregulated retinal para-inflammation mechanisms and retinal lesion development with aging, eventually leading to the development of dry AMD-like lesions in these mice.<sup>1;</sup><sup>9</sup> Other studies, however, have failed to show retinal lesions in these mice. Luhmann et al. reported increased subretinal macrophage accumulation, but no retinal degeneration in aged CCL2<sup>-/-</sup> mice.<sup>50</sup> Vessey et al. showed inner retinal (amacrine cell) dysfunction in 9-month-old CCL2/CX3CR1<sup>GFP/GFP</sup> mice.<sup>67</sup> In a recent publication, Chen et al. confirmed results of previous studies in which deficiency of CCL2 led to an identifiable dry AMD-like phenotype. Lesions appeared in these age-dependent CCL2<sup>-/-</sup>CX3CR1<sup>GFP/GFP</sup> mice not expressing the rd8 mutation, characterized by localized RPE and photoreceptor atrophy similarly to the human geographic atrophy dry type of AMD.<sup>9</sup> In line with these results, we performed experiments with CCL2<sup>-/-</sup> mice in order to establish an indirect link between age, complement activation, and age-related atrophic degeneration of the RPE. Retinas of CCL2<sup>-/-</sup> mice and age-matched wild-type mice were stained for  $\beta 5$  and  $\beta 5i$  proteasome subunits. Retinas of CCL2<sup>-/-</sup> mice showed an increased  $\beta 5i:\beta 5$  ratio. This was related to a higher content of  $\beta 5i$  in the RPE of the knockout mouse model when compared with the age-matched control. The increase in the  $\beta 5i:\beta 5$  ratio observed in CCL2<sup>-/-</sup> mice could be one of the rescue mechanisms against retinal toxicity and oxidative stress. Our study presents some limitations. It remains inconclusive why retinas of CCL2<sup>-/-</sup> mice show an increased  $\beta 5i:\beta 5$  ratio. A link with the *in vitro* experiments with HRPE cells cannot be established. We could not prove, *in vitro*, that the induction of  $\beta 5i$  was specific for complement. The retinas and RPE of CCL2<sup>-/-</sup> mice might be exposed to other inflammatory mediators that trigger the observed change in proteasome conformation. Another limitation of our study deals with estimating subunit composition from Western immunoblots in RPE homogenates. Unassembled subunits cannot be distinguished from those that are part of the functional complex. Such mechanism of subunit assembly may be altered by C3a stimulation. Another limitation of our method is the inability to differentiate proteasomes in different cellular compartments. C3a-associated changes in subcellular localization would not be detected using our method. Specific functions, for instance the degradation of misfolded proteins by proteasomes docked outside the endoplasmic reticulum, could be affected should the subcellular content of proteasomes be altered.

In conclusion, our results suggest a link between complement activation and proteasome activity in HRPE cells, which may have implications in the development of age-related maculopathy and AMD (Fig. 10). This alteration in UPS activity is not caused by changes in the proteasome composition itself, and probably occurs at a posttranslational level since it is not due to changes in gene expression or changes in the activity of specific proteasome subunits.

### LOCAL INFLAMMATION MODEL OF AMD

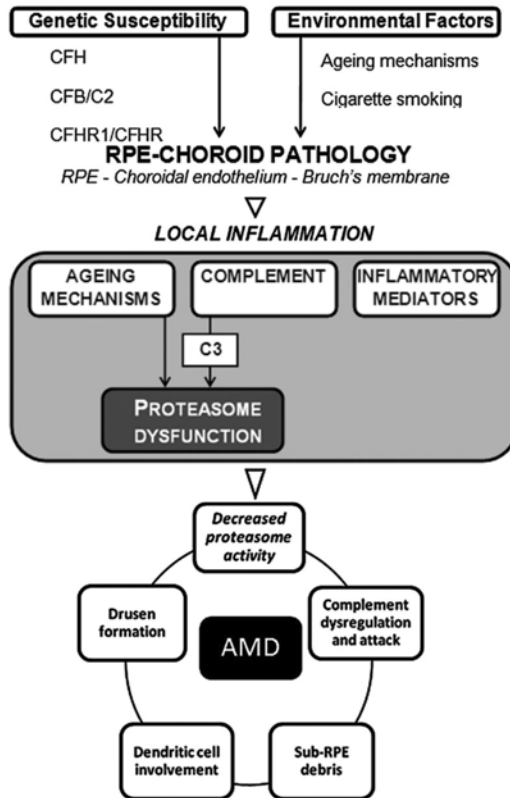


**Fig. 8.** Inflammation model of macular degeneration.<sup>6</sup> Age-related macular degeneration may be triggered by one or more environmental risk factors coupled with a genetic susceptibility profile conferred by variants in the CFH, CFB/C2, and/or C3 gene triad. Late in life, such features culminate in the development of pathologic changes in the RPE–choroid complex, which in turn generate a chronic, local inflammatory response characterized by complement over activation, and inflammation-mediated events. According to our results, release of anaphylatoxin C3a, a complement activation fragment, together with age-related changes, triggers decreased proteasome overall activity. Collectively, complement activation, inflammation-mediated events, and possibly proteasome dysfunction result in the photoreceptor degeneration and the loss of central vision that defines the clinical entity of AMD.

## Disclosure

Disclosure: J.E. Ramos de Carvalho, None; I. Klaassen, None; I.M.C. Vogels, None; S. Schipper-Krom, None; C.J.F. van Noorden, None; E. Reits, None; T.G.M.F. Gorgels, None; A.A.B. Bergen, None; R.O. Schlingemann, None

## References

1. Ambati J, Anand A, Fernandez S, et al.: An animal model of age-related macular degeneration in senescent Ccl-2-or Ccr-2-deficient mice. *Nat Med* 9:1390-1397, 2003
2. Anderson DH, Mullins RF, Hageman GS, Johnson LV: Perspective - A role for local inflammation in the formation of drusen in the aging eye. *Am J Ophthalmol* 134:411-431, 2002
3. Augood CA, Vingerling JR, De Jong PTVM, et al.: Prevalence of age-related maculopathy in older Europeans - The European Eye Study (EUREYE). *Arch Ophthalmol* 124:529-535, 2006
4. Berkers CR, van Leeuwen FWB, Groothuis TA, et al.: Profiling proteasome activity in tissue with fluorescent probes. *Molecular Pharmacology* 4:739-748, 2007
5. Bora NS, Jha P, Bora PS: The role of complement in ocular pathology. *Sem Immunopathol* 30:85-95, 2008
6. Bose S, Brooks P, Mason GGF, Rivett AJ: gamma-interferon decreases the level of 26 S proteasomes and changes the pattern of phosphorylation. *Biochem J* 353:291-297, 2001
7. Boulton M, Rozanowska M, Rozanowski B: Retinal photodamage. *J Photochem Photobiol B* 64:144-161, 2001
8. Burke JM, Skumatz CMB: Autofluorescent inclusions in long-term postconfluent cultures of retinal pigment epithelium. *Invest Ophthalmol Vis Sci* 39:1478-1486, 1998
9. Chen M, Forrester JV, Xu HP: Dysregulation in retinal para-inflammation and age-related retinal degeneration in CCL2 or CCR2 deficient mice. *PLoS One* 6:e22818, 2011
10. Coux O, Tanaka K, Goldberg AL: Structure and functions of the 20S and 26S proteasomes. *Annu Rev Biochem* 65:801-847, 1996
11. Crabb JW, Miyagi M, Gu XR, et al.: Drusen proteome analysis: an approach to the etiology of age-related macular degeneration. *Proc Natl Acad Sci U S A* 99:14682-14687, 2002
12. Dahlmann B, Ruppert T, Kuehn L, et al.: Different proteasome subtypes in a single tissue exhibit different enzymatic properties. *J Mol Biol* 303:643-653, 2000
13. Dawson TM, Dawson VL: Molecular pathways of neurodegeneration in Parkinson's disease. *Science* 302:819-822, 2003
14. Despriet DDG, Klaver CCW, Witteman JCM, et al.: Complement factor H polymorphism, complement activators, and risk of age-related macular degeneration. *JAMA* 296:301-309, 2006
15. Ding QX, Martin S, Dimayuga E, et al.: LMP2 knock-out mice have reduced proteasome activities and increased levels of oxidatively damaged proteins. *Antiox Redox Signal* 8:130-135, 2006
16. Donoso LA, Kim D, Frost A, et al.: The role of inflammation in the pathogenesis of age-related macular degeneration. *Surv Ophthalmol* 51:137-152, 2006
17. Dudek EJ, Shang F, Liu Q, et al.: Selectivity of the ubiquitin pathway for oxidatively modified proteins: relevance to protein precipitation diseases. *FASEB J* 19:1707-1709, 2005
18. Edwards AO, Ritter R, Abel KJ, et al.: Complement factor H polymorphism and age-related macular degeneration. *Science* 308:421-424, 2005
19. Fernandes AF, Guo WM, Zhang XY, et al.: Proteasome-dependent regulation of signal transduction in retinal pigment epithelial cells. *Exp Eye Res* 83:1472-1481, 2006
20. Ferrington DA, Hussong SA, Rochrich H, et al.: Immunoproteasome responds to injury in the retina and brain. *J Neurochem* 106:158-169, 2008
21. Florea BI, Verdoes M, Li N, et al.: Activity-based profiling reveals reactivity of the murine thymoproteasome-specific subunit beta 5t. *Chem Biol* 17:795-801, 2010
22. Goldberg AL, Cascio P, Saric T, Rock KL: The importance of the proteasome and subsequent proteolytic steps in the generation of antigenic peptides. *Mol Immunol* 39:147-164, 2002
23. Grimm C, Wenzel A, Behrens A, et al.: AP-1 mediated retinal photoreceptor apoptosis is independent of N-terminal phosphorylation of c-Jun. *Cell Death Differ* 8:859-867, 2001
24. Hageman GS, Anderson DH, Johnson LV, et al.: A common haplotype in the complement regulatory gene factor H (HF1/CFH) predisposes individuals to age-related macular degeneration. *Proc Natl Acad Sci U S A* 102:7227-7232, 2005
25. Hageman GS, Luthert PJ, Chong NHV, et al.: An integrated hypothesis that considers drusen as biomarkers of immune-mediated processes at the RPE-Bruch's membrane interface in aging and age-related macular degeneration. *Prog Ret Eye Res* 20:705-732, 2001
26. Hageman GS, Mullins RF: Molecular composition of drusen as related to substructural phenotype. *Mol Vis* 5, 1999
27. Haines JL, Hauser MA, Schmidt S, et al.: Complement factor H variant increases the risk of age-related macular degeneration. *Science* 308:419-421, 2005
28. Hayashi T, Faustman D: NOD mice are defective in proteasome production and activation of NF-kappa B. *Mol Cell Biol* 19:8646-8659, 1999
29. Hayashi T, Faustman DL: Genome and hormones: gender differences in physiology selected contribution: association of gender-related LMP2 inactivation with autoimmune pathogenesis. *J Appl Physiol* 91:2804-2815, 2001
30. Hohn A, Jung T, Grimm S, et al.: Lipofuscin inhibits the proteasome by binding to surface motifs. *Free Radic Biol Med* 50:585-591, 2011
31. Hollyfield JG: Age-related macular degeneration: the molecular link between oxidative damage, tissue-specific inflammation and outer retinal disease. The Proctor lecture. *Invest Ophthalmol Vis Sci* 51:1276-1281, 2010
32. Hope AD, de Silva R, Fischer DF, et al.: Alzheimer's associated variant ubiquitin causes inhibition of the 26S proteasome and chaperone expression. *J Neurochem* 86:394-404, 2003
33. Iuvone PM, Brown AD, Haque R, et al.: Retinal melatonin production: role of proteasomal proteolysis in circadian and photic control of arylalkylamine N-acetyltransferase. *Invest Ophthalmol Vis Sci* 43:564-572, 2002

34. Jahngnehodge J, Cyr D, Laxman E, Taylor A: Ubiquitin and ubiquitin conjugates in human lens. *Exp Eye Res* 55:897-902, 1992
35. Jakobsdottir J, Conley YP, Weeks DE, et al.: C2 and CFB Genes in age-related maculopathy and joint action with CFH and LOC387715 genes. *PLoS One* 3, 2008
36. Javitt JC, Zhou ZY, Maguire MG, et al.: Incidence of exudative age-related macular degeneration among elderly Americans. *Ophthalmology* 110:1534-1539, 2003
37. Johnson LV, Leitner WP, Staples MK, Anderson DH: Complement activation and inflammatory processes in drusen formation and age related macular degeneration. *Exp Eye Res* 73:887-896, 2001
38. Johnson LV, Ozaki S, Staples MK, et al.: A potential role for immune complex pathogenesis in drusen formation. *Exp Eye Res* 70:441-449, 2000
39. Kappahn RJ, Bigelow EJ, Ferrington DA: Age-dependent inhibition of proteasome chymotrypsin-like activity in the retina. *Exp Eye Res* 84:646-654, 2007
40. Katz ML: Factors influencing lipofuscin accumulation in the retinal pigment epithelium of the eye. *Arch Biol* 96:360-360, 1985
41. Katz ML, Drea CM, Eldred GE, et al.: Influence of early photoreceptor degeneration on lipofuscin in the retinal pigment epithelium. *Exp Eye Res* 43:561-573, 1986
42. Katz ML, Eldred GE: Retinal light damage reduces autofluorescent pigment deposition in the retinal pigment epithelium. *Invest Ophthalmol Vis Sci* 30:37-43, 1989
43. Katz ML, Norberg M, Stientjes HJ: Reduced phagosomal content of the retinal pigment epithelium in response to retinoid deprivation. *Invest Ophthalmol Vis Sci* 33:2612-2618, 1992
44. Katz ML, Shanker MJ: Development of lipofuscin-like fluorescence in the retinal pigment epithelium in response to protease inhibitor treatment. *Mech Ageing Dev* 49:23-40, 1989
45. Kijlstra A, La Heij EC, Hendrikse F: Immunological factors in the pathogenesis and treatment of age-related macular degeneration. *Ocul Immunol Inflamm* 13:3-11, 2005
46. Klare N, Seeger M, Janek K, et al.: Intermediate-type 20 S proteasomes in HeLa cells: "Asymmetric" subunit composition, diversity and adaptation. *J Mol Biol* 373:1-10, 2007
47. Klein RJ, Zeiss C, Chew EY, et al.: Complement factor H polymorphism in age-related macular degeneration. *Science* 308:385-389, 2005
48. Li ZM, Arnaud L, Rockwell P, Figueiredo-Pereira ME: A single amino acid substitution in a proteasome subunit triggers aggregation of ubiquitinated proteins in stressed neuronal cells. *J Neurochem* 90:19-28, 2004
49. Louie JL, Kappahn RJ, Ferrington DA: Proteasome function and protein oxidation in the aged retina. *Exp Eye Res* 75:271-284, 2002
50. Luhmann UFO, Robbie S, Munro PMG, et al.: The drusenlike phenotype in aging Ccl2-knockout mice is caused by an accelerated accumulation of swollen autofluorescent subretinal macrophages. *Invest Ophthalmol Vis Sci* 50:5934-5943, 2009
51. Maller JB, Fagerness JA, Reynolds RC, et al.: Variation in complement factor 3 is associated with risk of age-related macular degeneration. *Nature Gen* 39:1200-1201, 2007
52. Mattapallil MJ, Wawrousek EF, Chan CC, et al.: The Rd8 mutation of the Crbl1 gene is present in vendor lines of C57BL/6N mice and embryonic stem cells, and confounds ocular induced mutant phenotypes. *Invest Ophthalmol Vis Sci* 53:2921-2927, 2012
53. Molday RS, Hicks D, Molday L: Peripherin - A rim-specific membrane protein of rod outer segment disks. *Invest Ophthalmol Vis Sci* 28:50-61, 1987
54. Mullins RF, Aptsiauri N, Hageman GS: Structure and composition of drusen associated with glomerulonephritis: implications for the role of complement activation in drusen biogenesis. *Eye* 15:390-395, 2001
55. Murata S, Yashiroda H, Tanaka K: Molecular mechanisms of proteasome assembly. *Nat Rev Mol Cell Biol* 10:104-115, 2009
56. Nozaki M, Raisler BJ, Sakurai E, et al.: Drusen complement components C3a and C5a promote choroidal neovascularization. *Proc Natl Acad Sci U S A* 103:2328-2333, 2006
57. Papermaster DS: Preparation of retinal rod outer segments. *Meth Enzymol* 81:48-52, 1982
58. Rivett AJ, Bose S, Brooks P, Broadfoot KI: Regulation of proteasome complexes by gamma-interferon and phosphorylation. *Biochimie* 83:363-366, 2001
59. Rock KL, Gramm C, Rothstein L, et al.: Inhibitors of the proteasome block the degradation of most cell proteins and the generation of peptides presented on MHC class-I molecules. *Cell* 78:761-771, 1994
60. Sambrook J, Gething MJ: Protein structure - chaperones, paperones. *Nature* 342:224-225, 1989
61. Shang F, Gong X, Palmer HJ, et al.: Age-related decline in ubiquitin conjugation in response to oxidative stress in the lens. *Exp Eye Res* 64:21-30, 1997
62. Spencer KL, Hauser MA, Olson LM, et al.: Protective effect of complement factor B and complement component 2 variants in age-related macular degeneration. *Hum Mol Gen* 16:1986-1992, 2007
63. Spencer KL, Olson LM, Anderson BM, et al.: C3 R102G polymorphism increases risk of age-related macular degeneration. *Hum Mol Gen* 17:1821-1824, 2008
64. Tanaka K, Tanahashi N, Tsurumi C, et al.: Proteasomes and antigen processing. *Adv Immunol*, Vol 64 64:1-38, 1997
65. Vandesompele J, De Preter K, Pattyn F, et al.: Accurate normalization of real-time quantitative RT-PCR data by geometric averaging of multiple internal control genes. *Genome Biol* 3(7):RESEARCH0034 2002
66. Verdoes M, Florea BI, Menendez-Benito V, et al.: A fluorescent broad-spectrum proteasome inhibitor for labeling proteasomes in vitro and in vivo. *Chem Biol* 13:1217-1226, 2006
67. Vessey K, Greferath U, Jobling A, et al.: Ccl2/Cx3Cr1 knock-out mice have inner retinal dysfunction but are not an accelerated model of age-related macular degeneration. *Clin Exp Ophthalmol* 40:131-131, 2012
68. Wassell J, Ellis S, Burke J, Boulton M: Fluorescence properties of autofluorescent granules generated by cultured human RPE cells. *Invest Ophthalmol Vis Sci* 39:1487-1492, 1998
69. Wenzel A, Grimm C, Seeliger MW, et al.: Prevention of photoreceptor apoptosis by activation of the glucocorticoid receptor. *Invest Ophthalmol Vis Sci* 42:1653-1659, 2001
70. Witmer AN, Vrensen GEJM, Van Noorden CJF, Schlingemann RO: Vascular endothelial growth factors and angiogenesis in eye disease. *Prog Ret Eye Res* 22:1-29, 2003
71. Zarepari S, Branham KEH, Li MY, et al.: Strong association of the Y402H variant in complement factor H at 1q32 with susceptibility to age-related macular degeneration. *American Journal of Human Genetics* 77:149-153, 2005
72. Zhang XY, Zhou JL, Fernandes AF, et al.: The proteasome: a target of oxidative damage in cultured human retina pigment epithelial cells. *Invest Ophthalmol Vis Sci* 49:3622-3630, 2008

4

# Involvement of the ubiquitin-proteasome system in the expression of extracellular matrix genes in retinal pigment epithelial cells

J. Emanuel Ramos de Carvalho<sup>a</sup>, Milan T. Verwoert<sup>a</sup>, Ilse M.C. Vogels<sup>a</sup>, Eric A. Reits<sup>b</sup>, Cornelis J.F. Van Noorden<sup>a,b</sup>, Ingeborg Klaassen<sup>a</sup>, Reinier O. Schlingemann<sup>a</sup>

<sup>a</sup> Ocular Angiogenesis Group, Departments of Ophthalmology and Medical Biology, Academic Medical Center, University of Amsterdam, Amsterdam, The Netherlands

<sup>b</sup> Department of Medical Biology, Academic Medical Center, University of Amsterdam, Amsterdam, The Netherlands

## **Abstract**

Emerging evidence suggests that dysfunction of the ubiquitin-proteasome system is involved in the pathogenesis of numerous senile degenerative diseases including retinal disorders. The aim of this study was to assess whether there is a link between proteasome regulation and retinal pigment epithelium (RPE)-mediated expression of extracellular matrix genes. For this purpose, human retinal pigment epithelial cells (ARPE-19) were treated with different concentrations of transforming growth factor- $\beta$  (TGF $\beta$ ), connective tissue growth factor (CTGF), interferon- $\gamma$  (IFN $\gamma$ ) and the irreversible proteasome inhibitor epoxomicin. First, cytotoxicity and proliferation assays were carried out. The expression of proteasome-related genes and proteins was assessed and proteasome activity was determined. Then, expression of fibrosis-associated factors fibronectin (FN), fibronectin EDA domain (FN EDA), metalloproteinase-2 (MMP-2), tissue inhibitor of metalloproteinases-1 (TIMP-1) and peroxisome proliferator-associated receptor-  $\gamma$  (PPAR $\gamma$ ) was assessed. The proteasome inhibitor epoxomicin strongly arrested cell cycle progression and downregulated TGF $\beta$  gene expression, which in turn was shown to induce expression of pro-fibrogenic genes in ARPE-19 cells. Furthermore, epoxomicin induced a directional shift in the balance between MMP-2 and TIMP-1 and was associated with down-regulation of transcription of extracellular matrix genes FN and FN-EDA and up-regulation of the anti-fibrogenic factor PPAR $\gamma$ . In addition, both CTGF and TGF $\beta$  were shown to affect expression of proteasome-associated mRNA and protein levels. Our results suggest a link between proteasome activity and pro-fibrogenic mechanisms in the RPE, which could imply a role for proteasome-modulating agents in the treatment of retinal disorders characterized by RPE-mediated fibrogenic responses.

## Introduction

Age-related macular degeneration (AMD) is a progressive disease of the central retina-choroid tissue complex and one of the leading causes of blindness worldwide.<sup>5</sup> The retinal pigment epithelium (RPE), a polarized monolayer of epithelial cells that separates the neural retina from the vascularized choroid, has been implied to play an important role in the pathogenesis of the disease. Early AMD is characterized by focal drusen deposits in the macula, mostly located between the basal lamina of the RPE and the inner collagenous layer of Bruch's membrane.<sup>101</sup> Drusen contain carbohydrates, zinc and nearly 150 proteins including vitronectin, apolipoproteins E and B, clusterin, connective tissue growth factor (CTGF) and complement system components.<sup>19;84</sup> Advanced AMD is divided into nonexudative or dry AMD which affects 8% of patients and is characterized by macular RPE atrophy and ensuing photoreceptor degeneration, and exudative or neovascular AMD (nAMD) which affects 5% of patients and is characterized by the development of choroidal neovascularization (CNV).<sup>65</sup> CNV may ultimately lead to the development of a fibrous plaque or disciform scar that leads to secondary atrophy of the neurosensory retina and irreversible and untreatable loss of macular visual function.<sup>10; 40; 58; 76; 98</sup> The advent of anti-vascular endothelial growth factor (VEGF) therapy has greatly improved the prognosis of nAMD patients, stabilizing or even improving visual function.<sup>49; 117; 118</sup> Subretinal fibrosis, however, is a common ensuing process of CNV membrane formation, occurring in approximately half of anti-VEGF treated eyes.<sup>10; 21; 98</sup> Fibrosis may be considered as a dysregulated wound healing response to tissue damage.<sup>55; 98; 121</sup> Angiogenesis occurs in this process as an initial trigger for fibrin deposition, tissue repair, oxygen supply and recruitment of inflammatory cells to the wound.<sup>39; 98</sup> In AMD, angiogenesis occurs in the subretinal or sub-RPE space, leading to exudation, hemorrhage and eventually fibrosis. During this process, various types of cells such as RPE cells, glial cells, fibroblasts, myofibroblast-like cells and macrophages infiltrate and/or proliferate, secreting pro-angiogenic and pro-fibrogenic factors that interact with inflammatory cytokines and growth factors. Prevention of visual loss in AMD may therefore depend on the development of successful therapeutic regimens that can halt subretinal fibrosis and preserve the RPE.

The fibrogenic response is stimulated by inflammatory-derived cytokines and growth factors, including transforming growth factor- $\beta$  (TGF $\beta$ ),<sup>113</sup> an ubiquitously expressed growth factor belonging to the large superfamily of activins/bone morphogenetic proteins<sup>100</sup> and connective tissue growth factor (CTGF), a member of the connective tissue growth factor/cysteine-rich 61/nephroblastoma overexpressed (CCN) family of extracellular matrix (ECM) proteins, also known as CCN2.<sup>63; 72</sup> The expression of CTGF is regulated by TGF $\beta$ <sup>9; 77; 120</sup> and, likewise, CTGF has been shown to be an important mediator of TGF $\beta$  signaling and its effects in different cell types.<sup>4; 16; 42; 77; 85; 87; 93; 107; 119</sup> We and others have shown that both TGF $\beta$  and CTGF are major players in the fibrogenic response in the retina.<sup>55; 63; 67; 68; 69; 70; 71; 84; 106; 108; 109</sup>

The ubiquitin-proteasome system (UPS), a multi-catalytic cytoplasmic and nuclear

protein complex present in all eukaryotic cells, is responsible for non-lysosomal proteolysis and thus maintenance of a normal protein homeostasis in cells.<sup>18</sup> Mounting evidence suggests that UPS dysfunction is a major pathogenic mechanism in senile degenerative disorders,<sup>13</sup> including AMD and other ophthalmic conditions.<sup>22; 24; 29; 30; 31; 34; 53; 57; 75; 78; 114</sup> Proteasomes diffuse rapidly in the cytoplasm and nucleus where they encounter intracellular proteins that are appropriately tagged or misfolded. Proteins are tagged by ubiquitination processes and as such recognized by the 19S regulatory particle of the proteasome.<sup>92</sup> Ubiquitin has been shown to be uniformly expressed in the RPE-Bruch's membrane complex of patients afflicted with AMD.<sup>114</sup> The 19S regulatory particle, combined with the 20S catalytic core, forms the standard proteasome. Within the proteasome core, specialized catalytic subunits are responsible for the cleavage of the carboxyl termini of proteins. There are 3 catalytic subunits in the standard proteasome:  $\beta 1$  for acidic amino acids,  $\beta 2$  for basic amino acids, and  $\beta 5$  for hydrophobic amino acids. The standard proteasome may in some instances undergo a change in configuration into the immunoproteasome. This is achieved upon replacement of the constitutive subunits in the standard proteasome by inducible subunits,  $\beta 1i$ ,  $\beta 2i$ , and  $\beta 5i$ .<sup>20; 64</sup> Although uninjured RPE contains a baseline level of immunoproteasome subunits,<sup>22</sup> cellular stress, such as retinal injury by cytotoxic T-lymphocytes,<sup>34</sup> optic nerve trauma,<sup>99</sup> aging mechanisms,<sup>29; 53</sup> complement overactivation,<sup>22</sup> chronic oxidative stress<sup>52</sup> and exposure to pro-inflammatory cytokines<sup>22; 41</sup> may increase the number of active immunoproteasome subunits. Therefore, the ratio between the nascent ( $\beta 1$ ,  $\beta 2$ , and  $\beta 5$ ) and inducible subunits ( $\beta 1i$ ,  $\beta 2i$ , and  $\beta 5i$ ) may be used as a marker of cellular stress.<sup>34; 52; 53</sup> The aim of the present study was to characterize the involvement of the proteasome pathway in TGF $\beta$  and CTGF-mediated expression of ECM genes in RPE cells. Likewise, potential anti-fibrogenic effects of the selective proteasome inhibitor epoxomicin were assessed in ARPE-19 cell cultures.

## **Materials and methods**

### **Culture, maintenance and treatment of ARPE-19 cells**

Experiments were conducted using ARPE-19 cells, a human RPE cell line that has structural and functional properties that are characteristic of RPE cells in vivo. Monolayers of cells cultured on transwell filters reached a transepithelial resistance of 30-40  $\Omega \text{ cm}^2$  after 3 weeks of culture and expressed CRALBP, as detected by RT-PCR. Cells were cultured at 37°C in 5% CO<sub>2</sub> in gelatin-coated T75 cell culture flasks (Corning, Lowell, MA, USA) in Dulbecco Modified Eagle Medium (DMEM; Gibco Life Technologies, Carlsbad, CA, USA), low glucose, pyruvate in the presence of 1% penicillin/streptomycin and 10% fetal calf serum. Cell growth was monitored and medium was changed twice a week. For passaging of cells, TrypLE Express (Invitrogen, Carlsbad, CA, USA) was used and cell suspensions were diluted 3-fold. For experiments, cells were cultured in 6-well plates. Upon confluence, cells were washed once with

phosphate-buffered saline (PBS), serum starved for 24 h and then treated with various concentrations of the selective and irreversible proteasome inhibitor epoxomicin (Sigma-Aldrich, St. Louis, MO, USA), rhCTGF (ProSpec-Tany TechnoGene, Rehovot, Israel), rhTGF $\beta$ 1 (ProSpec) and interferon- $\gamma$  (IFN $\gamma$ ) (PBL Biomedical, Piscataway, NJ, USA). All experiments were performed in triplicate and repeated at least twice.

Gene	GenBank	Forward primer	Reverse Primer	Size (bp)	T <sub>m</sub> (°C)
PSME1	NM_006263	CAGCCCCATGTGGGTGATTATC	GCTTCTCGAAGTTCTTCAGGATGAT	139	82
PSMA7	NM_002792	CCTGGAAGGCCAATGCCATAG	TTTGCCACCTGACTGAACCACTTC	149	82
PSMB5	NM_002797	CCATGATCTGTGGCTGGGATAAG	GGTCATAGGAATAGCCCCGATC	144	83
PSMB8	NM_004159	CTGGAGGCGTTGTCAATATGTACC	GCAGCAGGTCCTGACATCTGTAC	81	76
VEGFA	NM_003375	GGCAGAAGGAGGAGGGCAGAAT	CACCAGGGTCTCGATTGGATGG	91	80
FN1	NM_002026	TGGGACCGTCAGGGAGAAAATG	CAGGAGCAAATGGCACCAGAT	167	82
FN EDA	XM_005246414	GCAGTGACCAACATTGATCGC	ACCCTGTACCTGGAACCTTGCC	110	80
MMP2	NM_004530	GGAATGCCATCCCCGATAACC	CCAGCTTCAGGTAATAGGCACCTT	93	83
TIMP1	NM_003254	ACTTCCACAGGTCCACAACCG	AGGGAAACACTGTGCATTCCTCAC	180	84
PPARG	NM_138712	CCTGCGAAAGCCTTTTGGTGAC	AAACCTGGGCGGTCTCCACT	135	79

**Table 1.** Primer details.

### Protein extraction

Cells were harvested using TrypLE Express (Invitrogen), collected in Eppendorf tubes and centrifuged for 10 min at 400 g. Supernatant was removed and the pellet was suspended in TSDG buffer (10 mM Tris, pH 7.5, 25 mM KCl, 10 mM NaCl, 1.1 mM MgCl<sub>2</sub>, 0.1 mM EDTA, and 8% glycerol), 5 mM ATP and 1x protease inhibitor (Roche Applied Science, Penzberg, Germany).

Cells were lysed with 3 cycles of freezing in liquid nitrogen and thawed at room temp. After centrifugation (15 min, 10,000 g), the protein concentration was determined using a Bradford protein assay (Serva, Heidelberg, Germany). All experiments were performed in triplicate and repeated at least twice.

## Cell cycle and cell viability assays

To assess the viability of healthy ARPE-19 cells and to assess the toxic effects of different stimulants used throughout assays, the PrestoBlue cytotoxicity assay (Invitrogen) was performed according to the manufacturer's instructions. The assays were carried out in 96-well plates (roughly 10,000-25,000 cells per well). After cells were conditioned and washed, PrestoBlue reagent was added to each well. The plates were subsequently incubated at 37 °C for the recommended time period (20-30 min). After incubation, the solution containing PrestoBlue reagent from the wells of the assay plates was transferred to new wells in a 96-well plate, and absorbance was read on a plate reader (Bio-Rad) with the excitation/emission wavelengths set at 570/600 nm.

To evaluate the effects of different stimulants on cell proliferation, the Click-iT EdU Alexa Fluor 488 imaging kit (Invitrogen) was applied according to the protocol provided by the manufacturer. Briefly, ARPE-19 cells at 30-50% confluence were treated with EdU (10  $\mu$ M). EdU was added 2 h prior to the addition of CTGF and TGF $\beta$  (both 24 h incubation) and epoxomicin (16 h incubation). Subsequently, cells were fixed, permeabilized, and click-labeled. As a negative control, untreated cells were used. Following incubation, fluorescence readout was determined using a FACS LSR II (Becton Dickinson, Breda, The Netherlands) to determine percentages of EdU-proliferative cells in S and M phase and EdU-negative quiescent cells in G0 and G1 phase. The experiment was performed in triplicate and repeated twice (n = 2).

## Proteasome activity labeling

Proteasome subunits were labeled in the lysate with 0.5  $\mu$ M activity-based probe BODIPY-epoxomicin for 1 h at 37 °C (BodipyFl-Ahx3L3VS, MV121, provided by H. Overkleeft, Institute of Chemistry, Leiden, The Netherlands)<sup>112</sup> and sample buffer (350 mM Tris-HCl pH 6.8, 10% SDS, 30% glycerol, 6%  $\beta$ -mercaptoethanol, 0.02 % bromophenol blue), added to 20  $\mu$ g protein lysate. Samples were boiled for 5 min and loaded on a 12.5% SDS-PAGE gel. As a positive control, maximal proteasome activity was determined after treatment with IFN $\gamma$  (50 U). After running the proteins on the gel, fluorescence imaging was performed on a Trio Typhoon (GE Medical Systems, Little Chalfont, UK) using the 580 bandpass filter to detect the probe directly on the gel. Proteasome total activity values were normalized according to the total proteasome content in cells as indicated by the levels of the  $\alpha$ 7 subunit of the 20S proteasome (1:1000; MCP72; Enzo Life Sciences, Zandhoven, Belgium). The experiment was performed in triplicate and repeated three times (n = 3).

## Western blot analysis

Proteins were isolated using a 1% Triton X-100 cell lysis buffer (10 mM Hepes, 150 mM NaCl, 10% glycerol, 1.5 mM MgCl<sub>2</sub>, 1 mM EGTA, 1% Triton X-100 and 1x Complete Protease Inhibitors; Roche Biochemicals, Almere, The Netherlands). All samples were run on SDS-PAGE under denaturing conditions. Briefly, 20 µg of protein was loaded on a 12.5% SDS-PAGE gel, and after electrophoresis transferred to nitrocellulose membranes using a Trans-Blot Turbo Transfer System (Bio-Rad). Membranes were incubated overnight or longer at 4°C with a monoclonal antibody against the α7 subunit of the 20S proteasome (1:1000; BML-PW8110-0025, Enzo Life Sciences) and the following polyclonal antibodies: anti-β5 subunit (1:1000; BML-PW8895-0100; Enzo Life Sciences) and anti-β5i subunit (1:1000; ab3329; Abcam, Cambridge, UK). Anti β-actin (1:10,000; a5441; Sigma-Aldrich, St. Louis, MI, USA) was determined for the loading control. Intensity of bands was quantified by densitometric analysis using Odyssey (LI-COR Biosciences, Lincoln, NE, USA). Quantification was performed with Image studio Lite 4.0 (LI-COR). Values were normalized using β-actin (1:10,000; ab8227; Abcam). The experiment was performed in triplicate and repeated three times (n = 3).

## RNA isolation and mRNA quantification

Total RNA was isolated from ARPE-19 cell cultures using TRIzol reagent (Invitrogen) according to the manufacturer's instructions. ARPE-19 cells were stimulated with TGFβ (5 ng, 30 ng or 50 ng for 24 h), CTGF (50 ng or 200 ng for 24 h), epoxomicin (50 nM, 100 nM, 250 nM, 500 nM for 16 h) and IFNγ (50 U for 72 h) in 6-well plates. In addition, in order to assess whether epoxomicin treatment was able to counteract TGFβ-mediated responses, TGFβ-stimulated ARPE-19 cells were treated with 500 nM epoxomicin. Total RNA (1 µg) was treated with DNase I (amplification grade; Life Technologies) and reverse transcribed into first strand cDNA using a Maxima® First Strand cDNA Synthesis Kit (Thermo Scientific, Roskilde, Denmark). Real-time qPCR was performed using a CFX96 system (Bio-Rad) as described previously.<sup>62</sup> Primer details are given in Table 1. Ct-values were converted to absolute amounts with the formula  $2^{-Ct}$  and taken relative to the absolute amounts of control samples, that were set to 1. The experiment was performed in triplicate and repeated three times (n = 3).

## **Enzyme-linked immunosorbent assay (ELISA)**

ARPE-19 cell samples treated with epoxomicin (50 nM, 100 nM, 250 nM, 500 nM for 16 h) and supernatant was collected. Concentrations of activated TGF $\beta$ 2 were determined by Quantikine ELISA assays according to the manufacturer's protocol (R&D Systems, Minneapolis MS, USA). The experiment was performed in triplicate and repeated twice (n = 2).

## **Statistical analysis**

Data are presented as fold change, with a fold change of 1.0 meaning the same level as control samples. Asterisks (\*) indicate a significant change relative to the control samples. Differences between experimental conditions were calculated with one-way or two-way ANOVA with  $P < 0.05$  indicating a statistical difference. Statistical analysis of data was performed using IBM SPSS 20 (SPSS, Chicago, IL, USA).

## **Results**

### **TGF $\beta$ and epoxomicin arrest cell cycle progression**

CTGF (50 and 200 ng for 24 h), TGF $\beta$  (5 and 50 ng for 24 h) and epoxomicin (50 and 500 nM for 16 h) did not induce any significant cytotoxicity in ARPE-19 cells (data not shown). TGF $\beta$  significantly reduced cell proliferation (35-37% cell cycle arrest in G0/G1 phase corresponding to a 20% increase when compared to control), whereas CTGF did not show an anti-proliferative effect (Fig. 1). On the other hand, epoxomicin, a cell-permeable potent and selective irreversible proteasome inhibitor,<sup>79</sup> strongly arrested cell cycle progression (Fig. 1). These results suggest that epoxomicin has significant anti-proliferative effects in ARPE-19 cells.

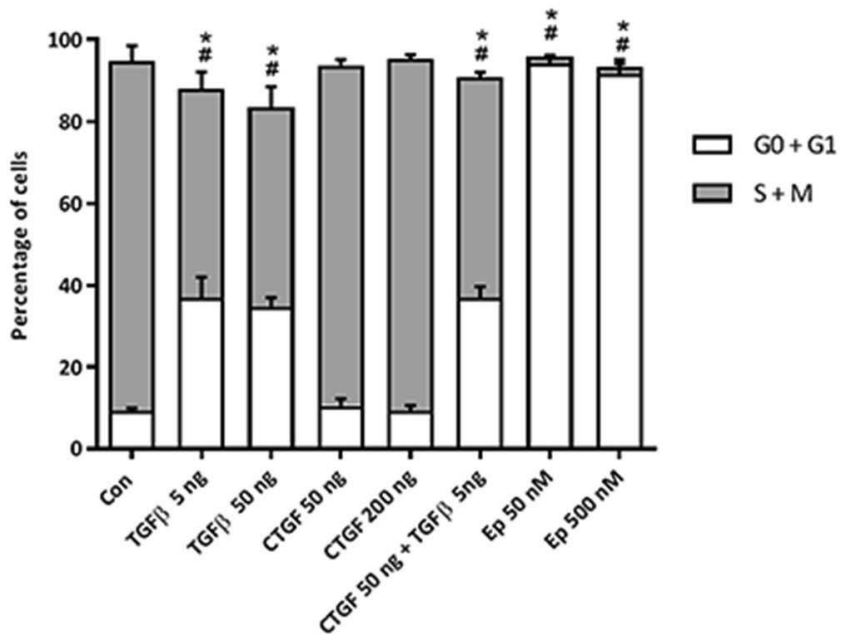


**Fig. 1.** Proliferation of ARPE-19 cells in the presence of TGF $\beta$ , CTGF, TGF $\beta$  and CTGF or epoxomicin expressed as percentage of cells in the S and M phase versus cells in the G0 and G1 phase after flow cytometric analysis of the percentage of cells that had incorporated EdU. \*Significant difference from control of percentage of cells in G0 and G1 phase. #Significant difference from control of percentage of cells in the S and M phase. The experiment was performed in triplicate and repeated twice (n = 2).

### CTGF and TGF $\beta$ affect proteasome subunit mRNA levels

As expected, treatment with high doses of epoxomicin significantly decreased mRNA levels of PA28A and  $\beta$ 5i (data not shown), whereas IFN $\gamma$  increased mRNA levels of  $\alpha$ 7 and  $\beta$ 5 (Fig. 2). CTGF marginally increased mRNA expression of subunit  $\beta$ 5 (Fig. 2). Upon TGF $\beta$  stimulation, mRNA levels of the immunoproteasome subunit  $\beta$ 5i and proteasome regulatory subunit PA28A were decreased.

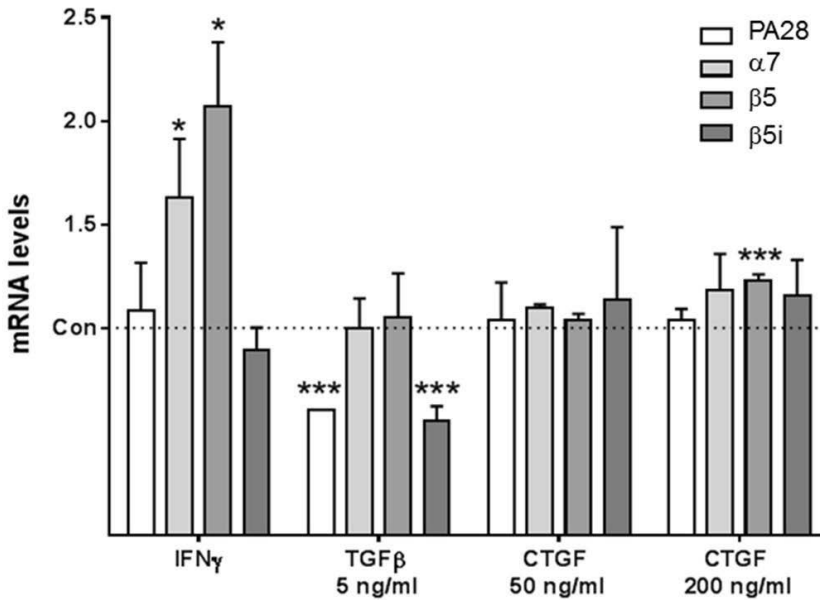


**Fig. 2.** Proteasome mRNA levels induced by IFN $\gamma$ , TGF $\beta$  or CTGF. mRNA levels of PA28 $\alpha$ ,  $\beta$ 5,  $\beta$ 5i, and  $\alpha$ 7 subunits of the proteasome in ARPE-19 cells, after stimulation with IFN $\gamma$ , TGF $\beta$  and low and high concentrations of CTGF. IFN $\gamma$  upregulates mRNA expression of  $\alpha$ 7 and  $\beta$ 5 subunits whereas TGF $\beta$  downregulates mRNA expression of PA28 $\alpha$  and  $\beta$ 5i subunits and CTGF upregulates mRNA expression of  $\beta$ 5 subunit. Values represent mRNA expression levels (mean  $\pm$  SD) relative to untreated control cells. \*, Significant change ( $P < 0.05$ ); \*\*\*, significant change ( $P < 0.001$ ). The experiment was performed in triplicate ( $n = 3$ ).

### CTGF increases the $\beta$ 5i/ $\beta$ 5 ratio

To assess whether the induced changes in expression of proteasome-associated genes was associated with increased protein expression levels of the respective subunits, we performed western blotting on ARPE-19 cells treated with CTGF (50 ng), TGF $\beta$  (50 ng), a combination of CTGF and TGF $\beta$ , and IFN $\gamma$  as positive control (Fig. 3). The ratio of  $\beta$ 5i and  $\beta$ 5 ( $\beta$ 5i/ $\beta$ 5) was taken as a marker of immunoproteasome activation. As expected, IFN $\gamma$  induced maximal immunoproteasome activation, as indicated by a 28-fold change in the  $\beta$ 5i/ $\beta$ 5 ratio (data not shown). Protein levels of  $\beta$ 5i were slightly higher in the presence of CTGF (Fig. 3A,B) which translated in a 19% increased  $\beta$ 5i/ $\beta$ 5 ratio (Fig. 3C), whereas TGF $\beta$  stimulation downregulated the expression level of the proteasome  $\beta$ 5i subunit by 33% (Fig. 3A,B), whereas the  $\beta$ 5i/ $\beta$ 5 ratio was not significantly affected (Fig. 3C).

These results indicate that, to a limited extent, expression of immunoproteasome  $\beta$ 5i subunit protein is upregulated by CTGF and downregulated by TGF $\beta$ .

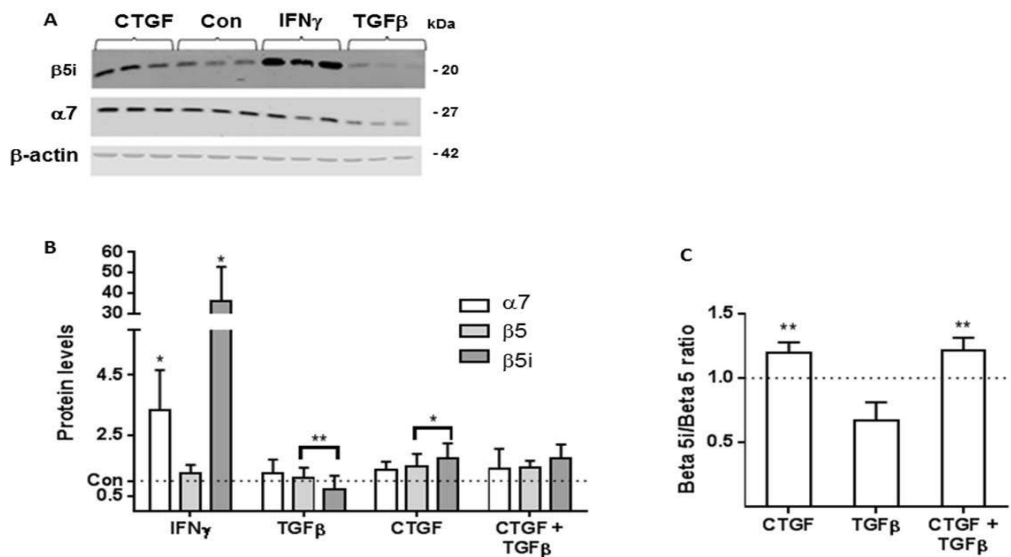


**Fig. 3.** Proteasome-specific subunit protein expression and  $\beta$ 5i: $\beta$ 5 ratios upon IFN $\gamma$ , CTGF, TGF $\beta$  or CTGF and TGF $\beta$  stimulation of ARPE-19 cells. (A) Western blot showing protein levels of  $\beta$ 5i,  $\alpha$ 7 and actin (loading control) in cells that had been incubated with IFN $\gamma$ , CTGF or TGF $\beta$ . (B) Protein levels of  $\beta$ 5 and  $\beta$ 5i subunits were assessed by western blot with actin as loading control and  $\alpha$ 7 subunit as proteasome content control. (C) Quantitative data of the average ratio of  $\beta$ 5i and  $\beta$ 5 relative to control samples after incubation in the presence or absence of CTGF, TGF $\beta$  or CTGF and TGF $\beta$ . Data are expressed as the mean  $\pm$  SD. \*, Significant change ( $P < 0.05$ ); \*\*, significant change ( $P < 0.01$ ). The experiment was performed in triplicate ( $n = 3$ ).

### CTGF upregulates proteasome activity in ARPE-19 cells

To assess whether proteasome gene expression and protein level changes induced by CTGF and TGF $\beta$  affect proteolytic activity of the proteasome, the activity of individual subunits after treatment of cells with CTGF, TGF $\beta$  or IFN $\gamma$  was determined (Fig. 4). IFN $\gamma$ , as expected, induced a substantial increase (4 to 5-fold change,  $P = 0.049$ ) in activity of all subunits. CTGF (50 ng) significantly upregulated the activity of the  $\beta$ 1/ $\beta$ 5i complex (2.6-fold change,  $P = 0.005$ ) and  $\beta$ 5/ $\beta$ 1i complex (1.5-fold change,  $P = 0.026$ ). TGF $\beta$  (30 ng) did not affect proteasomal activity, whereas a combination of CTGF (50 ng) and 6 h later TGF $\beta$  (5 ng) did not induce changes in the activity of the  $\beta$ 1/ $\beta$ 5i and  $\beta$ 5/ $\beta$ 1i complexes.

These results demonstrate that CTGF upregulates the activity of specific proteasome subunits, probably mediated by a change in the configuration of the standard proteasome into the immunoproteasome and up-regulation in mRNA and protein levels of proteasome  $\beta$ 5 and  $\beta$ 5i subunits.

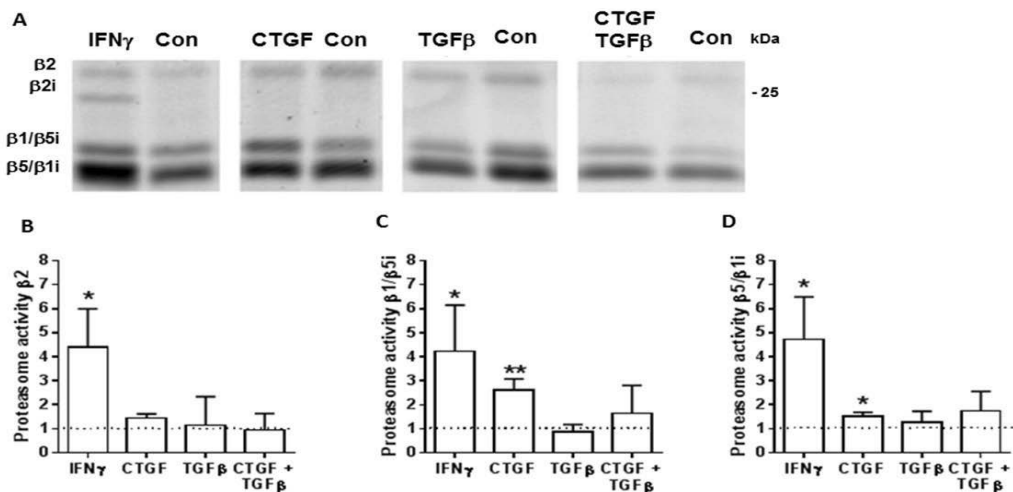


**Fig. 4.** Increased specific proteasome activity upon CTGF stimulation of ARPE-19 cells. (A) After treatment with IFN $\gamma$  (50 U), TGF $\beta$  (50 ng), CTGF (50 ng) or CTGF (50 ng) followed 6 h later by TGF $\beta$  (5 ng), ARPE-19 cells were harvested and proteasomes were labeled with a Bodipy-Ep activity probe. Proteasome activities were assessed by western blotting. Quantitative data of the proteasome activity are presented for proteasome subunit  $\beta$ 2 (B),  $\beta$ 1/ $\beta$ 5i complex (C), and  $\beta$ 5: $\beta$ 1i complex (D). \*, Significant change ( $P < 0.05$ ); \*\*, significant change ( $P < 0.01$ ). The experiment was performed in triplicate ( $n = 3$ ).

### TGF $\beta$ upregulates mRNA levels of ECM-associated genes

In order to characterize the effects of TGF $\beta$  and CTGF on the transcription of ECM-associated genes, we assessed the mRNA levels of CTGF, TGF $\beta$ 1 and TGF $\beta$ 2, VEGF, fibronectin (FN), fibronectin EDA domain (FN EDA), metalloproteinase-2 (MMP-2), tissue inhibitor of metalloproteinases-1 (TIMP-1) and peroxisome proliferator-associated receptor- $\gamma$  (PPAR $\gamma$ ) upon stimulation with CTGF, TGF $\beta$ , and CTGF followed by TGF $\beta$  (Fig. 5).

TGF $\beta$  upregulated mRNA levels of CTGF and VEGF (Fig. 5A). The same effect was observed when ARPE-19 cells were treated with CTGF followed by TGF $\beta$  (data not shown). This effect was dependent on the concentration of TGF $\beta$ , which implies that TGF $\beta$  may be the main mediator of this response in ARPE-19 cells.

With respect to fibrosis-related genes, TGF $\beta$ , but not CTGF, upregulated mRNA levels of FN EDA, FN and MMP-2 (Fig. 5B). Transcript levels of the anti-fibrogenic factor PPAR $\gamma$  were downregulated in the presence of TGF $\beta$  (Fig. 5B). Again, these effects were dependent on the concentration of TGF $\beta$ , irrespective of simultaneous treatment with different concentrations of CTGF (data not shown). These results confirm the role of TGF $\beta$  as a major pro-fibrogenic mediator in RPE cells.

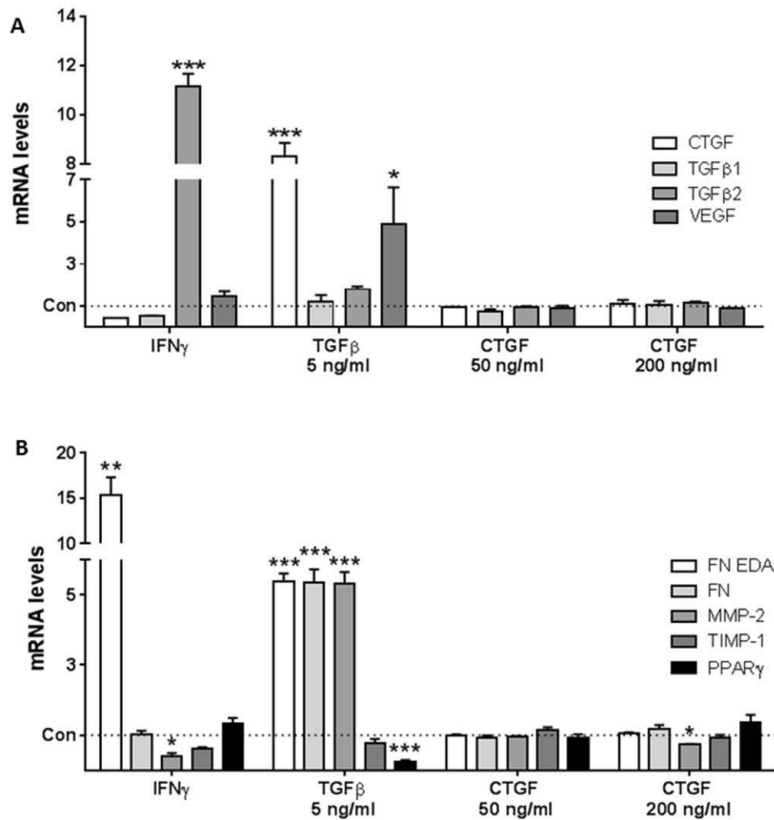


**Fig. 5.** TGF $\beta$  upregulates mRNA expression of CTGF, VEGF and pro-fibrogenic genes and downregulates mRNA expression of the anti-fibrogenic factor PPAR $\gamma$ . After stimulation with TGF $\beta$ , CTGF and IFN $\gamma$ , mRNA levels of (A) CTGF, TGF $\beta$ 1, TGF $\beta$ 2, VEGF and (B) FN, FN EDA, MMP-2, TIMP-1 and PPAR $\gamma$  were assessed in ARPE-19 cells. Values represent mRNA expression levels (mean  $\pm$  SD) relative to untreated control cells. \*, Significant change ( $P < 0.05$ ); \*\*, significant change ( $P < 0.01$ ); \*\*\*, significant change ( $P < 0.001$ ). The experiment was performed in triplicate ( $n = 3$ ).

### Proteasome inhibition by epoxomicin downregulates expression of ECM-associated genes

In order to test the effects of proteasome modulation on mRNA expression of CTGF, TGF $\beta$ 1, TGF $\beta$ 2, VEGF, FN, FN EDA, TIMP-1, MMP-2 and the anti-fibrogenic protein PPAR $\gamma$ , we assessed the effects of different concentrations of epoxomicin and TGF $\beta$  plus epoxomicin (Fig. 6).

Treatment of ARPE-19 cells with epoxomicin resulted in decreased mRNA levels of

TGF $\beta$ 1 and TGF $\beta$ 2 (Fig. 6A). Mean levels of activated TGF $\beta$ 2 protein were strongly reduced (to undetected levels when compared to untreated cells) after treatment of ARPE-19 cells with 50-500 nM epoxomicin (data not shown). At low concentrations (50 and 100 nM), epoxomicin downregulated VEGF mRNA expression (Fig. 6A). Furthermore, treatment with epoxomicin resulted in decreased mRNA levels of FN, FN EDA, TIMP-1 and a corresponding increase in MMP-2 mRNA levels (Fig. 6B). Down-regulation of mRNA expression of TGF $\beta$ 1, TGF $\beta$ 2, FN EDA and VEGF with 500 nM epoxomicin was also observed in TGF $\beta$ -treated ARPE-19 cells. In addition, epoxomicin, alone or in the presence of TGF $\beta$ , downregulated the expression of the anti-fibrogenic mediator PPAR $\gamma$  (Fig. 6B). These results suggest that epoxomicin, even upon TGF $\beta$  secretion, counteracts the pro-fibrogenic transcription effects of TGF $\beta$ .

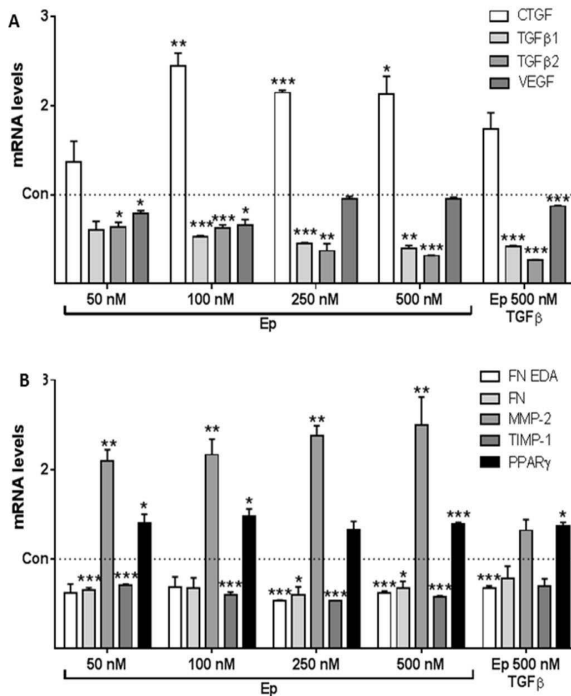


**Fig. 6.** Epoxomicin (Ep) downregulates mRNA expression of TGF $\beta$ 1, TGF $\beta$ 2, VEGF, FN, FN EDA, TIMP-1 and upregulates mRNA expression of CTGF and PPAR $\gamma$ . In the presence of TGF $\beta$ , epoxomicin downregulates mRNA expression of TGF $\beta$ 1, TGF $\beta$ 2, VEGF and FN EDA and expression of PPAR $\gamma$  is upregulated. After treatment with increasing concentrations of epoxomicin in untreated and TGF $\beta$ -treated ARPE-19 cells, mRNA levels of (A) CTGF, TGF $\beta$ 1, TGF $\beta$ 2, VEGF, (B) FN, FN EDA, MMP-2, TIMP-1 and PPAR $\gamma$  were assessed. Values represent mRNA expression levels (mean  $\pm$  SD) relative to untreated control cells. \*, Significant change ( $P < 0.05$ ); \*\*, significant change ( $P < 0.01$ ); \*\*\*, significant change ( $P < 0.001$ ). The experiment was performed in triplicate ( $n = 3$ ).

## Discussion

This study attributes a role to the proteasome pathway in modulation of part of the fibrogenic response of RPE cells which is a multifactorial response dependent on activation and suppression of a myriad of growth factors and cytokines. For the purpose of this study, we selected TGF $\beta$  and CTGF as both are regarded as important mediators of pathological fibrosis in the eye and other organs.<sup>4; 7; 9; 14; 16; 26; 42; 45; 46; 47; 59; 61; 63; 67; 69; 70; 71; 72; 73; 77; 84; 85; 90; 94; 106; 108; 109; 115; 119; 120</sup> Likewise, emerging evidence suggests a link between the fibrogenic response, proteasome modulation and TGF $\beta$  signaling in multiple systemic conditions.<sup>6; 35; 44; 50; 66; 83; 97; 116; 122; 123; 125</sup>

Routine passaging of ARPE-19 cells was used as an in vitro wound response model to study the fibrogenic response in the retina. Epithelial cells (such as the RPE in the retina) are considered to be the major mediators of fibrogenic responses to tissue injury.<sup>73; 98</sup> The RPE is a highly polarized monolayer of epithelial pigmented cells between the choroid and the neurosensory retina that plays a crucial role in the maintenance of visual function.<sup>102</sup> RPE cells proliferate and undergo epithelial-mesenchymal transition (EMT) when dissociated into single cells,<sup>43; 103</sup> whereas sheets of RPE cells in culture preserve their morphology for a longer period of time.<sup>23; 56</sup> Disorganization and extensive damage to the RPE such as during subretinal CNV membrane formation, is a prerequisite for development of subretinal fibrosis.<sup>55</sup> Accordingly, subretinal fibrosis is frequently reported in late stages of nAMD.<sup>10; 21</sup> Fibrosis in other organs such as lung, kidney, liver, skin and heart follows pathogenic pathways similar to subretinal fibrosis development in nAMD.<sup>36; 98</sup> In all these tissues, an intact epithelium is considered protective against fibrosis development.<sup>37</sup> Although the ARPE-19 cell line was deemed appropriate for the purpose of this study, confirmation of the attained results in an in vivo model is warranted. Our study is focused on the fibrogenic response of RPE cells, however, we acknowledge that RPE cells are only one of many other cell types involved in RPE-mediated fibrosis.

Our results demonstrate that CTGF is associated with activation of the proteasome as demonstrated by the increased proteolytic activity of specific proteasome complexes, namely  $\beta$ 1/ $\beta$ 5i and  $\beta$ 5/ $\beta$ 1i. The proteasome activity probe assay is unable to discriminate between the activities of the various proteasome subunits. Nevertheless, it is likely that the observed changes in proteasome activity stem from  $\beta$ 5 and  $\beta$ 5i increased proteolytic activity since these are known to be the rate-limiting subunits at the level of the RPE.<sup>57; 78</sup> Accordingly, these changes in proteasome activity are accompanied by a slight but significant up-regulation in  $\beta$ 5 and  $\beta$ 5i protein expression and  $\beta$ 5 mRNA levels. Conversely, TGF $\beta$  was associated with a down-regulation of  $\beta$ 5i and proteasome regulatory subunit PA28A mRNA levels. Association of PA28A with the 20S catalytic core has been shown to increase proteasome activity.<sup>25; 33; 91</sup> Studies have shown that expression of PA28A tends to decline in aged retina.<sup>29</sup> Unlike the effects of CTGF, proteasome activity assays in the presence of TGF $\beta$  demonstrated no changes in the proteolytic activity of specific proteasome subunit complexes. Recent evidence has

suggested that the immunoproteasome, besides its role in immune surveillance, may be considered as a rescue mechanism in response to cellular stress.<sup>22; 29; 32; 33; 34; 38; 41; 51; 52; 53; 99</sup> Correspondingly, immunoproteasome activation has been demonstrated in the RPE of a mouse model of age-related atrophic degeneration of the RPE<sup>22</sup> as well as in the retina of AMD human donors.<sup>29</sup>

There is converging evidence for TGF $\beta$  as an important pro-fibrogenic factor in the RPE. RPE cells from CNV membranes are strongly immunoreactive for TGF $\beta$ <sup>2</sup> and the RPE has been shown to be an intraocular secretion site of TGF $\beta$ .<sup>104</sup> Elevated mRNA levels of TGF $\beta$  (TGF $\beta$ 2 isoform) have been demonstrated in the RPE-choroid complex and retina of AMD patients<sup>86</sup> and in the vitreous of patients with proliferative vitreoretinopathy and proliferative diabetic retinopathy.<sup>17; 61</sup> TGF $\beta$  can induce EMT of RPE cells in suspension, but fails to do so when RPE cells have well-established cell-cell contacts.<sup>103</sup> Earlier studies have confirmed that TGF $\beta$  is an inducer of a number of growth factors such as CTGF, platelet-derived growth factor, fibroblast growth factors, and VEGF, as well as TGF $\beta$  itself.<sup>48; 110</sup> Likewise, in the presence of a TGF $\beta$  signaling inhibitor (A-83-01), RPE cells were more tolerant to continuous wound response triggers (such as routine passaging of cell cultures) and retained the capacity to acquire a pigmented epithelial morphology.<sup>90</sup> In addition, inhibition of TGF $\beta$  signaling did not prevent RPE differentiation or RPE-mediated wound repair.<sup>90</sup> Semaphorin 3A, a TGF $\beta$  inhibitor, suppressed laser-induced CNV formation in mice by inhibition of the Smad2/3 signaling pathway.<sup>8</sup> These and our results suggest that TGF $\beta$  may be regarded as a fibrogenic marker in disrupted RPE cells and that targeting of TGF $\beta$ -mediated effects may improve wound repair mechanisms. Our results demonstrate that inhibition of the proteasome by epoxomicin is associated with down-regulation of the expression of TGF $\beta$  (both isoforms TGF $\beta$ 1 and TGF $\beta$ 2) and a complete blockage of TGF $\beta$ 2 activity. These two isoforms were studied because in vivo roles and expression of the different TGF $\beta$  isoforms may not be uniform, although in vitro experiments often elicit similar responses.<sup>96</sup>

CTGF expression is regulated by several signaling mechanisms including pathways of TGF $\beta$ /Smad.<sup>74</sup> TGF $\beta$  is a major inducer of CTGF<sup>42; 72</sup> whereas CTGF has been shown to synergistically enhance the effects of TGF $\beta$ . Our results attribute an independent role for CTGF and TGF $\beta$  regarding modulation of the proteasome and fibrogenic response in RPE cells. When given consecutively, the effects of CTGF and TGF $\beta$  on proteasome expression and activity remained unchanged. Similarly, the pro-fibrogenic effects of TGF $\beta$  were not synergized by CTGF treatment. In other cell types, such as in hepatocytes, CTGF has been demonstrated to affect TGF $\beta$  signaling by facilitating binding of TGF $\beta$  to its receptor, down-regulation of the negative feedback loop via Smad7 and inhibition of receptor binding and signaling of the physiological TGF $\beta$  antagonist BMP-7.<sup>42</sup> Likewise, CTGF is considered to be a downstream mediator of certain effects attributed to TGF $\beta$  such as cell proliferation, migration, adhesion, ECM production and EMT.<sup>72</sup> In the eye, CTGF has been shown to accumulate in basal deposits and in Bruch's membrane of early AMD specimens.<sup>84</sup> In accordance with our results, CTGF secretion has been shown to be linked to up-regulation of the expression of the ECM

components FN, laminin and MMP-2 in ARPE-19 cells by mechanisms involving activation of ERK and p38 MAPK signaling pathways.<sup>84</sup> Furthermore, vitreous levels of CTGF correlated strongly with degree of fibrosis in vitreoretinal disorders such as proliferative vitreoretinopathy, proliferative diabetic retinopathy and macular hole.<sup>67</sup> Although expression of CTGF may occur independently of TGF $\beta$  in other retinal cell types,<sup>107</sup> our results suggest CTGF expression may be regulated by TGF $\beta$ -mediated pathways in RPE cells. In the presence of TGF $\beta$ , epoxomicin suppressed the strong up-regulation induced by TGF $\beta$  on CTGF mRNA levels. Since the pro-fibrogenic effects of TGF $\beta$  were more significant than those of CTGF, targeting of the TGF $\beta$  pathway instead of CTGF may have a more substantial anti-fibrogenic effect in subretinal fibrosis. Potential anti-fibrogenic effects were demonstrated after simultaneous treatment of RPE cell cultures with anti-VEGF (bevacizumab) and a CTGF inhibitor, but not when the CTGF inhibitor was administered alone.<sup>7</sup> Targeting the TGF $\beta$  pathway, however, could be less attractive due to concomitant inhibition of anti-inflammatory properties attributed to TGF $\beta$  alongside other important cellular effects.<sup>63</sup> Epoxomicin is one of the most selective inhibitors of the proteasome. Indeed, proteasomal subunits are the only cellular proteins covalently modified by the biotinylated derivatives of epoxomicin with no other proteolytic enzymes inhibited along this process.<sup>60</sup> Treatment of RPE cells with epoxomicin downregulated the expression of the pro-fibrogenic ECM mRNA levels of FN and FN-EDA. In the presence of TGF $\beta$ , epoxomicin still downregulated mRNA expression of FN EDA, VEGF, TGF $\beta$ 1 and TGF $\beta$ 2. FN, a glycoprotein that mediates cellular adhesion and migration of RPE cells, is one of the components of the ECM that is expressed in early phases of fibrosis.<sup>12</sup> FN is composed of two cross-linked subunits. Alternative splicing of the FN gene transcript results in several variants. One isoform (FN-EDA) has an extra domain in cellular FN.<sup>111</sup> Expression of FN-EDA is significantly increased in specific stages of embryonic development, during wound healing processes in the adult and in several fibrogenic diseases.<sup>59</sup>

Furthermore, epoxomicin led to a shift in the balance between MMP-2 and TIMP-1, as mRNA levels of MMP-2 were upregulated and TIMP-1 levels were downregulated. As demonstrated in other cell lines,<sup>27</sup> TGF $\beta$  increased MMP-2 levels without affecting mRNA levels of TIMP-1. RPE cells are known to express MMP-2 and TIMP-1,<sup>1,3</sup> MMPs are involved in a number of normal and physiological responses such as degradation of the basal lamina, remodeling of ECM, connective tissue turnover, angiogenesis and wound repair mechanisms.<sup>27</sup> TIMPs are the natural inhibitors of the functional effects of MMPs.<sup>11</sup> TIMPs have been shown to suppress angiogenesis and promote fibrosis by inhibiting the degradation and processing of ECM proteins.<sup>54</sup> TIMP-1, in particular, has a pivotal role in the fibrogenic response.<sup>54</sup> In vitreous samples of patients afflicted with proliferative diabetic retinopathy, TIMP-1 and MMP-2 were shown to be involved in angiogenesis, with TIMP-1 possibly acting as a natural anti-angiogenic factor.<sup>106</sup> Moreover, the balance between MMPs and TIMPs may be important for the integrity of ECM components, including, amongst others, collagens, vitronectin, fibronectin, laminin, elastin, and proteoglycans, and as such it may be regarded as indicative of

the initiation and progression of the fibrogenic response.<sup>55; 81</sup> The observed changes in the MMP/TIMP-1 balance by epoxomicin may result in improved breakdown of ECM components and subsequent attenuation of RPE cells' migration and fibrogenic responses. On the other hand, these effects on the MMP/TIMP ratio might be transitory, as evidenced in a previous study in which TGF $\beta$  inhibition had a late inhibitory effect on MMP-2 mRNA levels.<sup>6</sup>

The mechanism(s) by which proteasome inhibition protects against fibrosis remain unknown. Our results suggest that PPAR $\gamma$  modulation, alongside inhibition of TGF $\beta$  expression, may explain the anti-fibrogenic properties of epoxomicin. PPAR $\gamma$ , a member of the nuclear receptor superfamily, is a ligand-activated transcription factor known to be involved in various distinct physiological processes including fat cell differentiation, glucose homeostasis, lipid metabolism, aging and inflammatory and immune responses.<sup>95; 105</sup> Furthermore, PPAR $\gamma$  possesses important anti-angiogenic and anti-fibrogenic properties and is involved in the oxidative stress response.<sup>124</sup> In the retina, PPAR $\gamma$  has been shown to be involved in multiple molecular processes, including VEGF-induced choroidal angiogenesis response,<sup>82</sup> photoreceptor renewal process,<sup>28</sup> retinal neuroprotection<sup>126</sup> and protection from oxidative stress.<sup>88; 89</sup> Degradation of PPAR $\gamma$  has been reported to occur via the proteasome.<sup>80</sup> Inhibition of TGF $\beta$  signaling by PPAR $\gamma$  has been attributed to restriction of Smad 2,3 binding to TGF $\beta$ -responsive promoters.<sup>35</sup> After phosphorylation, Smad2,3 forms a complex with other Smad proteins, which in turn facilitate translocation to the nucleus. In the nucleus, coactivators or repressors (such as PPAR $\gamma$ ) regulate the binding of the Smad complex with DNA.<sup>116</sup> Our results demonstrate inhibition of the proteasome was able to counteract TGF $\beta$ -mediated down-regulation of PPAR $\gamma$ , an effect also demonstrated in other cell types.<sup>80</sup> Proteasome inhibitors may also impair late TGF $\beta$ -mediated responses by up-regulation of transcriptional corepressors such as Ski novel gene N and cellular Ski.<sup>116</sup>

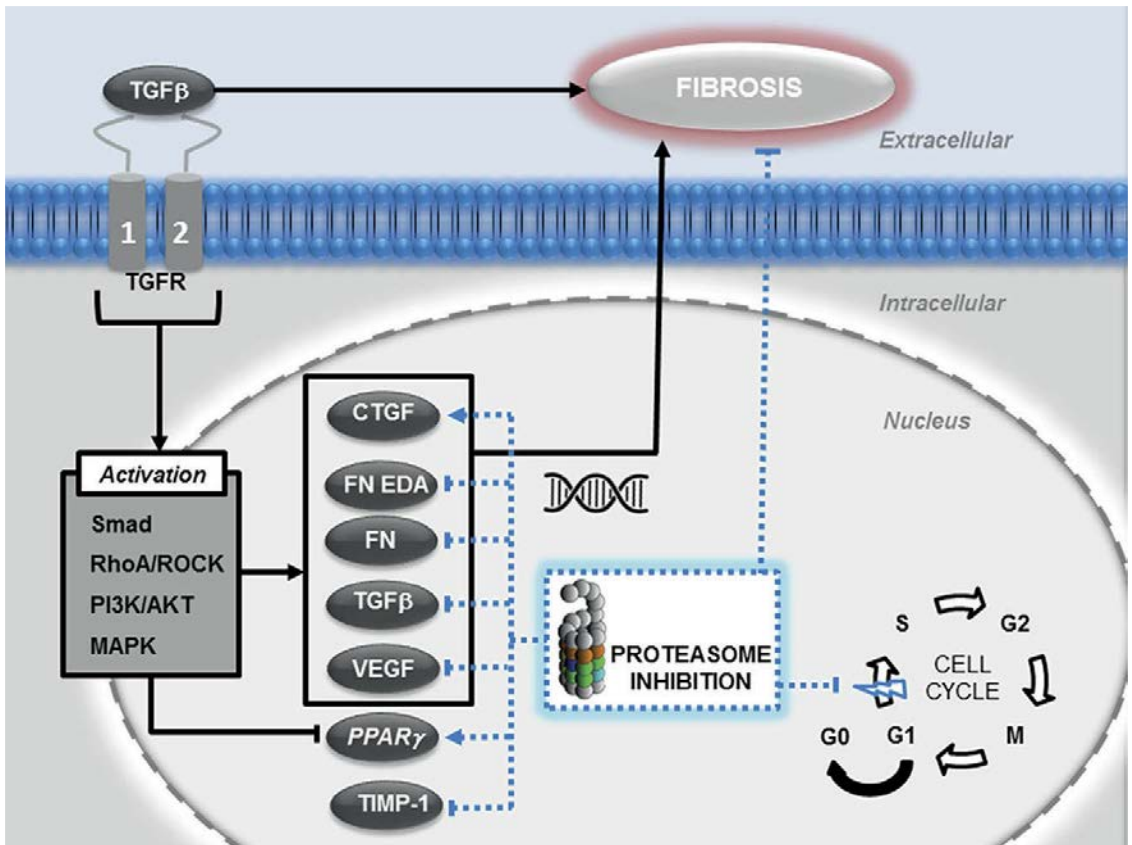


**Fig. 7.** A role for proteasome inhibition in the modulation of fibrogenic mechanisms mediated by RPE cells. TGFβ activates multiple pathways, including the Smad, Rho-like GTPase, PI3K/AKT and MAPK pathways, resulting in the transcription of several pro-fibrogenic genes such as CTGF, FN, FN EDA, VEGF and downregulation of PPARγ transcription. These effects contribute to epithelial-mesenchymal transition processes in RPE cells and initiation of fibrosis. Proteasome inhibition halts cell cycle progression and downregulates transcription of FN, FN EDA, TGFβ, VEGF and TIMP-1 whilst transcription of the anti-fibrogenic factor PPARγ is upregulated, also upon exposure to TGFβ. Effects of proteasome inhibition are depicted as dotted lines. Abbreviations: connective tissue growth factor (CTGF); fibronectin (FN); fibronectin EDA (FN EDA); MAP kinase pathway (MAPK); phosphatidylinositol-3-kinase pathway (PI3K/AKT); retinal pigment epithelial cells (RPE); Rho-like GTPase pathway (RhoA/ROCK); tissue inhibitor metalloproteinase-1 (TIMP-1); transforming growth factor β (TGFβ); transforming growth factor receptor (TGFR); vascular endothelial growth factor (VEGF).

Proteasome inhibition as a means to suppress pathological fibrogenic and proliferative responses has been proposed in various experimental studies. Proteasome inhibitors have been found to inhibit proliferation and induce apoptosis in renal interstitial fibroblasts,<sup>125</sup> prevent development of experimental dermal fibrosis,<sup>66</sup> attenuate diabetic nephropathy<sup>50</sup> and prevent hepatic fibrosis.<sup>15</sup> In Fig. 7 we propose a RPE-mediated fibrosis model and the signaling pathways affected by proteasome inhibition in the RPE.

In summary, we highlight specific fibrogenic and proliferative responses of RPE cells to proteasomal inhibition and propose mechanisms by which proteasomal inhibition may regulate TGF $\beta$  expression and signaling. Accordingly, the anti-fibrogenic properties of proteasome inhibitors may have a therapeutic role in RPE-mediated fibrosis. Further *in vivo* studies are required to elucidate the clinical value of these findings.

### **Acknowledgments**

This study was supported by grants of the Landelijke Stichting voor Blinden en Slechtzienden (LSBS), Stichting Blindenpenning and MaculaFonds; contributed through Uitzicht (Grant UitZicht 2011-15) and Stichting Oogfonds. The publishing of this article was supported by Edward and Marianne Blaauw Fonds voor Oogheelkunde (Edward and Marianne Fund for Ophthalmology). The funding organizations had no participation in the design or conduct of this study, data collection, management, analysis, interpretation, preparation, review or approval of this manuscript.

## References

- Alexander JP, Bradley JMB, Gabourel JD, Acott TS: Expression of matrix metalloproteinases and inhibitor by human retinal pigment epithelium. *Invest Ophthalmol Vis Sci* 31:2520-2528, 1990
- Amin R, Puklin JE, Frank RN: Growth-factor localization in choroidal neovascular membranes of age-related macular degeneration. *Invest Ophthalmol Vis Sci* 35:3178-3188, 1994
- An EK, Lu XN, Flippin J, et al.: Secreted proteome profiling in human RPE cell cultures derived from donors with age related macular degeneration and age matched healthy donors. *J Proteome Res* 6:1615-1615, 2007
- Arnott JA, Nuglozeh E, Rico M, et al.: Connective tissue growth factor (CTGF) is a downstream mediator of transforming growth factor-beta 1 (TGF-beta 1) in osteoblasts. *Mol Biol Cell* 15:417a-417a, 2004
- Augood CA, Vingerling JR, De Jong PTVM, et al.: Prevalence of age-related maculopathy in older Europeans - The European Eye Study (EUREYE). *Arch Ophthalmol* 124:529-535, 2006
- Awasthi N, Wang-Su ST, Wagner BJ: Downregulation of MMP-2 and-9 by proteasome inhibition: A possible mechanism to decrease LEC migration and prevent posterior capsular opacification. *Invest Ophthalmol Vis Sci* 49:1998-2003, 2008
- Bagheri A, Soheili ZS, Ahmadi H, et al.: Simultaneous application of bevacizumab and anti-CTGF antibody effectively suppresses proangiogenic and profibrotic factors in human RPE cells. *Mol Vis* 21:378-390, 2015
- Bai YJ, Liang ST, Yu WZ, et al.: Semaphorin 3A blocks the formation of pathologic choroidal neovascularization induced by transforming growth factor beta. *Mol Vis* 20:1258-1270, 2014
- Black SA, Trackman PC: Transforming growth factor-beta 1 (TGF beta 1) stimulates connective tissue growth factor (CCN2/CTGF) expression in human gingival fibroblasts through a RhoA-independent, Rac1/Cdc42-dependent mechanism - statins with forskolin block TGF beta 1-induced CCN2/CTGF expression. *J Biol Chem* 283:10835-10847, 2008
- Bloch SB, Lund-Andersen H, Sander B, Larsen M: Subfoveal fibrosis in eyes with neovascular age-related macular degeneration treated with intravitreal ranibizumab. *Am J Ophthalmol* 156:116-124, 2013
- Brew K, Dinakarandian D, Nagase H: Tissue inhibitors of metalloproteinases: evolution, structure and function. *Biochim Biophys Acta* 1477:267-283, 2000
- Campochiaro PA, Glaser BM: Platelet-derived growth-factor is chemotactic for human retinal pigment epithelial cells. *Arch Ophthalmol* 103:576-579, 1985
- Carvalho Marques F, Volovik Y, Cohen E: The roles of cellular and organismal aging in the development of late-onset maladies. *Annu Rev Pathol* 10:1-23, 2015
- Chen CL, Liang CM, Chen YH, et al.: Bevacizumab modulates epithelial-to-mesenchymal transition in the retinal pigment epithelial cells via connective tissue growth factor up-regulation. *Acta Ophthalmol* 90:e389-c398, 2012
- Chen H, He YW, Liu WQ, Zhang JH: Rosiglitazone prevents murine hepatic fibrosis induced by *Schistosoma japonicum*. *World J Gastroenterol* 14:2905-2911, 2008
- Chen MM, Lam A, Abraham JA, et al.: CTGF expression is induced by TGF-beta in cardiac fibroblasts and cardiac myocytes: a potential role in heart fibrosis. *J Mol Cell Cardiol* 32:1805-1819, 2000
- Connor TB, Roberts AB, Sporn MB, et al.: Correlation of fibrosis and transforming growth factor-beta type-2 levels in the eye. *J Clin Invest* 83:1661-1666, 1989
- Coux O, Tanaka K, Goldberg AL: Structure and functions of the 20S and 26S proteasomes. *Annu Rev Biochem* 65:801-847, 1996
- Crabb JW, Miyagi M, Gu XR, et al.: Drusen proteome analysis: An approach to the etiology of age-related macular degeneration. *Proc Natl Acad Sci U S A* 99:14682-14687, 2002
- Dahlmann B, Ruppert T, Kuehn L, et al.: Different proteasome subtypes in a single tissue exhibit different enzymatic properties. *J Mol Biol* 303:643-653, 2000
- Daniel E, Toth CA, Grunwald JE, et al.: Risk of scar in the comparison of age-related macular degeneration treatments trials. *Ophthalmology* 121:656-666, 2014
- de Carvalho JER, Klaassen I, Vogels IMC, et al.: Complement factor C3a alters proteasome function in human RPE cells and in an animal model of age-related RPE degeneration. *Invest Ophthalmol Vis Sci* 54:6489-6501, 2013
- Delpriore LV, Glaser BM, Quigley HA, et al.: Morphology of pig retinal pigment epithelium maintained in organ culture. *Arch Ophthalmol* 106:1286-1290, 1988
- Ding QX, Martin S, Dimayuga E, et al.: LMP2 knock-out mice have reduced proteasome activities and increased levels of oxidatively damaged proteins. *Antiox Redox Signal* 8:130-135, 2006
- Dubiel W, Pratt G, Ferrell K, Rechsteiner M: Purification of an 11-S regulator of the multicatalytic protease. *J Biol Chem* 267:22369-22377, 1992
- Duncan MR, Frazier KS, Abramson S, et al.: Connective tissue growth factor mediates transforming growth factor beta-induced collagen synthesis: downregulation by cAMP. *FASEB J* 13:1774-1786, 1999
- Eichler W, Friedrichs U, Thies A, et al.: Modulation of matrix metalloproteinase and TIMP-1 expression by cytokines in human RPE cells. *Invest Ophthalmol Vis Sci* 43:2767-2773, 2002
- Ershov AV, Bazan NG: Photoreceptor phagocytosis selectively activates PPARgamma expression in retinal pigment epithelial cells. *J Neurosci Res* 60:328-337, 2000
- Ethen CM, Hussong SA, Reilly C, et al.: Transformation of the proteasome with age-related macular degeneration. *FEBS Lett* 581:885-890, 2007
- Fernandes AF, Guo WM, Zhang XY, et al.: Proteasome-dependent regulation of signal transduction in retinal pigment epithelial cells. *Exp Eye Res* 83:1472-1481, 2006
- Fernandes AF, Zhou JL, Zhang XY, et al.: Oxidative inactivation of the proteasome in retinal pigment epithelial cells - a potential link between oxidative stress and up-regulation of interleukin-8. *J Biol Chem* 283:20745-20753, 2008
- Ferrington DA, Gregerson DS: Immunoproteasomes: structure, function, and antigen presentation. *Prog Mol Biol Transl Sci* 109:75-112, 2012
- Ferrington DA, Husom AD, Thompson LV: Altered proteasome structure, function, and oxidation in aged muscle. *FASEB J* 19:664-+, 2005
- Ferrington DA, Hussong SA, Roehrich H, et al.: Immunoproteasome responds to injury in the retina and brain. *J Neurochem* 106:158-169, 2008
- Fineschi S, Reith W, Guerne PA, et al.: Proteasome blockade

- exerts an antifibrotic activity by coordinately down-regulating type I collagen and tissue inhibitor of metalloproteinase-1 and up-regulating metalloproteinase-1 production in human dermal fibroblasts. *FASEB J* 20:562-564, 2006
36. Friedlander M: Fibrosis and diseases of the eye. *J Clin Invest* 117:576-586, 2007
  37. Friedman SL, Sheppard D, Duffield JS, Violette S: Therapy for fibrotic diseases: nearing the starting line. *Science Transl Med* 5, 2013
  38. Goldberg AL, Cascio P, Saric T, Rock KL: The importance of the proteasome and subsequent proteolytic steps in the generation of antigenic peptides. *Mol Immunol* 39:147-164, 2002
  39. Greaves NS, Ashcroft KJ, Baguneid M, Bayat A: Current understanding of molecular and cellular mechanisms in fibroplasia and angiogenesis during acute wound healing. *J Dermatol Sci* 72:206-217, 2013
  40. Green WR, Enger C: Age-related macular degeneration histopathologic studies - the 1992 Zimmerman, Lorenz, e Lecture. *Ophthalmology* 100:1519-1535, 1993
  41. Gregerson DS, Lew KL, McPherson SW, et al.: RPE cells resist bystander killing by CTLs, but are highly susceptible to antigen-dependent CTL killing. *Invest Ophthalmol Vis Sci* 47:5385-5394, 2006
  42. Gressner OA, Gressner AM: Connective tissue growth factor: a fibrogenic master switch in fibrotic liver diseases. *Liver Int* 28:1065-1079, 2008
  43. Grisanti S, Guidry C: Transdifferentiation of retinal pigment epithelial cells from epithelial to mesenchymal phenotype. *Invest Ophthalmol Vis Sci* 36:391-405, 1995
  44. Gruendler C, Lin Y, Farley J, Wang TW: Proteasomal degradation of Smad1 induced by bone morphogenetic proteins. *J Biol Chem* 276:46533-46543, 2001
  45. Guo CM, Wang YS, Hu D, et al.: Modulation of migration and Ca<sup>2+</sup> signaling in retinal pigment epithelium cells by recombinant human CTGF. *Curr Eye Res* 34:852-862, 2009
  46. He S, Jin ML, Worpel V, Hinton DR: A role for connective tissue growth factor in the pathogenesis of choroidal neovascularization. *Arch Ophthalmol* 121:1283-1288, 2003
  47. Hinton DR, He S, Jin ML, et al.: Novel growth factors involved in the pathogenesis of proliferative vitreoretinopathy. *Eye* 16:422-428, 2002
  48. Holmes A, Abraham DJ, Sa S, et al.: CTGF and SMADs, maintenance of scleroderma phenotype is independent of SMAD signaling. *J Biol Chem* 276:10594-10601, 2001
  49. Holz FG, Schmitz-Valckenberg S, Fleckenstein M: Recent developments in the treatment of age-related macular degeneration. *J Clin Invest* 124:1430-1438, 2014
  50. Huang W, Yang C, Nan QL, et al.: The proteasome inhibitor, MG132, attenuates diabetic nephropathy by inhibiting SnoN degradation in vivo and in vitro. *Biomed Res Int*, 2014
  51. Husom AD, Peters EA, Kolling EA, et al.: Altered proteasome function and subunit composition in aged muscle. *Arch Biochem Biophys* 421:67-76, 2004
  52. Hussong SA, Kappahn RJ, Phillips SL, et al.: Immunoproteasome deficiency alters retinal proteasome's response to stress. *J Neurochem* 113:1481-1490, 2010
  53. Hussong SA, Roehrich H, Kappahn RJ, et al.: A novel role for the immunoproteasome in retinal function. *Invest Ophthalmol Vis Sci* 52:714-723, 2011
  54. Iredale JP: Tissue inhibitors of metalloproteinases in liver fibrosis. *Int J Biochem Cell Biol* 29:43-54, 1997
  55. Ishikawa K, Kannan R, Hinton DR: Molecular mechanisms of subretinal fibrosis in age-related macular degeneration. *Exp Eye Res*, 2015
  56. Kamei M, Lewis JM, Hayashi A, et al.: A new wound healing model of retinal pigment epithelial cells in sheet culture. *Curr Eye Res* 15:714-718, 1996
  57. Kappahn RJ, Bigelow EJ, Ferrington DA: Age-dependent inhibition of proteasome chymotrypsin-like activity in the retina. *Exp Eye Res* 84:646-654, 2007
  58. Kent D, Sheridan C: Choroidal neovascularization: a wound healing perspective. *Molecular Vision* 9:747-755, 2003
  59. Khankan R, Oliver N, He SK, et al.: Regulation of fibronectin-EDA through CTGF domain-specific interactions with TGF beta 2 and its receptor TGF beta RII. *Invest Ophthalmol Vis Sci* 52:5068-5078, 2011
  60. Kisselev AF, Goldberg AL: Proteasome inhibitors: from research tools to drug candidates. *Chem Biol* 8:739-758, 2001
  61. Kita T, Hata Y, Kano K, et al.: Transforming growth factor-beta 2 and connective tissue growth factor in proliferative vitreoretinal diseases - possible involvement of hyalocytes and therapeutic potential of Rho kinase inhibitor. *Diabetes* 56:231-238, 2007
  62. Klaassen I, Hughes JM, Vogels IMC, et al.: Altered expression of genes related to blood-retina barrier disruption in streptozotocin-induced diabetes. *Exp Eye Res* 89:4-15, 2009
  63. Klaassen I, van Geest RJ, Kuiper EJ, et al.: The role of CTGF in diabetic retinopathy. *Exp Eye Res* 133:37-48, 2015
  64. Klare N, Seeger M, Janek K, et al.: Intermediate-type 20 S proteasomes in HeLa cells: "Asymmetric" subunit composition, diversity and adaptation. *J Mol Biol* 373:1-10, 2007
  65. Klein R, Chou CF, Klein BEK, et al.: Prevalence of age-related macular degeneration in the US Population. *Arch Ophthalmol* 129:75-80, 2011
  66. Koca SS, Ozgen M, Dagli F, et al.: Proteasome inhibition prevents development of experimental dermal fibrosis. *Inflammation* 35:810-817, 2012
  67. Kuiper EJ, de Smet MD, van Meurs JC, et al.: Association of connective tissue growth factor with fibrosis in vitreoretinal disorders in the human eye. *Arch Ophthalmol* 124:1457-1462, 2006
  68. Kuiper EJ, de Smet MD, van Meurs JC, et al.: Connective tissue growth factor in vitreous correlates with fibrosis in vitreoretinal disorders in the human eye. *Invest Ophthalmol Vis Sci* 45:U375-U375, 2004
  69. Kuiper EJ, Van Nieuwenhoven FA, de Smet MD, et al.: The angio-fibrotic switch of VEGF and CTGF in proliferative diabetic retinopathy. *PLoS One* 3(7), e2675 2008
  70. Kuiper EJ, van Zijderveld R, Roestenberg P, et al.: Connective tissue growth factor is necessary for retinal capillary basal lamina thickening in diabetic mice. *J Histochem Cytochem* 56:785-792, 2008
  71. Kuiper EJ, Witmer AN, Klaassen I, et al.: Differential expression of connective tissue growth factor in microglia and pericytes in the human diabetic retina. *Br J Ophthalmol* 88:1082-1087, 2004
  72. Leask A, Abraham DJ: The role of connective tissue growth factor, a multifunctional matricellular protein, in fibroblast biology. *Biochem Cell Biol* 81:355-363, 2003
  73. Leask A, Abraham DJ: TGF-beta signaling and the fibrotic response. *FASEB J* 18:816-827, 2004
  74. Leivonen SK, Hakkinen L, Liu D, Kahari VM: Smad3 and extracellular signal-regulated kinase 1/2 coordinately mediate transforming growth factor-beta-induced expression of connective tissue growth factor in human fibroblasts. *J Invest*

- Dermatol 124:1162-1169, 2005
75. Li Y, Wang YS, Shen XF, et al.: Alterations of activity and intracellular distribution of the 20S proteasome in ageing retinal pigment epithelial cells. *Exp Gerontol* 43:1114-1122, 2008
  76. Lim LS, Mitchell P, Seddon JM, et al.: Age-related macular degeneration. *Lancet* 379:1728-1738, 2012
  77. Liu Y, Liu H, Meyer C, et al.: Transforming growth factor-beta (TGF-beta)-mediated connective tissue growth factor (CTGF) expression in hepatic stellate cells requires Stat3 signaling activation. *J Biol Chem* 288:30708-30719, 2013
  78. Louie JL, Kappahn RJ, Ferrington DA: Proteasome function and protein oxidation in the aged retina. *Exp Eye Res* 75:271-284, 2002
  79. Meng LH, Mohan R, Kwok BHB, et al.: Epoxomicin, a potent and selective proteasome inhibitor, exhibits in vivo antiinflammatory activity. *Proc Natl Acad Sci U S A* 96:10403-10408, 1999
  80. Milam JE, Keshamouni VG, Phan SH, et al.: PPAR-gamma agonists inhibit profibrotic phenotypes in human lung fibroblasts and bleomycin-induced pulmonary fibrosis. *Am J Physiol Lung Cell Mol Physiol* 294:L891-901, 2008
  81. Moses MA, Sudhalter J, Langer R: Identification of an inhibitor of neovascularization from cartilage. *Science* 248:1408-1410, 1990
  82. Murata T, He S, Hangai M, et al.: Peroxisome proliferator-activated receptor-gamma ligands inhibit choroidal neovascularization. *Invest Ophthalmol Vis Sci* 41:2309-2317, 2000
  83. Mutlu GM, Budinger GRS, Wu MH, et al.: Proteasomal inhibition after injury prevents fibrosis by modulating TGF-beta(1) signalling. *Thorax* 67:139-146, 2012
  84. Nagai N, Klimava A, Lee WH, et al.: CTGF is increased in basal deposits and regulates matrix production through the ERK (p42/p44(mapk)) MAPK and the p38 MAPK signaling pathways. *Invest Ophthalmol Vis Sci* 50:1903-1910, 2009
  85. Nagaraja T, Chen L, Balasubramanian A, et al.: Activation of the connective tissue growth factor (CTGF)-transforming growth factor beta 1 (TGF-beta 1) axis in hepatitis C virus-expressing hepatocytes. *PLoS One* 7:e46526, 2012
  86. Newman AM, Gallo NB, Hancox LS, et al.: Systems-level analysis of age-related macular degeneration reveals global biomarkers and phenotype-specific functional networks. *Genome Med* 4, 2012
  87. Parada C, Li JY, Iwata J, et al.: CTGF mediates Smad-dependent transforming growth factor beta signaling to regulate mesenchymal cell proliferation during palate development. *Mol Cell Biol* 33:3482-3493, 2013
  88. Qin S, McLaughlin AP, De Vries GW: Protection of RPE cells from oxidative injury by 15-deoxy-delta12,14-prostaglandin J2 by augmenting GSH and activating MAPK. *Invest Ophthalmol Vis Sci* 47:5098-5105, 2006
  89. Qin SF, Lu YM, Rodrigues GA: Resveratrol protects RPE cells from sodium iodate by modulating PPAR alpha and PPAR delta. *Exp Eye Res* 118:100-108, 2014
  90. Radeke MJ, Radeke CM, Shih YH, et al.: Restoration of mesenchymal retinal pigmented epithelial cells by TGF beta pathway inhibitors: implications for age-related macular degeneration. *Genome Med* 7, 2015
  91. Reidlinger J, Pike AM, Savory PJ, et al.: Catalytic properties of 26 S and 20 S proteasomes and radiolabeling of MBI, LMP7, and C7 subunits associated with trypsin-like and chymotrypsin-like activities. *J Biol Chem* 272:24899-24905, 1997
  92. Reits EAJ, Benham AM, Plougastel B, et al.: Dynamics of proteasome distribution in living cells. *EMBO J* 16:6087-6094, 1997
  93. Ren SY, Babelova A, Moreth K, et al.: Transforming growth factor-beta 2 upregulates sphingosine kinase-1 activity, which in turn attenuates the fibrotic response to TGF-beta 2 by impeding CTGF expression. *Kidney Int* 76:857-867, 2009
  94. Roestenberg P, van Nieuwenhoven FA, Wieten L, et al.: Connective tissue growth factor is increased in plasma of type 1 diabetic patients with nephropathy. *Diabetes Care* 27:1164-1170, 2004
  95. Rosen ED, Spiegelman BM: PPARgamma: a nuclear regulator of metabolism, differentiation, and cell growth. *J Biol Chem* 276:37731-37734, 2001
  96. Saika S: TGF beta pathobiology in the eye. *Lab Invest* 86:106-115, 2006
  97. Sakairi T, Hiromura K, Takahashi S, et al.: Effects of proteasome inhibitors on rat renal fibrosis in vitro and in vivo. *Nephrology* 16:76-86, 2011
  98. Schlingemann RO: Role of growth factors and the wound healing response in age-related macular degeneration. *Graef Arch Clin Exp* 242:91-101, 2004
  99. Schuld NJ, Hussong SA, Kappahn RJ, et al.: Immunoproteasome deficiency protects in the retina after optic nerve crush. *PLoS One* 10:e0126768, 2015
  100. Shi YG, Massague J: Mechanisms of TGF-beta signaling from cell membrane to the nucleus. *Cell* 113:685-700, 2003
  101. Spaide RF, Curcio CA: Drusen characterization with multimodal imaging. *Retina* 30:1441-1454, 2010
  102. Strauss O: The retinal pigment epithelium in visual function. *Physiol Rev* 85:845-881, 2005
  103. Tamiya S, Liu LH, Kaplan HJ: Epithelial-mesenchymal transition and proliferation of retinal pigment epithelial cells initiated upon loss of cell-cell Contact. *Invest Ophthalmol Vis Sci* 51:2755-2763, 2010
  104. Tanihara H, Yoshida M, Matsumoto M, Yoshimura N: Identification of transforming growth-factor-beta expressed in cultured human retinal pigment epithelial cells. *Invest Ophthalmol Vis Sci* 34:413-419, 1993
  105. Tontonoz P, Hu E, Graves RA, et al.: mPPAR gamma 2: tissue-specific regulator of an adipocyte enhancer. *Genes Dev* 8:1224-1234, 1994
  106. Van Geest RJ, Klaassen I, Lesnik-Oberstein SY, et al.: Vitreous TIMP-1 levels associate with neovascularization and TGF-beta 2 levels but not with fibrosis in the clinical course of proliferative diabetic retinopathy. *J Cell Commun Signal* 7:1-9, 2013
  107. Van Geest RJ, Klaassen I, Vogels IMC, et al.: Differential TGF-beta signaling in retinal vascular cells: a role in diabetic retinopathy? *Invest Ophthalmol Vis Sci* 51:1857-1865, 2010
  108. Van Geest RJ, Leeuwis JW, Dendooven A, et al.: Connective tissue growth factor is involved in structural retinal vascular changes in long-term experimental diabetes. *J Histochem Cytochem* 62:109-118, 2014
  109. Van Geest RJ, Lesnik-Oberstein SY, Tan HS, et al.: A shift in the balance of vascular endothelial growth factor and connective tissue growth factor by bevacizumab causes the angioblastic switch in proliferative diabetic retinopathy. *Br J Ophthalmol* 96:587-590, 2012
  110. Van Obberghen-Schilling E, Roche NS, Flanders KC, et al.: Transforming growth factor-beta-1 positively regulates its own expression in normal and transformed cells. *J Biol Chem* 263:7741-7746, 1988
  111. Vartio T, Laitinen L, Narvanen O, et al.: Differential expression

- of the ED sequence-containing form of cellular fibronectin in embryonic and adult human tissues. *J Cell Sci* 88:419-430, 1987
112. Verdoes M, Florea BI, Menendez-Benito V, et al.: A fluorescent broad-spectrum proteasome inhibitor for labeling proteasomes in vitro and in vivo. *Chem Biol* 13:1217-1226, 2006
  113. Verrecchia F, Mauviel A: Transforming growth factor-beta signaling through the Smad pathway: Role in extracellular matrix gene expression and regulation. *J Invest Dermatol* 118:211-215, 2002
  114. Viiri J, Amadio M, Marchesi N, et al.: Autophagy activation clears ELAVL1/HuR-mediated accumulation of SQSTM1/p62 during proteasomal inhibition in human retinal pigment epithelial cells. *PLoS One* 8:e69563, 2013
  115. Watanabe D, Takagi H, Suzuma K, et al.: Expression of connective tissue growth factor and its potential role in choroidal neovascularization. *Retina* 25:911-918, 2005
  116. Weiss CH, Budinger GR, Mutlu GM, Jain M: Proteasomal regulation of pulmonary fibrosis. *Proc Am Thorac Soc* 7:77-83, 2010
  117. Witmer AN, Blaauwgeers HG, Weich HA, et al.: Expression patterns of VEGF receptors in healthy human and monkey retina: Involvement of VEGFs in physiology? *Invest Ophthalmol Vis Sci* 43:U654-U654, 2002
  118. Witmer AN, Vrensen GFJM, Van Noorden CJF, Schlingemann RO: Vascular endothelial growth factors and angiogenesis in eye disease. *Prog Ret Eye Res* 22:1-29, 2003
  119. Wu S, Duncan M, Grotendorst G, Bancalari E: Connective tissue growth factor (CTGF) mediates transforming growth factor-beta (TGF-beta) induced inhibition of lung morphogenesis in mouse embryo. *Pediatr Res* 53:29a-29a, 2003
  120. Wunsche C, Koch A, Goldschmeding R, et al.: Transforming growth factor beta 2 (TGF-beta(2))-induced connective tissue growth factor (CTGF) expression requires sphingosine 1-phosphate receptor 5 (S1P(5)) in human mesangial cells. *Biochim Biophys Acta* 1851:519-526, 2015
  121. Wynn TA: Common and unique mechanisms regulate fibrosis in various fibroproliferative diseases. *J Clin Invest* 117:524-529, 2007
  122. Zhang F, Laiho M: On and off: proteasome and TGF-beta signaling. *Exp Cell Res* 291:275-281, 2003
  123. Zhang F, Monkkonen M, Roth S, Laiho M: Proteasomal activity modulates TGF-beta signaling in a gene-specific manner. *FEBS Lett* 527:58-62, 2002
  124. Zhang S, Gu H, Hu N: Role of peroxisome proliferator activated receptor gamma in ocular diseases. *J Ophthalmol* 2015:275435, 2015
  125. Zhu BB, Jin YM, Han L, et al.: Proteasome inhibitor inhibits proliferation and induces apoptosis in renal interstitial fibroblasts. *Pharmacol Rep* 65:1357-1365, 2013
  126. Zhu J, Zhang J, Ji M, et al.: The role of peroxisome proliferator-activated receptor and effects of its agonist, pioglitazone, on a rat model of optic nerve crush: PPARgamma in retinal neuroprotect neuroprotection. *PLoS One* 8:e68935, 2013



5

# Modulation of the proteasome pathway by nano-curcumin and curcumin in retinal pigment epithelial cells

J. Emanuel Ramos de Carvalho<sup>a</sup>, Milan T. Verwoert<sup>a</sup>, Ilse M.C. Vogels<sup>a</sup>, Sabine Schipper-Krom<sup>b</sup>, Cornelis J.F. Van Noorden<sup>a,b</sup>, Eric A. Reits<sup>b</sup>, Ingeborg Klaassen<sup>a</sup>, Reinier O. Schlingemann<sup>a</sup>

<sup>a</sup> Ocular Angiogenesis Group, Departments of Ophthalmology and Medical Biology, Academic Medical Center, University of Amsterdam, Amsterdam, The Netherlands

<sup>b</sup> Department of Medical Biology, Academic Medical Center, University of Amsterdam, Amsterdam, The Netherlands

## Abstract

Curcumin has multiple biological effects including modulation of protein homeostasis by the ubiquitin-proteasome system. The purpose of this study was to assess the in vitro cytotoxic and oxidative effects of nano-curcumin and standard curcumin and characterize their effects on proteasome regulation in retinal pigment epithelial (RPE) cells.

Viability, cell cycle progression and reactive oxygen species (ROS) production were determined after treatment with nano-curcumin or curcumin. Subsequently, the effects of nano-curcumin and curcumin on proteasome activity and the gene and protein expression of proteasome subunits PA28 $\alpha$ ,  $\alpha$ 7,  $\beta$ 5 and  $\beta$ 5i were assessed.

Nano-curcumin (5 – 100  $\mu$ M) did not show significant cytotoxicity or anti-oxidative effects against H<sub>2</sub>O<sub>2</sub>-induced oxidative stress, whereas curcumin ( $\geq$  10  $\mu$ M) was cytotoxic and a potent inducer of ROS production. Both nano-curcumin and curcumin induced changes in proteasome-mediated proteolytic activity characterized by increased activity of the proteasome subunits  $\beta$ 2 and  $\beta$ 5i/ $\beta$ 1 and reduced activity of the  $\beta$ 5/ $\beta$ 1i proteasome subunits. Likewise, nano-curcumin and curcumin affected mRNA and protein levels of household and immunoproteasome subunits.

Our results demonstrate that nano-curcumin is less toxic to RPE cells and less prone to induce ROS production when compared to curcumin. Both nano-curcumin and curcumin increase proteasome-mediated proteolytic activity. These results suggest that nano-curcumin may be regarded as a proteasome-modulating agent of limited cytotoxicity for RPE cells.

## Introduction

Curcumin [1,7-bis-(4-hydroxy-3-methoxyphenyl)-1,6-heptadiene-3,5-dione] is the orange and water-insoluble pigment extract of turmeric, the rhizome of *Curcuma longa*. The therapeutic potential of curcumin is currently being tested in several clinical trials after promising preliminary observations.<sup>52</sup> In ophthalmology, curcumin has been proposed as a potential therapeutic strategy for several conditions including dry eye syndrome,<sup>10</sup> diabetic retinopathy,<sup>23; 63</sup> diabetic retinal neurodegeneration,<sup>35</sup> age-related macular degeneration (AMD),<sup>39</sup> retinitis pigmentosa<sup>59; 67</sup> and light and oxidative stress-induced retinal neurodegeneration.<sup>42</sup> On the other hand studies have warned of potential toxic effects of curcumin in RPE cells<sup>1; 27; 64</sup> and retinal endothelial cells.<sup>53</sup>

One of the major obstacles precluding implementation of curcumin as a therapeutic agent lies in its poor bioavailability in organs and tissues other than the gastrointestinal tract when given orally.<sup>3</sup> At present, various curcumin formulations with improved bioavailability, including nanoparticles as drug delivery systems, are being assessed.<sup>69</sup> However, these different formulations do not have comparable biological properties.<sup>49</sup> Recently, a highly absorptive curcumin dispersed with polysaccharide nanoparticles (Theracurmin® or nano-curcumin) has been developed. The oral absorption efficacy of

nano-curcumin is approximately 40-fold higher than that of curcumin in both rats and humans<sup>58</sup> which implies that this specific formulation is taken up by epithelial cells of the gastrointestinal tract and reaches blood levels that are deemed sufficient for bioactivity.<sup>46; 47</sup> The ubiquitin-proteasome system (UPS), a multicatalytic cytoplasmic and nuclear protein complex present in all eukaryotic cells, is responsible for nonlysosomal proteolysis.<sup>11</sup> Intracellular proteins are tagged for proteolysis after binding of ubiquitin moieties. These are then recognized by the 19S regulatory particle of the proteasome which in combination with the 20S catalytic core forms the household or 'classical' proteasome.<sup>55</sup> Within the proteasome core, 3 different specialized catalytic subunits are responsible for proteolytic cleavage of the carboxyl end of proteins:  $\beta$ 1 for acidic amino acids (caspase-like),  $\beta$ 2 for basic amino acids (trypsin-like) and  $\beta$ 5 for hydrophobic amino acids (chymotrypsin-like). In response to stress and injury, the household proteasome changes its configuration into the so-called immunoproteasome which is formed upon replacement of the constitutive subunits by inducible subunits,  $\beta$ 1i,  $\beta$ 2i, and  $\beta$ 5i.<sup>13; 34</sup> Therefore, the ratio between the household ( $\beta$ 1,  $\beta$ 2, and  $\beta$ 5) and inducible subunits ( $\beta$ 1i,  $\beta$ 2i, and  $\beta$ 5i) is a marker of cellular stress.<sup>21; 28; 29</sup>

Curcumin has been shown to modulate proteasome function by different mechanisms. First, the carbonyl carbons of curcumin interact with the hydroxyl group of the amino-terminal threonine residue of the  $\beta$ 5 subunit which results in suppression of the protease activity of the proteasome and in particular that of the chymotrypsin-like ( $\beta$ 5) subunit.<sup>45</sup> Second, curcumin inhibits COP9 signalosome (CSN) kinase activity.<sup>26; 66</sup> CSN is a protein complex that controls the stability of many proteins such as ligases<sup>60</sup> and possesses structural similarities with multiple non-ATPase subunits of the 19S lid of the proteasome.<sup>25</sup> The ligases interact with specific ubiquitin-conjugating enzymes in the ubiquitination of substrates and as such, CSN functions as an interface between signal transduction and ubiquitin-dependent proteolysis.<sup>6</sup> Third, curcumin has been shown to inhibit ubiquitin isopeptidases, a family of cysteine proteases (deubiquitinases) responsible for the re-utilization of ubiquitin by the 26S proteasome.<sup>22; 45; 50</sup> Curcumin contains an  $\alpha,\beta$ -unsaturated ketone and 2 sterically accessible  $\beta$ -carbons that mediate inhibition of these enzymes.<sup>25</sup>

A steadily increasing number of clinical trials are investigating the potential therapeutic effects of curcumin and other curcuminoid formulations. Yet, recent reports of curcumin-mediated retinal cytotoxicity<sup>1; 27; 53; 64</sup> could imply that chronic intake of curcumin negatively affects retinal function. The aims of the present study are: 1) to assess and characterize cytotoxic and oxidative effects of nano-curcumin and standard curcumin in RPE cells *in vitro*; and 2) to investigate the *in vitro* effects of nano-curcumin and standard curcumin on proteasome expression and activity in RPE cells so to ascertain whether nano-curcumin and/or standard curcumin can be used as proteasome-modulating agents in retinal disorders.

## **Methods**

### **Culture, maintenance and treatment of ARPE-19 cells**

Experiments were conducted using ARPE-19 cells, a human RPE cell line that has structural and functional properties that are characteristic of RPE cells *in vivo*. Cells were cultured at 37°C in 5% CO<sub>2</sub> in gelatin-coated T75 cell culture flasks (Corning, Lowell, MA, USA) in Dulbecco Modified Eagle Medium (DMEM; Gibco Life Technologies, Carlsbad, CA, USA), low glucose, pyruvate in the presence of 1% penicillin/streptomycin and 10% fetal calf serum. Cell growth was monitored and medium was changed twice a week. For passaging of cells, TrypLE Express (Invitrogen, Carlsbad, CA, USA) was added for trypsinization of the cells and cell suspensions were diluted 3-fold. For experiments, cells were cultured in 6-well plates. Upon confluence, cells were washed once with phosphate-buffered saline (PBS) and were serum starved for 24 h and then treated with different concentrations of nano-curcumin (Theracurmin®, kindly provided by Dr. C. Tamura, Theravalues, Tokyo, Japan) and curcumin (kindly provided by Dr. E. Kemper, Academic Medical Center, Amsterdam, The Netherlands). Both nano-curcumin and standard curcumin were dissolved in sterile water.

### **Protein extraction**

Cells were harvested using TrypLE Express (Invitrogen), collected in Eppendorf tubes and centrifuged for 10 min at 400 g. Supernatant was removed and the pellet was suspended in TSDG buffer (10 mM Tris, pH 7.5, 25 mM KCl, 10 mM NaCl, 1.1 mM MgCl<sub>2</sub>, 0.1 mM EDTA, and 8% glycerol), 5 mM ATP and 1x protease inhibitor (Roche Applied Science, Penzberg, Germany).

Cells were lysed by 3 cycles of freezing in liquid nitrogen and thawing at room temp. After centrifugation (15 min; 10,000 g), protein concentrations were determined using a Bradford protein assay (Serva, Heidelberg, Germany).

### **Cytotoxicity assays of ARPE-19 cells treated with nano-curcumin or curcumin**

To assess the viability of untreated ARPE-19 cells and possible toxic effects of nano-curcumin and curcumin, the PrestoBlue cytotoxicity assay (Invitrogen) was performed according to the manufacturer's instructions. A resazurin-based compound is converted to its reduced form in intact mitochondria of viable cells which causes a shift in its color and fluorescence which can be quantified fluorometrically or spectrophotometrically. The assay was also used to test whether nano-curcumin or curcumin (incubated for 3 h at concentrations of 20 μM) affect cytotoxicity of 0 – 1000 μM hydrogen peroxide (H<sub>2</sub>O<sub>2</sub>) in ARPE-19 cells.

The assays were carried out in 96-well plates (10,000-25,000 cells per well). After cell adherence and subsequent washing, PrestoBlue reagent was added to each well. The plates were then incubated at 37 °C for 20-30 min. After incubation, the solution containing PrestoBlue was transferred from the wells of the assay plates to new wells in a 96-well plate, and absorbance was read on a plate reader (Bio-Rad, Hercules, CA) with the excitation and emission wavelengths set at 570 and 600 nm, respectively.

### **Cell cycle progression analysis of ARPE-19 cells treated with nano-curcumin or curcumin**

In order to evaluate the effects of nano-curcumin and curcumin on cell proliferation, the Click-iT EdU Alexa Fluor 488 imaging kit (Invitrogen) was applied according to the protocol provided by the manufacturer. Briefly, ARPE-19 cells at 30-50% confluence were incubated for 24 h with EdU (5-ethynyl-2'-deoxyuridine). EdU, an analog of thymidine, is incorporated into newly synthesized DNA and subsequently recognized by azide dyes via a copper-mediated ("click") reaction. As a negative control, untreated cells were assessed and fluorescence per cell was detected using a FACS LSRII cell sorter (Becton Dickinson, Breda, The Netherlands).

### **Analysis of reactive oxygen species production of ARPE-19 cells treated with nano-curcumin or curcumin**

Production of ROS in ARPE-19 cells in the presence or absence of nano-curcumin or curcumin (5 or 50  $\mu\text{M}$ ) was determined by a FACS-based ROS detection kit (Enzo Life Sciences, Plymouth Meeting, PA, USA) using a modified protocol <sup>24</sup>. Untreated and unstained cells were used alongside a positive control with a ROS inducer (200  $\mu\text{M}$  pyocyanine) and a negative control with a ROS inhibitor (5 mM N-acetyl-L-cysteine). ARPE-19 cells incubated with nano-curcumin or curcumin were also treated with 250  $\mu\text{M}$   $\text{H}_2\text{O}_2$ . After staining for 30 min, fluorescence per cell in the green channel was detected using a FACS LSRII.

### **Measurement of activity of proteasome subunit complexes after treatment of RPE cells with nano-curcumin or curcumin**

We investigated the potential role of nano-curcumin and curcumin as proteasome-modulating agents in RPE cells. Proteasome catalytic subunits  $\beta_2$ ,  $\beta_5\text{i}/\beta_1$  and  $\beta_5/\beta_1\text{i}$  were labeled in lysates of ARPE-19 cells treated with nano-curcumin or curcumin (5, 50 or 100  $\mu\text{M}$ ) with a 0.5  $\mu\text{M}$  activity-based probe BODIPY-epoxomicin for 1 h at 37°C (BodipyFl-Ahx3L3VS, MV121, provided by Prof. Dr. H. Overkleeft, Institute of

Chemistry, Leiden, The Netherlands)<sup>68</sup> Sample buffer (350 mM Tris-HCl pH 6.8, 10% SDS, 30% glycerol, 6%  $\beta$ -mercaptoethanol, 0.02 % bromophenol blue) was added to 20  $\mu$ g protein lysate. The samples were boiled for 5 min and loaded on a 12.5% SDS-PAGE gel. After running the proteins on the gel, fluorescence imaging was performed using a Trio Typhoon (GE Medical Systems, Little Chalfont, UK) and a 580 bandpass filter to detect the probe directly on the gel. Proteasome total activity values were normalized on the basis of the total proteasome content in cells as indicated by the levels of the  $\alpha$ 7 subunit of the 20S proteasome (1:1000; MCP72; Enzo Life Sciences).

### **Western blot analysis of isolated RPE proteasome subunits after treatment with nano-curcumin or curcumin**

Western blot analysis was performed as described previously.<sup>57</sup> After treatment with nano-curcumin or curcumin (5, 10, 20 or 50  $\mu$ M at 24 h and 50  $\mu$ M at 48 h), 20  $\mu$ g of RPE cell protein was loaded on a 12.5% SDS-PAGE gel, and, after electrophoresis, transferred to nitrocellulose membranes and semi-quantitatively analyzed. Membranes were incubated overnight or longer at 4°C in the presence of either a monoclonal antibody against the  $\alpha$ 7 subunit of the 20S proteasome (1:1000; BML-PW8110-0025; Enzo Life Sciences) or one of the following polyclonal antibodies: anti- $\beta$ 5 subunit of the 20S proteasome (1:1000; BML-PW8895-0100; Enzo Life Sciences) or anti- $\beta$ 5i subunit of the 20S proteasome (1:1000; ab3329; Abcam, Cambridge, UK). Anti- $\beta$ -actin (1:10000; a5441; Sigma-Aldrich, St. Louis, MO, USA) was used as loading control. Intensity of bands was quantified by absorbance measurements using Odyssey (LI-COR Biosciences, Lincoln, NE, USA). Quantification was performed with Image studio Lite 4.0 (LI-COR). Values were normalized using  $\beta$ -actin (1:10,000; ab8227; Abcam).

### **RNA isolation and quantification of RPE mRNA after treatment with nano-curcumin or curcumin**

Real-time quantitative PCR experiments were performed to detect mRNA expression of proteasome regulatory subunit PA28A (PSME),  $\alpha$ 7 (PSMA7),  $\beta$ 5 (PSMB5) and  $\beta$ 5i (PSMB8) proteasome subunits. Total RNA was isolated from ARPE-19 cell cultures (6 samples per experimental condition) according to the manufacturer's instructions (TRIzol; Invitrogen) after incubation with low (10  $\mu$ M) and high (50  $\mu$ M) concentrations of nano-curcumin and curcumin.

Total RNA (1  $\mu$ g) was treated with DNase I (amplification grade; Life Technologies) and reverse transcribed into first strand cDNA using a Maxima® First Strand cDNA Synthesis Kit (Thermo Scientific, Roskilde, Denmark). Real-time qPCR was performed using a CFX96 system (Bio-Rad) as described previously.<sup>33</sup> Primer details are presented in

Table 1. The specificity of the primers was confirmed by NCBI BLAST. The presence of a single PCR product was verified by both the presence of a single melting temperature peak and detection of a single band of the expected size on 3% agarose gel. Non-template controls were included to verify the method and the specificity of the primers. Ct values were converted to arbitrary absolute amounts ( $2^{-Ct} \times 1E^{12}$ ).

Gene	GenBank	Forward primer	Reverse Primer	Size (bp)	T <sub>m</sub> (°C)
<i>PSME1</i>	NM_006263	CAGCCCCATGTGGGTGATTATC	GCTTCTCGAAGTTCTTCAGGATGAT	139	82
<i>PSMA7</i>	NM_002792	CCTGGAAGGCCAATGCCATAG	TTTGCCACCTGACTGAACCACTTC	149	82
<i>PSMB5</i>	NM_002797	CCATGATCTGTGGCTGGGATAAG	GGTCATAGGAATAGCCCCGATC	144	83
<i>PSMB8</i>	NM_004159	CTGGAGGCGTTGTCAATATGTACC	GCAGCAGGTCACTGACATCTGTAC	81	76

**Table 1.** Primer details. Gene nomenclature, GenBank accession code, primer sequences, predicted size and melting temperature (T<sub>m</sub>) of the amplified product.

### Statistical analysis

Data are presented as fold change, with a fold change of 1.0 meaning the same level as control samples. Asterisks (\*) indicate a significant change relative to the control samples. Differences between experimental conditions were calculated with one-way or two-way ANOVA with  $P < 0.05$  indicating a statistical difference. Statistical analysis of data was performed using IBM SPSS 20 (SPSS, Chicago, IL, USA).

## Results

### Nano-curcumin is not cytotoxic for ARPE-19 cells, unlike curcumin, and does not protect against oxidative stress-mediated cell death

We found no significant cytotoxicity in ARPE-19 cells exposed to 5 – 100  $\mu\text{M}$  of nano-curcumin, whereas exposure to 20 – 100  $\mu\text{M}$  curcumin induced significant cytotoxic effects (Fig. 1a). Hardly any viable cells were found after incubation in the presence of 50 – 100  $\mu\text{M}$  curcumin (Fig. 1a). Next, we assessed whether nano-curcumin or curcumin prevented cytotoxic effects of 125 – 1000  $\mu\text{M}$   $\text{H}_2\text{O}_2$ . The highest non-lethal concentration of curcumin (20  $\mu\text{M}$ ) was selected and compared to a similar concentration of nano-curcumin. As expected, exposure to  $\text{H}_2\text{O}_2$  caused dose-dependent cytotoxicity in ARPE-19 cells (Fig. 1b). Pretreatment with 20  $\mu\text{M}$  curcumin increased cytotoxicity of RPE cells when exposed to 125  $\mu\text{M}$   $\text{H}_2\text{O}_2$ , contrary to nano-curcumin which showed a mild protective effect ( $P = 0.04$ ). This effect subsided upon higher concentrations of  $\text{H}_2\text{O}_2$  (Fig. 1b).

Curcumin (15  $\mu\text{M}$ ) treatment of RPE cells was previously shown to arrest cell cycle progression with arrest in the G1 phase.<sup>64</sup> Cell cycle progression of ARPE-19 cells exposed to 0 – 50  $\mu\text{M}$  nano-curcumin did not show significant changes in cell proliferation (Fig. 2).

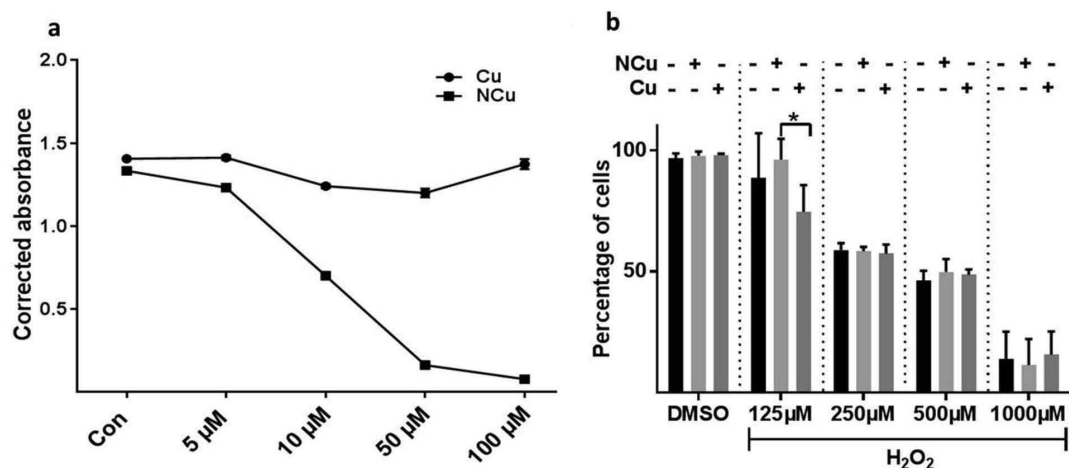


**Fig. 1.** Effects of nano-curcumin and curcumin on cell viability. Viability assays of ARPE-19 cells exposed to 0-100  $\mu\text{M}$  nano-curcumin (NCu) or standard curcumin (Cu) in the presence of 0-1000  $\mu\text{M}$   $\text{H}_2\text{O}_2$ . (a) Concentration-dependent effects of nano-curcumin and curcumin on ARPE-19 cell viability expressed as corrected absorbance. (b) Cytotoxicity effects of 0 - 1000  $\mu\text{M}$   $\text{H}_2\text{O}_2$  on ARPE-19 cells after pretreatment or not with nano-curcumin or curcumin (20  $\mu\text{M}$  for 3 h) and expressed as mean percentage of viable cells  $\pm$  standard deviation (SD) when compared to untreated cells (0.1% DMSO). \*, Significant change ( $P < 0.05$ ).

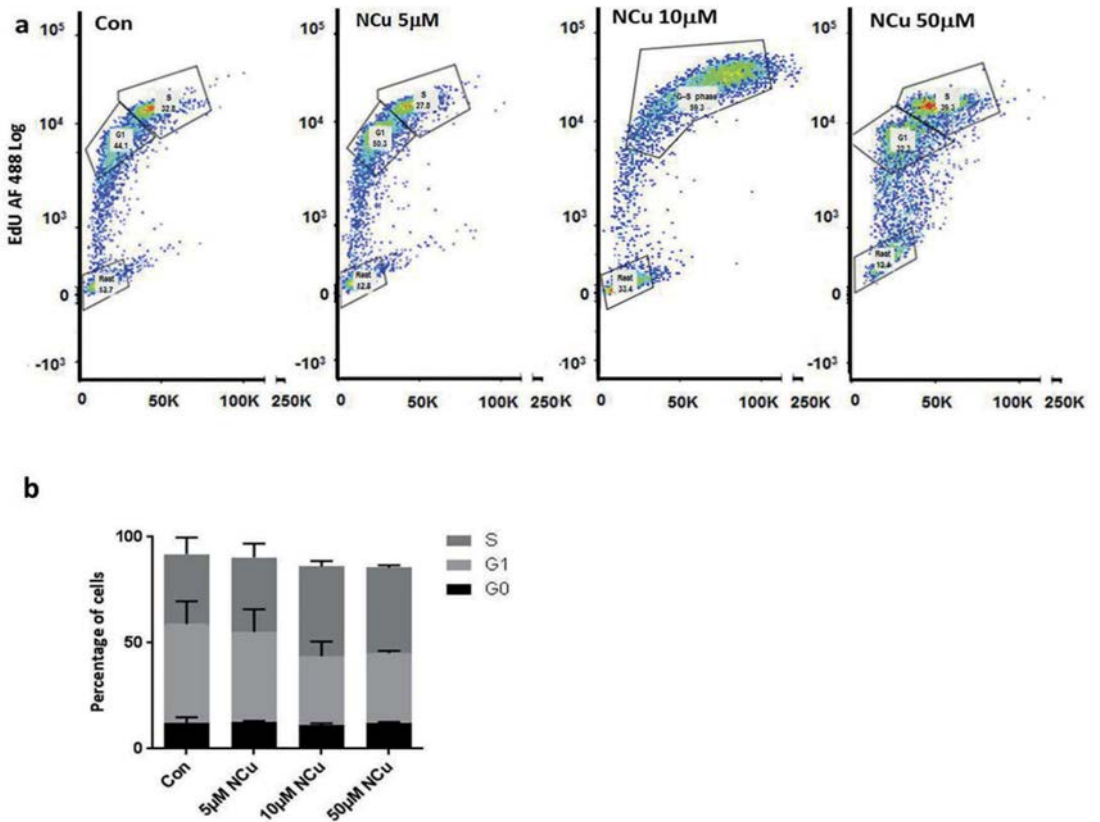


**Fig. 2.** Effects of nano-curcumin on cell proliferation. Cell proliferation assay of ARPE-19 cells in the presence of 0-50  $\mu\text{M}$  nano-curcumin (NCu) expressed as percentage of cells in the G0, G1 and S phase after flow cytometric analysis of fluorescence of incorporated EdU. (a) Contour plot of cells treated with 0, 5, 10 and 50  $\mu\text{M}$  nano-curcumin. (b) Percentages of cells in the different cell phases. Con: control, untreated. No significant differences were found.

### **Nano-curcumin is a mild ROS inducer and curcumin is a potent ROS inducer in ARPE-19 cells**

ROS cause damage to cells and extracellular matrix.<sup>7</sup> Because of the high retinal consumption of oxygen, the retina may be particularly susceptible to oxidative damage. Accordingly, oxidative stress has been linked to several senile degenerative diseases of the retina, including AMD.<sup>5; 17; 72</sup>

We determined the percentage of ROS-producing cells in the presence of 5 or 50  $\mu\text{M}$  nano-curcumin or curcumin and assessed whether the oxidative effects of nano-curcumin differed from those of standard curcumin. We demonstrated strong ROS-inducing effects

in cells treated with both low and high concentrations of curcumin, comparable to the pro-oxidative effects of pyocyanin which was used as a positive control (Fig. 3). These effects may explain the dose-dependent cytotoxic effects of curcumin as shown in Fig. 1. Low concentrations of nano-curcumin (5  $\mu\text{M}$ ) did not induce significant ROS production, with ROS levels that were comparable to those obtained in unstained untreated cells. High doses of nano-curcumin (50  $\mu\text{M}$ ) induced significant ROS production. These results attribute significant pro-oxidative effects to curcumin whereas low concentrations of nano-curcumin do not lead to significant ROS production in RPE cells.

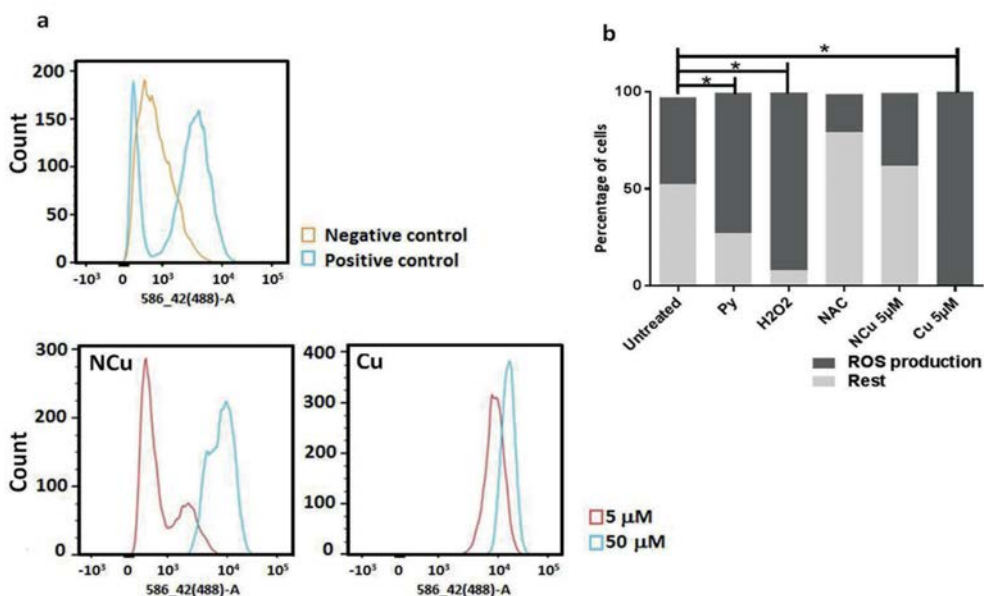


**Fig 3.** Effects of nano-curcumin and curcumin on ROS production. Detection of ROS production in ARPE-19 cells treated with low (5  $\mu\text{M}$ ) and high (50  $\mu\text{M}$ ) concentrations of nano-curcumin (NCu) or curcumin (Cu). Cells were also treated with 200  $\mu\text{M}$  pyocyanin (general ROS inducer, positive control) and 5 mM N-acetyl-L-cysteine (general ROS inhibitor, negative control). Cells were stained with ROS-ID™ Total ROS Detection Reagent and analyzed using flow cytometry. Untreated cells were used as a control. Cell debris was ungated. The cells with increased levels of oxidative stress demonstrate bright green fluorescence in the presence of the ROS detection solution. (a) Histogram plots showing cells incubated in the presence of pyocyanin (positive control), N-acetyl-L-cysteine (negative control), nano-curcumin and curcumin. Bright green fluorescence depicting increased ROS production (as observed in the positive control) is demonstrated in cells incubated with 50  $\mu\text{M}$  nano-curcumin and 5 and 50  $\mu\text{M}$  curcumin. (b) Percentage of cells actively producing ROS as compared to untreated cells, incubated with pyocyanin, H<sub>2</sub>O<sub>2</sub>, N-acetyl-L-cysteine, nano-curcumin and curcumin. All 3 independent experiments were carried out in triplicate. Py: pyocyanin; NAC: N-acetyl-L-cysteine; ROS: reactive oxygen species. \*, Significant change ( $P < 0.05$ ).

## **Nano-curcumin and curcumin affect the proteolytic activity of proteasome catalytic subunits $\beta 2$ , $\beta 5i/\beta 1$ and $\beta 5/\beta 1i$**

In order to assess whether nano-curcumin and curcumin affect the proteolytic activity of individual proteasome subunits, a proteasome activity-based probe assay was conducted. At present, available proteasome activity probes are unable to distinguish  $\beta 1$  and  $\beta 5$  from their inducible counterparts  $\beta 1i$  and  $\beta 5i$  because the subunits run identically in gels (Fig. 4a). Nano-curcumin, at low concentrations (5  $\mu\text{M}$ ) downregulates activity of the  $\beta 5/\beta 1i$  proteasome catalytic subunits (0.57 fold-change,  $P = 0.0009$ ). Intermediate (10  $\mu\text{M}$ ) and high (50  $\mu\text{M}$ ) concentrations of nano-curcumin upregulate activity of the  $\beta 2$  (1.27 fold-change,  $P = 0.03$  and 1.55 fold-change,  $P = 0.0005$ , respectively) and  $\beta 5i/\beta 1$  proteasome catalytic subunits (1.46 fold-change,  $P = 0.01$  and 1.54 fold-change,  $P = 0.04$ , respectively). Intermediate (10  $\mu\text{M}$ ) and high (50  $\mu\text{M}$ ) concentrations of curcumin downregulate activity of the  $\beta 5/\beta 1i$  proteasome catalytic subunits (0.89 fold-change,  $P = 0.009$  and 0.92 fold-change,  $P = 0.015$ , respectively). Similar to the effects observed with nano-curcumin, high (50  $\mu\text{M}$ ) concentrations of curcumin upregulate activity of the  $\beta 2$  and  $\beta 5i/\beta 1$  proteasome catalytic subunits (1.55 fold-change,  $P = 0.002$  and 1.40 fold-change,  $P = 0.035$ , respectively) (Fig. 4b). These results suggest that nano-curcumin and curcumin have dose-dependent effects on proteasome-mediated proteolytic activity.

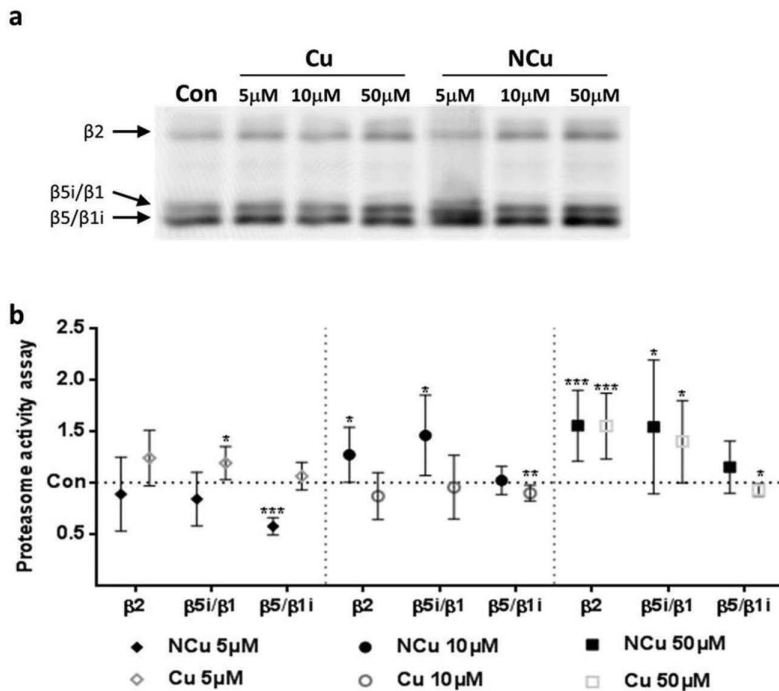


**Fig. 4.** Effects of nano-curcumin and curcumin on proteasome activity. Proteasome activity labeling in ARPE-19 cell lysates. (a) After treatment with 0 - 50  $\mu\text{M}$  nano-curcumin (Ncu) or curcumin (Cu), ARPE19 cells were harvested and proteasomes were labeled with a proteasome activity probe. Activity of the  $\beta_2$ ,  $\beta_1/\beta_{5i}$  and  $\beta_5/\beta_{1i}$  proteasome catalytic subunits was determined by fluorescence imaging. (b) Data are expressed as mean proteolytic activity per subunit complex  $\pm$  SD, normalized on the basis of the total proteasome content in cells as indicated by the levels of proteasome a7 subunit. \*, Significant change ( $P < 0.05$ ); \*\*, ( $P < 0.01$ ); \*\*\*, ( $P < 0.001$ ).

#### Nano-curcumin induces a mild activation of the immunoproteasome

Protein levels of proteasome subunits  $\beta_5$ ,  $\beta_{5i}$  and  $\alpha_7$  were assessed after treatment with various concentrations of nano-curcumin and curcumin. The ratio between  $\beta_{5i}$  and  $\beta_5$  was calculated at two time-points as a marker of immunoproteasome activation. Protein levels of the  $\alpha_7$  subunit of the 20S proteasome depict the total pool of proteasomes in cells. Nano-curcumin (50  $\mu\text{M}$  and 20  $\mu\text{M}$ ) increased protein levels of proteasome subunits  $\beta_{5i}$  (mean 1.6 fold-change,  $P = 0.01$ , data not shown) resulting in an increased  $\beta_{5i}/\beta_5$  ratio when compared to unstimulated and curcumin-treated RPE cells (Fig. 5a). This effect is both concentration and time-dependent, as shown in Fig. 5b which demonstrates that at 48 h, the increase in  $\beta_{5i}/\beta_5$  ratio is overturned. Neither nano-curcumin or curcumin had a significant effect on the protein levels of the proteasome  $\alpha_7$  subunits (Fig. 5c). These results suggest nano-curcumin may induce a mild activation of the immunoproteasome.

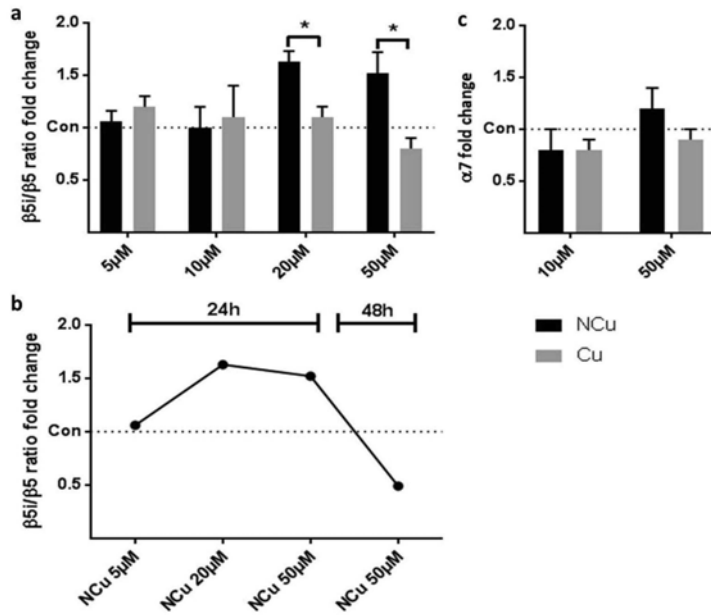


**Fig 5.** Effects of nano-curcumin and curcumin on proteasome protein expression. Protein levels of proteasome subunits  $\beta 5$ ,  $\beta 5i$  and  $\alpha 7$  were assessed by western blot with actin expression as loading control after incubation of ARPE-19 cells with 0-50  $\mu\text{M}$  nano-curcumin (NCu) and curcumin (Cu) at 24 h ( $\beta 5$ ,  $\beta 5i$  and  $\alpha 7$ ) and 48 h ( $\beta 5$  and  $\beta 5i$ ). (a)  $\beta 5i/\beta 5$  ratio fold-change at 24 h induced by 0-50  $\mu\text{M}$  nano-curcumin and curcumin, corrected for actin and relative to control samples. (c) Time-dependent effects in the  $\beta 5i/\beta 5$  ratio fold-change induced by nano-curcumin at 24 and 48 h, corrected for actin and relative to control samples. (c) Protein levels of proteasome subunit  $\alpha 7$  induced by 0-50  $\mu\text{M}$  nano-curcumin and curcumin, corrected for actin and relative to control samples. Data are expressed as the mean  $\pm$  SD. \*, Significant change ( $P < 0.05$ ).

### Nano-curcumin and curcumin affect the transcription of proteasome-related genes

In order to assess whether nano-curcumin affected the transcription of proteasome-related genes, qPCR of ARPE-19 cells treated for 72 h with 10 and 50  $\mu\text{M}$  nano-curcumin and curcumin was performed. Fig. 6 shows that 10  $\mu\text{M}$  nano-curcumin increased gene expression of proteasome  $\alpha 7$  subunit (1.56 fold-change,  $P = 0.03$ ),  $\beta 5$  subunit (1.18 fold-change,  $P = 0.004$ ) and  $\beta 5i$  subunit (1.11 fold-change,  $P = 0.04$ ). Ten  $\mu\text{M}$  curcumin increased gene expression of proteasome PA28A subunit (1.12 fold-change,  $P = 0.01$ ) and  $\beta 5i$  subunit (1.10 fold-change,  $P = 0.04$ ). Higher concentrations of curcumin (50  $\mu\text{M}$ ) strongly reduced gene expression of all proteasome-related genes ( $P < 0.001$ ). These results show that nano-curcumin and curcumin have concentration-dependent effects on the transcription of proteasome-related genes.

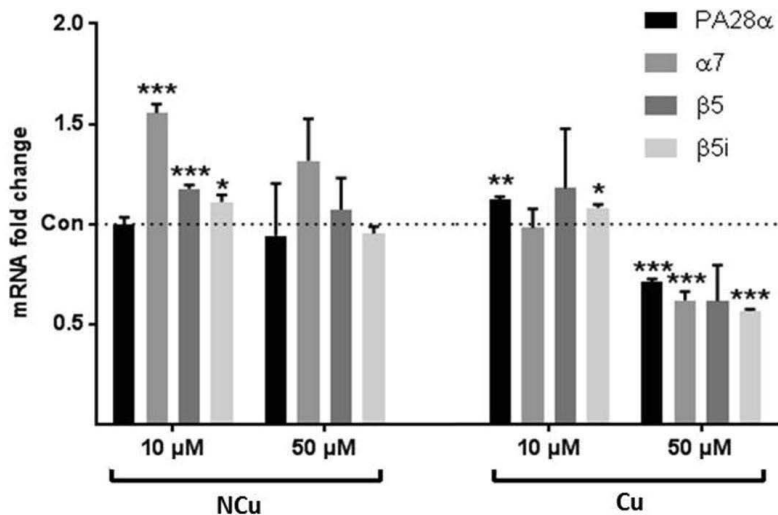


**Fig 6.** Expression of proteasome-related genes after exposure to nano-curcumin and curcumin. mRNA levels of proteasome subunits PA28α, α7, β5 and β5i after 72 h treatment with nano-curcumin and curcumin (0, 10, 50 μM). mRNA expression levels of α7 are increased upon stimulation with 10 μM nano-curcumin, and mRNA levels of β5 and β5i is increased upon stimulation with 10 μM and 50 μM nano-curcumin. Treatment with 10 μM curcumin increased PA28α and β5i mRNA levels. Higher concentrations of curcumin (50 μM) significantly decreased mRNA levels of PA28α, α7 and β5i. Values represent mRNA expression levels ± SD relative to untreated control cells. \*, Significant change ( $P < 0.05$ ); \*\*, ( $P < 0.01$ ); \*\*\*, ( $P < 0.001$ ).

## Discussion

The results of the present study support the pleiotropic properties of curcumin and its various formulations. A consensus regarding the effects of curcumin in the retina is yet to be reached. In this study, it was demonstrated that nano-curcumin induces changes in proteasome modulation with limited cytotoxic effects at low concentrations, suggesting that this specific formulation is a safe alternative for the retina and RPE. While some studies praise the beneficial effects of curcumin and its potential use in ophthalmic disease, others advocate retinal function ought to be monitored during the intake of curcumin. Such contradictory findings may be explained by the hormetic properties attributed to curcumin, i.e., toxic at high doses but able to exert adaptive stress responses at low doses.<sup>43; 44</sup> In addition, certain biological effects of curcuminoids may depend on the specific formulation of curcumin used.<sup>30; 49</sup> For instance, the number of methoxy groups dictates the anti-oxidative potency of curcumin,<sup>31</sup> whereas the presence of phospholipids in curcumin formulations affect its biological activity.<sup>12</sup> Therefore, the use of different curcuminoid formulations may lead to contradictory results.

Our study demonstrates significant cytotoxic effects of standard curcumin in RPE cells at concentrations higher than 20  $\mu\text{M}$ . These findings are in accordance with the data of previous studies in which curcumin exhibited pro-apoptotic effects in RPE cells at concentrations  $\sim 20 \mu\text{M}$ .<sup>1;27</sup> These concentrations are in the same concentration range that is supposed to be effective in cancer cells.<sup>9; 48; 54; 56; 62</sup> On the other hand, nano-curcumin, a formulation of curcumin dispersed with polysaccharide nanoparticles, shows no major cytotoxicity in RPE cells. The differences in cytotoxicity between these two formulations may be explained by the smaller size and increased solubility of nano-curcumin compared to curcumin. Curcumin, hardly soluble in water, forms particles that are larger than 20  $\mu\text{M}$  in diameter in aqueous solutions whereas the average diameter of nano-curcumin in aqueous solutions is 100 times smaller (0.2  $\mu\text{M}$ ).<sup>58</sup> Furthermore, nano-curcumin is more stable due to the formation of an amorphous state upon hydrogen bonding.<sup>70</sup> This suggests that monitoring of retinal toxicity is not required during concomitant intake of nano-curcumin, this may not hold true for standard curcumin.

The uptake of nano-curcumin in RPE cells was not investigated in this study, however, other studies provide evidence that RPE cells, similar to other cell lines, take up nano-curcumin. Epithelial cells of the gastrointestinal tract of rat and human *in vivo* absorb nano-curcumin over 40 times more efficiently when compared to standard curcumin<sup>47; 58</sup> and nano-curcumin has been shown to be taken up by esophageal cancer cells and non-cancer cells *in vitro*.<sup>46</sup>

Our findings suggest that curcumin-mediated cytotoxicity may be partly caused by increased ROS production. Contrary to curcumin, low concentrations of nano-curcumin (5  $\mu\text{M}$ ) do not induce ROS production in non-oxidative conditions and have significant less pro-oxidative effects when compared to curcumin. Higher concentrations of nano-curcumin, however, significantly induce ROS production. These results are in accordance with data from previous studies with other cell lines in which curcumin was shown to possess rapid ROS-inducing effects.<sup>4; 8; 65</sup> In contrast, other *in vitro* ARPE-19 cell studies attribute anti-oxidative properties to curcumin in aging and  $\text{H}_2\text{O}_2$ -mediated oxidative stress.<sup>71; 73</sup> According to our findings, and taking into account both the conflicting and supportive results reported in other studies, it appears that curcumin exhibits both pro- and anti-oxidative properties. Differences in experimental setup, such as concentration and stimulation time may partly explain the contradictory findings.

Recent evidence shows that dysfunction of the UPS may contribute to the pathogenesis of several eye diseases<sup>16; 18; 19; 20; 21; 29; 32; 38; 41</sup> Modulation of this pathway remains, however, an unexplored therapeutic target in retinal degenerative diseases. Curcumin has been reported to affect proteasome activity and expression in a biphasic dose-dependent manner.<sup>25</sup> Low concentrations of curcumin were found to upregulate proteasome activity whereas high concentrations of curcumin inhibited proteasome activity.<sup>25</sup> Chymotrypsin-like activity was increased by 46% after treatment of human keratinocytes with curcumin (up to 1  $\mu\text{M}$  for 24 h) whereas higher concentrations of curcumin were inhibitory. At 10  $\mu\text{M}$ , proteasome activity decreased to 46% of its initial value.<sup>2</sup> A possible explanation for this biphasic mechanism could be the fact that curcumin is both pro-oxidative and

anti-oxidative. Mild or transient oxidative stress upregulates proteasome activity and transiently enhances intracellular proteolysis whereas severe or continuous oxidative stress impairs proteasome function and decreases intracellular proteolysis.<sup>61</sup>

Our study demonstrates that both nano-curcumin and curcumin exert concentration-dependent changes in the activity of proteasome individual subunits in RPE *in vitro*. A recently developed activity-based probe assay was used instead of the more commonly used ubiquitin-independent fluorogenic peptides and ubiquitin-dependent fluorescent reporters. Activity-based probes can detect alterations in proteasomal activity in gels and can also be applied to visualize active proteasomes in living cells.<sup>36; 37; 40</sup> Unlike fluorescence-labeled tags, activity-based probes label only completely assembled and active proteasome complexes which may explain why results obtained with these two different methods are incomparable and at times inconsistent. Overall, activity of the  $\beta 2$  and  $\beta 5i/\beta 1$  proteasome catalytic subunits is upregulated with increasing concentrations of nano-curcumin and curcumin whilst activity of the  $\beta 5/\beta 1i$  proteasome catalytic subunits is downregulated after treatment of RPE cells with both nano-curcumin and curcumin. Short-term treatment of cells with high concentrations of both nano-curcumin and curcumin induces expression of  $\beta 5i$  subunits which translates in a higher number of  $\beta 5i$  subunits when compared to  $\beta 5$  subunits, i.e., the household proteasome undergoes a change in configuration with activation of the immunoproteasome. This effect is not explained by an increase in the number of proteasomes as the protein expression levels of the  $\alpha 7$  subunit remain unchanged after nano-curcumin and curcumin treatment. The pool of proteasome subunits is replenished after treatment with low concentrations of nano-curcumin, as demonstrated by the increased mRNA expression of  $\alpha 7$ ,  $\beta 5$  and  $\beta 5i$  proteasome subunits. Of note, the effects on mRNA expression observed after treatment with 50  $\mu\text{M}$  curcumin, namely downregulation of the transcription of all proteasome-related genes, possibly reflect the potent cytotoxic effects at similar concentrations.

The pro-oxidative state induced by high concentrations of nano-curcumin and curcumin may explain the changes found in proteasome activity, and gene and protein expression. Indeed, oxidative stress has been shown to affect proteasome function.<sup>15; 51</sup> Notably, in the RPE, the activity of  $\beta 5$  is the rate-limiting step of proteasome activity.<sup>11; 41; 45</sup> Changes due to nano-curcumin treatment approximate those in other conditions that have been shown to be associated with  $\beta 5$  proteasome activity inhibition, namely ageing<sup>32</sup> and complement overactivation.<sup>14</sup> Changes in the ratio between immunoproteasome and classic proteasome are indicative of cellular stress, inflammation and oxidative stress.<sup>14; 18; 21; 28; 29</sup> It has been suggested that a continuous expression of the immunoproteasome in the retina is protective against neuronal stress and promotes repair mechanisms.<sup>21</sup> A possible mechanism for the inactivation of the  $\beta 5$  subunit lies in the chemical structure of curcumin, via inhibition of the ubiquitin isopeptidase activity located at the 19S regulatory subunit of the 26S proteasome. Curcumin belongs to a class of compounds with  $\alpha, \beta$ -unsaturated ketones and two sterically accessible  $\beta$  carbons.<sup>50</sup> Furthermore, curcumin has been shown to bind directly to the 20S proteasome.<sup>45</sup> A recent study has confirmed that both carbonyl groups of curcumin are indeed susceptible to nucleophilic

attack by N-terminal threonine of the  $\beta 5$  chymotrypsin-like subunit of the proteasome thereby inhibiting its proteolytic activity.<sup>45</sup>

The formulation of curcumin, duration of culture and concentration used may account for the contradictory results described hitherto in several studies. It appears that the cytotoxic profile of each formulation of curcumin depends on its bioavailability, absorption and cellular uptake. Further in vivo studies are required to assess the molecular effects of supplementation of curcumin in relation to retinal function. It is not known whether systemic administration of curcumin reaches the RPE and the neurosensory retina at concentrations capable of inducing significant molecular effects. If so, our findings suggest that curcumin may promote the development of RPE and retinal dysfunction which in turn can accelerate development of age-related retinal diseases. On the other hand, our results show that two different formulations of curcumin show different biological effects. Nano-curcumin may be a safer alternative in clinical trials in the future. Finally, our results attribute significant proteasome-modulating properties to both nano-curcumin and curcumin. The changes in proteasome activity incurred after nano-curcumin treatment are characterized by an activation of the immunoproteasome with consequent changes in the protein and gene expression of proteasome-related subunits.

### **Acknowledgments**

This study was supported by grants of the Landelijke Stichting voor Blinden en Slechtienden (LSBS), Stichting Blindenpenning and MaculaFonds that contributed through UitZicht (Grant UitZicht 2011-15) and Stichting Oogfonds. The founding organizations had no participation in design or conduct of this study, data collection, management, analysis, interpretation, preparation, review or approval of this manuscript.

## References

- Alex AF, Spitznas M, Tittel AP, et al.: Inhibitory effect of epigallocatechin gallate (EGCG), resveratrol, and curcumin on proliferation of human retinal pigment epithelial cells in vitro. *Curr Eye Res* 35:1021-1033, 2010
- Ali RE, Rattan SIS: Curcumin's biphasic hormetic response on proteasome activity and heat-shock protein synthesis in human keratinocytes. *Ann Ny Acad Sci* 1067:394-399, 2006
- Anand P, Kunnumakkara AB, Newman RA, Aggarwal BB: Bioavailability of curcumin: Problems and promises. *Mol Pharmaceut* 4:807-818, 2007
- Atsumi T, Tonosaki K, Fujisawa S: Comparative cytotoxicity and ROS generation by curcumin and tetrahydrocurcumin following visible-light irradiation or treatment with horseradish peroxidase. *Anticancer Res* 27:363-371, 2007
- Beatty S, Koh H, Phil M, et al.: The role of oxidative stress in the pathogenesis of age-related macular degeneration. *Surv Ophthalmol* 45:115-134, 2000
- Bech-Otschir D, Seeger M, Dubiel W: The COP9 signalosome: at the interface between signal transduction and ubiquitin-dependent proteolysis. *J Cell Sci* 115:467-473, 2002
- Beckman KB, Ames BN: The free radical theory of aging matures. *Physiol Rev* 78:547-581, 1998
- Bhaumik S, Anjum R, Rangaraj N, et al.: Curcumin mediated apoptosis in AK-5 tumor cells involves the production of reactive oxygen intermediates. *FEBS Lett* 456:311-314, 1999
- Burgos-Moron E, Calderon-Montano JM, Salvador J, et al.: The dark side of curcumin. *Int J Cancer* 126:1771-1775, 2010
- Chen M, Hu DN, Pan Z, et al.: Curcumin protects against hyperosmoticity-induced IL-1 beta elevation in human corneal epithelial cell via MAPK pathways. *Exp Eye Res* 90:437-443, 2010
- Coux O, Tanaka K, Goldberg AL: Structure and functions of the 20S and 26S proteasomes. *Annu Rev Biochem* 65:801-847, 1996
- Cuomo J, Appendino G, Dern AS, et al.: Comparative absorption of a standardized curcuminoid mixture and its lecithin formulation. *J Nat Prod* 74:664-669, 2011
- Dahlmann B, Ruppert T, Kuehn L, et al.: Different proteasome subtypes in a single tissue exhibit different enzymatic properties. *J Mol Biol* 303:643-653, 2000
- de Carvalho JER, Klaassen I, Vogels IMC, et al.: Complement factor C3a alters proteasome function in human RPE cells and in an animal model of age-related RPE degeneration. *Invest Ophthalmol Vis Sci* 54:6489-6501, 2013
- Ding QX, Keller JN: Proteasome inhibition in oxidative stress neurotoxicity: implications for heat shock proteins. *J Neurochem* 77:1010-1017, 2001
- Ding QX, Martin S, Dimayuga E, et al.: LMP2 knock-out mice have reduced proteasome activities and increased levels of oxidatively damaged proteins. *Antiox Redox Signal* 8:130-135, 2006
- Drobek-Slowik M, Karczewicz D, Safranow K: The potential role of oxidative stress in the pathogenesis of the age-related macular degeneration (AMD). *Postepy Hig Med Dosw (Online)* 61:28-37, 2007
- Ethen CM, Hussong SA, Reilly C, et al.: Transformation of the proteasome with age-related macular degeneration. *FEBS Lett* 581:885-890, 2007
- Fernandes AF, Guo WM, Zhang XY, et al.: Proteasome-dependent regulation of signal transduction in retinal pigment epithelial cells. *Exp Eye Res* 83:1472-1481, 2006
- Fernandes AF, Zhou JL, Zhang XY, et al.: Oxidative inactivation of the proteasome in retinal pigment epithelial cells - a potential link between oxidative stress and up-regulation of interleukin-8. *J Biol Chem* 283:20745-20753, 2008
- Ferrington DA, Hussong SA, Roehrich H, et al.: Immunoproteasome responds to injury in the retina and brain. *J Neurochem* 106:158-169, 2008
- Gupta SC, Prasad S, Kim JH, et al.: Multitargeting by curcumin as revealed by molecular interaction studies. *Nat Prod Rep* 28:1937-1955, 2011
- Gupta SK, Kumar B, Nag TC, et al.: Curcumin prevents experimental diabetic retinopathy in rats through its hypoglycemic, antioxidant, and anti-inflammatory mechanisms. *J Ocul Pharmacol Th* 27:123-130, 2011
- Hafer K, Iwamoto KS, Schiestl RH: Refinement of the dichlorofluorescein assay for flow cytometric measurement of reactive oxygen species in irradiated and bystander cell populations. *Radiat Res* 169:460-468, 2008
- Hasima N, Aggarwal BB: Targeting proteasomal pathways by dietary curcumin for cancer prevention and treatment. *Curr Med Chem* 21:1583-1594, 2014
- Henke W, Ferrell K, Bech-Otschir D, et al.: Comparison of human COP9 signalosome and 26S proteasome 'lid'. *Mol Biol Rep* 26:29-34, 1999
- Hollborn M, Chen R, Wiedemann P, et al.: Cytotoxic effects of curcumin in human retinal Pigment Epithelial Cells. *PLoS One* 8, 2013
- Hussong SA, Kappahh RJ, Phillips SL, et al.: Immunoproteasome deficiency alters retinal proteasome's response to stress. *J Neurochem* 113:1481-1490, 2010
- Hussong SA, Roehrich H, Kappahh RJ, et al.: A novel role for the immunoproteasome in retinal function. *Invest Ophthalmol Vis Sci* 52:714-723, 2011
- Jager R, Lowery RP, Calvanese AV, et al.: Comparative absorption of curcumin formulations. *Nutr J* 13, 2014
- Jayaprakasha GK, Rao LJ, Sakariah KK: Antioxidant activities of curcumin, demethoxycurcumin and bisdemethoxycurcumin. *Food Chem* 98:720-724, 2006
- Kappahh RJ, Bigelow EJ, Ferrington DA: Age-dependent inhibition of proteasome chymotrypsin-like activity in the retina. *Exp Eye Res* 84:646-654, 2007

33. Klaassen I, Hughes JM, Vogels IMC, et al.: Altered expression of genes related to blood-retina barrier disruption in streptozotocin-induced diabetes. *Exp Eye Res* 89:4-15, 2009
34. Klare N, Seeger M, Janek K, et al.: Intermediate-type 20 S proteasomes in HeLa cells: "asymmetric" subunit composition, diversity and adaptation. *J Mol Biol* 373:1-10, 2007
35. Li J, Wang PP, Zhu YX, et al.: Curcumin inhibits neuronal loss in the retina and elevates Ca<sup>2+</sup>/calmodulin-dependent protein kinase II activity in diabetic rats. *J Ocul Pharmacol Th* 31:555-562, 2015
36. Li N, Kuo CL, Paniagua G, et al.: Relative quantification of proteasome activity by activity-based protein profiling and LC-MS/MS. *Nat Protoc* 8:1155-1168, 2013
37. Li N, Overkleeft HS, Florea BI: Activity-based protein profiling: an enabling technology in chemical biology research. *Curr Opin Chem Biol* 16:227-233, 2012
38. Li Y, Wang YS, Shen XF, et al.: Alterations of activity and intracellular distribution of the 20S proteasome in ageing retinal pigment epithelial cells. *Exp Gerontol* 43:1114-1122, 2008
39. Li Y, Zou X, Cao K, et al.: Curcumin analog 1, 5-bis (2-trifluoromethylphenyl)-1, 4-pentadien-3-one exhibits enhanced ability on Nrf2 activation and protection against acrolein-induced ARPE-19 cell toxicity. *Toxicol Appl Pharm* 272:726-735, 2013
40. Liggett A, Crawford LJ, Walker B, et al.: Methods for measuring proteasome activity: current limitations and future developments. *Leuk Res* 34:1403-1409, 2010
41. Louie JL, Kappahn RJ, Ferrington DA: Proteasome function and protein oxidation in the aged retina. *Exp Eye Res* 75:271-284, 2002
42. Mandal MNA, Patlolla JMR, Zheng L, et al.: Curcumin protects retinal cells from light-and oxidant stress-induced cell death. *Free Radic Biol Med* 46:672-679, 2009
43. Mattson MP: Dietary factors, hormesis and health. *Ageing Res Rev* 7:43-48, 2008
44. Mattson MP, Cheng AW: Neurohormetic phytochemicals: low-dose toxins that induce adaptive neuronal stress responses. *Trends Neurosci* 29:632-639, 2006
45. Milacic V, Banerjee S, Landis-Piwowar KR, et al.: Curcumin inhibits the proteasome activity in human colon cancer cells in vitro and in vivo. *Cancer Res* 68:7283-7292, 2008
46. Milano F, Mari L, van de Luijngaerden W, et al.: Nano-curcumin inhibits proliferation of esophageal adenocarcinoma cells and enhances the T cell mediated immune response. *Front Oncol* 3:137, 2013
47. Morimoto T, Sunagawa Y, Katanasaka Y, et al.: Drinkable preparation of theracurmin exhibits high absorption efficiency - a single-dose, double-blind, 4-way crossover study. *Biol Pharm Bull* 36:1708-1714, 2013
48. Mudduluru G, George-William JN, Muppala S, et al.: Curcumin regulates miR-21 expression and inhibits invasion and metastasis in colorectal cancer. *Biosci Rep* 31:185-197, 2011
49. Mujtaba T, Kanwar J, Wan SB, et al.: Sensitizing human multiple myeloma cells to the proteasome inhibitor bortezomib by novel curcumin analogs. *Int J Mol Med* 29:102-106, 2012
50. Mullally JE, Fitzpatrick FA: Pharmacophore model for novel inhibitors of ubiquitin isopeptidases that induce p53-independent cell death. *Mol Pharmacol* 62:351-358, 2002
51. Okada K, Wangpoengtrakul C, Osawa T, et al.: 4-hydroxy-2-nonenal-mediated impairment of intracellular proteolysis during oxidative stress - identification of proteasomes as target molecules. *J Biol Chem* 274:23787-23793, 1999
52. Park W, Amin AR, Chen ZG, Shin DM: New perspectives of curcumin in cancer prevention. *Cancer Prev Res (Phila)* 6:387-400, 2013
53. Premanand C, Rema M, Samcer MZ, et al.: Effect of curcumin on proliferation of human retinal endothelial cells under in vitro conditions. *Invest Ophthalmol Vis Sci* 47:2179-2184, 2006
54. Puliappadamba VT, Cheriyan VT, Thulasidasan AK, et al.: Nicotine-induced survival signaling in lung cancer cells is dependent on their p53 status while its down-regulation by curcumin is independent. *Mol Cancer* 9:220, 2010
55. Reits EAJ, Benham AM, Plougastel B, et al.: Dynamics of proteasome distribution in living cells. *EMBO J* 16:6087-6094, 1997
56. Saha A, Kuzuhara T, Echigo N, et al.: Apoptosis of human lung cancer cells by curcumin mediated through up-regulation of "growth arrest and DNA damage inducible genes 45 and 153". *Biol Pharm Bull* 33:1291-1299, 2010
57. Sambrook J, Gething MJ: Protein structure - chaperones, paperones. *Nature* 342:224-225, 1989
58. Sasaki H, Sunagawa Y, Takahashi K, et al.: Innovative preparation of curcumin for Improved Oral Bioavailability. *Biol Pharm Bull* 34:660-665, 2011
59. Scott PA, Kaplan HJ, McCall MA: Prenatal exposure to curcumin protects rod photoreceptors in a transgenic Pro23His swine model of retinitis pigmentosa. *Transl Vis Sci Technol* 4:5, 2015
60. Seeger M, Kraft R, Ferrell K, et al.: A novel protein complex involved in signal transduction possessing similarities to 26S proteasome subunits. *FASEB J* 12:469-478, 1998
61. Shang F, Taylor A: Ubiquitin-proteasome pathway and cellular responses to oxidative stress. *Free Radic Biol Med* 51:5-16, 2011
62. Singh M, Singh N: Curcumin counteracts the proliferative effect of estradiol and induces apoptosis in cervical cancer cells. *Mol Cell Biochem* 347:1-11, 2011
63. Sulaiman RS, Basavarajappa HD, Corson TW: Natural product inhibitors of ocular angiogenesis. *Exp Eye Res* 129:161-171, 2014
64. Sun Y, You ZP: Curcumin inhibits human retinal pigment epithelial cell proliferation. *Int J Mol Med* 34:1013-1019, 2014
65. Thayyullathil F, Chathoth S, Hago A, et al.: Rapid reactive oxygen species (ROS) generation induced by curcumin leads to caspase-dependent and -independent apoptosis in L929 cells. *Free Radic Biol Med* 45:1403-1412, 2008
66. Uhle S, Medalia O, Waldron R, et al.: Protein kinase CK2 and protein kinase D are associated with the COP9 signalosome. *EMBO J* 22:1302-1312, 2003
67. Vasireddy V, Chavali VRM, Joseph VT, et al.: Rescue of photoreceptor degeneration by curcumin in transgenic rats with P23H rhodopsin mutation. *PLoS One* 6, 2011
68. Verdoes M, Florea BI, Mendez-Benito V, et al.: A fluorescent broad-spectrum proteasome inhibitor for labeling proteasomes in vitro and in vivo. *Chem Biol* 13:1217-1226, 2006
69. Vyas A, Dandawate P, Padhye S, et al.: Perspectives on new synthetic curcumin analogs and their potential anticancer properties. *Curr Pharm Design* 19:2047-2069, 2013
70. Wang C, Ma C, Wu Z, et al.: Enhanced bioavailability and anticancer effect of curcumin-loaded electrospun nanofiber: in vitro and in vivo study. *Nanoscale Res Lett* 10:439, 2015
71. Woo JM, Shin DY, Lee SJ, et al.: Curcumin protects retinal pigment epithelial cells against oxidative stress via induction of heme oxygenase-1 expression and reduction of reactive oxygen. *Mol Vis* 18:901-908, 2012
72. Yildirim Z, Ucgun NI, Yildirim F: The role of oxidative stress and antioxidants in the pathogenesis of age-related macular degeneration. *Clinics (Sao Paulo)* 66:743-746, 2011
73. Zhu W, Wu Y, Meng YF, et al.: Effect of curcumin on aging retinal pigment epithelial cells. *Drug Des Devel Ther* 9:5337-5344, 2015

6

# Reversal of threatening blindness after initiation of eculizumab in Purtscher-like retinopathy secondary to atypical hemolytic uremic syndrome

J. Emanuel Ramos de Carvalho<sup>a</sup>, Reinier O. Schlingemann<sup>a</sup>, Maarten Oranje<sup>b</sup>, Frederike J. Bemelman<sup>b</sup>, Mary J. van Schooneveld<sup>a</sup>

<sup>a</sup> Department of Ophthalmology, Academic Medical Center, University of Amsterdam, Amsterdam, The Netherlands

<sup>b</sup> Division of Internal and External Medicine, Department of Nephrology, Academic Medical Centre, University of Amsterdam, Amsterdam, The Netherlands

## **Abstract**

Purtscher-like retinopathy, a rare manifestation of systemic thrombotic microangiopathy, is a potentially visually debilitating condition with no effective proven treatment. Distinct pathogenic pathways have been proposed as etiological factors. In this short review of the literature, we revisit the etiology of Purtscher-like retinopathy based on the rapid response and profound visual acuity improvement achieved after initiation of systemic intravenous eculizumab, an inhibitor of the complement cascade, in a patient with Purtscher-like retinopathy secondary to familial atypical hemolytic uremic syndrome (aHUS) due to a mutation in complement factor H. We hypothesize the efficacy of eculizumab in this patient provides evidence for pathogenic events in the retina similar to those encountered in the renal microvasculature of aHUS patients, namely complement-mediated thromboembolization as a result of activation of the complement cascade in endothelial cells with release of tissue factor and development and amplification of a procoagulant state. To the best of our knowledge, this is the first report in the literature of eculizumab as an effective therapeutic strategy in Purtscher-like retinopathy.

## **Introduction**

Purtscher and Purtscher-like retinopathy is a rare, often bilateral, retinal occlusive microvasculopathy that occurs as a result of various clinical entities associated with vascular thromboembolic occlusion. The designation Purtscher retinopathy refers to cases associated with a traumatic etiology, whereas Purtscher-like retinopathy occurs secondary to non-traumatic causes.<sup>1</sup>

Several mechanisms have been brought forward as hypothetical triggers of Purtscher and Purtscher-like retinopathy.<sup>1; 2; 3</sup> Although the pathogenesis is likely multifactorial and differs according to the underlying predisposing condition, embolization of the retinal

microcirculation has been proposed as the common pathogenic ground for the retinal findings.<sup>4; 5; 6; 7</sup> Potential sources of toxic and/or obstructive emboli include air, fat, fibrin, platelet and leukocyte aggregates.<sup>1</sup> Other infrequent causes include emboli arising from orbital steroid injection,<sup>8</sup> after retrobulbar anesthesia<sup>8; 9; 10; 11</sup> and after childbirth due to amniotic fluid embolism.<sup>12</sup> Uncontrolled complement activation with the formation of C5-9 membrane attack complex and the anaphylatoxin C5a has also been proposed to play a major role in the pathogenesis of Purtscher-like retinopathy by mechanisms involving endothelial damage and activation of the clotting cascade<sup>5; 6; 13; 14</sup> and development of leukocyte and platelet aggregates<sup>1; 4</sup>. The size of the leukocyte aggregates (~50 to 80  $\mu\text{m}$ ) is greater than the diameter of precapillary arterioles (45  $\mu\text{m}$ ) which may then result in occlusion of the retinal microcirculation.<sup>15</sup> Clinical evidence supports a role for complement-mediated vascular thromboembolic occlusion, as a large proportion of patients show evidence of low serum complement, a marker for complement activation.<sup>16</sup> Other proposed mechanisms include intravascular volume surge such as in sudden expansion of retinal veins,<sup>1</sup> hyperviscosity,<sup>17</sup> intracephalic shock waves such as in sudden increase in intracranial pressure with resulting precapillary occlusion at the level of the lamina cribrosa,<sup>18</sup> capillary endothelial damage<sup>19</sup> and vascular endothelial dysregulation and ensuing endothelin-induced vasculopathy.<sup>18</sup> In sum, regardless of the causative factor, Purtscher-like retinopathy may be regarded as a multifactorial downstream occlusive thromboembolic retinopathy, which in a large proportion of cases may be mediated by uncontrolled complement activation. Associated systemic entities include acute pancreatitis,<sup>20; 21; 22; 23; 24; 25; 26; 27</sup> pancreatic adenocarcinoma,<sup>28</sup> systemic lupus erythematosus,<sup>16</sup> renal failure,<sup>29; 30</sup> amniotic fluid embolization,<sup>12</sup> thrombotic thrombocytopenic purpura,<sup>31; 32; 33; 34</sup> hemolytic uremic syndrome,<sup>32; 35</sup> and cryoglobulinemia.<sup>36; 37; 38</sup> In specific disorders, the diagnosis of Purtscher-like retinopathy accompanies multisystem organ failure and therefore portends a poor prognosis.<sup>39</sup>

The clinical diagnosis of Purtscher and Purtscher-like retinopathy is suggested by a sudden visual loss of variable severity, hours to days after the associated etiology. Some patients may be asymptomatic (or not able to report symptoms because of their serious general condition) which likely results in underreporting.<sup>4</sup> The majority of patients (83 – 92%) show funduscopy evidence of retinal nerve fiber layer infarcts (cotton-wool spots) and intraretinal hemorrhages.<sup>1; 2</sup> Purtscher “flecken” correspond to areas of intraretinal whitening with a clear zone (within 50  $\mu\text{m}$ ) on either side of the retinal arterioles, venules and precapillary arterioles. These lesions are the result of precapillary arteriolar occlusion, and, though pathognomonic, can be identified in only 50% of cases.<sup>2</sup> Other less frequent findings include macular edema, optic disc swelling and a pseudo-cherry red spot. Fluorescein angiography shows evidence of an occlusive thromboembolic retinopathy with areas of retinal non-perfusion and leakage of dye from retinal arterioles, capillaries, venules and optic disc.<sup>4</sup>

Although up to 40% cases may be associated with normalization of all retinal findings and restoration of good visual acuity, a significant number develop optic atrophy, mottling of the retinal pigment epithelial (RPE), retinal thinning and narrowing of retinal arteries.<sup>4; 40</sup>

The prognosis for the individual patient is difficult to predict, due to the lack of clear and validated predictors. Treatment strategies range from watchful waiting, plasmapheresis and use of high doses of systemic corticosteroids.<sup>2; 41; 42; 43</sup>

Hemolytic uremic syndrome is characterized by non-immune hemolytic anemia, thrombocytopenia, and renal impairment. Most cases (90%) are secondary to infection with Shiga-toxin-producing bacteria as well as other bacteria, such as *Streptococcus pneumoniae*. Non-infectious causes, classified as atypical hemolytic uremic syndrome (aHUS), are linked to uncontrolled complement activation. The familiar type of aHUS, as seen in this patient, has a particularly poor prognosis, with a reported mortality rate and progression to end-stage disease between 50 and 80%.<sup>44</sup> Purtscher-like retinopathy has been reported to occur in a minority of patients with hemolytic uremic syndrome.<sup>45; 46; 47</sup>

We present a case of Purtscher-like retinopathy secondary to aHUS due to *CFH* mutation and resulting complement overactivation, successfully treated with systemic intravenous administration of eculizumab (Soliris; Alexion Pharmaceuticals, Cheshire, CT, USA), an inhibitor of terminal complement activation. We hypothesize that eculizumab may be an alternative therapeutic strategy for severe Purtscher-like retinopathy associated with complement dysregulated activation and ensuing thromboembolic occlusion of the retinal microvasculature. Based on the response achieved after initiation of treatment, an alternative etiology for Purtscher-like retinopathy is proposed after a short review of the literature.

### **Case description**

A 20-year old Caucasian woman presented with complaints of subacute painless loss of vision of her left eye. She was referred to our clinic for intravitreal ganciclovir treatment after a putative diagnosis of bilateral cytomegalovirus retinitis made by an ophthalmologist in her local hospital the day before. She was one of three sisters known with familial aHUS due to a missense mutation (c.3572 C>T, Ser1191Leu) in exon 23 of Complement Factor H (*CFH* gene). At six years of age, she underwent bilateral nephrectomy followed one year later by a living-donor renal transplant. After one year, she developed a systemic cytomegalovirus infection with relapse of aHUS. Her immunosuppression was tapered to a calcineurin free regimen and chronic maintenance plasmapheresis was started. Four years later, a transplant biopsy showed chronic allograft nephropathy with global glomerulosclerosis and tubular atrophy. There were no treatment options other than supportive care and her renal function slowly declined hereafter. At 19 years old she reached end-stage failure, immunosuppression was further tapered and she was started on dialysis. The maintenance plasmaphereses were halted. During dialysis she complained of seeing “black spots” and was referred to the local ophthalmologist. Her family history included two sisters, one of them her identical twin, with aHUS and *CFH* mutation. Her brother was an asymptomatic carrier for the *CFH* mutation, and her younger sister was

not affected. She had no past history of ocular illness.

On ophthalmologic examination, best corrected visual acuity was 20/15 and 20/200<sup>-2</sup> in the right and left eyes, respectively. There was no relative afferent pupillary defect. Intraocular pressure was normal. The anterior chambers and vitreous were clear in both eyes. Fundus examination revealed nerve fiber layer infarcts and mild flame-shaped hemorrhages in both eyes. The left eye showed mild macular cystoid macular edema. The retinal vessels were of a normal caliber in both eyes. A small choroidal naevus was present in the nasal retina of the right eye. Fluorescein angiography revealed early hypofluorescence, areas of non-perfusion, capillary obstruction and dropout, retinal ischemia in the parafoveal and perifoveal zone corresponding with the areas of nerve fiber layer infarcts and perifoveal capillary leakage and staining in late frames. The left eye showed mild cystoid macular edema nasal to the fovea (Fig. 1). Mild peripapillary staining was noted in the late frames of the left eye. Besides a small hemorrhage peripherally, all other angiographic findings were confined to the posterior pole, namely within the macula and immediately nasal to the optic disc. Normal fluorescein transit times were observed. The degree of macular ischemia and perifoveal capillary dropout was more pronounced in the left eye which explained the visual acuity loss in that eye. These clinical findings, together with her medical history, were consistent with Purtscher-like retinopathy. At the time of referral to our clinic, she was awaiting a second living-donor renal transplantation. The ophthalmic findings were evidence of undertreated hemolytic uremic syndrome and uncontrolled systemic complement activation. In order to prevent further progression of her retinopathy, and due to the severe loss of vision in her left eye, we started treatment with eculizumab, a C5 complement inhibitor that has been praised as highly effective in the treatment of hemolytic uremic syndrome, also after transplantation. After four months, while being on chronic eculizumab therapy, a transplantectomy was performed followed by a second renal transplantation. Both procedures had an uncomplicated course. On follow-up, she reported a steady continuous improvement of her visual acuity. Five days after eculizumab administration, best corrected visual acuity was stable in her right eye and pinhole visual acuity improved to 20/50<sup>+2</sup> in her left eye. Fundus examination revealed a decrease in the size of the nerve fiber layer infarcts and optical coherence tomography showed total resolution of the cystoid macular edema in the left eye. On the 14<sup>th</sup> day after treatment, she reported total resolution of all her previous visual complaints. Best corrected visual acuity was stable in her right eye and had improved to 20/15<sup>-2</sup> in her left eye. Fundus examination revealed an improvement of all clinical findings, including the nerve fiber layer infarcts, flame-shaped hemorrhages and macular edema. She was referred back to her local ophthalmologist. At 6 months, visual acuity remained stable and patient reported no visual complaints.

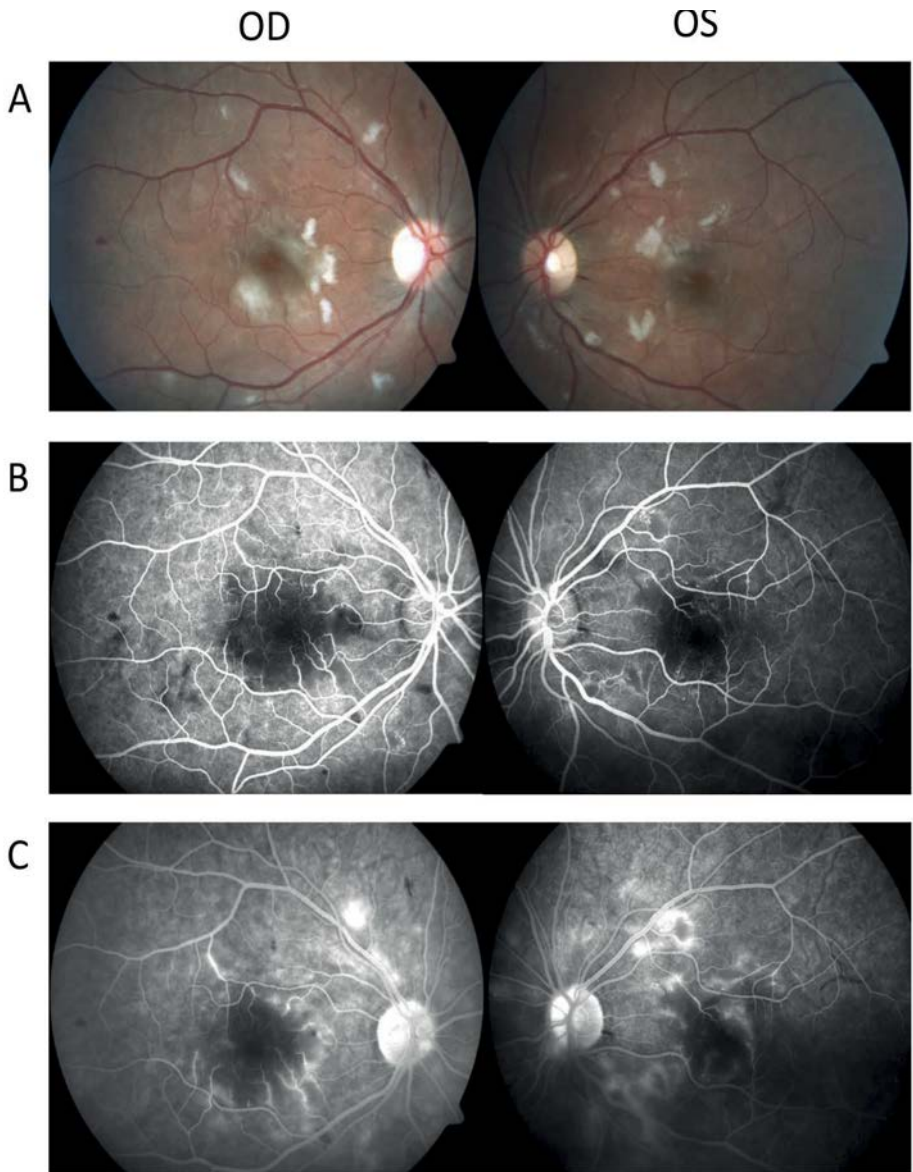


**Fig. 1.** Retinal photographs and fluorescein angiogram appearance at initial presentation. (A) Fundus appearance at presentation. Note the diffuse retinal nerve fiber layer infarcts, inner retinal ischemia and scattered retinal hemorrhages. Visual acuity was 20/15 and 20/200<sup>-2</sup> in the right and left eye, respectively. (B) Mid-phase intravenous fluorescein angiogram of the same patient at initial presentation. Note the parafoveal and perifoveal areas of capillary obstruction and retinal ischemia correspondent to the areas of inner retinal ischemia seen in the fundus picture. (C) Mid to late-phase fluorescein angiogram in the same patient. Note the parafoveal pericapillary leakage and mild macular edema with late leakage in the left eye. Angiographic findings were mostly confined to the macula and immediately nasal to the optic disc.

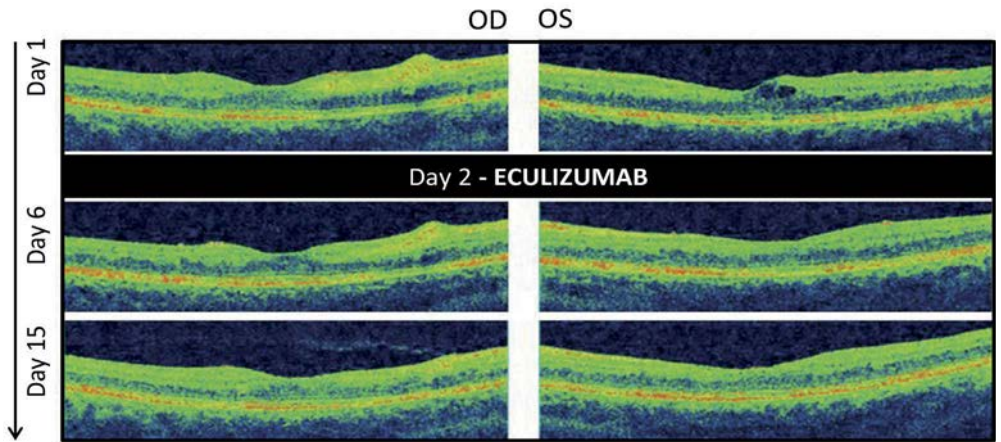


**Fig. 2.** Optical coherence tomography findings at initial presentation and at day 6 and 15. Inner retinal ischemia was evident in both eyes, corresponding to the cotton-wool spots demonstrated in the color photographs. The right eye, with normal visual acuity at presentation, had no evident macular edema. The left eye, with severe visual acuity loss, had mild cystoid macular edema which regressed rapidly after eculizumab administration. At day 15, visual acuity in the left eye had improved significantly alongside resolution of the macular oedema and inner retinal ischemia.

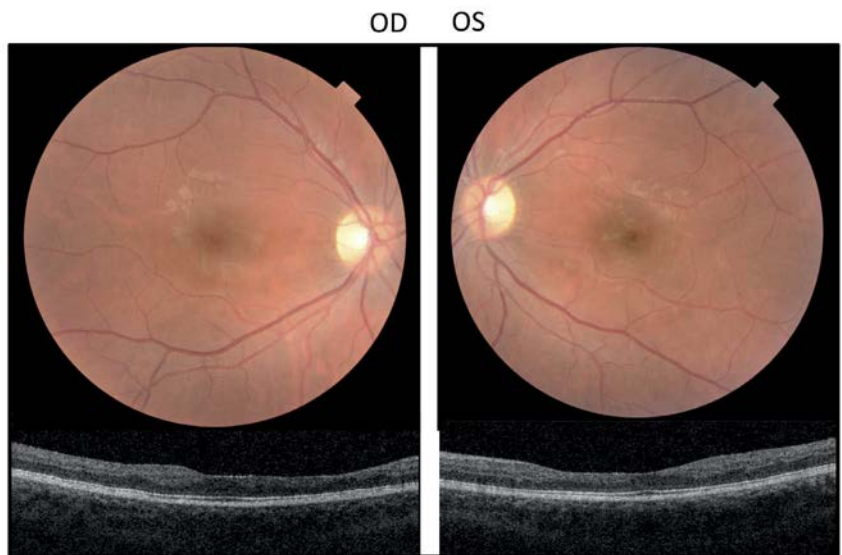


**Fig. 3.** Retinal photographs and optical coherence tomography 18 months after initial presentation. Color photographs of the right and left maculae show a normal appearance, albeit a significant thinning is evident on optical coherence tomography. The patient is asymptomatic and has normal visual acuity (20/15 in the right eye and 20/15<sup>-2</sup> in the left eye).

## Conclusion

This single case describes the favorable visual outcome achieved after systemic treatment with eculizumab in a patient with severe Purtscher-like retinopathy secondary to familial aHUS and *CFH* mutation.

In our view, the retinal findings were caused by uncontrolled systemic complement activation and as a result complement-mediated leukoembolization and/or complement activation of the coagulation cascade in endothelial cells and secondary development of a prothrombotic state. Leukoembolization as a cause of embolic retinal occlusion has been proposed as a potential pathogenic mechanism in Purtscher-like retinopathy.<sup>6; 15; 48</sup> However, recent experimental studies suggest endothelial activation of the coagulation cascade by complement with formation of microthrombi as the most plausible mechanism in the pathogenesis of aHUS,<sup>49</sup> and likewise, we propose this can be extrapolated not only to our case but to all cases of complement-driven Purtscher-like retinopathy. As previously mentioned, the patient was known to carry a mutation in the *CFH* gene which codes for a serum protein that regulates the alternative pathway of the complement system in the fluid phase as well as on host cell surfaces by binding through C3b and glycosaminoglycans via its C-terminal domain.<sup>50</sup> Mutations in the *CFH* gene of patients with aHUS are usually heterozygous in nature and cluster in C-terminal domain 19-20. This particular mutation, also found in this patient, results in normal levels of a folded, abnormal protein, that is unable to bind and regulate complement on host cells and platelets. Animal studies have confirmed development of aHUS with high C3 plasma levels in mice lacking the C-terminal end domain of factor H.<sup>51</sup> In contrast, complete *CFH* knockout mice develop a different renal disease pattern, namely membranoproliferative glomerulonephritis.<sup>52</sup> These studies support the evidence that the mutant *CFH* present in this patient fails to bind to and control complement activation on the glomerular endothelium, basement membrane, platelets and indirectly, the retinal endothelium, with subsequent development of a procoagulant state that in turn resulted in aHUS and Purtscher-like retinopathy.

Eculizumab is a monoclonal antibody directed against complement protein C5. It prevents activation of the terminal complement cascade and the generation of effector molecules C5a and C5b-9. The ability of eculizumab to suppress complement activity in native and transplanted kidney has revolutionized the care of patients with aHUS.<sup>53; 54; 55</sup> Without attenuation of complement activity, either through plasmapheresis, kidney-liver transplant (*CFH* and other complement factors are produced in the liver), or recently eculizumab, disease recurrence occurs in approximately 80% of *CFH* mutation carriers after renal transplantation since the isolated kidney allograft will not correct the underlying genetic defect.<sup>56</sup>

We hypothesize that complement inhibition by means of eculizumab, is likely to have resulted in the rapid resolution of clinical findings and dramatic restoration of visual acuity in this patient. We consider it unlikely that an expectant management or other treatment options such as dosage increase of systemic corticosteroids would have resulted in a similar outcome. We are, however, aware of the limitation of assuming efficacy based

on results obtained with only one patient. Confirmation of clinical efficacy requires validation from a larger clinical study. In this patient, plasmapheresis was considered as a possible treatment option; however, this would not have had an effect on complement activation which would have resulted in perpetuation of renal and (possibly) retinal findings. Eculizumab was considered the most viable option as an attempt to prevent visual loss in the other eye and halt reactivation of aHUS. In our opinion, increasing the dosage of systemic corticosteroids was not a valid therapeutic strategy. The beneficial effects of systemic corticosteroids in severe Purtscher-like retinopathy are inconsistent, with most studies confirming no differences in visual acuity improvement.<sup>1;4</sup> Interestingly, this patient developed Purtscher-like retinopathy whilst on systemic corticosteroids, albeit at a low dosage. It has been claimed that corticosteroids may lack efficiency in cases of Purtscher-like retinopathy primarily triggered by thrombotic microangiopathy, such as in aHUS.<sup>57</sup> Solely targeting the inflammatory component will not affect microembolization since other complex pathogenic events such as hemostasis, thrombosis and complement dysregulation will remain unanswered.<sup>57</sup>

Important clinical parameters support the favorable effect of eculizumab in this particular patient. First, pronounced visual acuity improvement occurred rapidly after eculizumab treatment (20/200<sup>2</sup> visual acuity at time of diagnosis improving to 20/15, 8 Snellen lines improvement, 14 days after initial examination). Evidence shows spontaneous visual improvement of at least 2 Snellen lines is likely to occur in half of cases, however, such improvement occurs mostly in patients with better visual acuity at presentation.<sup>2</sup> Poor visual acuity at presentation, such as observed in this patient, is regarded as a poor prognostic sign for visual improvement. Furthermore, studies have shown that early resolution of clinical findings is associated with better final visual outcomes.<sup>2</sup> Secondly, this patient possessed other established poor prognostic criteria,<sup>4</sup> namely female gender and intraretinal macular edema at presentation. Yet, visual acuity recovered dramatically after initiation of treatment. At six months, she reported no visual symptoms and visual acuity was stable in both eyes. The drop in visual acuity in this and other patients with Purtscher retinopathy is likely secondary to macular edema.<sup>4</sup> It has been hypothesized that the duration of retinal changes is the most important parameter for full recovery of vision and prevention of secondary development of retinal pigment epithelium and retinal nerve fiber layer atrophy with subsequent loss of differentiation between retinal layers.<sup>58</sup> Such findings are found in late-stage OCT examinations of patients with Purtscher retinopathy with profound visual loss.<sup>58</sup> Therefore, early reduction of macular edema and other findings should be a priority in therapeutic management in order to prevent end-stage degenerative changes. We did not perform visual field examination in this patient. Central, paracentral, or arcuate scotomata with preservation of the peripheral visual function have been reported in Purtscher retinopathy, also in cases in which macular edema and restoration of visual acuity occurred.<sup>1;59</sup> Since the patient reported no complaints, we believed there were no clinical grounds requiring visual field testing.

Mutations in complement-associated genes, and particularly in the *CFH* gene, have been

shown to be linked to development of age-related macular degeneration (AMD), one of the leading causes of blindness worldwide.<sup>60</sup> Several mutations in complement-associated genes reported in patients with aHUS patients, such as Arg1210Cys in *CFH*, were found to confer a high risk of AMD development. The relevance of this shared genetic association between two distinct clinical phenotypes remains unknown. Retrospective analysis of AMD databases did not reveal a higher incidence of renal disorders in carriers of complement gene mutations known to cause both aHUS and AMD.<sup>61</sup> On the other hand, patients afflicted with membranoproliferative glomerulonephritis type 2 (MPGN2), a renal disease that is also associated with *CFH* mutations, show AMD-like features. This suggests compound (genetic or environmental) factors may influence the final clinical outcome. Indeed, AMD and MPGN2 share a common pathogenic mechanism, i.e. the deposition of complement-containing material beneath the retinal pigment epithelial in AMD and along the glomerular basement membrane in MPGN2.<sup>62</sup> Disparately, the pathogenic mechanisms causative of Purtscher-like retinopathy are shared with those of aHUS, namely endothelial injury, activation of the coagulation cascade, and ultimately thromboembolic microangiopathy.<sup>51</sup> Moreover, some aHUS patients may carry multiple complement factor gene mutations, which could imply different cellular pathogenic mechanisms.<sup>63</sup> Cross-phenotype studies are required in order to understand similarities and differences in complement-mediated pathogenic mechanisms of both aHUS and AMD which could elucidate the effects of eculizumab and other complement-modulating agents in the treatment of AMD and other ophthalmic diseases. Recently, results of a phase 2 study in which eculizumab was administered for 24 weeks to patients with dry AMD (*COMPLETE* study), aimed at halting progression of geographic atrophy (GA), were published.<sup>64</sup> The authors concluded eculizumab failed to arrest GA progression. It is likely that, although complement dysregulation is knowingly associated with AMD, pathogenesis and progression of GA may occur independently of complement overactivation.<sup>65</sup> In our case report, complement overactivation likely had a direct effect as a facilitator and trigger of the retinal thromboembolic microangiopathy, and therefore it is highly probable that local complement inhibition by systemic eculizumab enabled the rapid resolution of the retinal microembolization with ensuing resolution of the macular intraretinal edema. These complement-mediated effects differ from those attributed to the complement pathway in diseases characterized by deposition of extracellular material such as AMD and MPGN2. Furthermore, complement inhibition has been demonstrated to occur within one hour after administration of eculizumab.<sup>54</sup> Therefore, eculizumab may be more efficacious in suppressing acute complement-mediated changes such as thromboembolic microangiopathy of retinal and renal vessels, as opposed to chronic changes induced by uncontrolled complement activation such as in AMD. The authors of the *COMPLETE* study argue that intravitreal administration of eculizumab might have resulted in a more favorable outcome. Our case provides indirect evidence that systemic eculizumab, at the administered dosage, does reach therapeutic concentrations at the level of the choroid and is able to penetrate the RPE and retina. In addition, the dosing regimen used for treatment of aHUS has been shown to reach drug

complement-inhibiting concentrations in the peripheral blood.<sup>55</sup>

The description of this case raises the possibility that eculizumab may be a valid therapeutic strategy in severe cases of Purtscher-like retinopathy in which the primary pathogenic trigger is attributed to dysregulated complement activity. The benefit of intervention over expectant management can only be convincingly assessed with a randomized clinical trial, which, given the rarity of the disease and the extreme high cost of the drug (about US \$350,000 per patient per year), is unlikely. The dramatic and rapid visual recovery demonstrated in this patient, even in the presence of established poor prognostic signs, namely, poor visual acuity at presentation, intraretinal macular edema and female gender, provides convincing evidence that eculizumab was causally related to the attained superior outcome. To the best of our knowledge, this is the first report in the literature of eculizumab as a potential therapeutic strategy in Purtscher-like retinopathy.

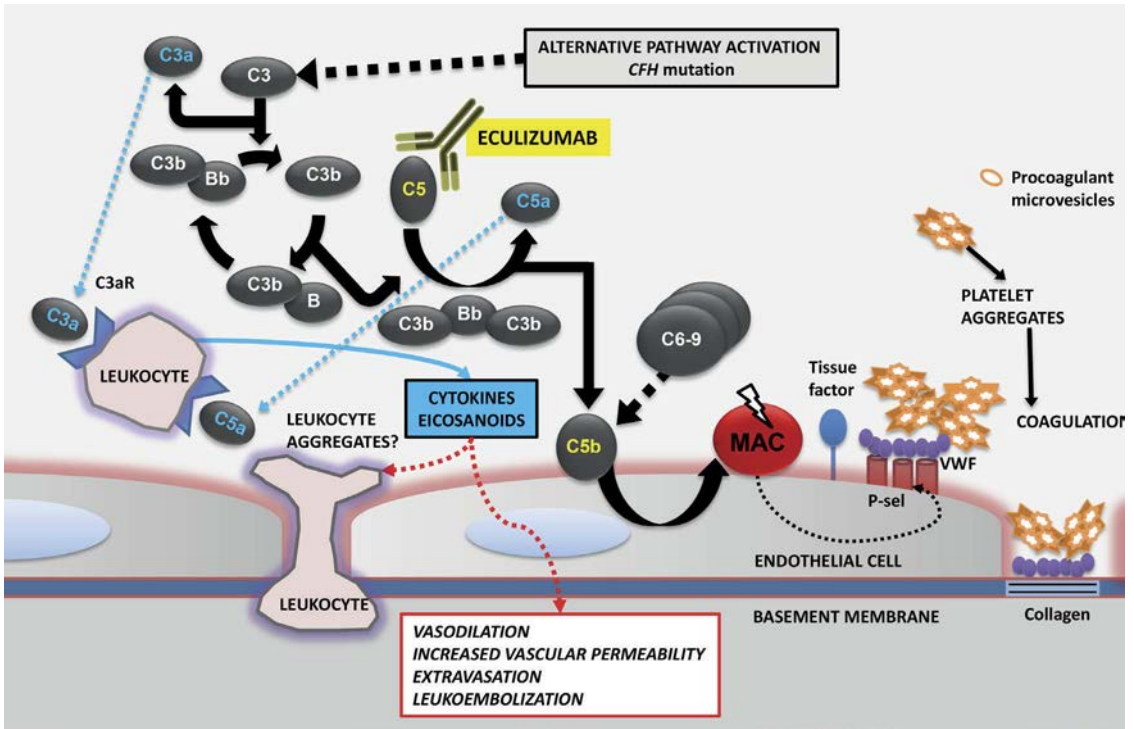


**Fig. 4.** Proposed pathogenic mechanisms of Purtscher-like retinopathy secondary to uncontrolled complement activation. The alternative pathway activates formation of C3b by C3; C3b interacts with factor B which is subsequently cleaved by factor D to form the alternative pathway C3 convertase (C3bBb). This enzyme complex is covalently attached to the target covalently via C3b whilst Bb is the catalytic serine protease subunit. Factor H regulates the alternative pathway by preventing the interaction of C3b with factor B, interacting with factor I-mediated cleavage of C3b and dissociating the C3 convertase of the alternative pathway (not shown). Unchecked, the terminal complement pathway is then activated with release of the complement anaphylatoxin C5a and formation of the membrane attack complex (MAC). Eculizumab binds C5 which is then unable to enter the C5 convertase (C3bBbC3b), impeding cleavage into the effector molecules, C5a and C5b and assembly of the terminal complement complex (C5b-9). This leads to exocytosis of adhesion molecules [P-selectin (P-sel)] and von Willebrand factor (VWF) which in turn will lead to platelet adhesion and aggregation, expression of tissue factor and activation of the coagulation cascade. Cell detachment exposes the subendothelial matrix, facilitating binding of VWF to collagen and subsequent amplification of the coagulation state. Platelet aggregates release procoagulant microvesicles that contain tissue factor. Receptors for C3a and C5a [C3a receptor (C3aR) and C5a receptor (C5aR)] in polymorphonuclear leukocytes and monocytes, bind these anaphylatoxins enhance the release of cytokines and eicosanoids contributing to an increase in vascular permeability, vasodilation, leukocyte extravasation and potentially formation of leukocyte aggregates.

## Disclosure

We report no proprietary or commercial interest in any product mentioned or concept discussed in this article. No financial support to disclose.

## References

1. Agrawal A, McKibbin MA: Purtscher's and Purtscher-like retinopathies: A review. *Surv Ophthalmol* 51:129-136, 2006
2. Agrawal A, McKibbin M: Purtscher's retinopathy: epidemiology, clinical features and outcome. *Br J Ophthalmol* 91:1456-1459, 2007
3. Pina JP, Ssi-Yan-Kai K, de Monchy I, et al.: Purtscher-like retinopathy: case report and review of the literature. *J Fr Ophthalmol* 31:609-613, 2008
4. Miguel AIM, Henriques F, Azevedo LFR, et al.: Systematic review of Purtscher's and Purtscher-like retinopathies. *Eye* 27:1-13, 2013
5. Behrensbaumann W, Scheurer G: M-Purtscher - range of clinical manifestations and pathogenesis. *Klin Monbl Augenheilkd* 198:99-107, 1991
6. Scheurer G, Praetorius G, Damerau B, Behrens-Baumann W: Vascular occlusion of the retina: an experimental model. I. Leukocyte aggregates. *Graefes Arch Clin Exp Ophthalmol* 230:275-280, 1992
7. Schroer H, Scheurer G, Behrens-Baumann W: Vascular occlusion of the retina--an experimental model. II. Platelet aggregates. *Graefes Arch Clin Exp Ophthalmol* 230:281-285, 1992
8. Wilkinson WS, Morgan CM, Baruh E, Gitter KA: Retinal and choroidal vascular occlusion secondary to corticosteroid embolisation. *Br J Ophthalmol* 73:32-34, 1989
9. Lemagne JM, Michiels X, Vancausenbroeck S, Snyers B: Purtscher-Like retinopathy after retrobulbar anesthesia. *Ophthalmology* 97:859-861, 1990
10. Blodi BA, Williams CA: Purtscher-like retinopathy after uncomplicated administration of retrobulbar anesthesia. *Am J Ophthalmol* 124:702-703, 1997
11. Lim BA, Ang CL: Purtscher-like retinopathy after retrobulbar injection. *Ophthalmic Surgery and Lasers* 32:477-478, 2001
12. Blodi BA, Johnson MW, Gass JD, et al.: Purtscher's-like retinopathy after childbirth. *Ophthalmology* 97:1654-1659, 1990
13. Lai JC, Johnson MW, Martonyi CL, Till GO: Complement-induced retinal arteriolar occlusions in the cat. *Retina* 17:239-246, 1997
14. Sacks T, Moldow CE, Craddock PR, et al.: Oxygen radicals mediate endothelial cell damage by complement-stimulated granulocytes. An in vitro model of immune vascular damage. *J Clin Invest* 61:1161-1167, 1978
15. Shapiro I, Jacob HS: Leukoembolization in ocular vascular occlusion. *Ann Ophthalmol* 14:60-62, 1982
16. Wu C, Dai RP, Dong FT, Wang Q: Purtscher-like retinopathy in systemic lupus erythematosus. *Am J Ophthalmol* 158:1335-1341, 2014
17. Nautiyal A, Amescua G, Jameson A, et al.: Sudden loss of vision: Purtscher retinopathy in multiple myeloma. *CMAJ* 181:E277-E277, 2009
18. Harrison TJ, Abbasi CO, Khraishi TA: Purtscher retinopathy: an alternative etiology supported by computer fluid dynamic simulations. *Invest Ophthalmol Vis Sci* 52:8102-8107, 2011
19. Stewart MW, Brazis PW, Guier CP, et al.: Purtscher-like retinopathy in a patient with HELLP syndrome. *Am J Ophthalmol* 143:886-887, 2007
20. Mayer C, Khoramnia R: Purtscher-like retinopathy caused by acute pancreatitis. *Lancet* 378:1653, 2011
21. Becheur H, Machevin L, Mostefa-Kara N, Zahedi R: Purtscher' ischemic retinopathy consecutive to an acute pancreatitis. *Gastroenterol Clin Biol* 25:922-924, 2001
22. Bui SK, O'Brien JM, Cunningham ET, Jr.: Purtscher retinopathy following drug-induced pancreatitis in an HIV-positive patient. *Retina* 21:542-545, 2001
23. Fumex L, Boizard Y, Burillon C, Denis P: Purtscher retinopathy in acute alcoholic pancreatitis. A case report. *J Fr Ophthalmol* 27:927-931, 2004
24. Carrera CR, Pierre LM, Medina FM, Pierre-Filho Pde T: Purtscher-like retinopathy associated with acute pancreatitis. *Sao Paulo Med J* 123:289-291, 2005
25. Krahulec B, Stefanikova J, Hlinst'akova S, et al.: Purtscher-like retinopathy - a rare complication of acute pancreatitis. *Vnitr Lek* 54:276-281, 2008
26. Bhan K, Ashiq A, Aralikatti A, et al.: The incidence of Purtscher retinopathy in acute pancreatitis. *Br J Ophthalmol* 92:151-153, 2008
27. Jeon SY, Jung E, Seol HJ, Hur YJ: Development of Purtscher-like retinopathy after pre-eclampsia combined with acute pancreatitis. *Obstet Gynecol Sci* 56:261-264, 2013
28. Tabandeh H, Rosenfeld PJ, Alexandrakis G, et al.: Purtscher-like retinopathy associated with pancreatic adenocarcinoma. *Am J Ophthalmol* 128:650-652, 1999
29. Stoumbos VD, Klein ML, Goodman S: Purtscher's-like retinopathy in chronic renal failure. *Ophthalmology* 99:1833-1839, 1992
30. Zwolinska D, Medynska A, Galar A, Turno A: Purtscher-like retinopathy in nephrotic syndrome associated with mild chronic renal failure. *Pediatr Nephrol* 15:82-84, 2000
31. Ong T, Nolan W, Jagger J: Purtscher-like retinopathy as an initial presentation of thrombotic thrombocytopenic purpura: a case report. *Eye (Lond)* 19:359-361, 2005
32. Patel MR, Bains AK, O'Hara JP, et al.: Purtscher retinopathy as the initial sign of thrombotic thrombocytopenic purpura/hemolytic uremic syndrome. *Arch Ophthalmol* 119:1388-1389, 2001
33. Power MH, Regillo MC, Custis PH: Thrombotic thrombocytopenic purpura associated with purtscher retinopathy. *Arch Ophthalmol* 115:128-129, 1997
34. Tajunisah I, Patel DK, Subrayan V: Purtscher retinopathy as an initial presentation of thrombotic thrombocytopenic purpura. *J Thromb Thrombolysis* 30:112-113, 2010
35. Lauer AK, Klein ML, Kovarik WD, Palmer EA: Hemolytic uremic syndrome associated with Purtscher-like retinopathy. *Arch Ophthalmol* 116:1119-1120, 1998
36. Myers JP, Di Bisceglie AM, Mann ES: Cryoglobulinemia associated with Purtscher-like retinopathy. *Am J Ophthalmol* 131:802-804, 2001
37. Sauer A, Nasica X, Zorn F, et al.: Cryoglobulinemia revealed by a Purtscher-like retinopathy. *Clin Ophthalmol* 1:555-557, 2007
38. Chebil A, Mammouri R, Abdallah MB, El Matri L: Purtscher-like retinopathy as a rare presentation of cryoglobulinemia. *Middle East Afr J Ophthalmol* 23:219-221, 2016
39. Hollo G: Frequency of Purtscher's retinopathy. *Br J Ophthalmol* 92:1159-1159, 2008
40. Yan Y, Shen X: Purtscher-like retinopathy associated with dermatomyositis. *BMC Ophthalmol* 13:36, 2013
41. Wang AG, Yen MY, Liu JH: Pathogenesis and neuroprotective treatment in Purtscher's retinopathy. *Jpn J Ophthalmol* 42:318-322, 1998
42. Atabay C, Kansu T, Nurlu G: Late visual recovery after intravenous methylprednisolone treatment of Purtscher's retinopathy. *Ann*

- Ophthalmol 25:330-333, 1993
43. Nautiyal A, Amescua G, Jameson A, et al.: Sudden loss of vision: Purtscher retinopathy in multiple myeloma. *CMAJ* 181:E277, 2009
  44. Noris M, Remuzzi G: Atypical hemolytic-uremic syndrome. *N Engl J Med* 361:1676-1687, 2009
  45. Laure AK, Klein ML, Kovarik WD, Palmer EA: Hemolytic uremic syndrome associated with purtscher-like retinopathy. *Arch Ophthalmol* 116:1119-1120, 1998
  46. Patel MR, Bains AK, O'Hara JP, et al.: Purtscher retinopathy as the initial sign of thrombotic thrombocytopenic purpura/hemolytic uremic syndrome. *Arch Ophthalmol* 119:1388-1389, 2001
  47. Sturm V, Menke MN, Landau K, et al.: Ocular involvement in paediatric haemolytic uraemic syndrome. *Acta Ophthalmol* 88:804-807, 2010
  48. Jacob HS, Goldstein IM, Shapiro I, et al.: Sudden blindness in acute pancreatitis. Possible role of complement-induced retinal leukoembolization. *Arch Intern Med* 141:134-136, 1981
  49. Noris M, Remuzzi G: Glomerular diseases dependent on complement activation, including atypical hemolytic uremic syndrome, membranoproliferative glomerulonephritis, and C3 glomerulopathy: core curriculum 2015. *Am J Kidney Dis* 66:359-375, 2015
  50. Schmidt CQ, Herbert AP, Kavanagh D, et al.: A new map of glycosaminoglycan and C3b binding sites on factor H. *J Immunol* 181:2610-2619, 2008
  51. Pickering MC, de Jorge EG, Martinez-Barricarte R, et al.: Spontaneous hemolytic uremic syndrome triggered by complement factor H lacking surface recognition domains. *J Exp Med* 204:1249-1256, 2007
  52. Pickering MC, Cook HT, Warren J, et al.: Uncontrolled C3 activation causes membranoproliferative glomerulonephritis in mice deficient in complement factor H. *Nat Genet* 31:424-428, 2002
  53. Fakhouri F, Hourmant M, Campistol JM, et al.: Terminal complement inhibitor eculizumab in adult patients with atypical hemolytic uremic syndrome: a single-arm, open-label trial. *Am J Kidney Dis* 68:84-93, 2016
  54. Legendre CM, Licht C, Muus P, et al.: Terminal complement inhibitor eculizumab in atypical hemolytic-uremic syndrome. *N Engl J Med* 368:2169-2181, 2013
  55. Noris M, Galbusera M, Gastoldi S, et al.: Dynamics of complement activation in aHUS and how to monitor eculizumab therapy. *Blood* 124:1715-1726, 2014
  56. Kavanagh D, Goodship TH: Atypical hemolytic uremic syndrome. *Curr Opin Hematol* 17:432-438, 2010
  57. Yusuf IH, Watson SL: Purtscher retinopathies: Are we aiming at the wrong target? *Eye* 27:783-785, 2013
  58. Holak HM, Holak S: Prognostic factors for visual outcome in Purtscher retinopathy. *Surv Ophthalmol* 52:117-118, 2007
  59. Gil P, Pires J, Costa E, et al.: Purtscher retinopathy: to treat or not to treat? *Eur J Ophthalmol* 25:E112-E115, 2015
  60. Despriet DD, Klaver CC, Witteman JC, et al.: Complement factor H polymorphism, complement activators, and risk of age-related macular degeneration. *JAMA* 296:301-309, 2006
  61. Duvvari MR, Paun CC, Buitendijk GH, et al.: Analysis of rare variants in the C3 gene in patients with age-related macular degeneration. *PLoS One* 9:e94165, 2014
  62. Mullins RF, Aptsiauri N, Hageman GS: Structure and composition of drusen associated with glomerulonephritis: implications for the role of complement activation in drusen biogenesis. *Eye* 15:390-395, 2001
  63. Esparza-Gordillo J, Goicoechea de Jorge E, Buil A, et al.: Predisposition to atypical hemolytic uremic syndrome involves the concurrence of different susceptibility alleles in the regulators of complement activation gene cluster in 1q32. *Hum Mol Genet* 14:703-712, 2005
  64. Yehoshua Z, de Amorim Garcia Filho CA, Nunes RP, et al.: Systemic complement inhibition with eculizumab for geographic atrophy in age-related macular degeneration: the COMPLETE study. *Ophthalmology* 121:693-701, 2014
  65. Ferris FL, 3rd, Wilkinson CP, Bird A, et al.: Clinical classification of age-related macular degeneration. *Ophthalmology* 120:844-851, 2013



7

# Spectral imaging of the ocular fundus using a 7-band retinal multispectral imaging system

J. Emanuel Ramos de Carvalho<sup>a</sup>, Richelle J.M. Hoveling<sup>b</sup>, Frank D. Verbraak<sup>a</sup>, Cornelis J. F. van Noorden<sup>a</sup>, Reinier O. Schlingemann<sup>a</sup>, Maurice C. G. Aalders<sup>b</sup>

<sup>a</sup> Ocular Angiogenesis Group, Departments of Ophthalmology and Medical Biology, Academic Medical Center, University of Amsterdam, Amsterdam, The Netherlands

<sup>b</sup> Department of Biomedical Engineering and Physics, Academic Medical Center, University of Amsterdam, Amsterdam, The Netherlands

## Abstract

Implementation of molecular imaging in ophthalmology relies on the availability of efficient imaging techniques that can detect and quantify chromophores to visualize molecular processes in vivo. We describe a 7-band retinal multispectral imaging (MSI) system and compare it with a hyperspectral imaging (HSI) device. Retinal oximetry studies were conducted as proof of principle.

Both devices incorporate optical bandpass filters in a mydriatic fundus camera. The MSI system scans the retina at 7 pre-defined wavelengths between 450 and 620 nm at which the absorption spectrum of hemoglobin has unique features. The HSI system acquires a full scan from 480 to 720 nm by tuning the transmission of a liquid crystal-based tunable filter over that wavelength range. The spectrally-resolved reflectance of light is then calculated for each individual pixel of the image. Two oximetry methods were used. The first calculates the absorbance ratio of oxygenated hemoglobin ( $\text{HbO}_2$ ) and reduced hemoglobin (HbR). The second method is based on a correction algorithm that compares the attained reflectance measurements with reflectance spectra of fully oxygenated and deoxygenated blood and allows an estimation of relative retinal oxygen saturation.

The MSI device can be customized with pre-selected filter sets optimized for a chromophore of interest and thereby be used in future ophthalmic molecular imaging strategies.

## Introduction

Molecular imaging of spatiotemporal distribution of molecular and cellular processes in the retina, in vivo, depends on the development of imaging techniques such as retinal spectral imaging, broadly divided in *hyperspectral imaging* (HSI) or *multispectral imaging*

(MSI). In HSI, acquisition of a dataset may be accomplished by different methods: point scanning (or whiskbroom), line scanning (or pushbroom) and area scanning (or staredown).<sup>12</sup> In a point scanning system, a complete spectrum is acquired for each single pixel. Light originating from one point enters the objective lens and is separated into different wavelengths by a spectrometer and detected by a linear array detector<sup>12</sup>. In a line scanning system, the spectra of all pixels in one image line are acquired simultaneously. The light is dispersed onto a 2D charge-coupled device (CCD) detector and a 2D data matrix with one spatial dimension is acquired.<sup>12</sup>

To obtain the full hypercube, containing two spatial ( $x,y$ ) dimensions and one wavelength ( $\lambda$ ) dimension, lateral scanning is performed. Finally, an area-scanning system generates a hypercube by collecting sequential spectral images for each wavelength band.<sup>12; 34</sup> Data acquisition occurs in small steps at a pre-defined wavelength range by using liquid crystal tunable filters (LCTF), acousto-optic tunable filters (AOTF),<sup>28</sup> Fourier transform spectrometers,<sup>6</sup> spectro-temporal scanners,<sup>17</sup> and, more recently, volume holographic methods.<sup>24</sup>

In MSI, a limited number of pre-defined wavelengths are selected according to the spectral signature of the chromophore of interest. Again, several approaches have been developed. The oldest and still most common technique uses a motorized filter wheel in front of the camera for sequential imaging at specific wavelengths. This type of camera is also used in our study. A more recent approach is the use of custom Bayer filters in front of the sensor so that each (group of) pixels has its own bandpass filter. With these so-called snapshot multispectral cameras it is possible to obtain a hypercube without scanning. This technique is still under development.

Both HSI and MSI spectroscopic imaging may be integrated in conventional ocular fundus cameras enabling acquisition of retinal spectral hypercubes that contain two spatial ( $x,y$ ) dimensions and one wavelength ( $\lambda$ ) dimension, thus acquiring a 3D dataset or hypercube.

Retinal spectral imaging techniques for ocular fundus imaging are usually integrated in commercially-available fundus cameras and as a result share many of its advantages such as large field of view, user friendliness, and high resolution.<sup>16; 22; 23; 27; 29; 30</sup> Notwithstanding, the development of efficient retinal spectral imaging devices must address several issues inherent to spectral imaging of living tissue: transmission of light, image misalignment, temporal differences in tissue perfusion and spectral and spatial calibration. Limited transmission of light by the filter renders imaging at wavelengths below 500 nm difficult, and the high degree of variability of background signals induced by wavelength-dependent scattering may complicate data interpretation.<sup>39</sup> Furthermore, image acquisition in the retina is very sensitive to cardiac-dependent differences in retinal perfusion patterns and eye movement artifacts.<sup>7; 26</sup> In MSI, acquisition time is shorter because images are captured at selected wavelengths rather than uniformly across the entire spectrum as in HSI. Lastly, the raw spectral imaging data from an ocular fundus are affected by the level and chemical composition of the scanned structure but also by the intensity and homogeneity of illumination, the sensitivity of the detector and the transmission of the

optics.<sup>15</sup> The effect of these factors is mostly wavelength dependent but is also sensitive to spatiotemporal variations. Image registration and alignment software allow images to be spatially aligned, but illumination levels may differ in the aligned regions of interest due to changes in angle of illumination because of movement and the anatomical curvature of the ocular fundus.<sup>13</sup>

The aim of the present study was to develop and evaluate a fast and affordable MSI system with a filter wheel in the optical path. This newly-developed imaging system was tested and compared with a purposely-built HSI system incorporating a LCTF. A new method was described for retinal oximetry analysis that can be explored in future ophthalmic molecular imaging strategies.

## **Materials and methods**

### **The hyperspectral fundus camera**

The HSI device consists of a commercial mydriatic fundus camera (TRC-50LX; Topcon, Tokyo, Japan) and a LCTF (VariSpec; CRI, Woburn, MA, USA) incorporated in the optical path. The LCTF is a narrow bandpass filter based on stacked Lyot filter with an optical tuning range from 480 to 720 nm. The bandwidth varies between 5 nm at short wavelengths, and 20 nm at longer wavelengths. The filtered light is captured by a high-resolution camera with a spatial resolution of 1280 x 1024 pixels (DCC1545M, high resolution CMOS camera; Applied Laser Technology, Best, The Netherlands). To reduce noise generated by light reflected by the cornea and crystalline lens, the annular stop of the fundus camera was optically conjugated with the pupil of the eye. A linear polarizer was attached to the front of the CMOS camera to reduce specular reflection from the objective and from within the eye. The integration time varied from 50 to 150 ms per wavelength. The field of view corresponded to approximately 35 degrees. Eye fixation was maintained by using a fixation light for the contralateral eye. The average time to acquire a full data set depended on the selected range of wavelengths; for a full spectrum, with 5 nm steps, the acquisition time was approximately 15 sec. All acquired images were combined into a hypercube data set for further analysis. The HSI system was controlled with a customized software program, written in LabView (National Instruments, Austin, TX, USA). A saturation histogram, live feed of the CCD recording, and retinal spectral image stacks were displayed on the software user interface.

### **The multispectral fundus camera**

Our MSI system was similar to the one described above with exception of the tunable filter and camera. The incorporated tunable filter was a SpectroCam Multispectral Imaging System (Pixelteq, Duiven, The Netherlands). The SpectroCam featured a high

speed continuously rotating filter wheel containing 7 interchangeable optical filters. The following filters were selected 450 nm (15 nm bandwidth), 480 nm (25 nm bandwidth), 509 nm (10 nm bandwidth), 542 nm (10 nm bandwidth), 558 nm (5 nm bandwidth), 578 nm (10 nm bandwidth) and 620 nm (20 nm bandwidth). This filter set was optimized to match the spectral signatures of the main chromophores in the visible spectrum of oxygenated hemoglobin (HbO<sub>2</sub>) and reduced hemoglobin (HbR). A wideband CCD camera, with a resolution of 1392 x 1040 pixels, sensitive from ultraviolet to near infrared was used to enable the electronic capturing of retinal images. A linear polarizer was attached to the front of the CCD to reduce an artifact caused by the specular reflection from the two surfaces of the objective lens within the fundus camera and from the air-cornea-lens interface. The field of view corresponded to approx. 20 degrees. The MSI imaging system was controlled with a software program provided by the manufacturer (Pixelteq). A saturation histogram, live feed of the CCD recording and retinal spectral image stack were displayed on the software interface.

### **Participants and image acquisition**

This study adhered to the tenets of the Declaration of Helsinki. Informed consent was obtained from each subject before imaging. Thirty voluntary participants with ages between 18 and 79 were scanned. Ten eyes were imaged using the HSI device and 20 eyes were imaged using the MSI device. Exclusion criteria included poor quality images with significant artifact, or subject's inability to abstain from blinking or movement during image acquisition. The original light source of the commercial mydriatic fundus camera (Topcon) was maintained in the setup of both HSI and MSI cameras thus complying with the established safety criteria for photobiological safety of lamps and ophthalmic instruments.<sup>9</sup>

Prior to eye scanning, the pupil was dilated using tropicamide 1% (1 drop). Eye fixation was maintained by instructing the subject to focus on a red fixation light with the contralateral eye. Acquisition time was 15 sec for the HSI device and 2.5 sec for the MSI device [0.8 sec when 2 wavelengths were applied (e.g. for ratio calculations)]. Scanning was repeated whenever large eye movements or blinking was observed, usually 3 times per participant. The best quality scan with the least amount of motion artifact was selected for analysis.

### **Data pre-processing and analysis**

#### **Calibration and spectral pre-processing**

Pre-processing was performed to eliminate or minimize unwanted artifacts such as noise, dead and spiked pixels, specular reflections, scattering effects and other instrumental variations. First, the dark response [ $I_{dark,ij}(\lambda)$ ] of the camera was subtracted. In order to correct for wavelength-dependent intensity differences in the light source, the background

response of a white reference plane (blank paper) at all wavelengths [ $I_{white}(\lambda)$ ], previously corrected for the dark response, was:

$$R_{ij}(\lambda) = \frac{I_{ij}(\lambda) - I_{dark, ij}(\lambda)}{I_{white}(\lambda) - I_{dark, ij}(\lambda)}$$

$R$  is reflectance,  $I$  is light intensity and  $i$  and  $j$  are horizontal and vertical pixel indices. Reflectance spectra obtained from the HSI measurements were corrected using the standard normal variate algorithm.<sup>1</sup> All data analysis was performed using custom-made scripts written in MATLAB (The Mathworks, Natick, MA, USA).

### Image registration and processing

A cross-correlation technique was used for image registration in which similarities in consecutive images were used for alignment. The cross-correlation techniques requires similar features between images irrespective of the wavelength. However, as the appearance of spectral images change with wavelength, sequential spectral retinal images were acquired in such a way that the main features in retinal images (optic disc and large retinal vessels) were located in similar positions in the image field. Automatic motion correction was performed using ImageJ and the tool “linear stack alignment via Scale Invariant Feature Transform”<sup>25</sup> to transform image data into scale-invariant coordinates relative to local features.

Alternatively, a single wavelength image was selected that showed the highest contrast between different components based on absorbance differences. Compositional contrast between pixels in an image was displayed by grayscale with intensity scaling. Image quality was highly variable and depended on clarity of the media (presence of cataract), movement of the subject, fixation of the eye and intolerance to standard illumination levels. Images of each eye were acquired until quality was deemed acceptable for analysis (mean of 3 scans per eye). Poor quality images (defocused or with high movement between frames) were discarded after evaluation by 2 observers (JERC and RJMH). Data analysis was performed using custom-made scripts written in MATLAB (The Mathworks).

### Measurement of reflectance signals

Two different methods for retinal spectroscopy using hemoglobin as an intrinsic chromophore are presented.

The first (indicative) method was based on the spectral signature of HbO<sub>2</sub> and HbR. Fig. 1 shows that the spectrum of HbO<sub>2</sub> has absorbance peaks at 542 nm and 578 nm and an absorbance trough at 558 nm, whereas the spectrum of HbR has an absorbance peak at 558 nm. The measured reflectance depends on contributions of both HbO<sub>2</sub> and HbR and from other chromophores. In a low oxygenation state the contribution of HbR is increased, resulting in a low ratio between reflectance values at 558 nm and 578 nm. In cases of a high oxygenation state, the contribution of HbO<sub>2</sub> is increased, resulting in a high 558/578 ratio. These ratios are affected by scattering and light absorbance by chromophores other than hemoglobin. The reflectance measurements have not been directly validated (e.g. against *ex vivo* measurements in phantom or Monte-Carlo simulations), therefore the acquired data can only be used to obtain an estimation of HbO<sub>2</sub>/HbR ratios which were expressed as the logarithm of the ratio of the reflectance value at 558 nm and that at 578 nm.

The second method was based on an algorithm that corrects for the influence of non-hemoglobin absorption as well as tissue scattering. The measured reflectance spectra are corrected by linear transformation in order to match these with reference spectra of HbO<sub>2</sub> and HbR at three isosbestic points, as first described by Hammer et al<sup>21</sup>. The O<sub>2</sub> saturation can then be determined by assuming a linear relationship with the corrected intensity at a wavelength showing a high contrast between HbO<sub>2</sub> and HbR (e.g. 558 nm). The original algorithm uses data at 3 isosbestic wavelengths (522 nm, 569 nm and 586 nm) as well as 560 nm. The quality of the HSI data at these wavelengths precluded application of this correction method to images obtained with the HSI technique. We selected 4 wavelengths for images obtained with the MSI device, 509 nm, 542 nm, 578 nm and 558 nm resulting in  $X_{509}$ ,  $X_{542}$ ,  $X_{578}$  and  $X_{558}$  as reflectance measurements. The theoretical reflectances  $R_{509}$ ,  $R_{542}$ ,  $R_{582}$ ,  $R_{558}^{0\%}$  and  $R_{558}^{100\%}$  were derived from the reference data. The reference data stems from the data shown in the Fig. 1 which depicts the absorption spectra for the pure components HbR and HbO<sub>2</sub>. In practice a mixture of two absorbers is measured, resulting in an absorption value somewhere between these two extremes. The superscripts 0% and 100% denote deoxygenated and oxygenated blood, respectively.  $X$  is again expressed as the logarithm of the reflectance value in the pixel and  $R$  as the logarithm of the reflectance value of HbR and HbO<sub>2</sub>. We performed a simulation to assess the performance of the algorithm with our selected wavelengths. Results of the simulations are expressed as ‘estimated’ oxygenation values versus ‘absolute’ oxygenation status.

The algorithm comprised the following 5 steps. Each letter (A-D) in the algorithm corresponds to a specific set of wavelengths used in this and other studies (Table 1).

1. A linear function  $g(\lambda)$  with  $g(A) = R_A$  and  $g(C) = R_C$  is determined.
2. A linear function  $f(\lambda)$  with  $f(A) = X_A$  and  $f(C) = X_C$  is determined.
3. The measured data are added by the difference between  $g(\lambda)$  and  $f(\lambda)$ :

$$X'(\lambda) = X(\lambda) + g(\lambda) - f(\lambda)$$

The correction forces the values of the measurements to be identical with that of the reflectance data at the isosbestic wavelengths  $A$  and  $C$ . Thus it compensates for any extinction (by absorption or scattering) other than hemoglobin absorption provided that extinction is linear with wavelength in a logarithmic scale (i.e. an exponential function of the wavelength).

4. A second correction step is applied to the data  $X'(\lambda)$  in order to correct for different conditions of illumination and measurement between the sample spectra and the reference spectra. In this correction step the data  $X'(\lambda)$  is stretched and compressed around the line  $g(\lambda)$  to match the reference data at isosbestic wavelength  $B$ , applying

$$X''(\lambda) = g(\lambda) - \frac{(X'(\lambda) - g(\lambda))(R^D - g(D))}{X'(B) - g(B)}$$

5. The oxygen saturation (OS) is indicated by  $X''(D)$  on a linear scale between  $R^{0\%}(D)$  and  $R^{100\%}(D)$

$$OS = \frac{X''(D) - R^{0\%}(D)}{R^{100\%}(D) - R^{0\%}(D)} \times 100\%$$

	MSI	Hammer	Braaf	Isosbestic
A	509	522	530	522
B	542	569	542	549
C	578	586	582	586
D	450	560	562	560

**Table 1.** Wavelengths (nm) used for oxygenation estimation.

## Results

### The ocular fundus hypercube

HSI and MSI images of the ocular fundus are analogous to a stack of images, each acquired at a narrow spectral band. The resulting data set is a 3D block of data, the so-called hypercube (Fig. 1), with two spatial (x,y) dimensions and one wavelength ( $\lambda$ ) dimension. This hypercube provides images for each wavelength ( $\lambda_i$ ) and a reflectance spectrum in each individual pixel ( $x_j, y_k$ ). Fig. 2 shows a typical retinal spectral data set at specific wavelengths obtained with the MSI and HSI devices. Image analysis demonstrates that light penetration is wavelength-dependent which results in an inhomogeneous representation of retinal structures at different wavelengths. At wavelengths above 590 nm, the choroidal vasculature becomes visible with both techniques.

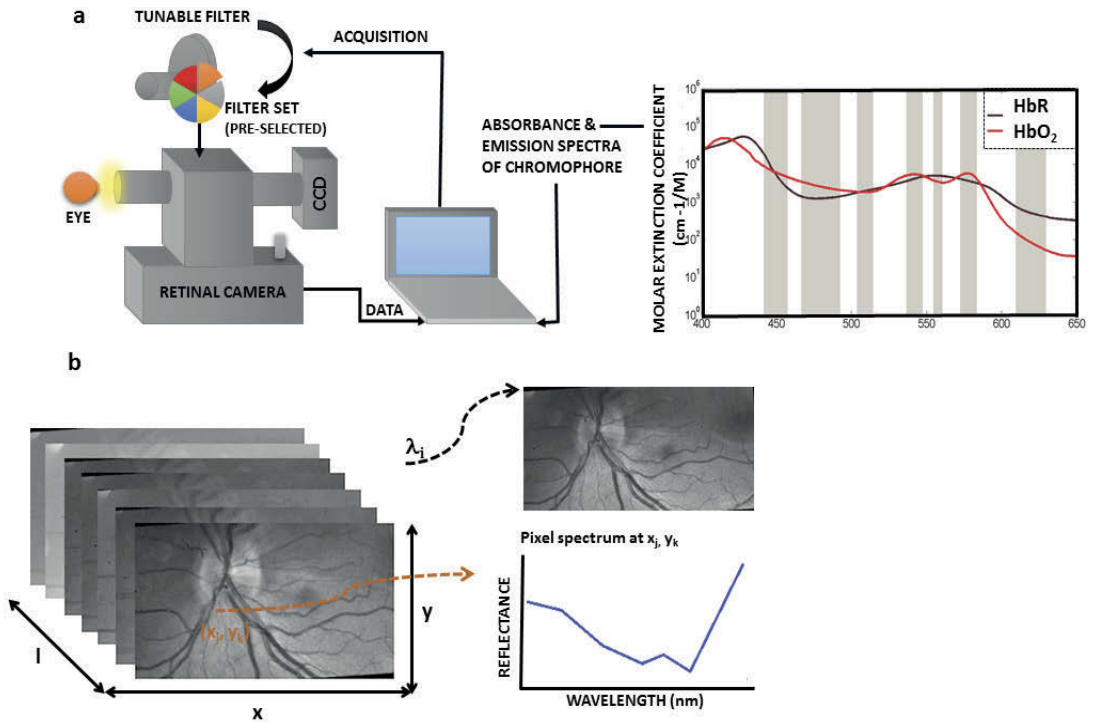


**Fig. 1.** Illustration of the steps involved in retinal spectral imaging (a) Schematic representation of the multispectral retinal imaging device. The spectral signature of a chromophore of interest (Hb and HbR) is determined by optical spectroscopy. The resulting spectrum is presented as reflectance versus wavelength. A specific wavelength filter set is pre-selected in MSI with gain adjusted per wavelength. In HSI, a tunable filter is used for image acquisition at a range of wavelengths. The tunable filter is incorporated in the optical pathway of a commercially-available mydriatic fundus camera. (b) Retinal multispectral dataset (or hypercube), with two spatial (x,y) and one wavelength ( $\lambda$ ) dimension. An image plane of the hypercube is shown for one wavelength ( $\lambda_i$ ) and a reflectance spectrum is obtained of one pixel ( $x_j, y_k$ ).

### Comparison of MSI with HSI

Images obtained with MSI were of better quality when compared to images obtained with HSI (Fig. 2). The gain was optimized for each wavelength that was used for measurements with MSI, resulting in good quality measurements at lower wavelengths. The HSI device failed to capture acceptable quality images at wavelengths < 558 nm and was more prone to artifacts. Acquisition time was longer for the HSI device (15 sec versus 2.5 sec), which in turn resulted in increased image misalignment. For this reason, we did not use HSI data for further analysis. Table 2 summarizes the main advantages and disadvantages of each method.

**Multispectral Imaging**  
Acquisition time: 2.5 sec

**Hyperspectral Imaging**  
Acquisition time: 15 sec

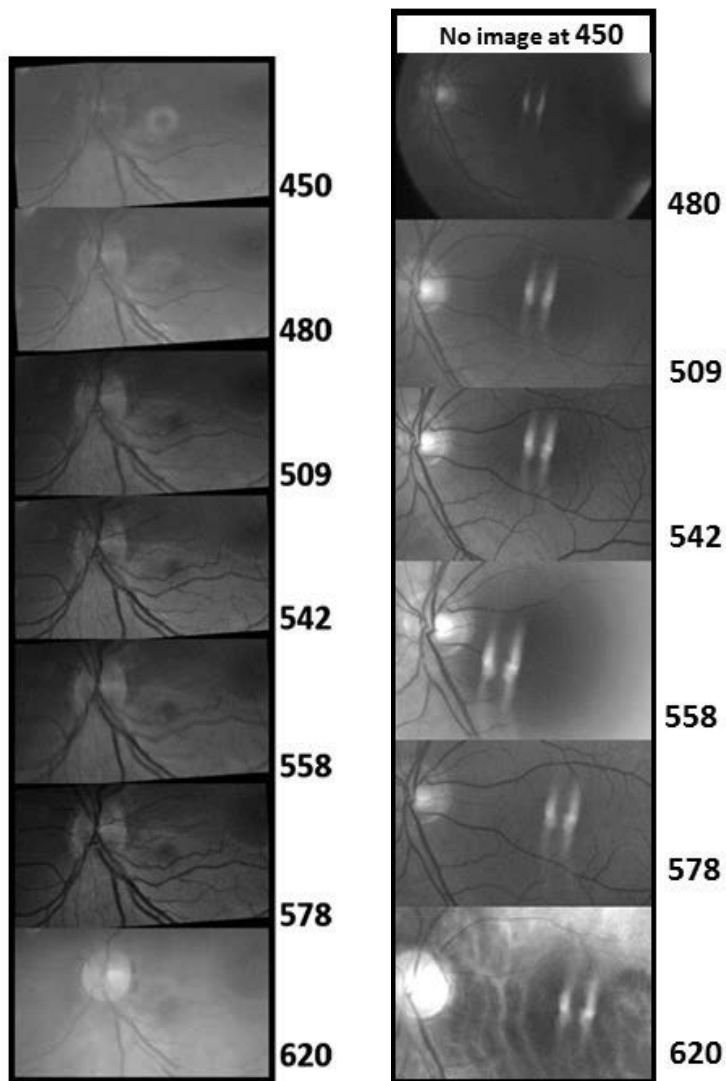


**Fig. 2.** Comparison of ocular fundus images captured with MSI and HSI. With MSI, images are captured at pre-selected wavelengths (with adjustment of gain per wavelength) based on the spectral properties of hemoglobin in blood. A full spectral scan (480 - 800 nm) is performed with the HSI system. The MSI system has a shorter acquisition time, captures images at lower wavelengths (> 450 nm) produces less image artifacts and the alignment and overall image quality are superior. Images are normalized and registered.

## Hemoglobin reflectance measurements in the retina

The reflectance spectra of different regions of the retina are presented in Fig. 3. Distinct reflectance minima are present at 540 nm and 585 nm, which correspond to the absorbance peaks of HbO<sub>2</sub>. A distinct reflectance peak is present at ~ 560 nm and corresponds to the absorbance peak of HbR.

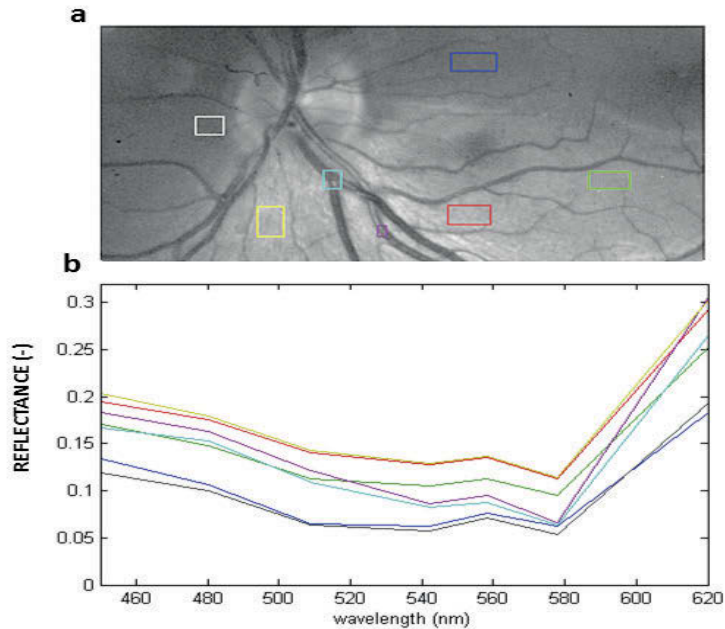


**Fig. 3.** Reflectance spectrum of different retinal regions. (a) MSI ocular fundus image at 542 nm. (b) Corresponding reflectance spectra (colored squares correspond to colored lines) of different regions in the retina. Reflectance demonstrates troughs at 542 nm and 578 nm corresponding to the absorbance spectrum of HbO<sub>2</sub>.

## Reflectance spectra ratios of hemoglobin

We obtained 2D distributions of HbO<sub>2</sub> and HbR in the retina by calculating the ratio of the reflectance values at 558 and 578 nm (Fig. 4). A smoothing filter was applied to the data to reduce noise. A higher ratio indicates a larger contribution of HbO<sub>2</sub> with respect to HbR, which may provide an estimation of relative oxygen saturation levels. In Fig. 5, a reflectance spectrum from one pixel from a retinal arteriole and venule are shown. In the wavelength range 540 – 580 nm, the reflectance spectra differ with higher ratios in the artery. This reflects physiological levels of oxygen saturation. These values are expected to approximate relative oxygen saturation; the actual oxygen saturation levels are unknown because the experiments lack proper validation.

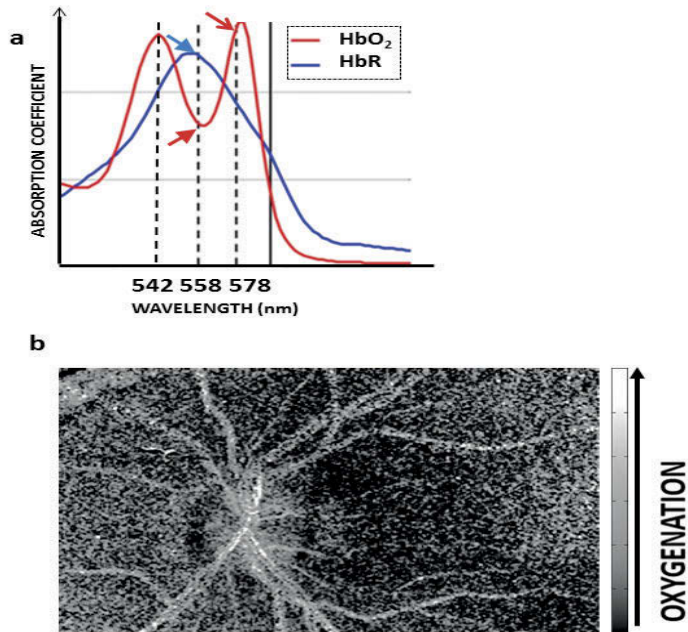


**Fig. 4.** Visualization of a 2-wavelength ratio of reflectance spectra. (a) Absorbance spectra of HbO<sub>2</sub> and HbR showing 3 selected wavelengths, 558 nm with a peak of HbR (blue arrow) and a trough of HbO<sub>2</sub> (red arrow) and the dual peak of HbO<sub>2</sub> at 542 and 578 nm (red open arrow). (b) Grayscale image of the ratios of reflectance at 558 nm and 578 nm. Regions in white correspond to areas of high relative oxygenation.

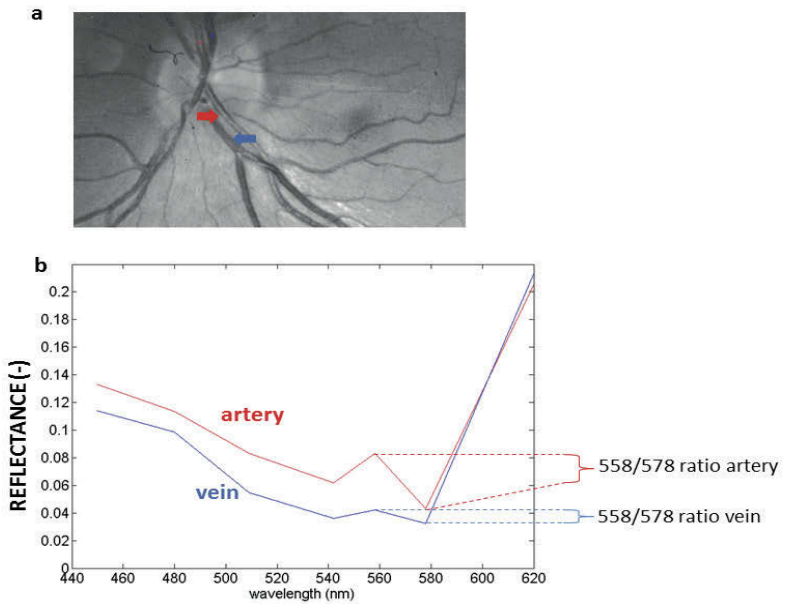


**Fig. 5.** Reflectance spectra of artery and vein. (a) Multispectral image of the peripapillary region showing an artery (red) and a vein (blue), selected for reflectance measurements. (b) Reflectance measurements in the artery and vein. The 558/578 ratio corresponds to reflectance measured at 558 nm corresponding to the combination of the trough absorbance of  $\text{HbO}_2$  and at 578 nm corresponding to the peak absorbance of  $\text{HbO}_2$ ; the artery shows a higher 558/578 ratio which means that the contribution of  $\text{HbO}_2$  is higher than the contribution of  $\text{HbR}$ .

### Estimation of relative retinal oxygen saturation by the Hammer correction algorithm

2D distributions of relative retinal oxygen saturation as calculated using the Hammer correction algorithm are presented in Fig. 6. The correction algorithm was applied to the reflectance spectra obtained in each pixel of the retinal vessels and tissue. The filter set used in our MSI setup differed from the setup described by Hammer et al <sup>21</sup>. Other studies reported adaptations to the original method by using different wavelengths for the estimation of oxygenation (Table 1). We plotted the estimated oxygenation values obtained with the wavelengths selected in the present study and other studies with absolute (or ideal) oxygenation levels (Fig. 6c). Data shows that measurements with our MSI setup underestimate oxygen saturation levels at low oxygen saturation status, whereas estimates of higher oxygen saturation levels approximate ideal oxygenation measurements.

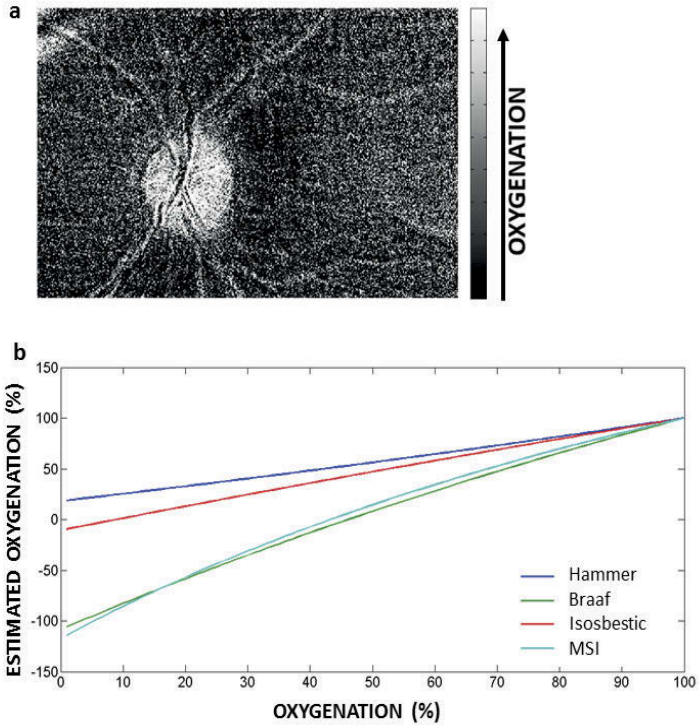


**Fig. 6.** Visualization of relative retinal oxygen saturation. (a) Determination of the relative saturation of oxygen by comparing the measured reflectance with reference spectra of fully oxygenated and deoxygenated blood (in grayscale). The algorithm is applied to measured reflectance data of the ocular fundus, with unknown oxygen saturation, at the wavelengths described for the MSI in Table 1. (b) Simulation of oxygen saturation levels using reflectance at various wavelengths described in Table 1. Estimated oxygenation values obtained with the wavelength settings used for the MSI device underestimated the relative oxygen saturation measurements when plotted against low absolute levels of oxygen saturation. At higher levels of estimated oxygen saturation, the values were similar independently of the wavelength.

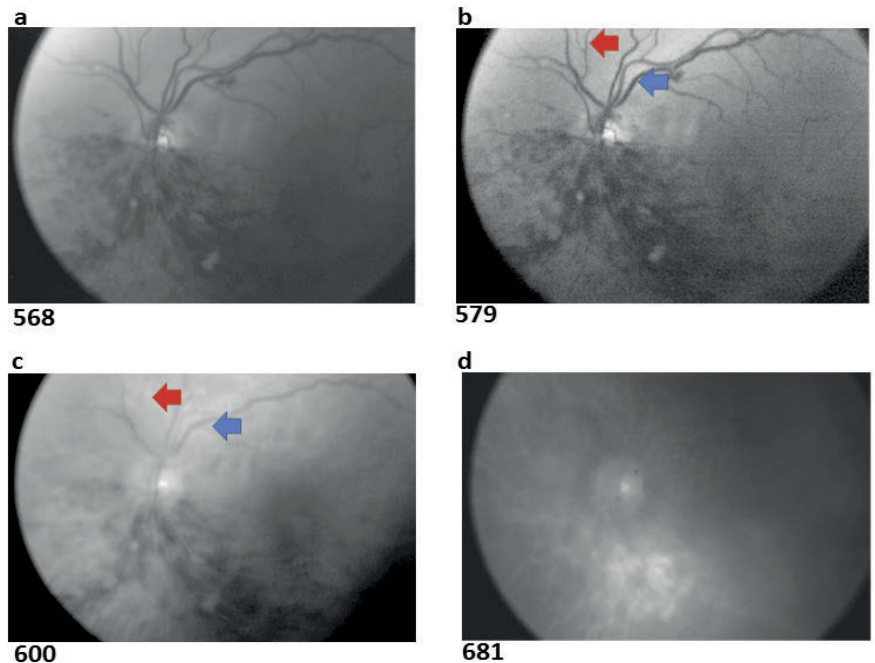


**Fig. 1 Suppl.** Wavelength-dependent penetration depth in retinal tissue. Ocular fundus images of a branch retinal vein occlusion at specified wavelengths. Images captured at wavelengths  $< 600$  nm show arterioles (red arrows) and venules (blue arrows) and hemorrhages alongside the inferior vascular arcade (a, b). At wavelengths  $\geq 600$  nm (c), arterioles are less visible as compared with venules. The choroid is visualized at wavelengths  $\geq 650$  nm (d) due to higher penetration of light. At these wavelengths, blood is no longer visible.

## Discussion

In our study, we compared efficiency and applicability of two spectral retinal imaging techniques, HSI and MSI. Development of molecular imaging contrast agents and approval for human use have been slower than expected. Therefore, hemoglobin was selected as an example of a naturally-occurring chromophore for retinal oximetry studies. MSI showed important advantages over the HSI system. First, the spatial resolution of the images obtained with MSI was higher. The short acquisition time of MSI reduces image alignment issues that may interfere with image pre-processing and spectral analysis. Moreover, exposure time can be adjusted per wavelength, which increases efficiency and comfort for the patient when compared to the HSI system. Nevertheless, our setup is affected by inherent difficulties similar to other retinal spectral imaging devices. Both techniques are prone to image acquisition artifacts in the raw reflectance images. Corneal reflections, blinking, and inability to hold the eyes open during

acquisition produce artifacts that at times cannot be corrected by image pre-processing techniques. Several methods have been described to reduce these artifacts which involve the exclusion of pixels when the model fit does not conform to expected.<sup>36</sup> Inaccurate measurements may also result from variations in illumination due to different light paths through the eye and the concave shape of the ocular fundus. In the case of retinal tissue oximetry, scattered light from blood vessels may interfere with measurements in surrounding tissue, which confounds reflectance measurements of hemoglobin in that region. This creates a low-pass filter effect, where the spectrum of each pixel represents an averaged spectrum of bordering pixels.

The spectral signature of a specific chromophore refers to distinct absorbance peaks at specific wavelengths that in turn can be used to recognize the chromophore of interest. Monte Carlo simulations have shown that at lower wavelengths, macular pigment and choroidal melanin affect reflectance measurements.<sup>38</sup> The method proposed by Hammer et al. is suitable for the calculation of blood oxygenation from reflection measurements at 4 wavelengths.<sup>21</sup> Moreover, tissue scattering can often be approximated by an exponential function of the wavelength which allows determining the compensation of scattering losses.<sup>20</sup>

We proceeded to evaluate the efficacy of the MSI device in its application to human subjects. Oximetry refers to the spectroscopic determination of blood saturation by oxygen, which is defined as the percentage (ratio) of HbO<sub>2</sub> over the total amount of hemoglobin. Several methods have been described for this purpose. Light absorbance can be measured at 2,<sup>3</sup> 3,<sup>31</sup> 4,<sup>14; 21</sup> or 5<sup>32</sup> different wavelengths that are relevant for the determination of blood saturation by oxygen. The main component of human blood that absorbs light is hemoglobin. Therefore, the absorbance characteristics are taken as an approximation of that of blood. The first retinal oximetry studies using spectral recordings were reported by Hammer and Schweitzer.<sup>33; 35</sup> Most studies on retinal oximetry measure oxygenation in retinal vessels.<sup>2</sup> Retinal tissue oxygenation measurements are complex to validate due to the dual vasculature of the neurosensory retina and wavelength-dependent penetration depth of the laser light.

We present 2 absorbance spectroscopy methods that can be applied for purposes other than oximetry. The first method is a simple assessment of the ratio between the absorbance peaks of hemoglobin. This simplified analysis ignores several considerations that are specific to retinal imaging, namely absorption by other chromophores such as melanin and loss of light due to tissue scattering. Light scattering by erythrocytes affects the absorbance spectrum of whole blood.<sup>4</sup> Spectra measured in retinal blood vessels reflect the absorbance by hemoglobin and scattering from erythrocytes and surrounding tissues. In addition, spectra are also affected by the presence of melanin in the retinal pigment epithelial and the choroid.<sup>19</sup> As a consequence, spectra measured in retinal blood vessels may be affected by the optical properties of the surrounding tissue.<sup>8; 33; 37</sup> Furthermore, the raw reflectance data are affected by the non-homogeneous distribution of blood in the retina. Therefore, the concentration of a specific chromophore cannot be obtained without accurately determining the diameters of the vessels, which is complex

for *in vivo* measurements with the current setup. The first method presented in this study is therefore not fit to retrieve validated oxygenation maps of the retina. However, the reflectance spectra of arteries and veins shown in Fig. 4 are in agreement with what was expected.

In an attempt to validate our measurements, we applied a spectroscopic technique based on the correction algorithm described by Hammer et al.<sup>21</sup> Measurements of oxygen saturation in the clinic are relative and not absolute, because these rely on standard calibrated models (such as the 2-wavelength model) dependent on arterial and venous oxygen saturation values that are used to compute calibration constants.<sup>5</sup> In this method, we assume a linear relationship of percentage of blood oxygen saturation and absorbance of hemoglobin in solution and blood.<sup>3; 40</sup> This method retrieves retinal oxygenation maps that demonstrate a significant underestimation of retinal oxygenation in tissue and vessels. At higher oxygen saturation, estimated oxygenation levels approach ideal estimates. The oxygenation maps shown in Fig. 6 can only be used as an indication of differences in oxygenation levels in the retina, since the data is not validated for absolute oxygenation levels in the human eye. Validation of retinal tissue spectral imaging data requires accurate modeling of light transport (for instance by Monte Carlo simulations) as well as analysis of the spectral properties of each tissue layer. This method, however, can be modified when used in combination with extrinsic molecular imaging agents. Any process on a molecular level affects measurements of specific parameters because the emission wavelength of probes depends on their microenvironment. Therefore, the spectra shift by changes in the environment such as pH. These spectra can be attained with this technique similar to as it has been described for hemoglobin.

We found an uneven distribution of HbO<sub>2</sub> in retinal tissue. This speckled pattern has also been demonstrated in other studies of retinal tissue oximetry<sup>10</sup> and is caused by a combination of factors. Studies have shown that at wavelengths above 590 nm, retinal spectroscopy also probes the choroid, which in turn affects oxygenation measurements due to its high blood flow.<sup>10</sup> This is exemplified in Suppl. Fig. 1, in which spectral imaging of the choroid at wavelengths > 600 nm was not affected by a large hemorrhage. On the other hand, Monte Carlo simulations demonstrated that in the 500 – 600 nm range, hemoglobin reflectance originates from the neurosensory retina in a larger proportion than choroidal hemoglobin does which means that measurements up to 600 nm depict the contribution of the inner retinal vasculature<sup>38</sup>. In addition, pigmentation differences between ocular fundi may result in different contributions of the choroid to outer retinal oxygenation.<sup>10</sup> The patchy oxygenation pattern may also be explained by image acquisition noise, which was not smoothed in our analysis at the expense of a lower spatial resolution. The speckled pattern may also reflect a ‘true’ unequal oxygen distribution in the retina, similar to findings in brain tissue. Brain tissue oxygenation studies have shown large partial pressure of oxygen (PO<sub>2</sub>) differences in areas outside arterioles and venules.<sup>11</sup>

In summary, our study demonstrates the superior properties of a MSI device over a HSI device for ocular fundus spectral imaging. The MSI technique enables the acquisition

of high-resolution images both at low and high wavelengths. The ability to select spectral filters based on the spectral properties of specific chromophores opens up new possibilities for MSI to be applied in a wider range of molecular imaging applications. The development of extrinsic contrast imaging agents will dictate further development of the field of retinal spectral molecular imaging.

### **Disclosure**

We report no proprietary or commercial interest in any product mentioned or concept discussed in this article. No financial support to disclose.

## References

1. Barnes RJ, Dhanoa MS, Lister SJ: Standard normal variate transformation and de-trending of near-infrared diffuse reflectance spectra. *Appl Spectrosc* 43:772-777, 1989
2. Beach J: Pathway to Retinal Oximetry. *Transl Vis Sci Technol* 3:2, 2014
3. Beach JM, Schwenzler KJ, Srinivas S, et al.: Oximetry of retinal vessels by dual-wavelength imaging: calibration and influence of pigmentation. *J Appl Physiol* 86:748-758, 1999
4. Bosschaart N, Edelman GJ, Aalders MCG, et al.: A literature review and novel theoretical approach on the optical properties of whole blood. *Laser Med Sci* 29:453-479, 2014
5. Braaf B. NA, Faber D., Ter Wee R., Van Leeuwen T., Aalders M. : Blood oxygen saturation of frozen tissue determined by hyperspectral imaging. *Proc SPIE* 6859 685907-1, 2008
6. Choi H, Wadduwage D, Matsudaira PT, So PTC: Depth resolved hyperspectral imaging spectrometer based on structured light illumination and Fourier transform interferometry. *Biomed Opt Express* 5:3494-3507, 2014
7. de Carvalho JER, Verbraak FD, Aalders MC, et al.: Recent advances in ophthalmic molecular imaging. *Surv Ophthalmol* 59:393-413, 2014
8. Delori FC: Noninvasive technique for oximetry of blood in retinal vessels. *Appl Opt* 27:1113-1125, 1988
9. Delori FC, Webb RH, Sliney DH: Maximum permissible exposures for ocular safety (ANSI 2000), with emphasis on ophthalmic devices. *J Opt Soc Am A* 24:1250-1265, 2007
10. Desjardins M, Sylvestre JP, Jafari R, et al.: Preliminary investigation of multispectral retinal tissue oximetry mapping using a hyperspectral retinal camera. *Exp Eye Res* 146:330-340, 2016
11. Devor A, Sakadzic S, Saisan PA, et al.: "Overshoot" of  $O_2$  is required to maintain baseline tissue oxygenation at locations distal to blood vessels. *J Neurosci* 31:13676-13681, 2011
12. Edelman GJ, Gaston E, van Leeuwen TG, et al.: Hyperspectral imaging for non-contact analysis of forensic traces. *Forensic Sci Int* 223:28-39, 2012
13. Everdell NL, Styles IB, Calcagni A, et al.: Multispectral imaging of the ocular fundus using light emitting diode illumination. *Rev Sci Instrum* 81, 2010
14. Fenton BM, Gayeski TEJ: Determination of microvascular oxyhemoglobin saturations using cryospectrophotometry. *Am J Physiol* 259:H1912-H1920, 1990
15. Geladi P, Burger J, Lestander T: Hyperspectral imaging: calibration problems and solutions. *Chemometr Intell Lab* 72:209-217, 2004
16. Gorman A, Fletcher-Holmes DW, Harvey AR: Generalization of the Lyot filter and its application to snapshot spectral imaging. *Opt Express* 18:5602-5608, 2010
17. Gramatikov BI: Modern technologies for retinal scanning and imaging: an introduction for the biomedical engineer. *Biomed Eng Online* 13:52, 2014
18. Hagen N, Kudenov MW: Review of snapshot spectral imaging technologies. *Opt Eng* 52, 2013
19. Hammer M, Leistriz S, Leistriz L, Schweitzer D: Light paths in retinal vessel oxymetry. *IEEE T Bio-Med Eng* 48:592-598, 2001
20. Hammer M, Roggan A, Schweitzer D, Muller G: Optical properties of ocular Fundus tissues - an in vitro study using the double-integrating sphere technique and inverse Monte-Carlo simulation. *Phys Med Biol* 40:963-978, 1995
21. Hammer M, Thamm E, Schweitzer D: A simple algorithm for in vivo ocular fundus oximetry compensating for non-haemoglobin absorption and scattering. *Phys Med Biol* 47:N233-N238, 2002
22. Hirohara Y, Okawa Y, Mihashi T, et al.: Validity of retinal oxygen saturation analysis: Hyperspectral imaging in visible wavelength with fundus camera and liquid crystal wavelength tunable filter. *Opt Rev* 14:151-158, 2007
23. Johnson WR, Wilson DW, Fink W, et al.: Snapshot hyperspectral imaging in ophthalmology. *J Biomed Opt* 12, 2007
24. Liu W, Barbastathis G, Psaltis D: Volume holographic hyperspectral imaging. *Appl Opt* 43:3581-3599, 2004
25. Lowe DG: Distinctive image features from scale-invariant keypoints. *Int J Comput Vision* 60:91-110, 2004
26. Masquelier T, Portelli G, Kornprobst P: Microsaccades enable efficient synchrony-based coding in the retina: a simulation study. *Sci Rep-Uk* 6, 2016
27. Mordant DJ, Al-Abboud I, Muyo G, et al.: Spectral imaging of the retina. *Eye* 25:309-320, 2011
28. Morris HR, Hoyt CC, Treado PJ: Imaging spectrometers for fluorescence and Raman microscopy - acoustooptic and liquid-crystal tunable filters. *Appl Spectrosc* 48:857-866, 1994
29. Muqit MMK, Denniss J, Nourrit V, et al.: Spatial and spectral imaging of retinal laser photocoagulation burns. *Invest Ophthalmol Vis Sci* 52:994-1002, 2011
30. Nourrit V, Denniss J, Muqit MMK, et al.: High-resolution hyperspectral imaging of the retina with a modified fundus camera. *J Fr Ophthalmol* 33:686-692, 2010
31. Pittman RN, Duling BR: Measurement of percent oxyhemoglobin in microvasculature. *J Appl Physiol* 38:321-327, 1975
32. Pittman RN, Duling BR: New method for measurement of percent oxyhemoglobin. *J Appl Physiol* 38:315-320, 1975
33. Schweitzer D, Hammer M, Kraft J, et al.: In vivo measurement of the oxygen saturation of retinal vessels in healthy volunteers. *IEEE Trans Biomed Eng* 46:1454-1465, 1999
34. Schweitzer D, Hammer M, Scibor M: Imaging spectrometry in ophthalmology - principle and applications in microcirculation and in investigation of pigments. *Ophthalmic Res* 28:37-44, 1996
35. Schweitzer D, Thamm E, Hammer M, Kraft J: A new method for the measurement of oxygen saturation at the human ocular fundus. *Int Ophthalmol* 23:347-353, 2001
36. Shore J, Lubin B: Spectral goodness of fit for network models. *Soc Networks* 43:16-27, 2015
37. Smith MH: Optimum wavelength combinations for retinal vessel oximetry. *Appl Opt* 38:258-267, 1999
38. Styles IB, Calcagni A, Claridge E, et al.: Quantitative analysis of multi-spectral fundus images. *Med Image Anal* 10:578-597, 2006
39. Tiedeman JS, Kirk SE, Srinivas S, Beach JM: Retinal oxygen consumption during hyperglycemia in patients with diabetes without retinopathy. *Ophthalmology* 105:31-36, 1998
40. Vankampen EJ, Zijlstra WG: Spectrophotometry of hemoglobin and hemoglobin derivatives. *Adv Clin Chem* 23:199-257, 1983

8

# Recent advances in ophthalmic molecular imaging

J. Emanuel Ramos de Carvalho<sup>a</sup>, Frank D. Verbraak<sup>a</sup>,  
Maurice C. Aalders<sup>b</sup>, Cornelis J. van Noorden<sup>a</sup>,  
Reinier O. Schlingemann<sup>a</sup>

<sup>a</sup> Ocular Angiogenesis Group, Departments  
of Ophthalmology and Medical Biology, Academic  
Medical Center, University of Amsterdam,  
Amsterdam, The Netherlands

<sup>b</sup> Department of Biomedical Engineering and Physics,  
Academic Medical Center, University of Amsterdam,  
Amsterdam, The Netherlands

## **Abstract**

The aim of molecular imaging techniques is the visualization of molecular processes and functional changes in living animals and human patients before morphological changes occur at the cellular and tissue level. Ophthalmic molecular imaging is still in its infancy and has mainly been used in small animals for pre-clinical research. The goal of most of these pre-clinical studies is their translation into ophthalmic molecular imaging techniques in clinical care. We discuss various molecular imaging techniques and their applications in ophthalmology.

## **Introduction**

The eye, compared to other tissues and organs, offers unique opportunities for imaging because of the presence of clear optical media. This means that images can be acquired repeatedly in a noninvasive manner. Most existing *in vivo* imaging methods of the eye visualize anatomical and morphological features and not molecular processes. Molecular imaging techniques allow the visualization of functional changes before these are visible otherwise. Convergence of molecular cell biology with non-invasive, high-resolution *in vivo* imaging techniques has proven to be of great value in the unraveling of disease-causing molecular processes in cells and tissues. Molecular imaging is used for the study of a multitude of biological processes such as assessment of molecular interactions, visualization of multiple molecular events, pharmacokinetics, gene expression and effects of gene therapy—all accomplished in a reliable, fast, and quantitative manner. The ability to image pre-pathological mechanisms occurring in the natural micro-environment of cells and tissues in the body has already led to great advances in experimental medicine using laboratory animals.<sup>179</sup> It is expected that in the near future molecular imaging techniques will not only be used for basic

medical research, but also for customized patient care in a new era of molecular medicine.<sup>116, 139, 188</sup> Ophthalmic molecular imaging is still evolving, but progress is being made. In vivo imaging of ophthalmic molecular processes occurring in eyes of both human patients and experimental animals has already been achieved by several research groups worldwide.

Molecular imaging strategies are based on the use of endogenous or exogenous molecular probes or contrast agents to image molecular processes in cells or tissues of interest non-invasively, thus combining morphological information with real-time imaging of molecular processes. Many currently used imaging modalities are explored for molecular imaging, whereas others have been purposely developed. Molecular imaging modalities include optical imaging techniques such as fluorescence imaging, bioluminescence imaging, reflectance-based approaches, magnetic resonance imaging (MRI), radionuclide techniques such as positron emission tomography (PET) and single photon emission tomography (SPECT), ultrasonography, and computed tomography (CT).<sup>89, 92, 101, 108</sup> Thus far, molecular imaging has been largely applied in pre-clinical research using experimental animals due to the fact that the pharmacological and toxicological profiles of molecular probes have not yet been elucidated and thus are not approved for use in humans. Nevertheless, new contrast agents have been recently approved, and the use of endogenously expressed molecular probes or contrast agents is being explored.

We summarize recent developments that have been achieved by the application of molecular imaging techniques in ophthalmology (Table 1). In addition, modalities that have been adapted or developed for ophthalmic molecular imaging purposes are reviewed (Table 2).

Imaging modality	Measurement site	Information	Contrast agent or metabolite	Subjects	Refs.
<b><i>Apoptosis</i></b>					
Heidelberg retinal angiograph and scanning laser ophthalmoscope	Inner retina	Retinal ganglion cell apoptosis	Fluorescently labeled annexin 5	Murine	56, 109, E
Scanning laser ophthalmoscope	Inner and outer retina	Inner and outer retina apoptosis after laser overexposure	Fluorescently labeled annexin 5	Murine	118, 156
<b><i>Ocular Oxygen Homeostasis</i></b>					
Magnetic resonance imaging	Vitreous body	PO <sub>2</sub> gradients in the vitreous body	Oxygen – paramagnetic characteristics	Murine	8, 9, 78, 147, 148, 176, 204
Fluorine-19 magnetic resonance spectroscopy	Vitreous body	PO <sub>2</sub> gradients in the vitreous body	Perfluorocarbon droplet	Murine Human	60, 189, 204, 205

Optical phosphorescence imaging	Retina (tissue and vasculature)	PO <sub>2</sub> gradients in the retinal vessels and retinal tissue	Oxygen-sensitive molecular probe, OxyphorR2 <sup>39,40</sup>	Murine	161,162
Multispectral retinal imaging	Retina (tissue and vasculature), opticnerve head	PO <sub>2</sub> gradients in the retinal vessels and retinal tissue	Oxygen – absorbance spectrum	Human	52, 71, 120, 123, 131
Spectrophotometric retinal oximeter	Retina (vasculature)	PO <sub>2</sub> gradients in the retinal vessels	Oxygen – absorbance spectrum	Human	61, 62, 63, 64, 65, 133, 157, 173, 175, 202
<b>Ocular Immune Responses</b>					
Stereofluorescent microscope; Epifluorescent microscope	Cornea	Infiltration of inflammatory cells (neutrophils) into the cornea	eGFP-marked inflammatory cells	Murine	22, 172
Intravital microscopy	Cornea	Visualization of corneal dendritic cell networks	CD11c-YFP-marked dendritic cells	Murine	97
Intravital microscopy	Cornea	T cell migration into and within the cornea	Labeled ovalbumin-specific T cells	Murine	172
Epifluorescent microscope	Iris	Trafficking and uveitogenic potential of CD4 <sup>+</sup> T cells	Labeled ovalbumin-specific CD4 <sup>+</sup> T cells	Murine	6
Intravital microscopy and scanning laser ophthalmoscope	Iris	Leukocyte dynamics in the iris	Carboxylated fluorescent microspheres conjugated with glycoprotein ligand-1	Murine	193
Scanning laser ophthalmoscope	Retina (vasculature)	Leukocyte dynamics in the retina	Labeled calcein-AM syngeneic T cells	Murine	30, 195, 196, 197, 198
Scanning laser ophthalmoscope	Retina (vasculature)	Leukocyte dynamics in the retina	Acridine Orange	Murine	58
Scanning laser ophthalmoscope	Choriocapillaries	Endothelial injury in choriocapillaries in a model of endotoxin-induced uveitis	Fluorescent microspheres conjugated to rOSFL-Ig	Murine	119
Scanning laser ophthalmoscope	Retina	Microglia cells, dendritic cells and macrophages visualization	Replacement of one copy of the fractalkine receptor (CX3CR1) gene by GFP	Murine	44
<b>Microscopic Retinal Structures</b>					
Scanning laser ophthalmoscope	Retina	Visualization of retinal ganglion cells	Thy-1-CFP-marked retinal ganglion cells	Murine	100
Scanning laser ophthalmoscope	Retina	Visualization of retinal ganglion cells	Fluorescent 4-DiA marked retinal ganglion cells	Murine	69
Scanning laser ophthalmoscope	Retina	Visualization of retinal ganglion cells	Calcium fluorescent markers for retinal ganglion cells	Murine	141, 151

Scanning laser ophthalmoscope	Retina	Visualization of retinal ganglion cells	Rhodamine dextran-marked retinal ganglion cells	Primates	53
Scanning laser confocal microscope	Retina	Visualization of retinal ganglion cells dendrites and amacrine cells	Fluorescent reporters expressed in retinal ganglion cells	Zebrafish	122
Fluorescence Microscope	Retina	Visualization of retinal ganglion cells, axonal growth plasticity	Fluorescent carbocyanine dye Dil targeting of retinal ganglion cells	Goldfish	32
<b>Transplanted Cells</b>					
Scanning laser microscope	Retina (vasculature)	Visualization of stem cells and retinal vasculature	Bone-marrow derived lineage-negative haematopoietic GFP-expressing stem cells	Murine	146
<b>Ion Activity</b>					
Manganese-enhanced magnetic resonance imaging	Retina	Determination of changes in ion activity and retinal thickness	Manganese	Murine	10
Contrast-enhanced proton magnetic resonance imaging	Anterior and posterior eye chamber	Plasma protein diffusion into the aqueous humor	Gd-DTPA	Rabbits; monkeys	91
Deuterium magnetic resonance imaging	Anterior and posterior eye chamber	Water movement	Deuterated saline	Murine	132
<b>Neural Visual Response</b>					
Positron emission tomography (PET)	Occipital visual cortex and lateral geniculate nuclei	Attenuation of the central visual pathway due to unilateral hypertension glaucoma	2- <sup>[18F]</sup> fluoro-2-deoxy-glucose and <sup>[11C]</sup> PK11195	Monkeys	76
Single-photon emission computed tomography (SPECT)	Occipital visual cortex	Hypoperfusion of the occipital visual cortex in ophthalmoplegia	Tc-99m hexamethylpropylene amineoxime	Humans	55
Manganese-enhanced magnetic resonance imaging	Retina	Detection of ectopic expression of channelrhodopsin-2	GFP-channelrhodopsin-2 fusion construct	Murine	79
Diffusion magnetic resonance imaging	Optic nerve	Axonal and myelin damage	Water diffusion properties	Murine	199
<b>Blood-Retinal Barrier Permeability</b>					
Scanning laser ophthalmoscope	Retina (vasculature and tissue)	Blood-retinal barrier permeability	Rhodamine-labeled nanoparticles, rhodamine-labeled Lutrol-SDS particles, rhodamine-labeled DEAE-Lutrol particles	Murine	141, 151

Fluorescence mediated tomography	Vitreous body	Blood-retinal barrier permeability	Cy 5.5	Murine	67
Dynamic contrast enhanced magnetic resonance imaging	Vitreous body	Blood-retinal barrier permeability	Gd-DTPA	Murine	11
<b>Retinal Gliosis</b>					
Scanning laser ophthalmoscope	Optic disk astrocytes, retinal glial cells	Retinal gliosis	GFAP-GFP transgene	Murine	72, 95
<b>Pharmacokinetics</b>					
Manganese-enhanced magnetic resonance imaging	Anterior segment and vitreous body	Assessment of the electrical current pathways and the sites of drug delivery in transscleral and transcorneal iontophoresis	Manganese	Rabbits	102
Magnetic resonance imaging	Vitreous body and posterior segment	Real-time movement of a drug surrogate released from a polymer-based intravitreal implant	Gd-DTPA	Rabbits	85
Dynamic contrast enhanced magnetic resonance imaging	Anterior and posterior segment	Distribution and clearance of Gd-DTPA	Gd-DTPA	Rabbits	87
Micro-positron emission tomography	Vitreous body and posterior segment	Distribution and clearance of bevacizumab and ranibizumab in the vitreous cavity	I-124	Rabbits	28
Ocular fluorophotometry	Anterior segment	Distribution and clearance of fluoresceinated dextrans	Fluorescein	Rabbits	7
<b><math>\beta</math>-Amyloid Retinal Plaques</b>					
Fluorescence microscope, multispectral retinal imaging	Retina	Visualization of $\beta$ -amyloid retinal plaques	Curcumin (diferuloylmethane)	Murine	93

**Table 1.** Characterization of molecular processes imaged by ophthalmic molecular imaging techniques.

Imaging modality	Applications	Advantages	Disadvantages
<i>Optical Imaging</i>			
Fluorescence mediated tomography	Blood–retinal barrier studies	Monitoring of multiple molecular processes; Wide applicability; Relatively inexpensive	Low penetration depth, especially at visible wavelengths; Not applicable in humans; Limited anatomical information
Scanning laser ophthalmoscope	Apoptosis imaging; Ocular immune response; Retinal ganglion cells imaging; Stem cells imaging; Blood–retinal barrier studies	Relatively low cost; Optics of the eyes serve as an objective lens; In clinical use	Monochromatic images
Retinal multispectral imaging	Retinal oxygen homeostasis; Optic nerve head imaging; $\beta$ -amyloid retinal plaques imaging	Potential for future applications with molecular imaging probes; In clinical use	Experimental setup; Long exposure times; Uncomfortable for the patient
Optical coherence tomography (OCT)	No in vivo experiments reported	Cross-sectional anatomical and morphological information combined with molecular imaging; Can be used almost universally in humans; Relatively low cost; In clinical use	Probes need to be ionized; Probes need to accumulate at the region of interest
In vivo scanning laser microscopy	Cellular imaging of the cornea; Ocular immune response	High resolution for ocular surface tissues; In clinical use	Surface contact required; Limited penetration depth

Multiphoton excitation fluorescence microscopy	Cellular imaging of the cornea;  Intra-operative monitoring during corneal surgery;  Imaging of trabecular meshwork	High resolution;  Potentially less phototoxicity and bleaching when compared to confocal microscopy;  High penetration depth	Not in clinical use;  Optics of the eye reduce efficacy;  Numerical aperture limited by large distance between plane of focus and anterior pole of the eye in retinal imaging
<b>Radionuclide imaging</b>			
Positron emission tomography (PET)	Neural visual cortex response	High sensitivity;  Quantitative;  High penetration depth;  Operates at concentrations as low as picomolar;  In clinical use	Cost;  Low resolution for ocular structures
Single-photon emission computed tomography (SPECT)	Detection of uveal melanoma;  Neural visual cortex response	High sensitivity;  Quantitative;  High penetration depth;  Relatively low cost;  Detection of multiple probes  In clinical use	Low resolution for ocular structures
<b>Magnetic Resonance Imaging (MRI)</b>	Oxygenation studies;  Blood-retinal barrier studies;  Ion activity in the eye:  Ocular drug delivery studies	High spatial resolution;  Excellent for morphological and functional imaging;  Good soft tissue contrast;  In clinical use	Low sensitivity;  Needs high molecular imaging probe concentration;  Cannot be used universally in humans;  Expensive;  Long acquisition time

**Table 2.** Characterization of imaging modalities currently used in ophthalmic molecular imaging.

## **Molecular imaging modalities in ophthalmology**

### **Optical imaging**

In vivo optical imaging techniques use light emitted through fluorescence, bioluminescence, absorbance, or reflectance as a source of contrast in tissues. Optical image capture systems are based on diffuse optical tomography, surface-weighted imaging (reflectance diffuse tomography), phase-array detection, confocal imaging, multiphoton imaging, or microscopic imaging with intravital microscopy.<sup>188</sup> Optical imaging techniques relevant for ophthalmic molecular imaging will be discussed in the following sections.

### **Fluorescence and bioluminescence imaging**

In fluorescence optical imaging, an external light source or laser excites target fluorescent molecules that then emit a signal with different spectral characteristics. Target cells are modified to express a specific fluorescent protein or a fluorescent tagged reporter is constructed into the animal. Imaging of fluorescent proteins such as green fluorescent protein (GFP), whose expression is regulated by the promoter of a gene of interest in specifically constructed transgenic mice, has revolutionized cell biology<sup>89, 188</sup> and pathology.<sup>73, 74</sup> A vast number of fluorescent proteins are now available. Translating these imaging techniques to patient care is promising.<sup>107, 188</sup>

Bioluminescence imaging exploits the emission of photons at specific wavelengths by luciferases that have been cloned from different organisms.<sup>89</sup> In the firefly, luciferase utilizes energy from adenosine triphosphate to convert its substrate, luciferin, to oxyluciferin with the emission of a photon. Expression of the luciferase gene can be controlled by the promoter of a gene of interest. This technique does not require an external light source and can be used to image distribution patterns and growth kinetics of, for example, cancer and bacterial organisms or to image the spatial distribution of gene expression products. So far, bioluminescence imaging has only been used in ex vivo ophthalmic research.

Bioluminescence imaging allows imaging at greater depth, higher sensitivity, and lower background signal when compared to fluorescence imaging. In bioluminescence, light has to travel only once through the tissue, whereas in fluorescence imaging both the excited as well as the emitted light are absorbed and scattered by various tissues, thus increasing the background signal and penetration depth.<sup>89</sup> Depth of penetration is related to scattering and absorption of light. The latter is primarily a function of the wavelength of the light. The longer the wavelength, the better tissue penetration is achieved.<sup>73</sup> One of the major advantages of fluorescence imaging is the ability to study different molecular processes in the same cell or animal model due to the many available fluorescent proteins with different emission spectra.

## Reflectance imaging

Reflectance-based imaging modalities measure reflectance of light. Three main reflectance-based techniques are used in ophthalmic molecular imaging: the scanning laser ophthalmoscope (SLO), retinal multispectral imaging, and optical coherence tomography (OCT). These modalities may use adaptive optic systems to improve their performance. Adaptive optics attenuates the effects of dynamic optical distortion. These systems incorporate a wavefront sensor to measure the distortions induced by the ocular media, a deformable mirror (or a material with variable refractive properties) that lies in the optical path, and a computer that receives input from the detector and calculates the ideal mirror shape to correct the distortions.<sup>59</sup>

The SLO, a retinal optical imaging device based on standard scanning laser microscopy<sup>185</sup> is an imaging technique that scans the fundus with a highly collimated narrow laser beam. Reflected light from a particular spot is detected by a photomultiplier and synchronously decoded to build up an image. Incident and reflected light follow a coaxial path—that is, a small aperture is used for illumination, and the remaining large area of the pupil is used for collection of reflected light.<sup>136, 164</sup> In the SLO, the optics of the eye serve as the objective lens, and individual ocular aberrations can be overcome by adaptive optics systems. Scanning laser ophthalmoscopes and microscopes, when equipped with a confocal aperture, offer fundamentally better performance than conventional imaging instruments due to elimination of scattered light. The confocal SLO generates high contrast images and is able to do optical sectioning through weakly scattering media, making it ideal for imaging the multilayered retina. This technique has been widely used in ophthalmic pre-clinical research in various applications such as apoptosis imaging,<sup>56, 109, 118, 153, D</sup> blood–retinal barrier studies,<sup>141,151</sup> imaging of retinal ganglion cells,<sup>53, 69, 100, 141, 151</sup> immune response assessment,<sup>30, 42, 58, 119, 195, 196, 197,198</sup> and stem cell imaging<sup>146</sup> (Table 1). Image improvement has enabled the visualization of the lamina cribrosa in glaucoma,<sup>182</sup> localized retinal vessel blood flow, and individual photoreceptor imaging.<sup>41, 149</sup> Clinically, the most popular SLO instrument is the Heidelberg retinal tomograph, which is currently used to acquire topographical images of the optic nerve head to study changes in this anatomical region.<sup>54</sup> The Heidelberg retinal angiograph is an adaptation of the Heidelberg retinal tomograph designed for simultaneous fluorescein and indocyanine green angiography. This device detects fluorescence and is used in the clinic for fluorescein angiography and measurement of fundus autofluorescence derived from lipofuscin accumulation.<sup>5, 35, 75</sup>

Retinal multispectral imaging measures reflectance of light from the retina. A liquid crystal wavelength tunable filter generate light of a series of narrow wavelength bands. The camera captures images of the light reflected by the retina while the filter tunes over the spectrum, and in that way, creates a stack of images of light of different wavelengths over the entire spectrum. Halogen or xenon lamp systems are the light source, and a set of relay lens systems and collimating optics optimize the signal.<sup>71, 123, 131, A, B</sup> This multispectral imaging system has the advantages of a fundus camera: large field of view, user

friendliness, and high resolution. One of the disadvantages of the technique is that the recording takes place sequentially over time at the different wavelengths that can induce cardiac-dependent differences in retinal oxygenation patterns and eye movement artifacts. Low transmission of light by the filter renders imaging below 460 nm difficult, and the high degree of variability induced by wavelength-dependent scattering may make data interpretation difficult.<sup>68, 173</sup>

Retinal multispectral imaging devices are used in oxygenation studies of the posterior eye segment in humans.<sup>52, 71, 120, 123, A, B</sup> Oxygenation studies of the retina use the principle of oximetry by means of spectrophotometry. Oximetry is based on the Lambert-Beer law ( $A = \epsilon \times b \times c$  in which  $A$  = absorbance,  $\epsilon$  = molecular extinction coefficient,  $b$  = the length of the path that the light traverses, and  $c$  = concentration of the light-absorbing compound in solution). The law states that light transmission through a solution diminishes exponentially as the concentration of the solution and the distance through it increase. Oximetry measures how much light is differentially absorbed at a given wavelength by reduced hemoglobin and oxyhemoglobin. Hemoglobin is the main light-absorbing component of human blood. Therefore, absorbance at a specific location in a retinal vessel is assumed to be mainly caused by hemoglobin. Retinal multispectral imaging thus generates a stack of images of the retina at a series of wavelengths, enabling the calculation of the absorbance of retinal arterioles and venules. The oxygen saturation is then calculated for a particular retinal vessel. Retinal multispectral imaging uses fluorescent probes that tag specific molecules. In this approach, a fluorescent probe is used and the specific excitation and emission wavelengths for that probe used.<sup>93</sup> When molecular probes are approved for human use, multispectral imaging may well become a versatile technique to retrieve information from a specific probe in the eye with known spectral characteristics.

Finally, OCT is a form of reflectance-based imaging that has already revolutionized ophthalmology by its widespread clinical applications. All OCT techniques are based on the principle of low-coherence interference in which light reflected from the eye interacts with light that has travelled a known path. This so-called interferometric setup, known as a Michelson interferometer, divides the emitted light in two directions towards a reference mirror and the sample, the eye. The beams then recombine at the beamsplitter and are guided to a detector. When the reference mirror is moved and the eye is at a fixed position, the detector measures an interference pattern. Because the path length of the reference light beam is known, the path length of the sample light beam, and thus the position of the reflecting structure in the eye, can be calculated. On the basis of that information, a so-called A-scan can be constructed that refers to the measurement of the reflectivity (the power of the interference pattern) versus depth. The final image is the longitudinal OCT or B-scan, which is constructed from serial A-scans with reflectivity plotted on a grayscale or false-color scale.<sup>33</sup> Van Velthoven et al. describe the advances of ophthalmic OCT technology in a recent review article.<sup>180</sup> The most frequently used OCT technique has been time-domain OCT (TD-OCT), recently replaced by the Fourier-domain OCT (FD-OCT; also named spectral-domain OCT [SD-OCT]). In this

technique the reference mirror is stationary, but the reflected light is detected by a spectrometer as a detector. In swept-source OCT, the reference mirror is also stationary, but the OCT signal is acquired by varying the (narrowband) wavelength of the light source in time and by using a single detector. The depth scan can be calculated in both systems by Fourier transformation from the acquired spectra without movement of the reference arm.<sup>126, 180, 192</sup>

Interpretation of OCT is based on the anatomy and morphology of the tissue that has been imaged with serial optical sections. In order to use OCT in ophthalmic molecular imaging, one has to use a naturally occurring (endogenous) contrast agent or an exogenous contrast agent. There are three approaches for molecular contrast OCT: attenuation-based molecular contrast OCT, coherent emission-based molecular contrast OCT, and nanoparticle-based molecular contrast OCT.<sup>200</sup>

Attenuation-based molecular contrast OCT measures changes in the spectral attenuation characteristics of tissue, at one point in time or over time. Light absorbance and scattering properties of a tissue depend on the presence of endogenous and exogenous contrast agents. For example, oxymetry may be performed when exploiting hemoglobin as an endogenous contrast agent. Near-infrared dyes with a known absorbance spectrum can be used as well.<sup>194</sup> In order to reduce the effects of endogenous light scattering and absorbance within the sample, the spectrum of the light source may be divided into three equal bands, with the middle band centered around the absorbance peak of the contrast agent. The OCT scans taken with three bands enable an easier detection of the contrast agent.<sup>201</sup> The ability to image over time allows detection of differences in the absorbance profile that occur when using contrast agents with a specific optically excitable transition, like methylene blue<sup>145</sup> or phytochrome-A.<sup>201</sup>

The second approach is coherent emission-based molecular contrast OCT. In this technique, endogenous contrast agents such as fluorophores are used. These absorb incident light and emit light of different wavelength. Detection takes place by means of an interferometer, using either a second-harmonic OCT setup<sup>81, 152</sup> or a setup based on coherent anti-Stokes Raman scattering (CARS) interferometry.<sup>17, 110, 183</sup> A typical OCT uses the linear and elastic scattering properties of tissues and is thus limited to the detection of asymmetric structures or polarization properties of the tissue. Second-harmonic OCT captures a standard OCT pattern and simultaneously another pattern produced by the second-light harmonic light phenomenon, which is a nonlinear optical effect generated only by molecules that are non-centrosymmetric. This phenomenon generates biological images in which contrast is a function of the specimen's molecular structure and its orientation relative to the laser beam. Coherent anti-Stokes Raman spectroscopy is a form of spectroscopy sensitive to vibrational signatures of molecules. The molecular vibrations of multiple molecules are addressed by multiple photons and a signal is produced in which the emitted waves are coherent with one another. OCT setups with CARS interferometry, also referred to as vibrational spectroscopy or molecular sensitive OCT,<sup>17, 110, 183</sup> may be able to simultaneously image multiple molecules within a sample,<sup>200</sup> for each specific molecule has a specific CARS signature.

The third approach is nanoparticle-based molecular contrast OCT, also called nanoparticle-assisted optical molecular imaging (NAOMI).<sup>E</sup> An additional signal is created, either using engineered scatterers that cause additional reflections<sup>21, 98</sup> or magnetic particles that cause additional Doppler signals under the influence of an external magnetic field.<sup>134</sup> The concentration of the used contrast agent correlates with the size of the measured signal. Several particles have been proposed for this purpose, for example, engineered microspheres which are oil-filled spheres with shells made out of melanin, gold, or carbon nanoparticles with a high scattering and low absorption coefficient<sup>98</sup> and smaller gold nanocages.<sup>21</sup> Specific antibodies directed against specific molecular and cellular targets can be used with these microspheres and nanocages to visualize those targets. An OCT setup can detect changes in optical scattering arising from nanoparticles.<sup>200</sup> Recently, gold nanoshells injected in an enucleated porcine eye were visualized on the basis of contrast enhancement due to their engineered backscattering cross section.<sup>E</sup> The application of NAOMI techniques to the human eye depends on the approval of nanoparticles as exogenous contrast agents. Thus far, these techniques have remained experimental. They will undoubtedly play a major role in molecular medicine in the future, either as drug-carrying vehicles or as exogenous contrast agents.

Considering the great progress made with introduction of OCT in clinical ophthalmic care, OCT could even further revolutionize ophthalmology by allowing the combination of cross-sectional anatomical and morphological information with specific visualization of molecular processes by a wide range of contrast agents, each with a specific signature that allow simultaneous multiple detections within a measurement. Some innovative OCT techniques other than scattering-based molecular contrast OCT, such as CARS interferometry and absorption spectrum-based molecular contrast OCT may also be explored to expand the use of contrast agents.

### **Confocal scanning microscopy**

In vivo confocal scanning microscopy is a noninvasive imaging technique used daily in ophthalmic practice, usually for the imaging of ocular surface structures such as the cornea.<sup>95</sup>

In confocal microscopy, reflected light passes through an aperture and is focused by a condenser (illumination system) within a small volume of the cornea. Reflected light then passes through an objective (observation system) that has the same focal point as the condenser. Light contamination from out of focus structures is eliminated which results in better contrast in the images. Magnifications of approximately 600 times enable the examination of the cornea at the cellular level with the signals being detected by a charge-coupled device (CCD).<sup>16</sup> To increase the field-of-view, current devices move the condenser to scan across the cornea.<sup>23</sup> In vivo confocal microscopes require contact between objective and cornea, either by the use of a coupling viscous gel in between cornea and objective, or by direct applanation on the cornea. Currently, there are three

devices available, the tandem scanning confocal microscope,<sup>137</sup> the slit scanning confocal microscope,<sup>117</sup> and the HRT II Rostock Corneal Module.<sup>14</sup> Clinically, confocal microscopy is already in use for differential diagnosis of corneal dystrophies, corneal structure examination, and visualization of infectious agents. Molecular imaging studies with this imaging modality have mostly been used in ophthalmology to visualize inflammatory cells in the cornea of small animals. Limited tissue penetration of this technique limits its use to superficial ocular structures.

### **Multiphoton excitation fluorescence microscopy**

Multiphoton excitation fluorescence microscopy, is a new technique that is capable of *in vivo* high-resolution imaging and functional analysis based on tissue autofluorescence. This technique evolved from fluorescence and confocal microscopy. Developed in order to increase penetration imaging depth into tissues, it is a promising technique for application in living subjects and animals. In fluorescence microscopy, a fluorescent probe is used to stain and label a specific molecule or biochemical process of interest. As in standard light microscopy, fluorescence microscopy can only give a two-dimensional view. This happens because the detected fluorescence includes the emission from areas outside the plane of focus of the excitation light. In confocal microscopy, the presence of an adjustable pinhole aperture in front of the detector guarantees that only fluorescence from the focusing plane is detected, and all superfluous fluorescence is neglected. A three-dimensional view is created by moving the plane of focus up and down through the specimen. These systems require an intense light source for excitation because a significant amount of fluorescence is neglected, bringing forward the problem of phototoxicity and fluorophore bleaching.<sup>77</sup> In 1990,<sup>34</sup> a new technique derived from fluorescence and confocal microscopy was described: two-photon excitation microscopy. This relies on the simultaneous absorption in a single quantitized event of two near-infrared photons in the spectral range of 800–1200 nm after an infrared beam is focused on the specimen.<sup>77, 140, 154</sup> The probability that two photons are simultaneously absorbed by a molecule of the fluorophore is substantially increased due to the high concentration of photons at the focal plane. The phototoxicity and fluorophore bleaching that can occur in confocal microscopy is reduced in two-photon excitation microscopy because excitation takes place only at the plane of focus. This feature, combined with the high penetration depth of the stimulating light beam because of the long infrared wavelengths of light used, has allowed imaging of live tissues and even of whole animals over extended periods of time. A pinhole aperture is not required in this technique because excitation and emission occur at the focal plane only—or in other words, fluorescence is generated at the focal plane only.<sup>77,140</sup> This enables the detection of more scattered emitted light, thus improving the signal-to-noise ratio at the expense of a lower spatial resolution when compared to confocal microscopy. To achieve better spatial resolution, a descanned detector

with an aperture placed in front can be used, which at the same time will decrease signal intensity. In order to image biological structures with subcellular resolution, two types of signals can be used: fluorescence and second-harmonic generation. Whereas the former is used to monitor the dynamic behavior of the chemical components of tissues, the latter is a novel way to study the spatial organization of different tissues. When imaging a specimen, and in particular the eye, one needs to account for intrinsic autofluorescence of tissues.

Multiphoton excitation fluorescence microscopy shows promise for application in humans and animals. Several clinical applications using this imaging technique are currently being explored.<sup>31, 43, 203</sup> In ophthalmic research, two-photon microscopy has proved valuable in the understanding of structure, metabolism, and signal transduction in the eye. The infrared illumination makes it ideal to visualize endogenous fluorophores present in the retinal pigment epithelium. For example, Palczewska et al used multiphoton excitation fluorescence microscopy to target retinosomes in retinal pigment epithelium and other fluorophores present in eyes of aging mice.<sup>135</sup> Another study with possible application in living animals explored the use of two-photon microscopy to obtain images of the trabecular meshwork in enucleated mouse eyes after labeling of blood vessels by fluorescein-conjugated dextran. The authors were able to show promise non-invasively to visualize structures relevant to aqueous flow in these mice, and further studies are ongoing to extrapolate the technique to living animals.<sup>82</sup> Two-photon microscopy can also be used for studies of the architecture of the cornea and lens. For example, analysis of two-photon-generated second harmonic signals originating from the collagen fibers of the corneal stroma identified three stromal layers with different patterns of fiber packing.<sup>121</sup> Collagen architecture studies at the level of the cornea are indeed one of the first *in vivo* applications of two-photon microscopy since it does not require any artificial labeling of the specimen.<sup>77</sup>

In summary, two-photon microscopy has so far led to major advances in the understanding of retinoid processing in the retina, visualization of important structures affected in glaucoma, and collagen organization in the cornea. Most studies have been performed *in vitro* and/or *ex vivo*. As stated before, it is expected that this technique will be extrapolated to clinical research and to clinical use as a molecular imaging device. Imaging of the retina and retinal pigment epithelium by two-photon microscopy would be a major breakthrough in the care of patients afflicted with retinal neurodegenerative diseases. Two limitations need to be overcome in order to achieve this. The human eye is an optically distorted structure, and this greatly influences the efficacy of two-photon excitation. Another issue is the large distance between the anterior and posterior pole of the eye, which limits the numerical aperture of the fundus ophthalmoscope for human eyes.<sup>77</sup>

## Radionuclide imaging

Radionuclide imaging techniques (PET and SPECT) utilize radiopharmaceuticals to probe a specific protein, usually an enzyme or a receptor. The enzyme or receptor to be targeted can be expressed either intracellularly or extracellularly. Intracellular proteins are not recognized by the immune system. The major advantages of targeting surface-expressed receptors and enzymes are better controllable kinetics (because the tracer does not have to penetrate into cells) and the fact that synthetic receptors can be engineered to recognize approved imaging probes such as perrhenate.<sup>186</sup>

PET imaging utilizes positron-emitting isotopes. These positrons annihilate nearby electrons, emitting two photons at an angle of 180° of each other. These photons are then detected by the scanner based on coincident collisions in the detector. Radioisotopes include C<sup>11</sup>, N<sup>13</sup>, O<sup>15</sup>, F<sup>18</sup>, Cu<sup>64</sup>, Cu<sup>62</sup>, I<sup>124</sup>, Br<sup>76</sup>, Rb<sup>82</sup>, and Ga<sup>68</sup>. F<sup>18</sup> is the most often used PET radiopharmaceutical. One of the major disadvantages of PET is that the radiotracers must be made with a cyclotron. Because each of these radionuclides has a half-life of minutes to hours, the cyclotron has to be in close proximity to the imaging facility. This significantly increases the costs of PET radionuclides. Because PET imaging relies on physiological or biochemical phenomena of disease processes, it retains many advantages when compared with anatomic imaging modalities such as MRI and CT scan and is used extensively in oncology for its ability to distinguish malignant from benign lesions where other imaging modalities fail to do so.<sup>F</sup> It is more sensitive than SPECT, capable of detecting probes in picomolar concentrations.<sup>143</sup>

SPECT uses gamma-ray emissions to generate images. The imaging agent used in SPECT decays and emits non-coincident gamma rays, as opposed to the coincident gamma rays associated with positron emitters (such as F<sup>18</sup>) used in PET. There is a range of radiotracers (such as Tc<sup>99m</sup>, In<sup>111</sup>, I<sup>123</sup>, Tl<sup>201</sup>) that can be used in SPECT, depending on the specific application. Radiotracers for SPECT are long-lasting, thus making the application of SPECT more economic than that of PET. Another major advantage of SPECT imaging over PET imaging is that it can potentially allow for concomitant imaging of multiple radionuclides.

Radionuclide imaging techniques have been used to study alterations in cortical activity secondary to ophthalmic diseases, but never in direct imaging of the eye with the exception of uveal melanoma detection with *N*-isopropyl-*p*-<sup>123</sup>I-iodoamphetamine SPECT.<sup>83</sup>

## Magnetic resonance imaging

Magnetic resonance imaging is based on the phenomenon of alignment of unpaired nuclear spins, called magnetic dipoles, when placed into a magnetic field. A magnetic field surrounding the subject under investigation is produced by a strong magnet located in the MRI scanner. “Coils” within the magnet produce a gradient in the magnetic field in the *x*, *y*, and *z* directions. The magnet also contains a radiofrequency coil that can pro-

duce a temporary radiofrequency pulse to change the alignment of the spins. Following the pulse, the magnetic dipoles return to their baseline orientation, which is detected (also by the radiofrequency coil) as a change in electromagnetic flux. An important function of the scanner is to determine the rate at which these dipoles relax to their baseline orientation. This measurement is translated into a MRI signal. Dipoles such as water molecules have different relaxation times in different physicochemical environments, and thus generate different MRI signals and subsequently image contrast.<sup>116</sup> The two most frequently used timing parameters are known as  $T_1$  and  $T_2$  weighting.  $T_1$  is the longitudinal relaxation time. It indicates the time required for a substance to become magnetized after first being placed in a magnetic field or, alternatively, the time required to regain longitudinal magnetization following a radiofrequency pulse.  $T_1$  is determined by thermal interactions between the resonating protons and other protons or other magnetic nuclei in the magnetic environment. These interactions allow the energy absorbed by the protons during resonance to be dispersed to other nuclei in the magnetic environment.  $T_2$  is the “transverse” relaxation time. It is a measure of how long transverse magnetization lasts in a perfectly uniform external magnetic field. Alternatively, it is a measure of how long the resonating protons remain coherent or rotate “in phase” following a 90° radiofrequency pulse.  $T_2$  decay is due to magnetic interactions that occur between spinning protons. Unlike  $T_1$  interactions,  $T_2$  interactions do not involve a transfer of energy but only a change in phase, which leads to a loss of coherence.<sup>C</sup>

Variations on standard MRI techniques for greater functional analysis include diffusion-weighted MRI, which exploits the translational mobility of water molecules to obtain information on the microscopic behavior of tissues (presence of macromolecules, presence and permeability of membranes, equilibrium of intracellular–extracellular water) and perfusion-weighted MRI, which uses endogenous and exogenous reporter probes for monitoring their hemodynamic status.<sup>116</sup>

Magnetic resonance imaging and its variants have been used in pre-clinical ophthalmic research (Table 1). Oxygenation studies have been performed with MRI using the paramagnetic properties of oxygen ( $O_2$ ), which produces contrast (i.e., increased signal intensity) on a  $T_1$ -weighted image. Ion activity may also be studied by manganese-enhanced MRI. Manganese is a heavy metal that serves as a paramagnetic contrast agent as a surrogate marker of calcium ion flux. Blood–retinal barrier permeability and transfer studies have also been performed by MRI.

Magnetic resonance imaging, noninvasive not affected by media opacities such as cataract, is able to simultaneously survey the entire two-dimensional retinal surface. However, spatial resolution is rather low.<sup>94</sup> Furthermore, ocular oxygenation studies using this technique only measured indirect values of partial pressure of  $O_2$  in the vitreous body and not directly at the level of retinal tissue.

## Computed tomography

Computed tomography generates 3D images based on a large series of two-dimensional X-ray images taken around a single axis of rotation.<sup>20</sup> Lack of target-specific contrast agents preclude its use in molecular imaging. Its main advantage is the ability to provide an excellent spatial resolution in the sub-millimeter range, which can be of interest as complementary to PET systems. In theory, several obstacles need to be surmounted to enable the use of CT in molecular imaging. Specific CT-based probes to image biological processes have to be iodinated (or tagged with another high-atomic-number atom that absorbs X rays). Moreover, site-specific accumulation of large quantities of such probes have to be possible in order to detect differential attenuation of X rays that reflect the biological process in question.<sup>116</sup> Development of new CT contrast agents and hybrid devices that combine PET and SPECT may well attribute a role to CT in medical molecular imaging.<sup>19</sup>

## Ultrasonography

Ultrasonography is the most widely used clinical imaging modality because of its low cost, availability, and safety. Ultrasound images are obtained when high-frequency sound waves are emitted from an acoustic transducer placed on the skin and the ultrasound is reflected by the internal organs that are examined. Contrast in the images depends on the imaging algorithm used, backscatter, attenuation of the sound, and speed of sound. Development of microbubble contrast agents and higher-resolution ultrasound devices will likely render ultrasonography to be a feasible technique for molecular imaging in ophthalmology in the near future.<sup>20, 116</sup>

## Molecular imaging applications in ophthalmology

### Apoptosis

Apoptosis, or programmed cell death, occurs in ophthalmic diseases such as inherited retinal degenerations, diabetic retinopathy, age-related macular degeneration, pathologic myopia, retinal detachment, and glaucoma.<sup>3, 4, 29, 40, 48, 84, 142, H</sup> Objective and quantitative noninvasive imaging of apoptosis in living human eyes would be a significant advancement in the diagnosis of eye diseases as well as in the follow-up of local effects of experimental therapeutic agents.

Apoptosis in the eye has been experimentally imaged by targeting caspases, proteases that always have been considered to drive the apoptotic cascade. Absolute involvement of caspases in apoptosis has become controversial,<sup>36, 37, 38, 104</sup> however, suggesting that induction of apoptosis can occur independently of caspase activation.<sup>36, 37, 38</sup>

One of the most frequently used markers for identification of apoptosis in vivo and in vi-

tro is extracellular expression of annexin 5. Annexin 5 becomes externalized during the early stages of apoptosis before nuclear condensation and DNA fragmentation occur, and binds to phosphatidylserine, an anionic phospholipoid enriched in plasma membranes.<sup>12, 14, 39, 125, 206, H</sup> Extracellular expression of annexin 5 is related to caspase-activated apoptosis and, accordingly, cells that express annexin 5 extracellularly are also labeled when using anti-active-caspase 3 antibodies.<sup>18, 96, 99, 111, 112, 113, 114, 170, 181</sup>

An experimental study using fluorophore-labeled anti-annexin 5 in rats demonstrated that retinal ganglion cells undergoing apoptosis can be imaged *in vivo*.<sup>D</sup> Neuronal apoptosis was induced by different mechanisms such as administration of hypertonic saline in the episcleral veins of rats, thus resulting in an increase in ocular pressure by transection of fibers of the optic nerve to induce trans-synaptic degeneration of retinal ganglion cells, and by intravitreal administration of staurosporine, a nonselective protein kinase inhibitor that rapidly and extensively induces neuronal apoptosis. Images were acquired with a modified confocal SLO to detect the emitted fluorescent light. Single cells undergoing apoptosis in the rat eye were visualized.<sup>D</sup> This technique is called DARC (detection of apoptosing cells) and has proven to be useful for the assessment of the effects of neuroprotective measures in glaucoma.<sup>56</sup> The Heidelberg retinal angiograph was also used successfully to detect apoptosis in retinal ganglion cells in mice. Therefore, this approach may become available in the future to detect apoptosis of retinal ganglion cells in patients.<sup>109</sup>

Similar methodology has been used to identify apoptosis in retinal cells from the inner nuclear layer and ganglion cell layer of rat eyes after thermal damage due to laser exposure with high-intensity light.<sup>156</sup> Dose-dependent apoptosis and the extent of retinal damage were established quantitatively *in vivo* in relation to laser exposure. The size of the lesion induced by the laser correlated with the amount of apoptotic retinal cells showing the importance of controlling lesion size during laser treatment of the retina.<sup>156</sup>

It may be argued that these studies do not demonstrate photoreceptor apoptosis but rather photoreceptor necrosis and cell death. Short periods of image capturing may not assess apoptosis because apoptosis induction occurs over an extended period of time.<sup>156</sup> Although extracellular annexin 5 expression is generally considered to be an early marker of apoptosis,<sup>15, 94</sup> it may not distinguish between necrotic cells and apoptotic cells *in vivo* because they both express annexin 5.<sup>155</sup> Reduced laser light intensity and longer exposure times are required to investigate whether confocal SLO can visualize real-time *in vivo* apoptosis in photoreceptors.

## Oxygen homeostasis

The serious consequences of hypoxia or hyperoxia in the eye underline the importance of the development of molecular imaging methods to visualize and quantify the occurrence of these phenomena in the eye in a noninvasive manner. Oxygen homeostasis is

crucial for the metabolically most active tissue in the human body; the retina. Oxygen is needed for ATP production, regulation of membrane transport,<sup>51</sup> intracellular signaling,<sup>106</sup> gene expression,<sup>50, 158</sup> and initiation of apoptosis.<sup>21, 24</sup> Among the unique features affecting retinal oxygenation are the low oxygen tension at the level of photoreceptors, in particular during dark adaptation, the presence of a dual circulation, lack of metabolic regulation of the choroid, oxygen regulation of the retinal circulation, and the presence of large amounts of mitochondria in the photoreceptor inner segments.<sup>2, 184</sup>

Oxygen gradients can be measured in vessels (point of supply) or in tissue (point of consumption). Measurements of retinal perfusion by means of vessel caliber assessment, video fluorescein angiography, laser Doppler flowmetry and velocimetry, color Doppler ultrasound, and ocular pulse measurement all have limitations such as inability to quantify such measurements, the limited spatial resolution and sensitivity, and inter-patient differences like corneal opacity or presence of cataract.<sup>176</sup> Fluorescein angiography, currently the standard technique to assess capillary non-perfusion and consequently local ischemia and hypoxia in the retina, remains an invasive procedure that is unpleasant for the patient, time consuming, and prone to adverse reactions. In addition, it is an indirect method to assess ocular oxygen homeostasis. Molecular imaging methods aim at the visualization and quantification of oxygen in a direct manner, using oxygen and oxygenated hemoglobin as naturally occurring endogenous chromophores.

At present, four methods are available for molecular imaging of oxygen homeostasis: MRI-based methods, methods based on phosphorescence, multispectral retinal imaging techniques, and attenuation-based OCT. Only multispectral retinal imaging techniques have been successful in noninvasive retinal oximetry in human patients, whereas other techniques have been applied to small animals. OCT-based techniques have not thus far in provided in vivo oxygenation measurements. Nevertheless, theoretical principles of this approach are briefly discussed here as well.

*MRI-based oximetry methods* rely on the paramagnetic characteristics of oxygen, a chromophore that produces contrast in a  $T_1$ -weighted image. Changes in oxygen signal intensity in the vitreous, measured under normoxic and hyperoxic conditions, can be mapped as a reflection of the vitreous partial oxygen pressure. The recording is carried out in the pre-retinal vitreous which has been shown to reflect oxygen levels in the inner retina.<sup>103, 184</sup> Measurements are expressed as differences between intensities recorded during normoxia and hyperoxia.<sup>8, 9,13, 78, 147, 148, 204</sup>

Pre-retinal oxygen pressure can also be measured by fluorine-19 magnetic resonance spectroscopy when a perfluorocarbon droplet is instilled and placed on the surface of the retina via a minimally invasive needle. This approach has been applied to pre-clinical models and to a single vitrectomized human eye.<sup>1, 60, 198, 199, 204, 205</sup> Measurements can only be performed within the limited area of the droplet instillation. Nevertheless, this technique remains interesting because it can measure oxygen pressure where other techniques cannot, such as in eyes of newborn rats, mouse eyes, and eyes that do not have clear optical media.<sup>187, 204, 205</sup>

156 *Phosphorescence oximetry methods* are based on the principle that oxygen is the only molecule

in blood that can quench an excited phosphorescent molecule.<sup>202</sup> The decay time depends on the concentration of oxygen in the vicinity of molecules with phosphorescence properties. Thus, intravascular oxygen pressure can be deduced from measurements of these quenching effects.<sup>167</sup> Measurements of retinal oxygen pressure and consumption and retinal vascular oxygen pressure have been performed with this approach in a number of studies.<sup>19, 47, 127, 147, 150, 159, 160, 161, 163, 165, 166, 167, 168, 190, 191, 207</sup>

Shahidi et al<sup>167, 168, 169, 170</sup> described a method in which images of vascular layers equally displaced in depth were constructed by segmentation in combination with phosphorescence images acquired from adjacent areas in the retina of mice that were administered an oxygen-sensitive probe. A modified SLO with an infrared barrier filter installed with transmission overlapping the phosphorescence emission of the probe in the light path was used. By projecting a narrow focused laser beam at 532 nm at an oblique angle on the retina after intravenous injection of the probe, a phosphorescent optical section is acquired from the retina. Phase-delayed images were analyzed to generate oxygen pressure maps of the vasculature at different levels in the retina, and thus to differentiate phosphorescence of the retina from the choroid.<sup>162</sup> This method provided oxygen pressure measurements in retinal capillaries, which depict more correctly the oxygenation status of the retina than measurements in large retinal vessels. More recently, oxygen pressure in retinal tissue of rats was measured using a similar approach.<sup>161</sup> Limitations of these techniques include the risk of producing toxic oxygen free radicals, the lack of discrimination of signals being emitted either from the retina or choroid, and the quality of the acquired images.

*Retinal multispectral oximetry imaging* devices detect differences in light absorbance at a given wavelength between oxygenated and reduced hemoglobin.<sup>33, 66</sup> By measuring the variation in reflection in relation with the wavelength, information about the relative concentrations of the two forms of hemoglobin in vessels and capillaries can be deduced. In retinal oximetry with multiple wavelength reflectance oximeters, images are captured at two isosbestic wavelengths, at wavelengths where light absorbance by oxygenated and reduced hemoglobin is the same and at a wavelength above 650 nm at which tissue scattering dominates.<sup>80</sup> Multispectral retinal cameras scan the retina at multiple wavelengths at regular intervals. Measuring the optical density of retinal blood vessels (i.e., the attenuation of retinal blood vessels at several discrete wavelengths) gives a measurement of the oxygenation status of the retina. The absorbance at a retinal location is obtained by calculating the ratio of the measured reflected light intensity adjacent to the target retinal vessel relative to the reflected light intensity at the center of the retinal vessel. The oxygenation status of the retinal blood vessel can then be calculated after analyzing the absorbance at various wavelengths.<sup>120</sup> Other research groups have built their own systems in order to measure oxygen saturation in retinal blood vessels, all applying the same principles as described earlier. Mordant et al recently published a review on this topic.<sup>120</sup> Retinal oximetry with these imaging devices has been used to assess the oxygenation status of human retinal vessels and/or retinal tissue in diabetic retinopathy,<sup>65, 123, 131, 173</sup> glaucoma filtration surgery,<sup>62</sup> central retinal vein occlusion,<sup>64, 202</sup> primary

open angle glaucoma,<sup>133</sup> dark adaptation,<sup>61</sup> therapy response,<sup>175</sup> neurogenic optic atrophy,<sup>157</sup> and hyperoxia.<sup>63</sup> The use of retinal vessel oximetry in clinical care is still limited because there is no direct correlation with vessel oximetry and oxygenation status of retinal tissue. Retinal tissue oximetry is confounded by the effects of the choroidal vasculature, which can have a considerably different oxygen tension value than the retina. In order to reduce the long recording times of multispectral imaging cameras, a multispectral imaging device has been developed.<sup>52, 120, A</sup> This device has a shorter light exposure time than conventional retinal multispectral imaging devices, which makes it more patient-friendly and less prone to changes induced by cardiac activity and eye motion. The key component is an image replicating imaging spectrometer that uses polarizing interferometry and Wollaston prism polarizing beam splitters simultaneously to replicate images of the retina in multiple spectral bands onto a single detector array. The output image is spectrally demultiplexed into eight narrow-band images recorded on a cooled CCD detector array.<sup>52, 120, A</sup>

*Attenuation-based molecular contrast OCT oximetry techniques* measure oxygen saturation in blood on the basis of scattering properties of erythrocytes and the refractive indices of oxygenated hemoglobin and reduced hemoglobin. Oxygen saturation dependent scattering properties of whole blood were recently reported.<sup>44</sup> In vitro experiments demonstrated a saturation-dependent attenuation coefficient in the OCT signal at 780 and 820 nm.<sup>45</sup> This principle can be applied to calculate oxygen pressure gradients in retinal tissue and vessels. When applying this principle in in vivo experiments, Doppler shifts need to be taken into account in larger vessels.<sup>45</sup> Optical coherence tomography seems to retain the advantage of operating independently of variations in fundus pigmentation and vessel diameters which could be a major advantage when applied in the clinical practice.

## Ocular immune responses

The eye is functionally very sensitive to structural alterations. Even minimal inflammatory processes can result in optical distortion, which leads to impaired vision. The so-called immunologic privilege of the eye, however, limits tissue damage, but is at times not complete. Molecular imaging techniques have not been used thus far for the assessment of the ocular immune response in humans. Some of the techniques that may be of interest for application to human eyes in the future are in vivo confocal scanning microscopy for the anterior segment and SLO and retinal multispectral imaging for the posterior segment. Thus far, these molecular imaging techniques have been used for the analysis of interactions between cells that play a role in the ocular immune response of small animals.<sup>6, 22, 25, 30, 42, 58, 97, 119, 172, 193, 195, 196, 197, 198</sup>

Molecular imaging techniques can also be used to analyze the dynamics of phagocytic cells such as microglia cells, macrophages, as well as dendritic cells in the eye. Macrophages and resident dendritic cells play a major role in the immunological response of the

eye. Macrophages are known to generate tissue damage in response to ischemia-induced retinopathy and experimental autoimmune uveitis. These phagocytic cells are involved in tissue remodeling, release toxic mediators and remove cellular debris. Microglia cells have been shown to be involved in the inflammatory response of the eye but their exact role as immune cells is not known. Dendritic cells play a crucial role in the induction of adaptive immune responses and their presence in ocular tissue has been shown by histology and immunohistochemistry. Their precise role in the healthy and diseased eye has not yet been resolved due to the lack of adequate experimental systems to study these cells. Under physiological conditions, dendritic cells may promote the maintenance of the immunologic privilege of the eye by preventing the activation of T-cells.

Intravital microscopy has been used to visualize and characterize inflammatory cells that migrate into the corneal stroma during keratitis. For that purpose, mice were generated that expressed GFP in their hematopoietic cells. Keratitis was induced by administration of endotoxin. The dynamics of GFP-expressing inflammatory cells were studied by real-time *in vivo* imaging using a fluorescence microscope.<sup>22</sup> The same approach was used after application of silver nitrate to induce chemical injury to the cornea.<sup>172</sup> In both studies, a pattern of fast centripetal migration of inflammatory cells was detected under these stress conditions.

The dynamic behaviour of corneal dendritic cells including Langerhans cells, which are antigen-presenting cells, was studied in the cornea of transgenic mice that expressed enhanced yellow fluorescent protein under the control of the promoter for CD11c. The cell surface marker CD11c is expressed specifically on mouse dendritic cells and thus allows us to differentiate these cells from macrophages. These studies showed decreased migration of these cells upon injury with endotoxin or microspheres.<sup>97</sup> Ovalbumin-specific T-cells have been imaged *in vivo* during interactions with ovalbumin-bearing corneal cells.<sup>172</sup>

The iris is also an immunologically privileged compartment. Immune-mediated diseases in the iris have been studied in a murine model of experimental ovalbumin-induced uveitis. Trafficking and intercellular interactions between fluorescently labeled dendritic cells and macrophages were characterized by means of intravital microscopy.<sup>6</sup> Furthermore, the endogenous immune response in the iris of endotoxin-induced uveitic rats was quantified using carboxylated fluorescent microspheres conjugated with recombinant P-selectin glycoprotein ligand-1. The interactions between this ligand and P-selectin appeared to be a crucial step in the process of leukocyte rolling along vessel walls that was triggered during early stages of inflammation. Visualization by intravital microscopy and SLO of the adhesion between the microspheres and the endothelium showed increased leukocyte adhesion in uveitis.<sup>193</sup>

Leukocyte dynamics in the retina have been imaged using calcein-AM-labeled leukocytes with a SLO, after induction of uveoretinitis.<sup>30, 195, 196, 197, 198</sup> Rolling of leukocytes in blood vessels in the retina of rats has also been visualized by SLO in an experimental model of autoimmune uveoretinitis after staining with acridine orange.<sup>58</sup>

Endothelial expression of P-selectin and assessment of endothelial injury during uveitis

can be imaged *in vivo* in the choriocapillaris by SLO after administration of fluorescent microspheres conjugated to recombinant P-selectin glycoprotein ligand-1. This complex is tolerated in humans and thus it may be used for clinical application in the future. This approach could be of interest for early detection of endothelial changes in a vast array of ocular diseases, in particular uveitis.<sup>119</sup>

Phagocytic cells such as microglia cells, macrophages and dendritic cells express the fractalkine receptor (CX<sub>3</sub>CR1) and thus can be made fluorescent by replacing one copy of the constitutively expressed CX<sub>3</sub>CR1 gene by GFP, while leaving the promoter intact.<sup>26, 46, 49, 129, 171</sup> Dynamics of microglia cells, dendritic cells, and macrophages were visualized in the retina of heterozygous CX<sub>3</sub>CR1<sup>GFP/+</sup> mice using SLO. Argon laser coagulation was applied to the fundus and the response of mononuclear phagocytes to laser injury of the fundus was followed. It appeared that the number of microglia cells increased after laser injury to the retina, whereas macrophages and granulocytes remained for longer periods of time in the choroid infiltrate.<sup>42</sup>

### **Microscopic retinal structures and cells**

*In vivo* imaging of the dynamics of cells has increased our understanding of mechanisms of retinal diseases. Using SLO and adaptive optics, microscopic retinal structures can be imaged in human eyes, such as retinal pigment epithelial cells in patients with cone-rod dystrophies and bilateral progressive maculopathy, cone photoreceptors,<sup>115</sup> flow of single leukocytes in blood vessels,<sup>115</sup> and the lamina cribrosa.<sup>182</sup> Fundus cameras with adaptive optics systems can also visualize cone photoreceptors in patients with retinal dystrophies and optic neuropathy.<sup>26, 27</sup> These approaches are not regarded as molecular imaging techniques *per se*. The structure of the region of interest in the eye can also be informative, however, such as the finding that neurodegeneration in retinal ganglion cells occurs at a very early stage in patients with minimal diabetic retinopathy. Ganglion cell layer thickness measurements was made possible after automated segmentation of SD-OCT scans of human patients with diabetes.<sup>177, 178</sup>

For the visualization of retinal ganglion cells, molecular imaging techniques and fluorescent markers have been used. To investigate neurodegeneration in retinal ganglion cells and to assess the effect of potential neuroprotective measures against this process, imaging and subsequent evaluation of living retinal ganglion cells is indispensable. In experimental animals, retinal ganglion cells, dendrites, and amacrine neurites have been simultaneously imaged over time by means of SLO. Retinal ganglion cells were made fluorescent by expression of the cyan fluorescent protein under the control of a Thy-1 promoter, a marker for retinal ganglion cells.<sup>100</sup> Retinal ganglion cells were also visualized in retinas of rats after retrograde labeling with the fluorescent dye 4-(4-(di-hexadecylamino)styryl)-*N*-methylpyridinium iodine administered in the superior colliculus.<sup>69</sup> Calcium-sensitive dyes were applied in a similar way and numbers, dynamic changes, functional activation, and connectivity of retinal ganglion cells were studied

after optic nerve injury.<sup>141, 151</sup>

Primates and fish have also been used to study vision-related microscopical structures. Fluorescent images of primate retinal ganglion cells were acquired with an adaptive optics SLO after administration of rhodamine dextran in the lateral geniculate nucleus.<sup>53</sup> In vivo visualization of cell–cell interactions in retinas of zebrafish enabled the study of neural circuit formation and especially targeting of synaptic strata by retinal ganglion cells within the inner plexiform layer, the dendritic growth and arborization pattern of retinal ganglion cells and the role of the amacrine plexus in the processing of the neural circuitry.<sup>122</sup> In addition, goldfish have been used to study axonal growth plasticity after optic fiber targeting by fluorescent carbocyanine dye 1,1'-dioctodecyl-3,3,3',3'-tetramethylindocarbocyanine perchlorate and image acquisition with a fluorescence microscope.<sup>32</sup>

### **Transplanted cells**

Stem cell therapy in degenerated retinas to restore function of the neurosensory retina poses a number of challenging issues such as the generation of appropriate stem cells for transplantation, the technical aspects of transplanting cells into a degenerating retina, and restoration of visual function. Molecular imaging has already been used for the visualization of transplanted stem cells in the retina. Bone marrow–derived lineage-negative GFP-expressing hematopoietic stem cells were administered in the vitreous of mice and visualized in the retinal vasculature by SLO as proof of principle.<sup>146</sup>

### **Ion activity**

Ion activity plays a role in photoreceptor transduction, neuronal transmitter release in the retina, regulation of gap junction conductance, modulation of postsynaptic potentials in retinal ganglion cells, and light and dark adaptation.

Magnetic resonance imaging is the modality of choice when performing studies of ion activity. Manganese-enhanced MRI can be used to study calcium ion flux in eyes. After intraocular or systemic administration, manganese accumulates in the retina and optic nerve, serving as a surrogate marker of calcium ion flux. Calcium sequestration and release by mitochondria represented by manganese ions change signal intensity on a  $T_1$ -weighted image. The uptake of manganese is dependent on ion activity in the retina in relation to light/dark adaptation,  $\text{Na}^+/\text{K}^+$  ATPase activity and L-type calcium channels. One of the potential clinical applications of this technique is the monitoring of progression of retinopathy.<sup>9</sup> Because manganese highlights the optic nerve, this technique is also suitable for studies of optic nerve transport.<sup>57</sup>

Other approaches based on molecular imaging of ion activity have been applied to study diffusion in the eye and to calculate water flow.<sup>91, 132</sup> Contrast-enhanced proton MRI

has been used to investigate plasma-derived protein diffusion into the aqueous humor. The contrast agent gadopentetic acid (Gd-DTPA) containing gadolinium was administered in rabbits and monkeys and subsequent analyses of  $T_1$ -weighted images allowed the demonstration of diffusion from the stroma of the ciliary body to the anterior chamber across the iris root.<sup>91</sup> Water movement in rat eyes has been assessed by means of in vivo deuterium MRI after intraperitoneal administration of deuterated saline. Deuterium oxide is a freely diffusible tracer to study blood flow and tissue perfusion. Analysis of differences in signal intensity over time allowed the calculation of the flow rate of water in the rat eye.<sup>132</sup>

### **Neural visual response**

Positron emission tomography has been used to show degenerative changes occurring in the occipital visual cortex and lateral geniculate nucleus as a consequence of experimental glaucoma. 2-[<sup>19</sup>F]fluoro-2-deoxy-glucose and [<sup>11</sup>C]PK11195 were the radio-isotope labeled imaging probes. The degenerative changes were manifest upon visual stimulation of one eye affected with active hypertensive glaucoma whereas the other was used as control. Glaucoma translated in significantly reduced neural responses of the occipital visual cortex ipsilateral to the affected eye. Studies with [<sup>11</sup>C]PK11195 revealed selective accumulation of activated microglia in the lateral geniculate nuclei of both hemispheres which is indicative for neural degeneration.<sup>76</sup> Occipital visual cortex responses were also assessed in patients with external ophthalmoplegia using Tc-99 m hexamethylpropylene amineoxime brain SPECT imaging.<sup>55</sup>

Restoration of the capacity to detect light in degenerated retinas may involve ectopic expression of light-sensitive proteins, such as channelrhodopsin-2. Manganese-enhanced MRI was used to determine non-invasively retinal uptake of manganese as a biomarker of channelrhodopsin-2-mediated activity. Mice expressing a fusion protein of channelrhodopsin-2 and GFP were assessed to construct a map of manganese uptake. It appeared that manganese uptake in the retina was elevated in channelrhodopsin-2-GFP-expressing mice.<sup>79</sup>

Axonal and myelin damage in mouse models of optic nerve injury can be demonstrated by measurements of water diffusion parallel or perpendicular to the axonal tracts of the optic nerve using diffusion MRI. Demyelination did not alter water diffusion parallel to the axonal fibers but water diffusion perpendicular to the axonal fibers was increased, whereas axonal injury caused increased water diffusion in both directions. These principles were used to differentially assess axonal and myelin damage in the optic nerve after injury caused by retinal ischemia and autoimmune encephalomyelitis.<sup>199</sup>

## Blood–retinal barrier permeability

Loss of function of blood–retinal barrier due to endothelial cell dysfunction results in vascular leakage.<sup>155</sup> Subsequent development of macular edema is one of the major causes of visual loss and blindness.<sup>88</sup> Fluorescein angiography is the standard method to assess integrity of the blood–retinal barrier in humans. This technique uses fluorescein as tracer after systemic administration. An angiogram is obtained by imaging fluorescence emitted after illumination of the retina with blue light at a wavelength of 490 nm. The technique, however, can cause serious complications and even death of the patient. Furthermore, fluorescein angiography is not a quantitative method and cannot detect subtle dysfunction of the blood–retinal barrier or distinguish increased permeability for compounds that have a different molecular weight than fluorescein. In addition, a distinction between dysfunction of the inner or outer blood–retinal barrier is difficult or impossible.

Ocular fluorophotometry is a semi-quantitative blood–retinal barrier evaluation method which was developed in the 1980s. An advantage of this method is that both excitation and detection devices share a single mobile optical element, which allows for continuous fluorescence measurements along a straight line extending from the center of the cornea to the center of the posterior pole.<sup>144</sup>

A fluorescence optical imaging technique, fluorescence-mediated tomography, was used to assess experimental breakdown of the blood-retinal barrier in transgenic diabetic mice overexpressing insulin-growth factor 1 (IGF-1) which induces vascular alterations as may also be the case in human diabetic retinopathy. Breakdown of the blood–retinal barrier was assessed in a similar way as in fluorescein angiography using Cy5.5 as dye for the tracer studies. After administration of Cy5.5, intense fluorescence signal was found in the IGF-1 transgenic mice.<sup>67</sup> In vivo tomography of fluorescent tracers proved to be a reliable, safe, and fast method to assess permeability alterations in the blood–retinal barrier of small animals. The resolution of fluorescence-mediated tomography is, however, too low for this technique to be considered in humans.

Changes in vascular permeability have also been assessed in diabetic rats by dynamic contrast-enhanced MRI using Gd-DTPA as contrast agent. Passive permeability of the blood–retinal barrier was increased in diabetic rats and in VEGF-treated rats. Blood–retinal barrier disruption causes extravasation of Gd-DTPA to the vitreous directly affecting the surrounding proton spin-lattice relaxation rate ( $[T_1]^{-1}$ ). This triggers changes in signal intensity on  $T_1$ -weighted images that can be used to calculate passive blood–retinal barrier permeability.<sup>11</sup> Dynamic contrast-enhanced MRI methods are promising for the assessment of blood–retinal barrier permeability status both in pre-clinical and clinical studies. The blood–retinal barrier is a biological barrier that often limits drugs to reach therapeutic levels in ocular tissues. Therefore, one of the goals of blood–retinal barrier permeability studies is to investigate the enhanced delivery of drugs or genes to ocular tissue compartments. Delivery of nanoparticles containing the fluorescent marker rhodamine over the blood–retinal barrier has been investigated as well. Different nanoparticle formulations were injected and the fluorescence signal was imaged using a SLO.<sup>141, 151</sup>

## Retinal gliosis

Glial fibrillary acidic protein (GFAP) is expressed by astrocytes and Müller cells, the major glial cell types in the retina. Increased amounts of GFAP are produced in retinopathies such as retinal gliosis. Retinal gliosis has been quantified in transgenic mice expressing GFP under the control of the GFAP promoter after treatment with the excitatory neurotoxic agent kainic acid to induce gliosis. Gliosis in the retina was determined by SLO imaging and by measuring the expression of the GFAP-GFP. Intensity of the GFP fluorescent signal correlated with glial cell activity.<sup>71</sup> The same method was used for quantification of retinal gliosis development in time in response to diabetic retinopathy. Reactive retinal gliosis appeared to occur in early stages.<sup>95</sup>

## Pharmacokinetics

Molecular imaging approaches using MRI or PET as imaging modalities are frequently used to monitor drug delivery, pharmacokinetics, drug distribution, and elimination in the various tissues including ocular tissues.

Iontophoresis has been used to improve drug delivery across membranes with the assistance of an electric field. In the eye, a drug-containing electrode is placed on the surface and a second electrode is placed on another body surface. Assessment of the electrical current and the sites of drug delivery in the eye was performed by manganese-enhanced MRI.  $T_1$ -weighted images showed that for transscleral iontophoresis the probe ion was transported directly into the vitreous under the electrode whereas for transcorneal iontophoresis the site of delivery proved to be the anterior chamber.<sup>102</sup>

The frequently used MRI contrast agent Gd-DTPA has been used as a drug surrogate. Noninvasive real-time transport of Gd-DTPA released from an intravitreal polymer-based implant was imaged in rabbits.<sup>85</sup> It was also shown that episcleral implants at the equator of the eye do not deliver Gd-DTPA into the vitreous,<sup>86</sup> whereas intrascleral infusions were successful in transporting Gd-DTPA to the posterior segment from an anterior infusion site through the suprachoroidal space.<sup>87</sup> These results indicate that the suprachoroidal space is a compartment that can be used to deliver drugs to posterior structures of the eye.

Positron emission tomography is also used in pharmacokinetic studies. After radiolabeling of bevacizumab and ranibizumab with I-124, the pharmacokinetic properties of these drugs after intravitreal injection in rabbits were studied over time using a micro-PET device coupled with a CT scan. It was demonstrated that bevacizumab and ranibizumab were retained in the vitreous cavity up to 28 and 21 days, respectively.<sup>28</sup> Finally, fluorophotometry has recently been used to evaluate in vivo the transscleral delivery of fluorescein-conjugated dextrans to the posterior retina and choroid of rabbits.<sup>7</sup>

## **$\beta$ -amyloid retinal plaques**

It is assumed that the pathogenic mechanisms eventually leading to Alzheimer disease become manifest decades before the disease is recognized and are characterized by the accumulation of  $\beta$ -amyloid ( $A\beta$ ) in neural tissue. Identification of individuals who are prone to develop Alzheimer disease may have an impact on the clinical course of the disease. At the moment, several clinical trials are in progress investigating the potential beneficial role of  $\gamma$ -secretase inhibitors (LY450139) (ClinicalTrials.gov number, NCT00765115),<sup>169</sup> aggregation blockers, vaccination with  $A\beta$ , and monoclonal antibodies against various  $A\beta$  epitopes. Early detection of neural  $A\beta$  accumulation likely helps to understand progression of the disease and may be used as a surrogate marker to detect early effects of these new drugs.

In vivo identification of neural  $A\beta$  plaques is a major issue in research in neurodegenerative diseases. Presently, diagnosis of Alzheimer disease can only be established by the detection of  $A\beta$  accumulation and intracellular neurofibrillary tangles during a brain autopsy. Noninvasive in vivo detection of neuronal  $A\beta$  plaques in patients suspected of having Alzheimer disease and in animal models has been attempted,<sup>70, 124, 128</sup> but, so far, has not been successful, mainly because of the limited resolution.<sup>90, 105, 174</sup>

$\beta$ -amyloid plaques are formed in the retina as well and share properties with those in the brain. The retina can be considered the most accessible human neural tissue for imaging purposes. Transgenic mice carrying the mutated human genes APPSWE and Presenilin 1DE9, which lead to an early-onset familial Alzheimer disease, were found to develop  $A\beta$  deposits in the retina.<sup>130, 138</sup> Visualization of these deposits in the retina would allow noninvasive imaging of  $A\beta$  plaques as a pathological hallmark of Alzheimer disease already at early stages. For this purpose, curcumin (diferuloylmethane) was used, a natural and safe fluorochrome that binds and labels  $A\beta$  plaques. Eyes of mice that are models for Alzheimer disease have been imaged following systemic administration of curcumin using a retinal imaging microscope assembled with a specific set of filters suitable to detect curcumin fluorescence. Individual plaques or plaque clusters at high resolution were detected in the retinas of transgenic diseased mice, whereas control mice did not show any plaque formation. Moreover, numbers of these retinal plaques decreased after immune-based therapy, as they did in the brain. In addition,  $A\beta$  plaques were imaged in postmortem retinas of human patients at early and late stages of Alzheimer disease. The plaques were mainly located in the inner segments of the retina which facilitates in vivo imaging.<sup>93</sup> These studies indicate that retinal  $A\beta$  plaques may be used as diagnostic marker for Alzheimer disease in its early stages. It remains to be established whether the visualization of  $A\beta$  plaques in the retina of Alzheimer patients by multispectral imaging with adaptive optics is also feasible.

## **Future perspectives**

This overview shows the possibilities of application of molecular imaging techniques in ophthalmology. With the ongoing advancements in noninvasive imaging, molecular imaging will certainly be crucial to assess effects of novel therapies and diagnostic methods. Two major difficulties explain the delay in implementing molecular imaging into clinical practice: the lack of toxicity studies of molecular probes in humans and the lack of adequate imaging devices for high-resolution noninvasive imaging in the human body. Due to the easy accessibility of the eye, and the current technological developments such as multispectral imaging, it is assumed that ophthalmology might be one of the first medical fields to benefit from the use of these methods in the clinic. In the meantime, application of molecular imaging techniques in pre-clinical research is already leading to great advances in the understanding of the complex molecular interactions that eventually lead to disease states in the eye. Furthermore, molecular imaging methods may enable new possibilities to diagnose and characterize systemic diseases with repercussion in the eye such as Alzheimer disease.

## **Method of literature search**

For this review the Medline and Web of Science databases for the time period 1950 up to 15 October 2012 were searched on the Web of Knowledge System. Due to the broad nature of the subject and the different subtopics covered, we performed a separate search for each of the subtopics listed in the review. No limits were used so that all languages, all types of articles, all years, and all indexed publications were retrieved. In the second phase, all abstracts were scanned to identify relevant articles within the specific topics of our review. Our selection included articles in English, French, and German. Review articles were also included when relevant. Ophthalmic imaging articles were classified as “molecular imaging techniques” and “non-molecular imaging techniques”. Inclusion in the former category required the use of molecular probes and endogenous or exogenous contrast agents. All relevant ophthalmic imaging articles that were considered to fulfill the criteria of “molecular imaging techniques” were included. Other ophthalmic imaging articles that did not fulfill the criteria were included only when considered relevant for this review. Copies of the entire articles were obtained. The bibliographies of the retrieved articles were manually searched and additional references from key articles were incorporated into the text when deemed necessary. In the third stage, articles were reviewed and incorporated into the manuscript. Due to the rapid evolving nature of the subject, we included some information gathered from selected presentations at scientific meetings and from theoretical book chapters.

## Disclosure

We report no proprietary or commercial interest in any product mentioned or concept discussed in this article.

## References

1. Abdallah, W., Ameri, H., Barron, E. et al. Vitreal oxygenation in retinal ischemia reperfusion. *Invest Ophthalmol Vis Sci* 52:1035–1042, 2011
2. Arden, G.B., Sidman, R.L., Arap, W. et al. Spare the rod and spoil the eye. *Br J Ophthalmol*. 89:764–769, 2005
3. Arroyo, J.G., Yang, L., Bula, D. et al. Photoreceptor apoptosis in human retinal detachment. *Am J Ophthalmol* 139:605–610, 2015
4. Barber, A.J., Lieth, E., Khin, S.A. et al. Neural apoptosis in the retina during experimental and human diabetes - early onset and effect of insulin. *J Clin Invest* 102:783–791, 1998
5. Bartsch, D.U., Weinreb, R.N., Zinser, G. et al. Confocal scanning infrared-laser ophthalmoscopy for indocyanine green angiography. *Am J Ophthalmol* 120:642–651, 1995
6. Becker, M.D., Planck, S.R., Crespo, S. et al. Immunohistology of antigen-presenting cells in vivo: a novel method for serial observation of fluorescently labeled cells. *Invest Ophthalmol Vis Sci* 44:2004–2009, 2003
7. Berezovsky, D.E., Patel, S.R., McCarey, B.E. et al. In vivo ocular fluorophotometry: delivery of fluoresceinated dextrans via transscleral diffusion in rabbits. *Invest Ophthalmol Vis Sci* 52:7038–7045, 2011
8. Berkowitz, B.A., Kowluru, R.A., Frank, R.N. et al. Subnormal retinal oxygenation response precedes diabetic-like retinopathy. *Invest Ophthalmol Vis Sci* 40:2100–2105, 1999
9. Berkowitz, B.A., Luan, H.M., Gupta, R.R. et al. Regulation of the early subnormal retinal oxygenation response in experimental diabetes by inducible nitric oxide synthase. *Diabetes* 53:173–178, 2004
10. Berkowitz, B.A. and Roberts, R. Prognostic MRI biomarkers of treatment efficacy for retinopathy. *NMR Biomedicine* 21:957–967, 2008
11. Berkowitz, B.A., Roberts, R., Luan, H.M. et al. Dynamic contrast-enhanced MRI measurements of passive permeability through blood retinal barrier in diabetic rats. *Invest Ophthalmol Vis Sci* 45:2391–2398, 2004
12. Blankenberg, F.G. and Strauss, H.W. Will imaging of apoptosis play a role in clinical care? A tale of mice and men. *Apoptosis* 6:117–123, 2001
13. Blumenroder, S., Augustin, A.J., and Koch, F.H.J. The influence of intraocular pressure and systemic oxygen tension on the intravascular pO<sub>2</sub> of the pig retina as measured with phosphorescence imaging. *Surv Ophthalmol* 42:S118–S126, 1997
14. Bochert, R., Zhivov, A., Kraak, R. et al. Contribution to comprehension of image formation in confocal microscopy of cornea with Rostock cornea module. *Br J Ophthalmol* 89:1351–1355, 2005
15. Boersma, H.H., Kietselaer, B.L.J.H., Stolk, L.M.L. et al. Past, present, and future of annexin A5: From protein discovery to clinical applications. *J Nucl Med* 46:2035–2050, 2005
16. Bohnke, M. and Masters, B.R. Confocal microscopy of the cornea. *Prog Ret Eye Res* 18:553–628, 1999
17. Bredfeldt, J.S., Vinegoni, C., Marks, D.L. et al. Molecularly sensitive optical coherence tomography. *Opt Lett* 30:495–497, 2005
18. Bresnick, G.H., Frisch, G.D., Powell, J.O. et al. Ocular effects of argon laser radiation. Retinal damage threshold studies. *Invest Ophthalmol Vis Sci* 9:901–910, 1970
19. Buerk, D.G., Shonat, R.D., Riva, C.E. et al. O<sub>2</sub> gradients and countercurrent exchange in the cat vitreous-humor near retinal arterioles and venules. *Microvas Res* 45:134–148, 1993
20. Cai, W.B. and Chen, X.Y. Nanoplatforms for targeted molecular imaging in living subjects. *Small* 3:1840–1854, 2007
21. Cang, H., Sun, T., Li, Z.Y. et al. Gold nanocages as contrast agents for spectroscopic optical coherence tomography. *Opt Lett* 30:3048–3050, 2005
22. Carlson, E.C., Drazba, J., Yang, X.P. et al. Visualization and characterization of inflammatory cell recruitment and migration through the corneal stroma in endotoxin-induced keratitis. *Invest Ophthalmol Vis Sci* 47:241–248, 2006
23. Cavanagh, H.D., El-Agha, M.S., Petroll, W.M. et al. Specular microscopy, confocal microscopy, and ultrasound biomicroscopy - diagnostic tools of the past quarter century. *Cornea* 19:712–722, 2000
24. Chae, H.J., Kim, S.C., Han, K.S. et al. Hypoxia induces apoptosis by caspase activation accompanying cytochrome C release from mitochondria in MC3T3E1 osteoblasts. p38 MAPK is related in hypoxia-induced apoptosis 23:133–152, 2001
25. Chinnery, H.R., Ruitenber, M.J., Plant, G.W. et al. The chemokine receptor CXCR1 mediates homing of MHC class II - positive cells to the normal mouse corneal epithelium. *Invest Ophthalmol Vis Sci* 48: 1568–1574, 2007
26. Choi, S.S., Doble, N., Hardy, J.L. et al. In vivo imaging of the photoreceptor mosaic in retinal dystrophies and correlations with visual function. *Invest Ophthalmol Vis Sci* 47:2080–2092, 2006
27. Choi, S.S., Zawadzki, R.J., Keltner, J.L. et al. Changes in cellular structures revealed by ultra-high resolution retinal imaging in optic neuropathies. *Invest Ophthalmol Vis Sci* 49:2103–2119, 2008
28. Christoforidis, J.B., Carlton, M.M., Knopp, M.V., and Hinkle, G.H. PET/CT imaging of I-124-radiolabeled bevacizumab and ranibizumab after intravitreal injection in a rabbit model. *Invest Ophthalmol Vis Sci* 52:5899–5903, 2011
29. Cook, B., Lewis, G.P., Fisher, S.K. et al. Apoptotic photoreceptor degeneration in experimental retinal detachment. *Invest Ophthalmol Vis Sci* 36:990–996, 1995
30. Crane, I.J., Xu, H.P., Wallace, C. et al. Involvement of CCR5 in the passage of Th1-type cells across the blood-retina barrier in experimental autoimmune uveitis. *J Leukoc Biol* 79:435–443, 2006
31. DaCosta, R.S., Wilson, B.C., and Marcon, N.E. Optical techniques for the endoscopic detection of dysplastic colonic lesions. *Curr Opin Gastroenterol* 21:70–79, 2005

32. Dawson, A.J. and Meyer, R.L. Growth dynamics and morphology of regenerating optic fibers in tectum are altered by injury conditions: an in vivo imaging study in goldfish. *Exp Neurol* 210:592–601, 2008
33. Delori, F.C. Noninvasive technique for oximetry of blood in retinal vessels. *Appl Opt* 27:1113–1125, 1988
34. Denk, W., Strickler, J.H., and Webb, W.W. 2-Photon laser scanning fluorescence microscopy. *Science* 248:73–76, 1990
35. Dithmar, S., Holz, F.G., Burk, R.O.W. et al. Confocal indocyanine-green angiography using the Heidelberg retina angiograph. *Klin Monbl Augenheilkd* 207:11–16, 1995
36. Donovan, M., Carmody, R.J., and Cotter, T.G. Light-induced photoreceptor apoptosis in vivo requires neuronal nitric-oxide synthase and guanylate cyclase activity and is caspase-3 independent. *J Biol Chem* 276:23000–23008, 2001
37. Donovan, M. and Cotter, T.G. Caspase-independent photoreceptor apoptosis in vivo and differential expression of apoptotic protease activating factor-1 and caspase-3 during retinal development. *Cell Death Differ* 9:1220–1231, 2002
38. Doonan, F., Donovan, M., and Cotter, T.G. Caspase-independent photoreceptor apoptosis in mouse models of retinal degeneration. *J Neurosci* 23:5723–5731, 2003
39. Dumont, E.A., Reutlingsperger, C.P.M., Smits, J.F.M. et al. Real-time imaging of apoptotic cell-membrane changes at the single-cell level in the beating murine heart. *Nat Med* 7:1352–1355, 2001
40. Dunaief, J.L., Dentchev, T., Ying, G.S. et al. The role of apoptosis in age-related macular degeneration. *Arch Ophthalmol* 120:1435–1442, 2002
41. Duncan, J.L., Zhang, Y.H., Gandhi, J. et al. High-resolution imaging with adaptive optics in patients with inherited retinal degeneration. *Invest Ophthalmol Vis Sci* 48:3283–3291, 2007
42. Eter, N., Engel, D.R., Meyer, L. et al. In vivo visualization of dendritic cells, macrophages, and microglial cells responding to laser-induced damage in the fundus of the eye. *Invest Ophthalmol Vis Sci* 49:3649–3658, 2008
43. Evgenov, N.V., Medarova, Z., Dai, G.P. et al. In vivo imaging of islet transplantation. *Nat Med* 12:144–148, 2006
44. Faber, D.J., Aalders, M.C.G., Mik, E.G. et al. Oxygen saturation-dependent absorption and scattering of blood. *Phys Rev Lett* 93(2):028102, 2004
45. Faber, D.J., Mik, E.G., Aalders, M.C.G. et al. Toward assessment of blood oxygen saturation by spectroscopic optical coherence tomography. *Optics Lett* 30:1015–1017, 2005
46. Fang, I.M., Lin, C.P., Yang, C.M. et al. Expression of CX3C chemokine, fractalkine, and its receptor CX3CR1 in experimental autoimmune anterior uveitis. *Mol Vis* 11:443–451, 2005
47. Ferrez, P.W., Chamot, S.R., Petrig, B.L. et al. Effect of visual stimulation on blood oxygenation in the optic nerve head of miniature pigs: a pilot study. *Klin Monbl Augenheilkd* 221:364–366, 2004
48. Garcıavalenzuela, E., Shareef, S., Walsh, J. et al. Programmed cell-death of retinal ganglion-cells during experimental glaucoma. *Exp Eye Res* 61: 33–44, 1995
49. Geissmann, F., Jung, S., and Littman, D.R. Blood monocytes consist of two principal subsets with distinct migratory properties. *Immunity* 19:71–82, 2003
50. Giaccia, A.J., Simon, M.C., and Johnson, R. The biology of hypoxia: the role of oxygen sensing in development, normal function, and disease. *Genes Dev* 18:2183–2194, 2004
51. Gibson, J.S., Cossins, A.R., and Ellory, J.C. Oxygen-sensitive membrane transporters in vertebrate red cells. *J Exp Biol* 203:1395–1407, 2000
52. Gorman, A., Fletcher-Holmes, D.W., and Harvey, A.R. Generalization of the Lyot filter and its application to snapshot spectral imaging. *Opt Express* 18:5602–5608, 2010
53. Gray, D.C., Wolfe, R., Gee, B.P. et al. In vivo imaging of the fine structure of rhodamine-labeled macaque retinal ganglion cells. *Invest Ophthalmol Vis Sci* 49:467–473, 2008
54. Greaney, M.J., Hoffman, D.C., Garway-Heath, D.F. et al. Comparison of optic nerve imaging methods to distinguish normal eyes from those with glaucoma. *Invest Ophthalmol Vis Sci* 43:140–145, 2002
55. Grunwald, F., Zierz, S., Broich, K. et al. Brain spect imaging with Tc-99m Hmpao in ophthalmoplegia plus. *Clin Nucl Med* 16:20–23, 1991
56. Guo, L. and Cordeiro, M.F. Assessment of neuroprotection in the retina with DARC. Glaucoma: an open window to neurodegeneration and neuroprotection. *Prog Br Res* 173:437–450, 2008
57. Guy, J. MRI in experimental inflammatory and mitochondrial optic neuropathies. *NMR Biomed* 21: 968–977, 2008
58. Hamada, M., Ogura, Y., Miyamoto, K. et al. Retinal leukocyte behavior in experimental autoimmune uveoretinitis of rats. *Exp Eye Res* 65: 445–450, 1997
59. Hampson, K.M., Paterson, C., Dainty, C. et al. Adaptive optics system for investigation of the effect of the aberration dynamics of the human eye on steady-state accommodation control. *J Opt Soc Am A Opt Image Sci Vis* 23:1082–1088, 2006
60. Handa, J.T., Berkowitz, B.A., Wilson, C.A. et al. Hypoxia precedes the development of experimental preretinal neovascularization. *Graefes Arch Clin Exp Ophthalmol* 234:43–46, 1996
61. Hardarson, S.H., Basit, S., Jonsdottir, T.E. et al. Oxygen saturation in human retinal vessels is higher in dark than in light. *Invest Ophthalmol Vis Sci* 50:2308–2311, 2009
62. Hardarson, S.H., Gottfredsdottir, M.S., Halldorsson, G.H. et al. Glaucoma filtration surgery and retinal oxygen saturation. *Invest Ophthalmol Vis Sci* 50:5247–5250, 2009
63. Hardarson, S.H., Harris, A., Karlsson, R.A. et al. Automatic retinal oximetry. *Invest Ophthalmol Vis Sci* 47:5011–5016, 2006
64. Hardarson, S.H. and Stefansson, E. Oxygen saturation in central retinal vein occlusion. *Am J Ophthalmol* 150:871–875, 2010
65. Hardarson, S.H. and Stefansson, E. Retinal oxygen saturation is altered in diabetic retinopathy. *Br J Ophthalmol* 4:560–563, 2012
66. Harris, A., Dinn, R.B., Kagemann, L. et al. A review of methods for human retinal oximetry. *Ophthalmic Surg Lasers Imaging* 34:152–164, 2003
67. Haurigot, V., Villacampa, P., Ribera, A. et al. Increased intraocular insulin-like growth factor-I triggers blood-retinal barrier breakdown. *J Biol Chem* 284:22961–22969, 2009
68. Hickam, J.B. and Frayser, R. Studies of the retinal circulation in man. observations on vessel diameter, arteriovenous oxygen difference, and mean circulation time. *Circulation* 33:302–316, 1966
69. Higashide, T., Kawaguchi, I., Ohkubo, S. et al. In vivo imaging and counting of rat retinal ganglion cells using a scanning laser ophthalmoscope. *Invest Ophthalmol Vis Sci* 47:2943–2950, 2006
70. Hintersteiner, M., Enz, A., Frey, P. et al. In vivo detection of amyloid-beta deposits by near-infrared imaging using an oxazine-derivative probe. *Nat Biotechnol* 23:577–583, 2005
71. Hirohara, Y., Okawa, Y., Mihashi, T. et al. Validity of retinal

- oxygen saturation analysis: Hyperspectral imaging in visible wavelength with fundus camera and liquid crystal wavelength tunable filter. *Optical Review* 14:151–158, 2007
72. Ho, G., Kumar, S., Min, X.S. et al. Molecular imaging of retinal gliosis in transgenic mice induced by kainic acid neurotoxicity. *Invest Ophthalmol Vis Sci* 50:2459–2464, 2009
73. Hoffman, R.M. Green fluorescent protein imaging of tumour growth, metastasis, and angiogenesis in mouse models. *Lancet Oncol* 3:546–556, 2002
74. Hoffman, R.M. In vivo imaging with fluorescent proteins: the new cell biology. *Acta Histochem* 106:77–87, 2004
75. Holz, F.G., Bellmann, C., Rohrschneider, K. et al. Simultaneous confocal scanning laser fluorescence and indocyanine green angiography. *Am J Ophthalmol* 125:227–236, 1998
76. Imamura, K., Onoe, H., Shimazawa, M. et al. Molecular imaging reveals unique degenerative changes in experimental glaucoma. *Neuroreport* 20:139–144, 2009
77. Imanishi, Y., Lodowski, K.H., and Koutalos, Y. Two-photon microscopy: shedding light on the chemistry of vision. *Biochemistry* 46:9674–9684, 2007
78. Ito, Y. and Berkowitz, B.A. MR studies of retinal oxygenation. *Vision Res* 41:1307–1311, 2011
79. Ivanova, E., Roberts, R., Bissig, D. et al. Retinal channelrhodopsin-2-mediated activity in vivo evaluated with manganese-enhanced magnetic resonance imaging. *Mol Vis* 16:1059–1066, 2010
80. Jensen, P.S. and Glucksberg, M.R. Regional variation in capillary hemodynamics in the cat retina. *Invest Ophthalmol Vis Sci* 39:407–415, 1998
81. Jiang, Y., Tomov, I., Wang, Y.M. et al. Second-harmonic optical coherence tomography. *Opt Lett* 29:1090–1092, 2004
82. Johnson, A.W., Ammar, D.A., and Kahook, M.Y. Two-photon imaging of the mouse eye. *Invest Ophthalmol Vis Sci* 52:4098–4105, 2011
83. Kato, K., Kubota, T., Ikeda, M. et al. Low efficacy of F-18-FDG PET for detection of uveal malignant melanoma compared with I-123-IMP SPECT. *J Nucl Med* 47:404–409, 2006
84. Kerrigan, L.A., Zack, D.J., Quigley, H.A. et al. TUNEL-positive ganglion cells in human primary open-angle glaucoma. *Arch Ophthalmol* 115:1031–1035, 1997
85. Kim, H., Lizak, M.J., Tansey, G. et al. Study of ocular transport of drugs released from an intravitreal implant using magnetic resonance imaging. *Ann Biomed Eng.* 2005; 33: 150–164
86. Kim, H., Robinson, M.R., Lizak, M.J. et al. Controlled drug release from an ocular implant: an evaluation using dynamic three-dimensional magnetic resonance imaging. *Invest Ophthalmol Vis Sci* 45:2722–2731, 2004
87. Kim, S.H., Galban, C.J., Lutz, R.J. et al. Assessment of subconjunctival and intrascleral drug delivery to the posterior segment using dynamic contrast-enhanced magnetic resonance imaging. *Invest Ophthalmol Vis Sci* 48:808–814, 2007
88. Klaassen, I., Van Noorden, C.J., and Schlingemann, R.O. Molecular basis of the inner blood-retinal barrier and its breakdown in diabetic macular edema and other pathological conditions. *Prog Retin Eye Res* 34:19–48, 2013
89. Klerk, C.P.W., Overmeer, R.M., Niers, T.M.H. et al. Validity of bioluminescence measurements for noninvasive in vivo imaging of tumor load in small animals. *Biotechniques* 43:7–13, 2007
90. Klunk, W.E., Lopresti, B.J., Ikonomic, M.D. et al. Binding of the positron emission tomography tracer Pittsburgh compound-B reflects the amount of amyloid-beta in Alzheimer's disease brain but not in transgenic mouse brain. *J Neurosci* 25:10598–10606, 2005
91. Kolodny, N.H., Freddo, T.F., Lawrence, B.A. et al. Contrast-enhanced magnetic resonance imaging confirmation of an anterior protein pathway in normal rabbit eyes. *Invest Ophthalmol Vis Sci* 37:1602–1607, 1996
92. Koo, V., Hamilton, P.W., and Williamson, K. Non-invasive in vivo imaging in small animal research. *Cell Oncol* 28:127–139, 2006
93. Koronyo-Hamaoui, M., Koronyo, Y., Ljubimov, A.V. et al. Identification of amyloid plaques in retinas from Alzheimer's patients and noninvasive in vivo optical imaging of retinal plaques in a mouse model. *Neuroimage* 54:204–217, 2011
94. Kravtsov, V.D., Daniel, T.O., and Koury, M.J. Comparative analysis of different methodological approaches to the in vitro study of drug-induced apoptosis. *Am J Pathol* 155:1327–1339, 1999
95. Kumar, S. and Zhuo, L. Longitudinal in vivo imaging of retinal gliosis in a diabetic mouse model. *Exp Eye Res* 91:530–536, 2010
96. L'Esperance, F.A. Jr. and Kelly, G.R. The threshold of the retina to damage by argon laser radiation. *Arch Ophthalmol* 81:583–588, 1969
97. Lee, E.J., Rosenbaum, J.T., and Planck, S.R. Epifluorescence intravitral microscopy of murine corneal dendritic cells. *Invest Ophthalmol Vis Sci* 51:2101–2108, 2010
98. Lee, T.M., Oldenburg, A.L., Sitafalwalla, S. et al. Engineered microsphere contrast agents for optical coherence tomography. *Opt Lett* 28:1546–1548, 2003
99. Leibur, R., Davila, E., and Zemel, E. Development of laser-induced retinal damage in the rabbit. *Graefes Arch Clin Exp Ophthalmol* 237:991–1000, 1999
100. Leung, C.K.S., Lindsey, J.D., Crowston, J.G. et al. In vivo imaging of murine retinal ganglion cells. *J Neurosci Methods* 168: 475–478, 2008
101. Lewis, J.S., Achilefu, S., Garbow, J.R. et al. Small animal imaging: current technology and perspectives for oncological imaging. *Eur J Cancer* 38:2173–2188, 2002
102. Li, S.K., Jeong, E.K., and Hastings, M.S. Magnetic resonance imaging study of current and ion delivery into the eye during transscleral and transcorneal iontophoresis. *Invest Ophthalmol Vis Sci* 45:1224–1231, 2004
103. Linsenmeier, R.A., Goldstick, T.K., Blum, R.S. et al. Estimation of retinal oxygen transients from measurements made in the vitreous humor. *Exp Eye Res.* 32:369–379, 1981
104. Liu, C.D., Li, Y.W., Peng, M. et al. Activation of caspase-3 in the retina of transgenic rats with the rhodopsin mutation S334ter during photoreceptor degeneration. *J Neurosci* 19:4778–4785, 1999
105. Lockhart, A., Lamb, J.R., Osredkar, T. et al. PIB is a non-specific imaging marker of amyloid-beta (A beta) peptide-related cerebral amyloidosis. *Brain* 130: 2607–2615, 2007
106. Lopez-Barneo, J., Pardal, R., and Ortega-Saenz, P. Cellular mechanisms of oxygen sensing. *Annu Rev Physiol* 63:259–287, 2001
107. Luker, G.D. and Luker, K.E. Optical imaging: current applications and future directions. *J Nucl Med* 49:1–4, 2008
108. Lyons, S.K. Advances in imaging mouse tumour models in vivo. *J Pathol* 205:194–205, 2005
109. Maass, A., von Leithner, P.L., Luong, V. et al. Assessment of rat and mouse RGC apoptosis Imaging in vivo with different scanning laser ophthalmoscopes. *Curr Eye Res* 32:851–861, 2007

110. Marks, D.L. and Boppart, S.A. Nonlinear interferometric vibrational imaging. *Phys Rev Lett* 92(12):23905, 2004
111. Marshall, J., Hamilton, A.M., and Bird, A.C. Histopathology of ruby and argon laser lesions in monkey and human retina - comparative study. *Br J Ophthalmol* 59:610–630, 1975
112. Marshall, J. and Mellerio, H.J. Histology of retinal lesions produced with Q-switched lasers. *Exp Eye Res* 7:225–230, 1968
113. Marshall, J. and Mellerio, J. Histology of the formation of retinal laser lesions. *Exp Eye Res* 6:4–9, 1967
114. Marshall, J. and Mellerio, J. Pathological development of retinal laser photocoagulations. *Exp Eye Res* 6:303–308, 1967
115. Martin, J.A. and Roorda, A. Direct and noninvasive assessment of parafoveal capillary leukocyte velocity. *Ophthalmology* 112:2219–2224, 2005
116. Massoud, T.F. and Gambhir, S.S. Molecular imaging in living subjects: seeing fundamental biological processes in a new light. *Genes Dev* 17:545–580, 2003
117. Masters, B.R. and Bohnke, M. Three-dimensional confocal microscopy of the human cornea in vivo. *Ophthalmic Res* 33:125–135, 2001
118. Matsubara, A., Nakazawa, T., Noda, K. et al. Photodynamic therapy induces caspase-dependent apoptosis in rat CNV model. *Invest Ophthalmol Vis Sci* 48:4741–4747, 2007
119. Miyahara, S., Almulki, L., Noda, K. et al. In vivo imaging of endothelial injury in choriocapillaris during endotoxin-induced uveitis. *FASEB J* 22:1973–1980, 2008
120. Mordant, D.J., Al-Abboud, I., Muyo, G. et al. Spectral imaging of the retina. *Eye* 25:309–320, 2011
121. Morishige, N., Petroll, W.M., Nishida, T. et al. Noninvasive corneal stromal collagen imaging using two-photon-generated second-harmonic signals. *J Cataract Refract Surg* 32:1784–1791, 2006
122. Mumm, J.S., Williams, P.R., Godinho, L. et al. In vivo imaging reveals dendritic targeting of laminated afferents by zebrafish retinal ganglion cells. *Neuron* 52:609–621, 2006
123. Muqit, M.M.K., Denniss, J., Nourrit, V. et al. Spatial and spectral imaging of retinal laser photocoagulation burns. *Invest Ophthalmol Vis Sci* 52:994–1002, 2011
124. Nakada, T., Matsuzawa, H., Igarashi, H. et al. In vivo visualization of senile-plaque-like pathology in alzheimer's disease patients by MR microscopy on a 7T system. *J Neuroimaging* 18:125–129, 2008
125. Narula, J., Acio, E.R., Narula, N. et al. Annexin-V imaging for noninvasive detection of cardiac allograft rejection. *Nat Med* 7:1347–1352, 2001
126. Nassif, N., Cense, B., Park, B.H. et al. In vivo human retinal imaging by ultrahigh-speed spectral domain optical coherence tomography. *Opt Lett* 29:480–482, 2004
127. Nelson, D.A., Krupsky, S., Pollack, A. et al. Special report: noninvasive multi-parameter functional optical imaging of the eye. *Ophthalm Surg Lasers Imaging* 36:57–66, 2005
128. Ng, S., Villemagne, V.L., Berlangieri, S. et al. Visual assessment versus quantitative assessment of C-11-PIB PET and F-18-FDG PET for detection of Alzheimer's disease. *J Nucl Med* 48:547–552, 2007
129. Niess, J.H., Brand, S., Gu, X.B. et al. CXCR1-mediated dendritic cell access to the intestinal lumen and bacterial clearance. *Science* 307:254–258, 2005
130. Ning, A., Cui, J., To, E. et al. Amyloid-beta deposits lead to retinal degeneration in a mouse model of Alzheimer disease. *Invest Ophthalmol Vis Sci* 49:5136–5143, 2008
131. Nourrit, V., Denniss, J., Muqit, M.M.K. et al. High-resolution hyperspectral imaging of the retina with a modified fundus camera. *J Fr Ophthalmol* 33: 686–692, 2010
132. Obata, T., Ikehira, H., Shishido, F. et al. Deuterium MR in vitro imaging of the rat eye using (H<sub>2</sub>O)-H-2. *Acta Radiol* 36:552–555, 1995
133. Olafsdottir, O.B., Hardarson, S.H., Gottfredsdottir, M.S. et al. Retinal oximetry in primary open angle glaucoma. *Invest Ophthalmol Vis Sci* 52:6409–6413, 2011
134. Oldenburg, A.L., Gunther, J.R., and Boppart, S.A. Imaging magnetically labeled cells with magnetomotive optical coherence tomography. *Opt Lett* 30:747–749, 2005
135. Palczewska, G., Maeda, T., Imanishi, Y. et al. Noninvasive multiphoton fluorescence microscopy resolves retinol and retinal condensation products in mouse eyes. *Nat Med* 16:1444–1449, 2010
136. Paques, M., Sironnotti, M., Roux, M.J. et al. High resolution fundus imaging by confocal scanning laser ophthalmoscopy in the mouse. *Vision Res* 46:1336–1345, 2006
137. Patel, D.V. and McGhee, C.N.J. Contemporary in vivo confocal microscopy of the living human cornea using white light and laser scanning techniques: a major review. *Clin Experiment Ophthalmol* 35:71–88, 2007
138. Perez, S.E., Lumayag, S., Kovacs, B. et al. Beta-amyloid deposition and functional impairment in the retina of the APPsw/PS1 delta E9 transgenic mouse model of alzheimer's disease. *Invest Ophthalmol Vis Sci* 50:793–800, 2009
139. Phelps, M.E. Nuclear medicine, molecular imaging, and molecular medicine. *J Nucl Med* 43:13N–14N, 2002
140. Piston, D.W. Imaging living cells and tissues by two-photon excitation microscopy. *Trends Cell Biol* 9:66–69, 1999
141. Prilloff, S., Fan, J.Y., Henrich-Noack, P. et al. In vivo confocal neuroimaging (ICON): non-invasive, functional imaging of the mammalian CNS with cellular resolution. *Eur J Neurosci* 31:521–528, 2010
142. Quigley, H.A., Nickells, R.W., Kerrigan, L.A. et al. Retinal ganglion-cell death in experimental glaucoma and after axotomy occurs by apoptosis. *Invest Ophthalmol Vis Sci* 36:774–786, 1995
143. Rahmim, A. and Zaidi, H. PET versus SPECT: strengths, limitations and challenges. *Nucl Med Commun* 29:193–207, 2008
144. Raines, M.F. Vitreous fluorophotometry—a review. *JR Soc Med* 81:403–406, 1988
145. Rao, K.D., Choma, M.A., Yazdanfar, S. et al. Molecular contrast in optical coherence tomography by use of a pump-probe technique. *Opt Lett* 28:340–342, 2003
146. Ritter, M.R., Aguilar, E., Banin, E. et al. Three-dimensional in vivo imaging of the mouse intraocular vasculature during development and disease. *Invest Ophthalmol Vis Sci* 46:3021–3026, 2005
147. Riva, C.E. Noninvasive measurement of oxygen tension in the optic nerve head. *Curr Opin Ophthalmol* 9:56–60, 1998
148. Roberts, R., Zhang, W., Ito, Y. et al. Spatial pattern and temporal evolution of retinal oxygenation response in oxygen-induced retinopathy. *Invest Ophthalmol Vis Sci* 44:5315–5320, 2003
149. Roorda, A., Zhang, Y.H., and Duncan, J.L. High-resolution in vivo imaging of the RPE mosaic in eyes with retinal disease. *Invest Ophthalmol Vis Sci* 48:2297–2303, 2007
150. Rumsey, W.L., Vanderkooi, J.M., and Wilson, D.F. Imaging of phosphorescence—a novel method for measuring oxygen distribution in perfused tissue. *Science* 241:1649–1651, 1998
151. Sabel, B.A., Engelmann, R., and Humphrey, M.F. In vivo confo-

- cal neuroimaging (ICON) of CNS neurons. *Nat Med* 3:244–247, 1997
152. Sarunic, M.V., Applegate, B.E., and Izatt, J.A. Spectral domain second-harmonic optical coherence tomography. *Opt Lett* 30:2391–2393, 2005
  153. Sawai, H. and Domae, N. Discrimination between primary necrosis and apoptosis by necrostatin-1 in Annexin V-positive/propidium iodide-negative cells. *Biochem Biophys Res Comm* 411:569–573, 2011
  154. Schenke-Layland, K., Riemann, I., Damour, O. et al. Two-photon microscopes and in vivo multiphoton tomographs - powerful diagnostic tools for tissue engineering and drug delivery. *Adv Drug Deliv Rev* 58:878–896, 2006
  155. Schlingemann, R.O., Hofman, P., Vrensen, G.F. et al. Increased expression of endothelial antigen PAL-E in human diabetic retinopathy correlates with microvascular leakage. *Diabetologia* 42:596–602, 1999
  156. Schmitz-Valckenberg, S., Guo, L., Maass, A. et al. Real-time in vivo imaging of retinal cell apoptosis after laser exposure. *Invest Ophthalmol Vis Sci* 49:2773–2780, 2008
  157. Sebaj, J., Delori, F.C., Fekete, G.T. et al. Effects of optic atrophy on retinal blood flow and oxygen saturation in humans. *Arch Ophthalmol* 107:222–226, 1989
  158. Semenza, G.L. HIF-1: mediator of physiological and pathophysiological responses to hypoxia. *J Appl Physiol* 88:1474–1480, 2000
  159. Shahidi, M., Blair, N.P., Mori, M. et al. Feasibility of noninvasive imaging of chorioretinal oxygenation. *Ophthalmic Surg Lasers Imaging* 35:415–422, 2004
  160. Shahidi, M., Shakoor, A., Blair, N.P. et al. A method for chorioretinal oxygen tension measurement. *Curr Eye Res* 31:357–366, 2006
  161. Shahidi, M., Wanek, J., Blair, N.P. et al. Retinal tissue oxygen tension imaging in the rat. *Invest Ophthalmol Vis Sci* 51:4766–4770, 2010
  162. Shahidi, M., Wanek, J., Blair, N.P. et al. Three-dimensional mapping of chorioretinal vascular oxygen tension in the rat. *Invest Ophthalmol Vis Sci* 50:820–825, 2009
  163. Shakoor, A., Shahidi, M., Blair, N.P. et al. Noninvasive assessment of chorioretinal oxygenation changes in experimental carotid occlusion. *Curr Eye Res* 30:763–771, 2005
  164. Sharp, P.F., Manivannan, A., Xu, H. et al. The scanning laser ophthalmoscope—a review of its role in bioscience, and medicine. *Phys Med Biol* 49:1085–1096, 2004
  165. Shonat, R.D. and Johnson, P.C. Oxygen tension gradients and heterogeneity in venous microcirculation: a phosphorescence quenching study. *Am J Physiol* 41:H2233–H2240, 1997
  166. Shonat, R.D. and Kight, A.C. Oxygen tension imaging in the mouse retina. *Ann Biomed Eng* 31:1084–1096, 2003
  167. Shonat, R.D., Wilson, D.F., Riva, C.E. et al. Effect of acute increases in intraocular pressure on intravascular optic nerve head oxygen tension in cats. *Invest Ophthalmol Vis Sci* 33:3174–3180, 1992
  168. Shonat, R.D., Wilson, D.F., Riva, C.E. et al. Oxygen distribution in the retinal and choroidal vessels of the cat as measured by a new phosphorescence imaging method. *Appl Opt* 31:3711–3718, 1992
  169. Siemers, E.R., Quinn, J.F., Kaye, J. et al. Effects of a gamma-secretase inhibitor in a randomized study of patients with Alzheimer disease. *Neurology* 66:602–604, 2006
  170. Smiddy, W.E., Fine, S.L., Quigley, H.A. et al. Comparison of krypton and argon laser photocoagulation. Results of stimulated clinical treatment of primate retina. *Arch Ophthalmol* 102:1086–1092, 1984
  171. Soos, T.J., Sims, T.N., Barisoni, L. et al. CXCR1(+) interstitial dendritic cells form a contiguous network throughout the entire kidney. *Kidney Int* 70:591–596, 2006
  172. Spencer, D.B., Lee, E.J., Kawaguchi, T. et al. In vivo imaging of the immune response in the eye. *Semin Immunopathol.* 30: 179–190, 2008
  173. Tiedeman, J.S., Kirk, S.E., Srinivas, S. et al. Retinal oxygen consumption during hyperglycemia in patients with diabetes without retinopathy. *Ophthalmology.* 105:31–36, 1998
  174. Toyama, H., Ye, D., Ichise, M. et al. PET imaging of brain with the beta-amyloid probe, [C-11]6-OH-BTA-1, in a transgenic mouse model of Alzheimer's disease. *Eur J Nucl Med Mol Imaging* 32:593–600, 2005
  175. Traustason, S., Hardarson, S.H., Gottfredsdottir, M.S. et al. Dorzolamide-timolol combination and retinal vessel oxygen saturation in patients with glaucoma or ocular hypertension. *Br J Ophthalmol* 93:1064–1067, 2009
  176. Trick, G.L. and Berkowitz, B.A. Retinal oxygenation response and retinopathy. *Prog Ret Eye Res* 24:259–274, 2005
  177. van Dijk, H.W., Verbraak, F.D., Kok, P.H.B. et al. Decreased retinal ganglion cell layer thickness in patients with type 1 diabetes. *Invest Ophthalmol Vis Sci* 51:3660–3665, 2010
  178. van Dijk, H.W., Verbraak, F.D., Kok, P.H. et al. Early neurodegeneration in the retina of type 2 diabetic patients. *Invest Ophthalmol Vis Sci* 53:2715–2719, 2012
  179. Van Noorden, C.J.F. Imaging enzymes at work: metabolic mapping by enzyme histochemistry. *J Histochem Cytochem* 58:481–497, 2010
  180. van Velthoven, M.E.J., Faber, D.J., Verbraak, F.D. et al. Recent developments in optical coherence tomography for imaging the retina. *Prog Ret Eye Res* 26: 57–77, 2007
  181. Vermes, I., Haanen, C., Steffensnacken, H. et al. A novel assay for apoptosis - flow cytometric detection of phosphatidylserine expression on early apoptotic cells using fluorescein-labeled annexin-V. *J Immunol Methods* 184:39–51, 1995
  182. Vilupuru, A.S., Rangaswamy, N.V., Frishman, L.J. et al. Adaptive optics scanning laser ophthalmoscopy for in vivo imaging of lamina cribrosa. *J Opt Soc Am A Opt Image Sci Vis* 24:1417–1425, 2007
  183. Vinegoni, C., Bredfeldt, J.S., Marks, D.L. et al. Nonlinear optical contrast enhancement for optical coherence tomography. *Opt Express* 12:331–341, 2004
  184. Wangsa-Wirawan, N.D. and Linsenmeier, R.A. Retinal oxygen—fundamental and clinical aspects. *Arch Ophthalmol* 121:547–557, 2003
  185. Webb, R.H., Hughes, G.W., and Pomerantzeff, O. Flying spot TV ophthalmoscope. *Appl Opt* 19:2991–2997, 1980
  186. Weissleder, R. and Mahmood, U. Molecular imaging. *Radiology* 219:316–333, 2001
  187. Wilson, C.A., Benner, J.D., Berkowitz, B.A. et al. Transcorneal oxygenation of the preretinal vitreous. *Arch Ophthalmol* 112:839–845, 1994
  188. Wilson, C.A., Berkowitz, B.A., McCuen, B.W. et al. Measurement of preretinal oxygen-tension in the vitrectomized human eye using F-19 magnetic-resonance spectroscopy. *Arch Ophthalmol* 110:1098–1100, 1992
  189. Wilson, C.A., Berkowitz, B.A., Sato, Y. et al. Intravitreal steroid reduces blood-retinal barrier breakdown due to retinal photocoagulation. *Invest Ophthalmol Vis Sci.* 33:1125, 1992

## Other cited material

190. Wilson, D.F., Pastuszko, A., Digiacoio, J.E. et al. Effect of hyperventilation on oxygenation of the brain cortex of newborn piglets. *J Appl Physiol* 70:2691–2696, 1991
191. Wilson, D.F., Vanderkooi, J.M., Green, T.J. et al. A versatile and sensitive method for measuring oxygen. *Adv Exp Med Biol* 215:71–77, 1987
192. Wojtkowski, M., Bajraszewski, T., Gorczynska, I. et al. Ophthalmic imaging by spectral optical coherence tomography. *Am J Ophthalmol* 138:412–419, 2004
193. Xie, F., Sun, D.W., Schering, A. et al. Novel molecular imaging approach for subclinical detection of iritis and evaluation of therapeutic success. *Am J Pathol* 177:39–48, 2010
194. Xu, C.Y., Ye, J., Marks, D.L. et al. Near-infrared dyes as contrast-enhancing agents for spectroscopic optical coherence tomography. *Opt Lett* 29:1647–1649, 2004
195. Xu, H.P., Manivannan, A., Goatman, K.A. et al. Reduction in shear stress, activation of the endothelium, and leukocyte priming are all required for leukocyte passage across the blood-retina barrier. *J Leukoc Biol* 75:224–232, 2004
196. Xu, H.P., Manivannan, A., Goatman, K.A. et al. Improved leukocyte tracking in mouse retinal and choroidal circulation. *Exp Eye Res* 74:403–410, 2002
197. Xu, H.P., Manivannan, A., Jiang, H.R. et al. Recruitment of IFN-gamma-producing (Th1-like) cells into the inflamed retina in vivo is preferentially regulated by P-selectin glycoprotein ligand 1: P/E-Selectin interactions. *J Immunol* 172:3215–3224, 2004
198. Xu, H.P., Manivannan, A., Liversidge, J. et al. Involvement of CD44 in leukocyte trafficking at the blood-retinal barrier. *J Leukoc Biol* 72:1133–1141, 2002
199. Xu, J.Q., Sun, S.W., Naismith, R.T. et al. Assessing optic nerve pathology with diffusion MRI: from mouse to human. *NMR Biomed* 21:928–940, 2008
200. Yang, C.H. Molecular contrast optical coherence tomography: a review. *Photochem Photobiol* 81:215–237, 2005
201. Yang, C.H., Choma, M.A., Lamb, L.E. et al. Protein-based molecular contrast optical coherence tomography with phytochrome as the contrast agent. *Opt Lett* 29:1396–1398, 2004
202. Yoneya, S., Saito, T., Nishiyama, Y. et al. Retinal oxygen saturation levels in patients with central retinal vein occlusion. *Ophthalmology* 109:1521–1526, 2002
203. Zhang, E.Z., Laufer, J.G., Pedley, R.B. et al. In vivo high-resolution 3D photoacoustic imaging of superficial vascular anatomy. *Phys Med Biol* 54:1035–1046, 2009
204. Zhang, W., Ito, Y., Berlin, E. et al. Role of hypoxia during normal retinal vessel development and in experimental retinopathy of prematurity. *Invest Ophthalmol Vis Sci* 44:3119–3123, 2003
205. Zhang, W., Ito, Y., Berlin, E. et al. Specificity of subnormal Delta Po-2 for retinal neovascularization in experimental retinopathy of prematurity. *Invest Ophthalmol Vis Sci* 44:3551–3555, 2003
206. Zhao, M., Beauregard, D.A., Loizou, L. et al. Non-invasive detection of apoptosis using magnetic resonance imaging and a targeted contrast agent. *Nat Med* 7:1241–1244, 2001
207. Zuckerman, R., Cheasty, J.E., and Wang, Y.P. Optical mapping of inner retinal tissue PO2. *Curr Eye Res* 12:809–825, 1993
- A. Alabboud, I., Muyo, G., Gorman, A. et al. New spectral imaging techniques for blood oximetry in the retina. *Proc SPIE* 3:6631–22, 20 07
- B. Arimoto, H. and Furukawa, H. Retinal blood oxygen saturation mapping by multispectral imaging and morphological angiography. *Proc IEEE Eng Med Biol Soc* 1627–1630, 2007
- C. Bradley WG. Fundamentals of MRI: part II. Accessed online on 16 July 2012 <http://www.e-radiography.net/mrict/fund%20mr2/fundmri%202.htm>.
- D. Cordeiro, M.F., Guo, L., Luong, V. et al. Real-time imaging of single nerve cell apoptosis in retinal neurodegeneration. *Proc Natl Acad Sci USA* 101:13352–16, 2004
- E. Faber, D.J., van Velthoven, M.E.J., de Bruin, M. et al. NAOMI: nanoparticles assisted optical molecular imaging. *Proc SPIE* 6079:607905, 2006
- F. Grifeth, L.K. Use of PET/CT scanning in cancer patients: technical and practical considerations. *Proc Bayl Univ Med Cent* 18:321–330, 2005
- G. Laxman, B., Hall, D.E., Bhojani, M.S. et al. Noninvasive real-time imaging of apoptosis. *Proc Natl Acad Sci USA* 99:16551–16555, 2002
- H. Nakazawa, T., Hisatomi, T., Nakazawa, C. et al. Monocyte chemoattractant protein 1 mediates retinal detachment-induced photoreceptor apoptosis. *Proc Natl Acad Sci USA* 104:2425–2430, 2007



9

# Summary and conclusions

The first aim of this thesis was to investigate the role of the ubiquitin-proteasome system (UPS) in retinal pigment epithelial (RPE) cell-mediated proteostasis. We then addressed potential causes of proteasomal dysfunction in RPE cells, whether the UPS was involved in RPE-mediated fibrogenic pathways and investigated the effects of pharmacological inhibition and activation of the UPS in RPE cells. The second aim was to apply a newly-developed retinal multispectral imaging device to visualize the above-mentioned processes in the neurosensory retina.

In Chapter 3, we assessed potential triggers of proteasome dysfunction in RPE cells and, indirectly, the role of the proteasome in the pathogenesis of age-related macular degeneration (AMD). An AMD-like environment was induced in human RPE cell cultures to assess individual effects of specific AMD pathogens such as complement anaphylatoxins C3a and C5a, oxidative stress induced by  $H_2O_2$  and phagocytosis of photoreceptor outer segments. In addition, we characterized the effects of aging on proteasome overall activity and assessed the expression of proteasome classic and inducible subunits  $\beta 5$  and  $\beta 5i$  in a mouse model of age-related RPE degeneration. It was shown that complement activation, via complement factor C3a, was associated with decreased proteasome-mediated proteolytic activity and that aging was associated with decreased proteasome overall activity. Furthermore, expression of one of the immunoproteasome subunits was upregulated in a mouse model of age-related RPE degeneration. Immunoproteasome activation is presumed to be a cellular response to stress and mice deficient in this specific proteasome subunit ( $\beta 5i$ ) have been shown to be less resistant to oxidative stress. These results indicate an association between complement activation and ineffective RPE-mediated proteostasis. Further studies are warranted to establish the contribution of proteasome dysfunction to AMD pathogenesis.

In Chapter 4, we assessed whether the UPS was involved in fibrogenic and proliferative responses of RPE cells. Fibrosis in ophthalmic disorders, such as neovascular AMD and proliferative vitreoretinopathy, is irreversible and untreatable. Since the advent of efficacious anti-angiogenic drugs, the study of fibrogenic pathways in ophthalmic disorders

has been relegated. In recent years, proteasome inhibitors have been proposed as potential agents in the prevention and treatment of fibrotic disorders such as renal and hepatic fibrosis. Therefore, we assessed whether proteasome modulation affected expression of extracellular matrix genes in RPE cells. Epoxomicin, a proteasome selective and irreversible inhibitor, was used to guarantee maximal proteasome inhibition. Epoxomicin arrested cell cycle progression and downregulated expression of transforming growth factor- $\beta$  (TGF $\beta$ ) which in turn was found to be a major pro-fibrogenic factor. Likewise, epoxomicin not only downregulated the expression of important extracellular matrix genes, but also upregulated transcription of peroxisome proliferator-associated receptor- $\gamma$  (PPAR $\gamma$ ), an important anti-fibrogenic factor. These results suggest a link between UPS modulation and fibrogenic pathways in the RPE.

Next, we investigated exogenous drugs as proteasome-modulating agents, such as curcumin, the main curcuminoid of turmeric (*Curcuma longa*), which amongst other functions is also known to modulate proteasome function. Although a myriad of potential beneficial effects of curcumin have been described, its use as a therapeutic agent is hampered by the poor bioavailability profile of standard curcumin. Furthermore, it has been suggested that curcumin is toxic for RPE cells. The goal of Chapter 5 was dual: to assess the cytotoxic, proliferative and oxidative effects of nano-curcumin (Theracurmin®), a bioavailable curcumin that is dispersed with nano-colloidal particles, in comparison with standard curcumin, and to assess the effects of standard curcumin and nano-curcumin on proteasome expression and activity. We found nano-curcumin to be a safer alternative when compared to standard curcumin. Nano-curcumin did not show significant cytotoxicity and did not affect cell cycle progression whereas standard curcumin reduced cell viability and increased production of reactive oxygen species. This may stem from the more stable biochemical profile of nano-curcumin which is 100 times smaller in size and thus more soluble than standard curcumin. Both nano-curcumin and standard curcumin exerted significant changes in proteasome-mediated proteostasis with consequent changes in expression of proteasome subunits. Our results indicated that RPE function is negatively affected by curcumin supplementation. The question remains whether oral intake of curcumin reaches the eye at levels required for significant molecular effects.

In our studies, a link between dysregulated complement pathway activation and proteasome dysfunction was established. The complement system is an important pathogenic factor associated with the development of AMD and likewise, modulation of the complement pathway is currently being explored as strategy to halt progression of this disease. However, a phase II clinical trial of eculizumab, an inhibitor of complement factor C5, failed to show any clinical benefit in nonexudative AMD. In Chapter 6, we assessed the effects of eculizumab on Purtscher-like retinopathy, which, similarly to AMD, is known to be triggered by complement activation. In this particular case, complement activation was caused by a mutation in complement factor H, a regulator of the alternative pathway of the complement which is also known to increase susceptibility to the development of AMD. In this patient, systemic eculizumab treatment was associated with full visual

recovery and resolution of all clinical signs and symptoms indicating that therapeutic levels were reached in the choroid and retina. The outcome attained in this patient highlights the differences between acute complement activation, as seen in Purtscher-like retinopathies, and chronic complement activation which occurs in AMD. The pathogenesis of Purtscher-like retinopathies was reviewed based on the therapeutic effects attained in this patient and the recent description of the molecular pathways involved in hemolytic uremic syndrome, namely endothelial activation of the coagulation cascade by complement and the formation of microthrombi. This is the first report of an effective treatment of visually-threatening Purtscher-like retinopathy.

The second part of this thesis is focused on ophthalmic molecular imaging methods as a means to visualize ocular molecular processes in vivo. In Chapter 7, we describe the development of a retinal multispectral imaging system and compare its efficacy with that of a retinal hyperspectral imaging system incorporating a liquid crystal tunable filter. The clinical applications of ophthalmic molecular imaging techniques, as reviewed in Chapter 8, depend on the development of effective imaging devices and techniques that permit the visualization and quantification of extrinsic and intrinsic chromophores that enable molecular imaging. Our retinal multispectral imaging allows selection of filters needed to visualize the chromophore of interest. This selection of filters ultimately results in faster acquisition of images and higher quality image processing. Our initial aim was to use curcumin as an extrinsic contrast agent. However, we found that curcumin lacked the spectral characteristics required for spectral imaging. It became apparent during our study that ophthalmic molecular imaging techniques are hampered by the lack of contrast agents that are approved for clinical use. Therefore, we used hemoglobin as a naturally-occurring chromophore to demonstrate the feasibility of multispectral imaging in the human eye for the acquisition of retinal spectral images of high quality obtained with short capture times. Further studies are warranted to test the feasibility of our system with exogenous contrast molecular imaging agents.



10

# Nederlandse samenvatting

Het eerste onderwerp van het onderzoek beschreven in dit proefschrift was de rol van het ubiquitine-proteasoom systeem (UPS) in retinale pigment epitheel (RPE) celgemedieerde proteostase. Vervolgens werden mogelijke oorzaken van proteasomale disfunctie in RPE cellen bestudeerd. Verder is onderzocht of het UPS betrokken is bij RPE-gemedieerde fibrose en wat de effecten zijn van farmacologische remming en activatie van het UPS in RPE cellen. Het tweede onderwerp van dit proefschrift is de toepassing van een nieuw-ontwikkeld instrument voor het multispectraal imagen van de retina om de bovengenoemde processen in de neurosensorische retina te visualiseren. In Hoofdstuk 3 hebben we mogelijke oorzaken van proteasoom disfunctie in RPE cellen onderzocht en, indirect, de rol van het proteasoom in de pathogenese van leeftijdsgebonden macula degeneratie (AMD). Een AMD-achtige omgeving werd geïntroduceerd in humane RPE celkweken om effecten van specifieke AMD pathogenen vast te stellen, zoals de complement anaphylatoxines C3a en C5a, oxidatieve stress geïnduceerd door waterstof peroxide en fagocytose van de buitenste fotoreceptor segmenten. Bovendien hebben we de effecten van veroudering op proteasoom activiteit gekarakteriseerd en hebben we expressie van de klassieke en de induceerbare proteasoom subunits  $\beta 5$  en  $\beta 5i$  bestudeerd in een muismodel van leeftijdsafhankelijke RPE degeneratie. We hebben aangetoond dat complement activatie via complement factor C3a geassocieerd is met gereduceerde proteasoomgemedieerde proteolytische activiteit en dat afgenomen proteasoom activiteit samenhangt met veroudering. Bovendien hebben we gevonden dat expressie van een van de induceerbare immunoproteasoom subunits opgereguleerd is in een muismodel van leeftijdsafhankelijke RPE degeneratie. Immunoproteasoom activatie wordt verondersteld een cellulaire respons te zijn op stress en muizen die deficiënt zijn voor deze proteasoom subunit ( $\beta 5i$ ) zijn minder resistent tegen oxidatieve stress. Deze bevindingen duiden op een associatie tussen complement activatie en ineffektieve RPE-gemedieerde proteostase. Verder onderzoek is noodzakelijk om de bijdrage van proteasoom disfunctie aan de AMD pathogenese vast te stellen. In Hoofdstuk 4 hebben we onderzocht of het UPS betrokken is bij fibrose en proliferatie van RPE cellen. Fibrose in oogziekten zoals neovasculaire

AMD en proliferatieve vitreoretinopathie is irreversibel en onbehandelbaar. Sinds er effectieve anti-angiogenese geneesmiddelen beschikbaar zijn, is de studie naar oorzaken van fibrose in oogziekten in het slop geraakt. In de afgelopen jaren is gesuggereerd dat proteasoom remmers mogelijke agentia zijn voor preventie en behandeling van fibrose in nier en lever. Derhalve hebben we onderzocht of modulatie van het proteasoom een effect heeft op de expressie van genen van extracellulaire matrix eiwitten in RPE cellen. De selectieve en irreversibele remmer van het proteasoom, epoxomicine, hebben we gebruikt om maximale remming van proteasoom activiteit te bewerkstelligen. Epoxomicine remde de celcyclus en de expressie van transforming growth factor- $\beta$  (TGF $\beta$ ), wat een krachtige profibrogene factor is. Bovendien remde epoxomicine niet alleen de expressie van genen van belangrijke extracellulaire matrix eiwitten, maar induceerde ook transcriptie van peroxisoom proliferator-geassocieerde receptor- $\gamma$  (PPAR $\gamma$ ), een belangrijke anti-fibrogene factor. Deze resultaten suggereren een relatie tussen UPS modulatie en fibrogenese in RPE. Vervolgens onderzochten we verbindingen op hun proteasoom-modulerende activiteit, zoals curcumine, dat naast andere effecten ook bekend is vanwege proteasoommodulerende effecten. Een veelvoud van mogelijke effecten van curcumine zijn beschreven, maar het gebruik van curcumine als therapeutisch middel wordt beperkt door de geringe biologische beschikbaarheid van standaard curcumine. Bovendien is gesuggereerd dat curcumine toxisch is voor RPE cellen. Het doel van het onderzoek beschreven in Hoofdstuk 5 was tweeledig: het vaststellen van de cytotoxische, antiproliferatieve en oxidatieve effecten van nanocurcumine (Theracurmin®), een biologisch beschikbaar curcumine dat vermengd is met nanocolloïdale deeltjes, in vergelijking met standaard curcumine, en het bepalen van de effecten van standaard curcumine en nanocurcumine op de expressie en activiteit van het proteasoom in RPE cellen. We hebben gevonden dat nanocurcumine een veiliger alternatief is in vergelijking met standaard curcumine. Nanocurcumine was niet of nauwelijks cytotoxisch en had geen effect op de celcyclus, terwijl standaard curcumine de levensvatbaarheid van RPE cellen verminderde en de productie van reactieve zuurstof deed toenemen. Dit verschil in effecten kan verklaard worden door het stabielere biochemische profiel van nanocurcumine dat 100 keer kleiner is dan standaard curcumine en derhalve beter water-oplosbaar. Nanocurcumine en standaard curcumine vertoonden beiden significante effecten op proteasoom-gemedieerde proteostase en expressie van proteasoom subunits. Onze bevindingen duiden op een negatief effect van standaard curcumine op het functioneren van RPE. Bovendien blijft de vraag onbeantwoord of nanocurcumine en standaard curcumine bij oraal gebruik het oog in voldoende concentraties bereiken die noodzakelijk zijn voor significante moleculaire effecten. In onze studies is een relatie vastgesteld tussen een ontregelde activatie van het complement systeem en het dysfunctioneren van het proteasoom. Het complement systeem is een belangrijke pathogene factor die geassocieerd is met de ontwikkeling van AMD en modulatie van het complement systeem wordt momenteel onderzocht als therapeutische strategie om de progressie van AMD te remmen. Echter, een fase II klinische trial met eculizumab, een remmer van complement factor C5 liet geen klinische effecten zien in niet exudatieve AMD. In Hoofdstuk 6

beschrijven we de effecten van eculizumab in Purtscher-achtige retinopathie, die evenals AMD door complement activatie wordt geïnduceerd. In dit bijzondere geval werd complement activatie veroorzaakt door een mutatie in het gen van complement factor H, een regulator van het alternatieve complement systeem die beschouwd wordt ook de gevoeligheid voor de ontwikkeling van AMD te bevorderen. Systematische behandeling van deze patiënt met eculizumab was geassocieerd met volledig herstel van visus en het verdwijnen van alle klinische symptomen, hetgeen een indicatie is dat therapeutische concentraties verkregen werden in choroïd en retina. Deze resultaten bij de patiënt geven aan dat er verschil bestaat tussen acute complement activatie zoals die gevonden wordt in Purtscher-achtige retinopathie en chronische complement activatie bij AMD. Een overzicht van de pathogenese van Purtscher-achtige retinopathie is beschreven op basis van de therapeutische effecten die behaald werden bij deze patiënt. Bovendien zijn de moleculaire achtergronden van het syndroom van hemolytische uremie beschreven, te weten de endotheliale activatie van de coagulatie cascade door het complement systeem en de vorming van microthrombi. Dit is de eerste beschrijving van een effectieve behandeling van visus-bedreigende Purtscherachtige retinopathie. Het tweede deel van dit proefschrift is gericht op moleculaire imaging methodes voor het oog om moleculaire processen in vivo te visualiseren. In Hoofdstuk 7, beschrijven we de ontwikkeling van een multispectraal imaging systeem van de retina en vergelijken we de effectiviteit ervan met die van een hyperspectraal imaging systeem van de retina, waarbij een liquid crystal tunable filter wordt gebruikt. Klinische toepassingen van moleculaire imaging technieken in het oog, zoals beschreven in Hoofdstuk 8, zijn afhankelijk van de ontwikkeling van effectieve imaging apparatuur en technieken, die de visualisatie en kwantificering van extrinsieke en intrinsieke chromoforen mogelijk maken. Het multispectrale imaging systeem dat wij beschrijven maakt het mogelijk om filters te selecteren die nodig zijn om chromoforen die gebruikt worden te visualiseren. Deze selectie van filters leidt uiteindelijk tot een snellere acquisitie van beelden en hogere kwaliteit van image processing. Ons oorspronkelijke doel was het gebruik van curcumine als extrinsiek contrastmiddel. Echter, we hebben gevonden dat curcumine de spectrale karakteristieken miste die noodzakelijk zijn voor spectraal imaging. Tijdens ons onderzoek werd duidelijk dat moleculair imaging in het oog beperkt wordt door het gebrek aan contrastmiddelen die goedgekeurd zijn voor klinische toepassingen. Derhalve hebben we hemoglobine gebruikt als intrinsiek chromofoor om de geschiktheid van multispectraal imaging in het menselijk oog te bewijzen voor snelle acquisitie van spectrale beelden van de retina van hoge kwaliteit. Meer onderzoek is noodzakelijk om de geschiktheid van dit systeem met extrinsieke contrastmiddelen voor moleculair imaging te testen.



11

Addendum

Biography

Curriculum vitae

List of publications

Acknowledgements

## Biography

João Emanuel Ramos de Carvalho (born April 18, 1984, Portuguese-Canadian) is a London-based ophthalmologist with a special interest in Medical Retina, Neuro-ophthalmology and Ophthalmogenetics. In 2009, he completed a Master's Degree in Medicine at the University of Oporto, Portugal. His thesis, entitled "Congenital hydrocephalus due to LICAM mutation and Hirschsprung disease" was conducted under the supervision of Prof. dr. Rolando DelMaestro at the Montréal Neurological Hospital and McGill University in Montréal, Canada. During his medical degree, De Carvalho completed several clinical and research internships in Paediatric Neurosurgery at the Hospital for Sick Children, University of Toronto, in Neuro-oncology at the Klinikum Grosshadern, Ludwig Maximilian University of Munich, Germany and in Developmental Neurology at the University of Groningen, The Netherlands. He spent four months at the University of Milan as an exchange student during his final year in Medicine. During his medical training, he worked as a senior clerk in Neurosurgery at the University of Oporto and taught Neurology and General Movements' Assessment at the University of Oporto and Ludwig Maximilian University of Munich. In 2009, he was admitted to the combined residency and Ph.D. programme in Ophthalmology at the Academic Medical Centre of the University of Amsterdam. The research for his Ph.D. thesis was conducted at the Department of Medical Biology and Department of Biomedical Engineering. His research project focused on the role of the proteasome in age-related ophthalmic disorders and on the development of novel methods in ophthalmic molecular imaging. In 2016, soon after completion of his clinical residency programme, De Carvalho was admitted to a clinical fellowship programme in Medical Retina, Uveitis and Genetics at Moorfields Eye Hospital in London, United Kingdom. The subsequent year, he was appointed as Locum Consultant in Medical Retina and Acting Clinic Lead at the same institution, a role he combines with a clinical fellowship in Neuro-ophthalmology at Moorfields Eye Hospital and at the National Hospital for

Neurology and Neurosurgery, University College Hospital London. He maintains his affiliation with the Academic Medical Centre of the University of Amsterdam as a Clinical Lecturer in Ophthalmogenetics. De Carvalho has presented at multiple conferences and has been invited to serve as board member of the Young Retina Specialists EURETINA Association. He holds a special interest in visual arts and fiction writing. During his residency in Amsterdam, he set up a series of Op Art lectures drawing attention to how this art genre has evolved from theoretical principles based on visual and neuro-ophthalmic sciences.

## **Curriculum vitae**

### **Education and Licensure**

Residency in Ophthalmology, Academic Medical Centre, University of Amsterdam, Amsterdam, The Netherlands 2011 – 2016

Master's Degree in Medicine, Faculty of Medicine, University of Oporto, Oporto, Portugal 2002 – 2008

### **Appointments**

Locum Consultant Medical Retina Moorfields Eye Hospital, London, United Kingdom 2017 – 2018

Clinical Fellowship – Neuro-Ophthalmology Moorfields Eye Hospital, London, United Kingdom 2017 – 2018  
National Hospital for Neurology and Neurosurgery, London, United Kingdom

Clinical Fellowship - Medical Retina, Uveitis and Genetics Moorfields Eye Hospital, London, United Kingdom 2016 – 2018

Observership Medical Retina, Uveitis and Electrophysiology Moorfields Eye Hospital, London, United Kingdom 2015

Observership Orbit and Adnexal Surgery Moorfields Eye Hospital, London, United Kingdom 2015

Master's Degree in Congenital Hydrocephalus	2007 –
Thesis title: LICAM syndrome associated with Hirschsprung's disease	2008
<i>Research site:</i> The Brain Tumour Research Centre, Montréal Neurological Institute and Hospital, McGill University, Montréal, QC, Canada	
<i>Thesis defence:</i> Faculty of Medicine, University of Oporto, Oporto, Portugal	
Classification: 19 out of 20 (A+)	
Graduate Teaching Assistant in Developmental Neurology	2006 –
Faculty of Medicine, University of Oporto, Oporto, Portugal	2008
Junior Clerk in Neurosurgery – Neuro-Oncology	2007 –
Department of Neurosurgery, University of Oporto, Oporto, Portugal	2008
Senior Clerk in Neurosurgery, Graduate Teaching Assistant and Research Assistant - Microdissection Human Cortex	2007
Department of Neurosurgery, Klinikum Grosshadern, Ludwig- Maximillians University, Munich, Germany	
Senior Clerk and Research Assistant in Neurosurgery - Neuro-Oncology	2007
The Brain Tumour Research Centre, Montréal Neurological Institute and Hospital, McGill University, Montréal, QC, Canada	
Senior Clerk in Paediatric Neurosurgery	2007
Hospital for Sick Children, University of Toronto, Toronto, ON, Canada	
Research Assistant in Developmental Neurology	2006
Institute of Developmental Neurology, University Medical Centre Groningen, Groningen, The Netherlands	

## Professional Development

Perimetry Course (Dutch Ophthalmological Society, The Netherlands)	2014
Bay Area Ophthalmology Course (Stanford University, U.S.A.)	2011
Practical Biostatistics Course (University of Amsterdam, The Netherlands)	2011
DNA Technology Course (University of Amsterdam, The Netherlands)	2011
Clinical Epidemiology Course (University of Amsterdam, The Netherlands)	2010
Reference Manager Basic Course (University of Amsterdam, The Netherlands)	2010
Small Animal Optical Imaging Course (University of Leiden, The Netherlands)	2009
Advanced DNA Technology Course (University of Amsterdam, The Netherlands)	2009
Ophthalmic Genetics Course (University of Amsterdam, The Netherlands)	2009
Workshop in Substance Abuse (International Society of Addiction Medicine)	2006
Course in Surgical Treatment of Parkinson Disease (University of Oporto, Portugal)	2006

## Language Courses

Advanced Level Dutch Language Course (Elycio Talen School, The Netherlands)	2009
Advanced Level German Language Course (Goethe Institute, Portugal)	2007
Swedish Language Course (University of Oporto, Portugal)	2007
Italian Language Course (University of Milan, Italy)	2002
Certificate of Proficiency in English (CPE)	2001
International English Language Testing System (IELTS)	2001/2016
German Language and Germanic Studies Course (Minho University, Portugal)	1999

## National Ophthalmological Dutch Board Examinations

(American Academy of Ophthalmology)

Average classification: 9 out of 10

## Educational Activities

### Teaching Activities

Art and Ophthalmology – Part 1: From El Greco to Bridget Riley, 2012 –  
Ophthalmology applied to Visual Arts. Part 2: The Physiology of Op 2016  
Art. MD Programme - University of Amsterdam, Amsterdam,  
The Netherlands

Neurological Examination – Practical Course for Medical Students. 2007  
Klinikum Grosshadern, Ludwig-Maximilians University, Munich,  
Germany

Assessment of General Movements – Instructional Course for 2006 –  
Paediatricians and Medical Students. University of Oporto, Oporto, 2008  
Portugal

### Advising, Mentoring & Supervision:

Ilyes Messoussi, Bachelor of Medicine 2017 –  
Project: *Curcumin in eye diseases*. Faculty of Medicine, University of 2018  
Amsterdam, The Netherlands

Tessa Willems, M.Sc. Student Forensic Sciences 2014 –  
Project: *Multispectral Imaging of Retinal Haemorrhages*. Department of 2016  
Biomedical Engineering and Physics, University of Amsterdam, The  
Netherlands

Milan Verwoert, Bachelor Cell Biology 2014 –  
Project: *Retinal Fibrosis and Proteasome Dysfunction*. Department of 2016  
Molecular Biology, University of Amsterdam, The Netherlands

## Presentations & Abstracts

### Invited Presentations

<i>The Eye of the Artist</i> , Amsterdam Orbital Meeting, Amsterdam, The Netherlands	2018
<i>YOURS RETINA Complex Cases Moderator</i> , EURETINA Vienna, Austria	2018
<i>YOURS RETINA Complex Cases Moderator</i> , EURETINA Barcelona, Spain	2017
<i>Role of the Ubiquitin-Proteasome Pathway in Age-Related Macular Degeneration</i> , ProRetina International Meeting Potsdam, Germany	2015
<i>History of Op Art</i> , Worldwide Access to Medical Advances, Access to Ophthalmological Advances Conference, Paramaribo, Suriname	2015
<i>The Eye of The Artist</i> , Worldwide Access to Medical Advances, Access to Ophthalmological Advances Conference, Paramaribo, Suriname	2012
<i>Retinal Prosthetic Devices</i> , Worldwide Access to Medical Advances, Access to Ophthalmological Advances Conference, Paramaribo, Suriname	2010

### National/International Meetings

Ramos de Carvalho, Michaelides M. et al. <i>Longitudinal long-term natural history of patients with Enhanced S-Cone Syndrome</i> . European Retinal Association EURETINA, Barcelona, Spain	2017
Ramos de Carvalho JE, Maloca PM, Petzold A. <i>Three-dimensional volume rendering of optic nerve head drusen</i> . European Neuro-Ophthalmological Society Meeting EUNOS, Budapest, Hungary	2017
Ramos de Carvalho JE. <i>Complement overactivation and the ubiquitin-proteasome pathway in age-related macular degeneration</i> . European Retinal Association EURETINA, Nice, France	2016
Ramos de Carvalho JE, Grewal D, Thomas D. <i>Assessment of subclinical microvascular flow characteristics in aneurysmal retinal vasculitis using optical coherence tomography angiography</i> . The Association for Research in Vision and Ophthalmology: ARVO, Baltimore, U.S.A.	2013
Ramos de Carvalho JE, Strianese D, Baronnissi I, Mourits MP, Yang M, Saeed P. <i>Long-term analysis of 25 cases of orbital lymphangioma</i> . European Society of Ophthalmic Plastic and Reconstructive Surgery, Barcelona, Spain	2014
Ramos de Carvalho JE, Klaassen I, Vogels IM, Schipper-Krom S, van Noorden CJ, Reits E, Gorgels TG, Bergen AA, Schlingemann RO. <i>Characterization of the ubiquitin-proteasome system in the retina</i> . Dutch Ophthalmological Society	2012

## List of publications

1. Ramos de Carvalho JE, Klaassen I, Vogels IM, Schipper-Krom S, van Noorden CJ, Reits E, Gorgels TG, Bergen AA, Schlingemann RO. Complement factor C3a alters proteasome function in human RPE cells and in an animal model of age-related RPE degeneration. *Invest Ophthalmol Vis Sci.* 2013;3,54(10):6489-501. doi: 10.1167/iovs.13-12374
2. Ramos de Carvalho JE, Verbraak FD, Aalders MC, van Noorden CJ, Schlingemann RO. Recent advances in ophthalmic molecular imaging. *Surv Ophthalmol.* 2014;59(4):393-413
3. Ramos de Carvalho JE, Verwoert MT, Vogels IMC, Schipper-Krom S, Van Noorden CJF, Reits EA, Klaassen I, Schlingemann RO. Modulation of the proteasome pathway by nano-curcumin and curcumin in retinal pigment epithelial cells. *Ophthalmic Res.* 2018;59(2):98-109. doi: 10.1159/000481261.
4. Ramos de Carvalho JE, Verwoert MT, Vogels IMC, Schipper-Krom S, van Noorden CJ, Reits E, Klaassen I, Schlingemann RO. Involvement of the ubiquitin-proteasome system in the expression of extracellular matrix genes in retinal pigment epithelial cells. *Biochem Biophys Rep.* 2018 Jan 28;13:83-92. doi: 10.1016/j.bbrep.2018.01.005
5. Ramos de Carvalho JE, Willig A, Chung R, Peiretti E, Mura M. Current surgical treatment of age-related macular degeneration. *Exp Rev Ophthalmol.* 2014; 9,3:235-245
6. Ramos de Carvalho JE, Schlingemann RO, Oranje M, Bemelman FJ, Van Schooneveld MJ. Reversal of threatening blindness after initiation of eculizumab in Purtscher-like retinopathy secondary to atypical hemolytic uremic syndrome. *Int Ophthalmol.* 2018 Feb;38(1):399-407. doi: 10.1007/s10792-017-0470-1.
7. Maloca PM, Tufail A, Egan C, Zweifel S, Hasler P, Petzold A, Ramos de Carvalho, JE. Volume rendering of superficial optic disk drusen: a possible new imaging technique using optical coherence tomography Angiography. *Spektrum der Augenheilkunde* 2017; doi: 10.1007/s00717-017-0359-4
8. Maloca PM, Tufail A, Hasler PW, Rothenbuehler S, Egan C, Ramos de Carvalho JE, Spaide RF. 3D printing of choroidal vessels and tumors based on optical coherence tomography. *Acta Ophthalmol.* 2017; doi: 10.1111/aos.13637
9. Maloca PM, Spaide RF, Rothenbuehler S, Scholl HPN, Heeren T, Ramos de Carvalho JE, Okada M, Hasler PW, Egan C, Tufail A. Enhanced resolution and speckle-free 3D printing of macular optical coherence tomography angiography. *Acta Ophthalmol.* 2017; doi: 10.1111/aos.13567
10. Maloca PM, Hasler PW, Ramos de Carvalho JE, Mushtaq F, Mon-Williams M, Egan C, Tufail A, Cattin PC. High-performance virtual reality volume rendering of original optical coherence tomography point-cloud data enhanced with real-time ray casting. *Trans Vis Sci Tech.* 2018; doi: 10.1167/tvst.7.4.2
11. Maloca PM, Hasler PW, Barthelmes D, Arnold P, Mooser M, Scholl HPN,

- Balaskas K, Heeren T, Ramos de Carvalho JE, Egan C, Tufail A, Zweifel S. Safety and feasibility of a novel sparse optical coherence tomography device for patient-delivered retina home monitoring. *Trans Vis Sci Tech.* 2018; doi: 10.1167/tvst.7.4.8
12. Ramos de Carvalho JE, Hoveling RJM, Verbraak FD, van Noorden CJF, Schlingemann RO, Aalders MCG. Spectral imaging of the ocular fundus using a 7-band retinal multispectral imaging system (submitted, under revision)
  13. Maloca PM, Ramos de Carvalho JE, Studer HP, Scholl HPN, Schottenhamml J, Hasler PW, Balaskas K, Tufail A, Egan C. A novel application of sphericity and cylindricity indices on volume rendering optical coherence tomography angiography in normal and diabetic eyes (submitted, under revision)
  14. Maloca PM, Hasler PW, Barthelmes D, Arnold P, Mooser M, Scholl HPN, Balaskas K, Heeren T, Ramos de Carvalho JE, Egan C, Tufail A, Zweifel S. Feasibility of support vector machine learning in age-related macular degeneration using small sample yielding sparse optical coherence tomography data. *Transl Vis Sci Technol.* 2018; doi: 10.1167/tvst.7.4.8
  15. Maloca PM, Tufail A, Ramos de Carvalho JE, Okada M, Fasler K, Leung I, Hörmann B, Suter S, Hasler P, Egan E, Heeren T, Balaskas K, Lee A. Benchmarking and validation of open source human and automated artificial intelligence retina compartmentalization of optical coherence tomography images (submitted, under revision)

## Acknowledgements

The journey to completion of this thesis has been long and enjoyable and it is with great enthusiasm that I write these words. The combination of a clinical residency programme with doctorate research work appeared at times to be an unattainable task. It is therefore imperative that I hereby thank everyone that has supported me and accompanied me in this endeavour.

First and foremost, I would like to thank the staff from the Department of Medical Biology, Department of Biomedical Engineering and Department of Ophthalmology at the Academic Medical Centre University of Amsterdam. In particular, I would like to thank Prof. dr. Mourits for the courage in appointing a resident from a foreign country to a highly competitive Ph.D./clinical residency programme. I truly feel that this epitomises the values of a common European vision that at present is increasingly under scrutiny. Secondly, Ingeborg and Ilse who taught me valuable lab skills and guided me during these past years. Ingeborg, I admire your knowledge and devotion to your work. Ilse, thank you for your warm welcome, encouragement and invaluable help during all these years. Thank you both for your patience and commitment. To Milan I would like to extend my sincerest thanks; without your dedication and diligence I would not have completed the final chapters of the thesis. I wish you the very best for your future. Reinier, Ron and Maurice, thank you for your guidance and invaluable help and approachability. Ron, thank you for caring so deeply and for your dedication to excellency. Reinier, it has been truly an honour to have you as my promotor. Maurice, I have always felt at ease with you and I do hope we can find new projects to collaborate in the future. Eric and Sabine, you were key elements during the time I spent in the lab. I always felt that I was part of your extended research group and I am deeply grateful for your help and advice. Richelle, thank you for your input and effort. Without your help, it would not have been possible to complete one of the most complex topics of this project. Mary, Sarit, Marco, Ruthie, Peerooz, Frank thank you for your help and motivational words.

Theo and Arthur, thank you for allowing me access to your lab and all the support. Rob, Martin, John and Joanna, I could not have wished for kinder research colleagues. Thank you for welcoming me to the team. Joanna, a simple wish that you were here with us. To my residency colleagues, I will always cherish the moments we spent together. To all of you, best of luck for the future and please stay in touch. Violette and Barbara, how amazing it was to have shared the office for all those years. Alissa and Hester, thank you for your friendship and for standing by my side during the Ph.D. ceremony. Thank you to my dear friends, who have always been there for me in the good and bad moments. I am grateful to Zé and Guida for the kind support and to Harry for his generosity and friendship over the years. To Cas, Marian, Kasia, Constantin, Jared, Laura, Andrew, Sterre, Matthew, Maria, Julia, Barbara, Sezayi, Inês, Rita, Roy, Sarah, Hugo, Sami, Tina, Irena, Cédric and Steven: thank you for your loyal friendship. And to my new team at Moorfields, Adnan, Cathy, Peter, Stevie and Camiel: looking forward to our new endeavours!

Finally, to my parents and my sister, Tina, to Mels and Mildred, thank you for always being there whenever encouragement was needed. This thesis bears testament to your unconditional love and support.





In the post-genomic era, characterisation of pathways involved in protein turnover has been a major area of research in medicine. The discovery of ubiquitin and thereafter the proteasome has revolutionised the understanding of the mechanisms responsible for protein regulation, also known as proteostasis. The proteasome acts as a nanomachine in eukaryotic and archaeal cells, responsible for proteolysis of soluble proteins that are tagged for degradation. This is achieved by selective ubiquitination of target proteins, a process that involves the covalent attachment of a poly-ubiquitin chain to the protein that is marked for recycling. In recent years, dysfunction of the ubiquitin-proteasome system has been linked to numerous human diseases which has led to the development of novel therapies using proteasome inhibitors. In this dissertation, we explore the contributions of the proteasome to retinal pathology and discuss strategies of therapeutic proteasome modulation in the retinal pigment epithelium.

Emanuel Ramos de Carvalho is an ophthalmologist affiliated with Moorfields Eye Hospital NHS Foundation Trust in London where he specialises in Medical Retina, Neuro-ophthalmology and Genetics. His doctorate research was conducted at the Academic Medical Centre of the University of Amsterdam, The Netherlands. His primary areas of research include inherited eye diseases, artificial intelligence and virtual reality applied to ophthalmology.

ISBN 9789461829160



9 789461 829160